

ABSTRACT

Title of Document: EARLY TRANSITION METAL STUDIES OF
DINITROGEN CLEAVAGE AND METAL-
NITROGEN BOND REACTIVITY TOWARDS
CATALYTIC N₂ FIXATION

Andrew John Keane, Doctor of Philosophy

Directed By: Professor Lawrence R. Sita
University of Maryland – College Park

The development of energy efficient catalysts that provide a range of commodity chemicals derived from the fixation of N₂ is a highly attractive target due to the abundance of molecular nitrogen present in Earth's atmosphere. Studies have focused on the systematic investigation of several key components of metal-catalyzed N₂ fixation that detail molecularly discrete transformations involving the activation of N₂, cleavage of the strong N≡N triple bond and N-atom functionalization to provide ammonia and other organic molecules of scientific and industrial interest. To this end, an evaluation of group 5 N₂ cleavage using the pentamethylcyclopentadienyl, amidinate (CPAM) ligand framework that includes extensive kinetic and mechanistic investigations detailing the N-N cleavage reaction coordinate has been undertaken. Further studies conducted within group 5 include the synthesis and reactivity of tantalum imido complexes to elucidate metal-nitrogen bond reactivity and N-N cleavage relevant to the Chatt cycle. In group 6, photolytic N-N cleavage has been

further investigated. Most notably, chemistry has been discovered for N₂-derived metal nitride complexes of Mo and W that gives access to imido complexes capable of participating in nitrene group transfer (NGT) to carbon monoxide and isocyanides to provide isocyanates and carbodiimides respectively. For the first time, it has been demonstrated that imido complexes that participate in NGT chemistry can be derived from N₂ to provide N-C based organic products. Collectively, these results serve to establish a new platform for studying the catalytic viability of the discovered transformations.

EARLY TRANSITION METAL STUDIES OF DINITROGEN CLEAVAGE AND
METAL-NITROGEN BOND REACTIVITY TOWARDS CATALYTIC N₂
FIXATION

By

Andrew John Keane

Thesis submitted to the Faculty of the Graduate School of the
University of Maryland, College Park, in partial fulfillment
of the requirements for the degree of
Doctor of Philosophy
2015

Advisory Committee:
Professor Lawrence R. Sita, Chair
Professor Andrei Vedernikov
Professor Bryan W. Eichhorn
Professor Efrain E. Rodriguez
Professor Min Ouyang

© Copyright by
Andrew John Keane
2015

Dedication

The discoveries and advancements made during my tenure as a graduate student are dedicated to my family and close friends as well as teachers and professors that have served as my mentors over the years.

Acknowledgements

I want to thank my advisor Professor Sita for being a great mentor and giving me every opportunity to succeed as a graduate student. I have a deeper understanding of what it takes to conduct successful research and have confidence that I am capable of producing high quality work thanks to working in his lab and his guidance. The projects that I worked on were intellectually stimulating, challenging and geared towards making significant contributions to the field. The only limit to solving problems in these projects was my own creativity – I can only hope that I will have the opportunity to pursue similar research in the future. I have also had many unique opportunities as a graduate student and these would have not been possible without his support.

I would like to thank Sita group members in the past who I have worked with that include Brendan Yonke, Wonseok Hwang, Rennisha Wickham, Jia Wei, Jonathan Reeds and Gail Blakley. This group was extremely supportive and key to getting up to speed in the lab. Brendan Yonke was my glove box partner and taught me a lot of the tips and tricks to making and isolating new compounds. He was a nice person to work with and continues to be supportive even after his graduation. The current Sita lab members, Wes Farrell, Kaitlyn Crawford, Tessy Thomas, Kerry DeMella, Leila Duman, Kyle Augustine and Katie Pohida have been fun to work with and I have enjoyed discussing research with them. This is an extremely supportive group of people. Wes Farrell was my box-mate for the last half of my tenure in the Sita lab and it has been great to work with someone who is very enthusiastic about pursuing research. All in all, I feel privileged to have been a part of such a dedicated

group of graduate students. Having had the opportunity to get to know everyone closely, it amazes me how unique everyone's personality is and how each person contributes to the group. I have learned a lot about research and life in general and have been inspired by these people. I could have not asked for a better group to work with and I will be sad as I move on from this community.

I would like to thank our crystallographer Dr. Peter Zavalij who was critical to developing this research. The NMR staff Dr. Yui-Fai Lam and Dr. Yinde Wang were very generous and helpful. Finally, I would like to thank the department and the graduate school for fellowship awards that supported me throughout my tenure. The community as a whole (graduate students and professors outside of the Sita lab) was very supportive and made my graduate school experience the best it could be.

I made many sacrifices to pursue this Ph.D. degree and I want to thank my family and friends for the patience and support they have given me to make this a successful venture. Specifically, my parents David and Nancy Keane, my brother Brendan Keane, my sister-in-law Stacy Keane, their three children Avery, Mason and Penny as well as Kristen Jabanoski. The professors at Eckerd College in the NAS department were all inspiring and this would not have been possible without their guidance and support. Funding for this work was provided by the DOE (Grant DE-SC0002217) and NSF (Grant CHE-1361716).

Table of Contents

Dedication.....	ii
Acknowledgements	iii
Table of Contents.....	v
List of Abbreviations.....	viii
List of Tables.....	x
List of Figures	xi
List of Schemes	xvi
Chapter 1: Introduction to Nitrogen Fixation	1
1.1. Significance of Nitrogen Fixation.....	2
1.2. Developments in Homogeneous Nitrogen Fixation.....	2
1.2.1. Synthetic metal complexes capable of fixating N ₂	2
1.3. Strategies Employed in this Thesis	5
1.3.1. Previous N ₂ fixation work in the Sita lab.....	5
1.3.2. The focus of research in this thesis	6
1.4. References.....	6
Chapter 2: Synthesis and Reactivity of a CPGU Ta(IV) Imido.....	8
2.1. Introduction.....	9
2.2. CPGU Mononuclear Ta(IV, <i>d</i> ¹) Imido Studies.....	12
2.2.1. Synthesis and characterization of a CPGU Ta(IV) imido complex	12
2.2.2. Reactivity of a CPGU Ta(IV, <i>d</i> ¹) mononuclear imido complex	16
2.3. Conclusion	20
2.4. Experimental Section	21
2.4.1. General considerations.....	21
2.4.2. Synthesis of new compounds.....	22
2.5. References.....	27
Chapter 3: Chemistry and N-N Cleavage of Tantalum Hydrazido and Hydrazidium Complexes	30
3.1. Introduction.....	31
3.2. Mononuclear Ta(IV, <i>d</i> ¹) Hydrazido Studies	32
3.2.1. Synthesis and characterization of a mononuclear Ta(IV) hydrazido complex.....	32

3.2.2. Metal-centered reactivity of a mononuclear Ta(IV) hydrazido complex.....	35
3.3. Tantalum Hydrazidium Complexes and N-N Cleavage	39
3.3.1. Synthesis of Ta(V) and Ta(IV) hydrazidium complexes	39
3.3.2. Ta(IV) hydrazidium N-N cleavage studies	41
3.4. Structural and Electronic Comparisons of Ta Imido and Hydrazido Compounds.....	44
3.4.1. N β - substituent effects	44
3.5. Hydrazido Studies Extended to Group 6	46
3.5.1. Synthesis and reactivity of group 6 hydrazido complexes.....	46
3.6. Conclusion	48
3.7. Experimental Section	49
3.7.1. General considerations.....	49
3.7.2. Synthesis of new compounds.....	50
3.7.3. Supporting NMR spectra	57
3.8. References.....	58
Chapter 4: Group 5 Thermal N₂ Cleavage Studies	63
4.1. Introduction.....	64
4.2. Tantalum mediated N-N cleavage	66
4.2.1. Discussion of structural perturbations of pre-cleaved and cleaved dinitrogen complexes as a function of the amidinate derivative.....	66
4.2.2. Kinetic and mechanistic studies regarding N ₂ cleavage	68
4.2.3. Kinetic isotope effects and crossover experiments	71
4.3. CPAM Niobium Mediated N ₂ cleavage.....	75
4.3.1. Development of a well-defined Nb N ₂ cleavage system	75
4.3.2. Niobium mediated N ₂ cleavage kinetics	78
4.4. CPAM Vanadium N ₂ chemistry.....	80
4.4.1. Synthesis and reactivity of a CPAM vanadium N ₂ complex	80
4.5. Conclusion	82
4.6. Experimental Section	83
4.6.1. General considerations.....	83
4.6.2. Synthesis of new compounds.....	84
4.6.3. Mechanistic experiments	88
4.6.4. Supporting NMR and UV-vis spectra.....	90
4.7. References.....	93
Chapter 5: Group 6 CPAM N₂ Fixation.....	97
5.1. Introduction.....	98
5.2. Group 6 Photolytic N ₂ Cleavage Studies	100
5.2.1. UV-vis and NMR studies of photolytic Mo and W mediated N ₂ cleavage.....	100
5.3. Reactivity of Group 6 CPAM Nitride Complexes.....	103
5.3.1. Structural and electronic properties of group 6 CPAM bis- μ -nitrido complexes	103
5.3.2. Reaction of nitride complexes with silylating agents	105

5.3.3. Extension of silyl chemistry to group 14 monochloride reagents, R ₃ ECl	107
5.4. Dinitrogen Functionalization	110
5.4.1. Imido complexes derived from dinitrogen.....	110
5.4.2. Labeling studies and multinuclear NMR	113
5.5. On Pursuing Catalysis.....	116
5.5.1. Catalytic implications of discovered dinitrogen functionalization	116
5.5.2. Future direction for pursuing catalytic formation of N-C based products.....	117
5.6. Conclusion	120
5.7. Experimental Section	120
5.7.1. General considerations.....	120
5.7.2. Synthesis of new compounds.....	121
5.7.3. ¹ H NMR N ₂ photocleavage experiments	123
5.7.4. ¹ H NMR experiments of Mo and W nitride complexes with R ₃ ECl (R = Me, Ph; E = C, Si, Ge).....	124
5.7.5. ¹ H NMR experiments detailing N ₂ functionalization and fixation to R ₃ EN=C=O and Me ₃ SiN=C=NAr	130
5.7.6. Labeling studies and multinuclear NMR of group 6 ¹⁵ N imido species, [¹³ C, ¹⁵ N]-isocyanates and ¹⁵ N-carbodiimides.....	141
5.8. References.....	145
Chapter 6: Implications of Research and Future Work.....	148
6.1. Implications of Discoveries	149
6.2. Future Work	150
Appendix A: Group 6 Nitrene Transfer to Isocyanides.....	153
A.1. Introduction.....	154
A.2. Group 6 Imido Group Transfer Chemistry	155
A.2.1. Extension of imido group transfer chemistry to aryl isocyanide substrates.....	155
A.3. Conclusion	158
A.4. Experimental Section	159
A.4.1. General considerations.....	159
A.4.2. Synthesis of new compounds.....	159
A.5. References.....	160

List of Abbreviations

N ₂	dinitrogen
H ₂	dihydrogen
NH ₃	ammonia
NMe ₃	trimethylamine
HIPT	hexaisopropylterphenyl
BAr ^F ₄	tetrakis(pentafluorophenyl)borate
Cp	cyclopentadienyl
Cp*	pentamethylcyclopentadienyl
Me	methyl
ⁱ Pr	<i>iso</i> -propyl
^t Bu	<i>tert</i> -butyl
CPAM	pentamethylcyclopentadienyl amidinate
CPGU	pentamethylcyclopentadienyl guanidinate
Et ₂ O	diethylether
THF	tetrahydrofuran
Ar	aryl
CO	carbon monoxide
Ph	phenyl
TEMPO	(2,2,6,6,-tetramethyl-piperidin-1-yl)oxyl
MeI	methyl iodide
MeOTf	methyl trifluoromethanesulfonate

LiNMe ₂	lithium dimethylamide
H ₂ NNMe ₂	N,N-dimethylhydrazine
CNAr	2,6-dimethylphenyl isocyanide
NaHg	sodium amalgam
KC ₈	potassium graphite
RT	room temperature
NMR	nuclear magnetic resonance
VT-NMR	variable temperature – nuclear magnetic resonance
EPR	electron paramagnetic resonance
XRD	x-ray diffraction
ESI-MS	electrospray ionization – mass spectrometry
UV-vis	ultraviolet – visible
Abs	absorbance
min	minutes
h	hours
d	days
HOMO	highest occupied molecular orbital
LUMO	lowest unoccupied molecular orbital
UV	ultraviolet

List of Tables

Table 2.1. CPAM <i>tert</i> -butyl imido isostructural series spanning groups 4 through 6.	10
Table 3.1. Structural parameters for imido and hydrazido compounds.	45
Table 4.1. Structural parameters for group 5 pre-cleaved and cleaved dinitrogen compounds.	66
Table 4.2. Experimentally-derived activation parameters for thermal conversion of 4.1a-c to 4.3a-c	71
Table 5.1. Structural parameters for bis- μ -nitrido complexes 5.4a and 5.4b	103
Table 5.2. Multinuclear NMR of ^{15}N -labeled imido complexes 5.7a-e	114
Table 5.3. Multinuclear NMR (benzene- d_6 , 25 °C) of doubly labeled [^{13}C , ^{15}N]-isocyanates 5.10a-d and labeled [^{15}N]-carbodiimide 5.12	115

List of Figures

Figure 2.1. Molecular structures (30% thermal ellipsoids) of (top) 2.14 , (middle) 2.15 and (bottom) 2.16 . Hydrogen atoms except for H1 in 2.14 have been removed for the sake of clarity.	15
Figure 2.2. X-band EPR spectrum (toluene, 25 °C) of compound 2.16 ; $g_{\text{iso}} = 1.975$, $A_{\text{iso}}(^{181}\text{Ta}) = 600$ MHz.....	16
Figure 2.3. Molecular structures (30% thermal ellipsoids) of (top) 2.17 , (middle) 2.18 and (bottom) 2.19 . Hydrogen atoms have been removed for the sake of clarity.	18
Figure 2.4. Molecular structures (30% thermal ellipsoids) of 2.20 . Hydrogen atoms have been removed for the sake of clarity.....	20
Figure 3.1. Molecular structures (30% thermal ellipsoids) of (left) 3.3 and (right) 3.5 . Hydrogen atoms have been removed for the sake of clarity.	34
Figure 3.2. X-band EPR spectrum (toluene, 25 °C) of compound 3.5 ; $g_{\text{iso}} = 1.962$, $A_{\text{iso}}(^{181}\text{Ta}) = 439$ MHz.....	35
Figure 3.3. Molecular structures (30% thermal ellipsoids) of (top) 3.6 , (middle) 3.7 and (bottom) 3.8 . Hydrogen atoms except for H1 and H2 in 3.6 and H1 in 3.7 have been removed for the sake of clarity.	37
Figure 3.4. X-band EPR spectrum (toluene, 25 °C) of compound 3.10 ; $g_{\text{iso}} = 1.921$, $A_{\text{iso}}(^{181}\text{Ta}) = 422$ MHz.....	40
Figure 3.5. Molecular structures (30% thermal ellipsoids) of (top) 3.9 and (bottom) 3.10 . Hydrogen atoms have been removed for the sake of clarity.	41
Figure 3.6. Molecular structures (30% thermal ellipsoids) of (left) <i>cis</i> - 3.11 and (right) 3.12 . Hydrogen atoms except for H1 in 3.12 have been removed for the sake of clarity.....	43
Figure 3.7. Molecular structures (30% thermal ellipsoids) of 3.20 . Hydrogen atoms have been removed for the sake of clarity.....	47
Figure 3.8. Hydrazido(2-) versus isodiazene(0) resonance structures for hydrazido complexes.	48

Figure 3.9. ^1H NMR (400.13 MHz, C_6D_6 , 25 °C) experiment showing (top) pure 3.7 and (bottom) a mixture of 3.7 (+) and 3.6 (•) that was produced from the thermal disproportionation of 3.5 .	57
Figure 3.10. ^1H NMR (400.13 MHz, C_6D_6 , 25 °C) experiment showing (top) <i>trans</i> - 3.11 and (bottom) <i>trans</i> - 3.11 , both isolated from reductive N-N cleavage of compound 3.10 .	57
Figure 3.11. (top) ^{19}F NMR (376 MHz, C_6D_6 , 25 °C) and (bottom) ^1H NMR (400.13 MHz, C_6D_6 , 25 °C) of compound 3.12 isolated from N-N cleavage of 3.10 in toluene.	58
Figure 4.1. Spacefill models for (left column) pre-cleaved 4.1a-c and (right column) cleaved <i>trans</i> 4.3a-c with view of red Cp* remaining constant.	67
Figure 4.2. (a) Scanning UV-vis spectroscopy for ($^{15}\text{N}_2$, 98%)- 4.1a \rightarrow ($^{15}\text{N}_2$, 98%)- 4.3a at T = 318.15 K. (b) Kinetic analysis of $[\text{4.1a}]_t$ vs. time as monitored at $\lambda = 625$ nm.	69
Figure 4.3. (left) temperature dependent first order $\ln(A) = -kt + A_0$ plots for the conversion of ($^{15}\text{N}_2$, 98%)- 4.1a to ($^{15}\text{N}_2$, 98%)- 4.3a and (right) concentration dependence of rate constants and initial rates for the conversion of ($^{15}\text{N}_2$, 98%)- 4.1a to ($^{15}\text{N}_2$, 98%)- 4.3a .	69
Figure 4.4. Temperature-dependent first-order rate constants with least-squares fit to the Eyring equation, $k = (k_{\text{B}}T/h) \exp(\Delta S^\ddagger/R) \exp(-\Delta H^\ddagger/RT)$, for the conversion of 4.1a to 4.3a (circle), 4.1c to 4.3c (square) and 4.1b to 4.3b (triangle).	70
Figure 4.5. Kinetic isotope effect $k(^{14}\text{N})/k(^{15}\text{N})$ for the conversion of 4.1a to 4.3a .	72
Figure 4.6. Crossover study: ESI-MS (positive ion mode) of products from heating a mixture of 4.1a and 4.1b in THF for 3.5 h. No theoretical crossover product was observed.	73
Figure 4.7. Structural parameters for group 4 side-bound dinitrogen complexes.	74
Figure 4.8. Molecular structures (30% thermal ellipsoids) of (top) 4.4a , (middle) 4.2b and (bottom) 4.4b . Hydrogen atoms have been removed for the sake of clarity.	77

Figure 4.9. (top) Scanning UV-vis spectroscopy for 4.2b → 4.4b (T = 338.15 K, Δt = 3 min) and (bottom) temperature dependent first order $\ln(A) = -kt + A_0$ plots for the conversion of 4.2b to 4.4a .	79
Figure 4.10. Molecular structures (30% thermal ellipsoids) of (left) 4.7 and (right) 4.5 . Hydrogen atoms have been removed for the sake of clarity.	80
Figure 4.11. Molecular structures (30% thermal ellipsoids) of (left) 4.6 and (right) 4.7 . Hydrogen atoms have been removed for the sake of clarity.	81
Figure 4.12. ¹ H NMR (400.13 MHz, C ₆ D ₆ , 25 °C) experiment showing crude products (<i>cis/trans</i> - 4.3a) obtained from thermolysis of 4.1a at 70 °C for 2 h.	90
Figure 4.13. ¹ H NMR (400.13 MHz, C ₆ D ₆ , 25 °C) experiment showing crude products (<i>cis/trans</i> - 4.3b) obtained from thermolysis of 4.1b at 70 °C for 2 h.	90
Figure 4.14. ¹ H NMR (400.13 MHz, C ₆ D ₆ , 25 °C) experiment showing crude products (<i>cis/trans</i> - 4.3c) obtained from thermolysis of 4.1c at 85 °C for 2.5 h.	91
Figure 4.15. ¹ H NMR (400.13 MHz, C ₆ D ₆ , 25 °C) experiment showing crude products (<i>trans</i> - 4.4b) obtained from thermolysis of 4.2b at 70 °C for 2 h.	91
Figure 4.16. (top left) UV-vis scanning kinetics at 334.45 K, Δt = 3 min, (top right) temperature dependent first order $\ln(A) = -kt + A_0$ plots, and (bottom) rate constant and initial rate concentration dependence for the conversion of 4.1b to 4.3b . Error bars are at the 95% confidence interval.	92
Figure 4.17. (top left) UV-vis scanning kinetics at 343.15 K, Δt = 3 min, (top right) temperature dependent first order $\ln(A) = -kt + A_0$ plots, and (bottom) rate constant and initial rate concentration dependence for the conversion of 4.1c to 4.3c . Error bars are at the 95% confidence interval.	93
Figure 5.1. UV-vis spectra of 5.2a (c = 0.87 mM in methylcyclohexane) taken during photolysis (Quartz, med. Pressure Hg lamps) after timed intervals (Δt ≈ 1 h for total 4 h).	101

Figure 5.2. UV-vis spectra of 5.2b ($c = 0.86$ mM in methylcyclohexane) taken during photolysis (Quartz, med. pressure Hg lamps) after timed intervals ($\Delta t \approx 1$ h for total of 9 h).....	101
Figure 5.3. Molecular structures (30% thermal ellipsoids) within a co-crystal containing 5.4a and 5.5 (ratio of 5.4a to 5.5 is 1 to 3). (left) 5.4a and (right) 5.5 . Hydrogen atoms have been removed for the sake of clarity.....	102
Figure 5.4. X-band EPR spectrum (toluene, 25 °C) of compound 5.4a ; $g_{\text{iso}} = 1.975$, $A_{\text{iso}}(^{95/97}\text{Mo}) = 40$ MHz. Simulation was produced by EasySpin.	104
Figure 5.5. Molecular structure (30% thermal ellipsoids) of 5.7e . Hydrogen atoms have been removed for the sake of clarity.....	109
Figure 5.6. ^1H NMR (400.13 MHz, benzene- d_6 , 25 °C) of 5.2b (o) exposed to UV light after (a) 0 h, (b) 15.5 h, and (c) 60 h, showing production of 5.4b (+).....	124
Figure 5.7. ^1H NMR (400.13 MHz, benzene- d_6 , 25 °C) of (a) initial 5.4a and durene (*). (b) Reactivity of 5.4a with Me_3CCl (V) after heating at 80 °C for 31h to give 5.7a (o), isobutene (-) and isobutane (l).	125
Figure 5.8. ^1H NMR (400.13 MHz, benzene- d_6 , 25 °C) of (a) initial 5.4a and durene (*). (b) Reactivity of 5.4a with Me_3SiCl over 18 h to produce 5.7b (+) and 5.3a (O).	126
Figure 5.9. ^1H NMR (400.13 MHz, benzene- d_6 , 25 °C) of (bottom) initial 5.4b (-) and durene (*). (top) reactivity of 5.4b with Me_3SiCl (V) over 18 h to produce 5.7c (o) and 5.3b (+).	127
Figure 5.10. ^1H NMR (400.13 MHz, benzene- d_6 , 25 °C) of (a) initial 5.4a and durene (*). (b) Reactivity of 5.4a with $(\text{Me}_3\text{Si})_2\text{Hg}$ over 18 h to give 5.7b (o).....	128
Figure 5.11. ^1H NMR (400.13 MHz, benzene- d_6 , 25 °C) of (a) initial 5.4a and durene (*). (b) Reactivity of 5.4a with Ph_3SiCl for 15 min to give 5.7d (o) and 5.3a (+). The symbol # denotes diethyl ether impurities.	129
Figure 5.12. ^1H NMR (400.13 MHz, benzene- d_6 , 25 °C) of (a) initial 5.4a and durene (*). (b) reactivity of 5.4a with Me_3GeCl (^) over 1 h to give 5.7e (o) and 5.3a (+).....	130

Figure 5.13. ^1H NMR (400.13 MHz, benzene- d_6 , 25 °C) of (a) initial 5.2b (O), durene (*), and Me_3SiCl (^), (b) after photolyzing for 49 h showing partial conversion to 5.7c (+) and 5.8b (=) and (c) after photolyzing for 119 h to complete the conversion to 5.7c and 5.8b	131
Figure 5.14. ^1H NMR (400.13 MHz, benzene- d_6 , 25 °C) of (a) initial 5.2a (O) and durene (*), (b) after photolyzing for 65 h, (c) after adding <i>tert</i> -butyl chloride (^) and heating to provide 5.7a (+), isobutene (l) and isobutane (-) followed by (d) reacting with carbon monoxide for 23 h to provide 5.9a (=) and Me_3CNCO (5.10a).....	133
Figure 5.15. ^1H NMR (400.13 MHz, benzene- d_6 , 25 °C) of (a) initial 5.2a and durene (*), (b) after photolyzing for 65 h, (c) after adding Ph_3SiCl (^) to provide 5.7b (+) followed by (d) reacting with CO to provide 5.9a (=) and Me_3SiNCO (5.10b).	135
Figure 5.16. ^1H NMR (400.13 MHz, benzene- d_6 , 25 °C) of (a) initial 5.2a (O) and durene (*), (b) after photolyzing for 65 h, (c) after adding Ph_3SiCl (^) to provide 5.7d (+) followed by (d) reacting with CO to provide 5.9a (=) and Ph_3SiNCO (5.10c).....	137
Figure 5.17. ^1H NMR (400.13 MHz, benzene- d_6 , 25 °C) of (a) initial 5.2a and durene (*), (b) after photolyzing for 82.5 h, (c) after adding Me_3GeCl (^) to provide 5.7e (+) followed by (d) reacting with CO to provide 5.9a (=) and Me_3GeNCO (5.10d).....	139
Figure 5.18. ^1H NMR (400.13 MHz, benzene- d_6 , 25 °C) of (a) initial 5.2a (O), Me_3SiCl (V) and durene (*), (b) after photolyzing for 94 h to produce 5.7b (l) and (c) 8 h after addition of 2,6-dimethylphenyl isocyanide (CNAr') (X) to produce 5.11 (-) and $\text{Me}_3\text{SiNCNAr}$ (5.12) (+).	141
Figure A.1. ^1H NMR spectrum (400 MHz, benzene- d_6 , 25 °C) of (a) pure A.4 (O), (b) after reacting with 2,6-dimethylphenyl isocyanide (CNAr) (V) at room temperature for 15 m revealing a transient C_1 symmetric species attributed to A.11 (+), with partial conversion to A.12 (l), and $\text{Me}_3\text{Si-N=C=N-Ar}$ (A.13) (-), and (c) complete conversion to A.12 (l) and $\text{Me}_3\text{Si-N=C=N-Ar}$ (A.13) (-) after reacting for 12 h.	156
Figure A.2. ESI-MS (positive ion mode) of carbodiimide ArN=C=NSiMe_3 (A.13) (Ar = 2,6-dimethylphenyl).	157
Figure A.3. Molecular structures (30% thermal ellipsoids) of A.14 . Hydrogen atoms have been removed for the sake of clarity.....	158

List of Schemes

Scheme 1.1. First reported synthetic catalyst for N ₂ fixation to ammonia by Schrock.	3
Scheme 1.2. Synthetic catalysts capable of fixation dinitrogen to ammonia.....	3
Scheme 1.3. Production of N-C based organic molecules derived from N ₂	4
Scheme 1.4. Groups 4-6 CPAM isostructural series of N ₂ complexes.....	5
Scheme 2.1. Reactivity of CPAM Ta dinitrogen complex 2.1	9
Scheme 2.2. Synthetic route to CPAM Ta(IV) Imido 2.7	11
Scheme 2.3. Synthesis of CPGU Ta(IV) amido chloride 2.14	12
Scheme 2.4. Reactivity of CPGU Ta(IV) amido chloride 2.14	13
Scheme 2.5. Synthesis of 2.16 starting from the amido chloride precursor 2.14	14
Scheme 2.6. One-electron chemistry of 2.16 with methyl iodide.....	17
Scheme 2.7. Reactivity of 2.16 with diphenyl disulfide.....	19
Scheme 2.8. Reactivity of CPAM dinitrogen complex 2.1 with diphenyl disulfide.....	19
Scheme 3.1. Synthesis of CPAM Ta(V) hydrazido chloride 3.3	33
Scheme 3.2. Synthesis of CPAM Ta(IV) Hydrazido 3.5	33
Scheme 3.3. Thermal disproportionation of CPAM Ta(IV) Hydrazido 3.5	36
Scheme 3.4. Reactivity of 3.5 with trimethylsilylazide.....	38
Scheme 3.5. Synthesis of CPAM Ta(V) hydrazidium 3.9	39
Scheme 3.6. Synthesis of CPAM Ta(IV) hydrazidium 3.10	40
Scheme 3.7. N-N cleavage of a Ta(IV) hydrazidui complex.....	42
Scheme 3.8. Proposed mechanisms for the formation of 3.11 and 3.12	44

Scheme 3.9. Synthesis and reactivity of group 6 CPAM hydrazido compounds 3.18 and 3.19	46
Scheme 4.1. Tantalum mediated N ₂ cleavage and mechanistic pathways.....	65
Scheme 4.2. Synthesis and reactivity of CPAM Nb dinitrogen complexes.....	76
Scheme 4.3. Synthesis of a CPAM vanadium N ₂ complex.	80
Scheme 4.4. CPAM vanadium N ₂ displacement chemistry.....	81
Scheme 5.1. Previous research involving CPAM mediated group 6 N ₂ cleavage.....	99
Scheme 5.2. Products obtained from photolytic group 6 N ₂ cleavage.....	102
Scheme 5.3. Group 6 bis- μ -nitrido reactivity with Me ₃ SiCl.	105
Scheme 5.4. Reactivity of nitride compounds with (Me ₃ Si) ₂ Hg	107
Scheme 5.5. CPAM Molybdenum nitride chemistry with R ₃ ECl.	107
Scheme 5.6. Preparative synthesis of 5.7e	108
Scheme 5.7. Molybdenum bis- μ -nitrido reactivity with <i>tert</i> -butyl chloride.....	110
Scheme 5.8. Dinitrogen functionalization by Mo and W to provide isocyanates and carbodiimides.....	112
Scheme 5.9. Hypothetical cycle for production of isocyanates derived from N ₂	116
Scheme 5.10. General cycle for the production of organic products from N ₂	118
Scheme 5.11. Alternative proposed cycle for the formation of N-C based products derived from N ₂	119
Scheme A.1. Group 6 nitrene transfer to carbon monoxide.	154
Scheme A.2. Group 6 nitrene transfer to aryl isocyanides.	155
Scheme A.3. Synthesis and isolation of a tungsten η^2 -carbodiimide complex.....	157

Chapter 1: Introduction to Nitrogen Fixation

1.1. Significance of Nitrogen Fixation

The last century has hinged on the growth of industrial syntheses of a variety of commodity chemicals to support the needs of the current world population. While the industrial revolution made an enormous impact, current research must focus on new methods to replace old, inefficient processes for the production of commodity chemicals. Synthesis of ammonia (NH_3) is one of the largest industrial processes today, as it is a necessary building block for synthetic nitrogen containing molecules and is vital to support agriculture. However, only the Haber-Bosch process currently exists to make NH_3 on an industrial scale, which uses an estimated 1-3% of the world's total annual energy consumption due to its energy intensive processes.¹ Sustainable production of ammonia will be a key challenge in the 21st century to support the world population at its growing rate. Nitrogen (N_2) fixation has thus become an important academic focus in part due to the significant challenge that cleaving the strong triple bond present in N_2 , but more practically, the massive resource of N-atoms from nitrogen gas found within Earth's atmosphere that go untapped, or used at a high energy cost for the production of ammonia.

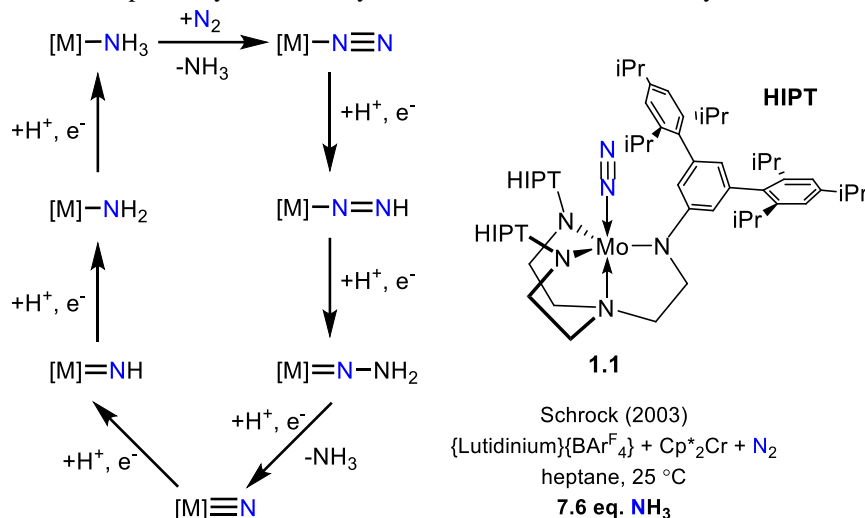
1.2. Developments in Homogeneous Nitrogen Fixation

1.2.1. Synthetic metal complexes capable of fixating N_2

The first example of catalytically reducing N_2 to ammonia under mild conditions was demonstrated by Schrock and coworkers in 2003.² Using a molybdenum catalyst supported by a bulky tris-amido amine ligand set to create a

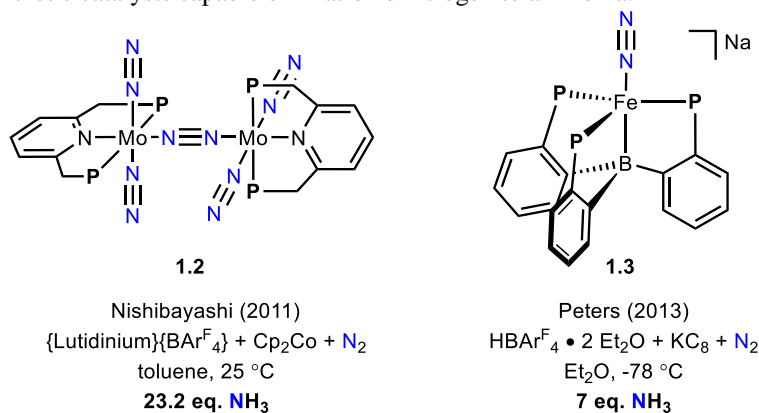
pocket for dinitrogen coordination, $[(\text{HIPTNCH}_2\text{CH}_2)_3\text{N}]^{3-}$ (HIPT = 3,5-(2,4,6- $\text{iPr}_3\text{C}_6\text{H}_2$) $_2\text{C}_6\text{H}_3$), four catalytic turnovers was achieved using a ‘Chatt Cycle’³

Scheme 1.1. First reported synthetic catalyst for N_2 fixation to ammonia by Schrock.



mechanism involving stepwise proton and electron transfers with a total of six protons and six electrons to convert dinitrogen into two equivalents of ammonia (Scheme 1.1). Isolation and full characterization of six intermediates within the catalytic cycle gave evidence for the proposed mechanism. Following this lead, Nishibayashi has improved on this system using other molybdenum catalysts to

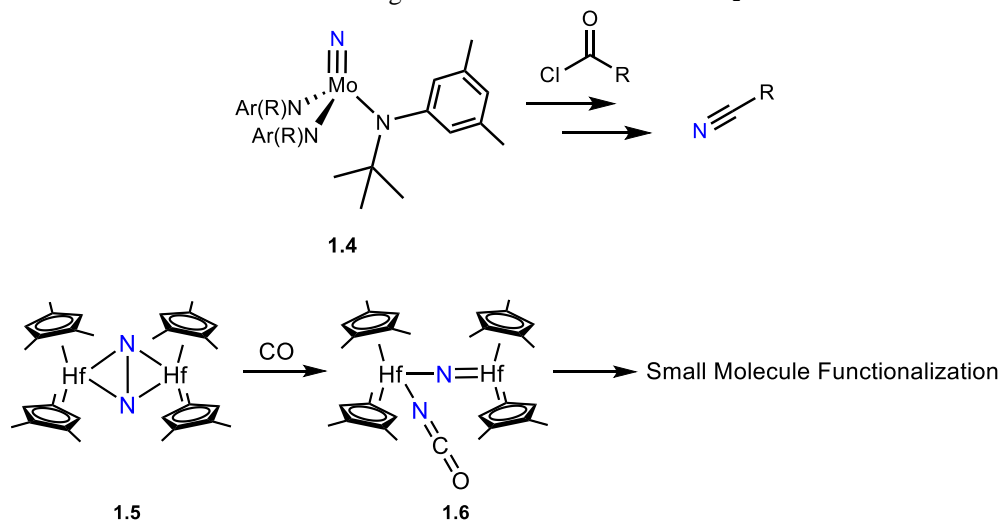
Scheme 1.2. Synthetic catalysts capable of fixation dinitrogen to ammonia.



produce up to 23.2 eq. of NH_3 ⁴ and Peters has extended this chemistry to include Fe catalysts⁴ capable of producing 7 eq. of NH_3 relative to the catalyst in the presence of proton and electron sources as described in Scheme 1.2.

While catalytic N-H formation chemistry to produce ammonia has seen significant development over the last five years, N_2 fixation involving N-C bond formation and production of more complex organic molecules has been much less developed. Cummins and coworkers made initial discoveries by using their tris-anilide molybdenum nitride complex with acyl chloride to make organic nitriles with

Scheme 1.3. Production of N-C based organic molecules derived from N_2 .



nitrogen atoms derived from N_2 .⁶ Chirik and coworkers have developed group 4 metallocene complexes that are able to coordinate N_2 and fully cleave the N-N bond after addition of carbon monoxide (CO). The resulting μ -nitrido species is active towards a variety of substrates to yield oxamides, formamides and carbodiimides that are coordinated to the metal center. Quenching with HCl liberates the free organic molecules.⁷ Finally, Kawaguchi and co-workers have developed vanadium chemistry

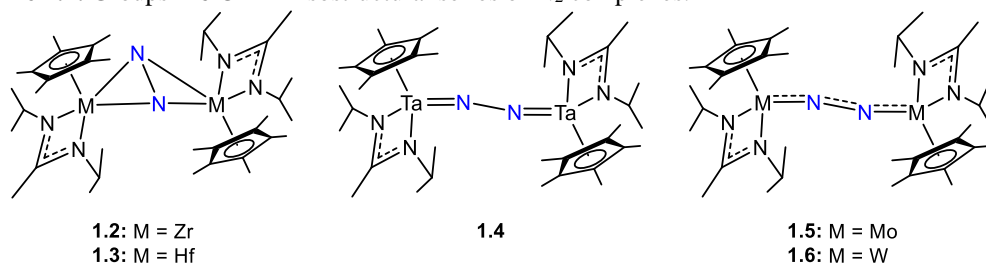
to produce potassium cyanate salts containing nitrogen atoms derived from N_2 .⁸ Despite these developments, however, a catalytic system has yet to be established.

1.3. Strategies Employed in this Thesis

1.3.1. Previous N_2 fixation work in the Sita lab

Within our group, the pentamethylcyclopentadienyl, amidinate (CPAM) ligand framework has provided a convenient platform for studying catalytic processes involving Ziegler-Natta polyolefin synthesis along with N- and O-atom transfer catalysis.⁹ Furthermore, the library of amidinate derivatives available in the literature allows us to easily synthesize derivatives to impart chirality for asymmetric conversions or fine-tune sterics and electronics to optimize reactivity or isolate metal complexes of fundamental interest. Within this framework, efforts have focused on

Scheme 1.4. Groups 4-6 CPAM isostructural series of N_2 complexes.



systematically evaluating the potential for N_2 fixation with early transition metals (groups 4 - 6) bearing the pentamethylcyclopentadienyl, amidinate ligand framework as shown in Scheme 1.4.¹⁰ Interestingly, both group 5 and 6 dinitrogen complexes have been shown to thermally^{10b} and photolytically cleave N_2 respectively and nitrene transfer chemistry has been developed within group 6 metals. Consequently, this chemistry has been a center of focus for N_2 fixation studies within our group.

1.3.2. The focus of research in this thesis

Primarily, the focus of this thesis is to develop a fundamental understanding of metal mediated N-N cleavage and M-N bond reactivity of relevant species along the pathway of N₂ fixation. This involves studying 1) N₂ coordination, activation and cleavage as well as 2) investigating metal nitrogen bond reactivity to ultimately yield Nitrogen and carbon based organic molecules. As demonstrated in the subsequent chapters of this thesis, fundamental discoveries have been made on these fronts that have established a new platform for studying the catalytic viability of forming N-C based organic molecules derived from N₂.

1.4. References

- 1) Smil, V. *Enriching the Earth: Fritz Haber, Carl Bosch, and the Transformation of World Food Production*, MIT Press, Cambridge, MA, 2001.
- 2) Yandulov, D. V.; Schrock, R. R. *Science* **2003**, *301*, 76-78.
- 3) Chatt, J.; Dilworth, J. R.; Richards, R. L. *Chem. Rev.* **1978**, *78*, 589-625.
- 4) Arashiba, K.; Miyake, Y.; Nishibayashi, Y. *Nature Chem.* **2011**, *3*, 120-125.
- 5) Anderson, J. S.; Rittle, J.; Peters, J. C. *Nature* **2013**, *501*, 84-87.
- 6) (a) Figueroa, J. S.; Piro, N. A.; Clough, C. R.; Cummins, C. C. *J. Am. Chem. Soc.* **2006**, *128*, 940-950. (b) Curley, J. J.; Sceats, E. L.; Cummins, C. C. *J. Am. Chem. Soc.* **2006**, *128*, 14036-14037. (c) Cozzolina, A. F.; Silvia, J. S.; Lopez, N.; Cummins, C. C. *Dalton Trans.* **2014**, *43*, 4639-4652.
- 7) (a) Knobloch, D. J.; Lobkovsky, E.; Chirik, P. J. *J. Am. Chem. Soc.* **2010**, *132*, 10553-10564. (b) Knobloch, D. J.; Lobkovsky, E.; Chirik, P. J. *J. Am. Chem. Soc.* **2010**, *132*, 15340-15350. (c) Semproni, S. P.; Lobkovsky, E.; Chirik, P. J. *J.*

- Am. Chem. Soc.* **2011**, *133*, 10406-10409. (d) Semproni, S. P.; Chirik, P. J. *J. Am. Chem. Soc.* **2013**, *135*, 11373-11383.
- 8) Ishida, Y.; Kawaguchi, H. *J. Am. Chem. Soc.* **2014**, *136*, 16990-16993.
- 9) (a) Yonke, B. L.; Reeds, J. P.; Zavalij, P. Y.; Sita, L. R. *Angew. Chem. Int. Ed.* **2011**, *50*, 12342-12346. (b) Yonke, B. L.; Reeds, J. P.; Fontaine, P. P.; Zavalij, P. Y.; Sita, L. R. *Organometallics* **2014**, *33*, 3239-3242.
- 10) (a) Hirotsu, M.; Fontaine, P. P.; Zavalij, P. Y.; Sita, L. R. *J. Am. Chem. Soc.* **2007**, *129*, 9284-9285. (b) Hirotsu, M.; Fontaine, P. P.; Zavalij, P. Y.; Sita, L. R. *J. Am. Chem. Soc.* **2007**, *129*, 12690-12692. (c) Fontaine, P. P.; Yonke, B. L.; Zavalij, P. Y.; Sita, L. R. *J. Am. Chem. Soc.* **2010**, *132*, 12273-12285.

Chapter 2: Synthesis and Reactivity of a CPGU

Ta(IV) Imido¹

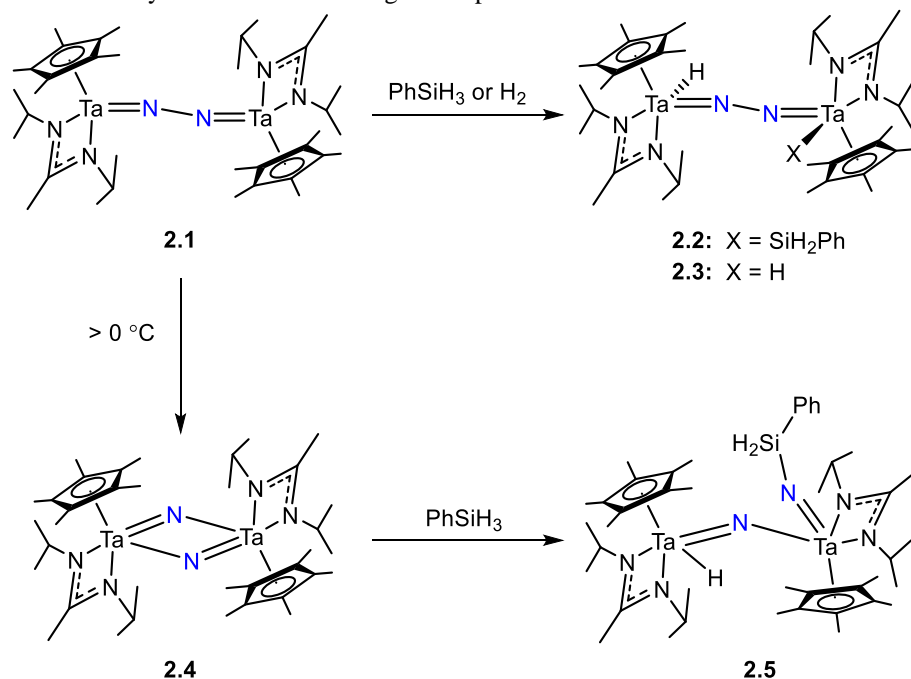
¹ Reproduced in part with permission from Yonke, B. L.; Keane, A. J.; Zavalij, P. Y.; Sita, L. R. *Organometallics* **2012**, *31*, 345-355. Copyright 2012 American Chemical Society.

2.1. Introduction

In the context of dinitrogen fixation, imido compounds serve an important role as potential intermediates along the pathway of dinitrogen reduction for the production of organic molecules. Imido compounds can also serve as models to explore reactivity of their respective dinitrogen complexes.¹ For example, the side-bound dinitrogen complex $[(\eta^5\text{-C}_5\text{Me}_4\text{H})_2\text{Zr}]_2[\mu\text{-}\eta^2:\eta^2\text{-N}_2]$ that was found to undergo hydrogenation by Chirik and co-workers is largely attributed to isomerization of the N_2 ligand to the end-on coordination mode, $[\text{Zr}]=\text{N}-\text{N}=[\text{Zr}]$, which possesses substantial imido character.² Zirconium and titanium imido compounds have previously been shown to readily react with dihydrogen.³ We have previously reported a CPAM tantalum end-on dinitrogen complex,

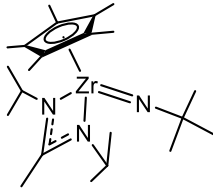
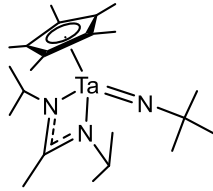
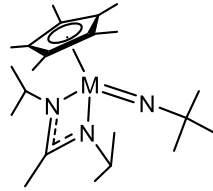
$[\text{Cp}^*[\text{N}(\text{iPr})\text{C}(\text{Me})\text{N}(\text{iPr})]\text{Ta}]_2[\mu\text{-}\eta^1:\eta^1\text{-N}_2]$ (**2.1**), that reacts with phenylsilane and

Scheme 2.1. Reactivity of CPAM Ta dinitrogen complex **2.1**.



dihydrogen to give the 1,4-addition products **2.2** and **2.3** as depicted in Scheme 2.1.⁴ Compound **2.1** was also found to thermally cleave N₂ under ambient condition to provide the bis- μ -nitrido product [Cp*₂[N(^{*i*}Pr)C(Me)N(^{*i*}Pr)]Ta(N)₂ (**2.4**) that underwent N-functionalization chemistry with phenylsilane to provide **2.5**. The end-on tantalum dinitrogen compound **2.1** has a dinuclear core, [Ta(IV), Ta(IV)], that possesses two Ta(IV, d^1) imido units with a central [N₂]⁴⁺ fragment as determined by structural parameters. The N-functionalization product **2.5** contains two Ta(V) imido units that could theoretically undergo further reactivity to provide N₂ fixation products. Thus, it was of interest to synthesize and fully investigate the chemical reactivity of model mononuclear CPAM Ta(IV) and Ta(V) imido compounds.⁵ In a broader context, these studies also fit within a CPAM isostructural series spanning

Table 2.1. CPAM *tert*-butyl imido isostructural series spanning groups 4 through 6.

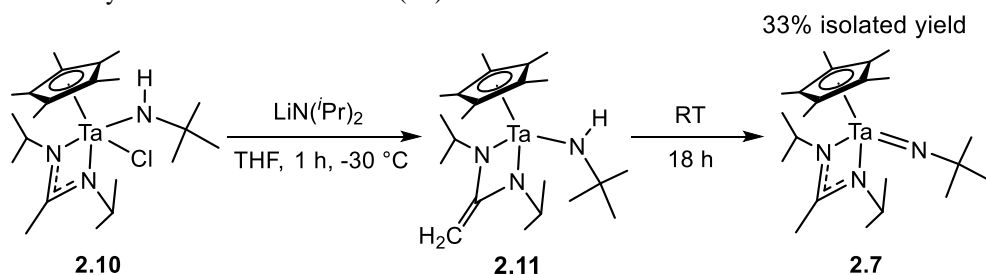
Group 4 M(IV, d^0) No Zr-N Reactivity	Group 5 M(IV, d^1) ?	Group 6 M(IV, d^2) Imido Group Transfer
 2.6	 2.7	 2.8: M = Mo 2.9: M = W

groups 4 through 6.⁶ To summarize this series, Zr-N bonds of Zr(IV, d^0) imido **2.6** have yet to be shown to be reactive, Ta(IV, d^1) imido (**2.7**) chemistry and not been fully evaluated, and imido group transfer to carbon monoxide (CO) to produce isocyanates has been discovered for group 6 CPAM imido complexes Mo(IV, d^2) (**2.8**) and W(IV, d^2) (**2.9**) mononuclear imido compounds. Therefore, it was of further

interest to understand the extent of reactivity for the CPAM Ta(IV, d^1) imido analogue to determine its chemical profile within this CPAM isostructural series.

The successful synthesis and characterization of **2.7** has been achieved previously within our group, representing the first example of a mononuclear Ta(IV) imido compound. The route to **2.7**, as outlined in Scheme 2.2, involves the Ta(IV) amido chloride precursor **2.10**. Traditional routes to imido complexes from amido chloride compounds typically involve deprotonation of the amide group with organolithium reagents with concomitant formation of the corresponding salt *e.g.* LiCl. In this case, however, the amidinate ligand was the site of deprotonation as

Scheme 2.2. Synthetic route to CPAM Ta(IV) Imido **2.7**.



opposed to the amido ligand, leading to the kinetic formation of the ‘enol-amido’ compound **2.11**. Allowing this compound to stir over 18 h at room temperature led to tautomerization that provided the Ta(IV) imido compound **2.7** as the thermodynamic product. Although synthesis of the target Ta(IV) imido **2.7** was achieved (representing the first example of a mononuclear Ta(IV) imido), the synthetic route suffered from low yields that hindered the complete evaluation of its chemical reactivity profile. Thus, a more straightforward, traditional route to the target Ta(IV) imido compound was desired in order to fully evaluate the chemical reactivity.

This chapter focuses on the development of a traditional, high yielding route to the target Ta(IV) imido. Furthermore, metal-centered one-electron chemistry of

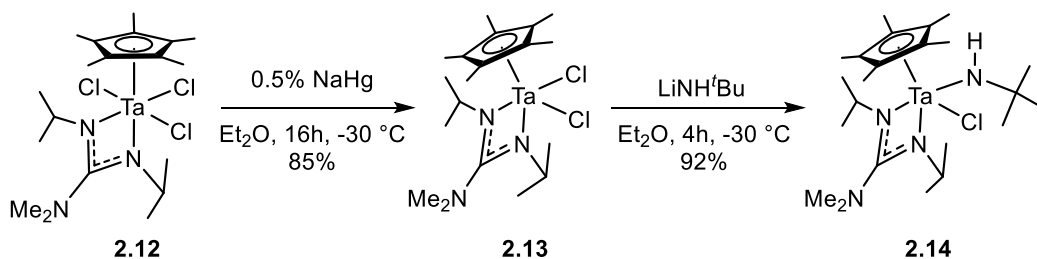
the Ta(IV) imido was discovered and applied to dinitrogen complex **2.1**. This work completes a general reactivity survey of a group 4 – 6 CPAM imido isostructural series and provides insight into the chemical nature of dinitrogen complex **2.1**.

2.2. CPGU Mononuclear Ta(IV, d^1) Imido Studies

2.2.1. Synthesis and characterization of a CPGU Ta(IV) imido complex

While the target CPAM Ta(IV) imido compound (**2.7**) was successfully synthesized, the synthetic route involved the kinetic deprotonation of the non-innocent amidinate ligand in **2.10** with $\text{LiN}(\text{tPr})_2$ to provide the ‘enol-amido’ intermediate **2.11**, which tautomerized to the target Ta(IV) imido **2.7** in low isolated yields (33%). In an effort to block the kinetic deprotonation of the amidinate thereby

Scheme 2.3. Synthesis of CPGU Ta(IV) amido chloride **2.14**.

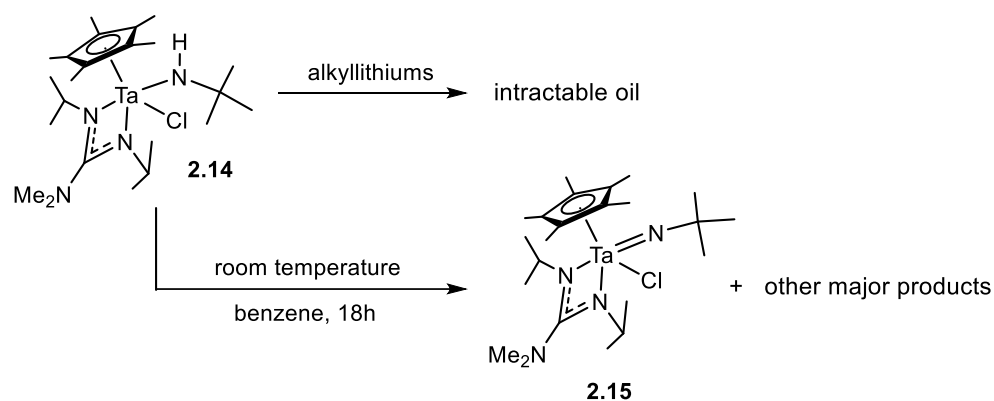


directing the site of deprotonation to the amido fragment, the guanidinate ligand, $[\text{N}(\text{tPr})\text{C}(\text{NMe}_2)\text{N}(\text{tPr})]$, employing a dimethylamino substituent in the distal position was pursued. Following a similar synthetic route to CPAM Ta(IV) amido chloride **2.10**, $\text{Cp}^*[\text{N}(\text{tPr})\text{C}(\text{NMe}_2)\text{N}(\text{tPr})\text{Ta}(\text{V})\text{Cl}_3$ (**2.12**) was first reacted with 0.5% sodium amalgam in Et_2O to provide dark orange crystals of paramagnetic CPGU Ta(IV) Cl_2 (**2.13**) in 85% yield. Subsequently, **2.13** was reacted with $\text{LiNH}(\text{tBu})$ in Et_2O over 3 h, where workup and crystallization of a concentrated pentane solution at $-30\text{ }^\circ\text{C}$ provided the desired amido chloride product **2.14** as a

purple crystalline solid in excellent yields as described in Scheme 2.3. Elemental analysis and single crystal X-ray diffraction (XRD) served to further confirm the structure and composition of this paramagnetic material, of which the latter is presented in Figure 2.1.

Having established a preparative route to **2.14**, efforts were focused towards deprotonating the amido group of this compound with strong bases (*i.e.* organolithiums) to provide a direct route to the target Ta(IV) imido.^{6a} Various organolithium reagents including methyl lithium, *n*-butyl lithium and *tert*-butyl

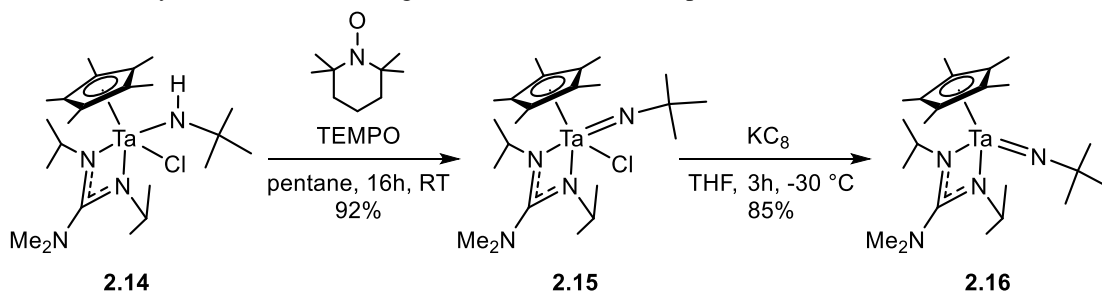
Scheme 2.4. Reactivity of CPGU Ta(IV) amido chloride **2.14**.



lithium were pursued; however, all attempts failed to cleanly produce the Ta(IV) imido and instead produced complex oily mixtures that were unable to be identified. While it was discouraging that the originally planned synthetic route to the Ta(IV) imido could not be realized, a curious observation was noted concerning the thermal stability of **2.14**: analytically pure solutions of this compound in benzene-*d*₆ decomposed over the course of 18 h as evidenced by a color change from purple to colorless. ¹H NMR studies of this transformation revealed that disproportionation had occurred, as all broad, paramagnetic resonances had converted to a spectrum of diamagnetic peaks indicating a mixture of products. Fortunately, crystallization of

this mixture of crude products in a concentrated pentane solution furnished colorless single crystals that were analyzed by single crystal XRD and identified as the Ta(V) imido chloride **2.15**. In comparing structural parameters for **2.14** and **2.15**, there is a clear contraction of the Ta1-N1 bond length from 1.978(2) Å (**2.14**) to 1.775(2) Å (**2.15**) and straightening of the Ta1-N1-C1 bond angle from 143.90(17)° to 165.0(2)°. Interestingly, production of **2.15** from **2.14** implies formal loss of a hydrogen atom (H•) with oxidation of the metal center from Ta(IV) to Ta(V). Although this degradative pathway led to low yields of **2.15**, it was envisioned that reaction of **2.14** with a hydrogen atom acceptor could provide a quantitative pathway to **2.15**.⁷ The compound (2,2,6,6,-tetramethyl-piperidin-1-yl)oxyl (TEMPO) was chosen as a suitable reagent, and reaction of **2.14** with one equivalent of TEMPO in pentane solution following work-up provided **2.15** in 92% yield with elemental analysis

Scheme 2.5. Synthesis of **2.16** starting from the amido chloride precursor **2.14**.



further establishing the purity of the material. Discovery of this chemistry opened a new pathway for obtaining the Ta(IV) imido involving reduction of the imido chloride **2.15** to provide the Ta(IV) imido directly. Following this lead, compound **2.15** was reacted with potassium graphite in THF solution at -30 °C over a 3 h period to produce a red solution with a black, graphite suspension. Subsequently, this

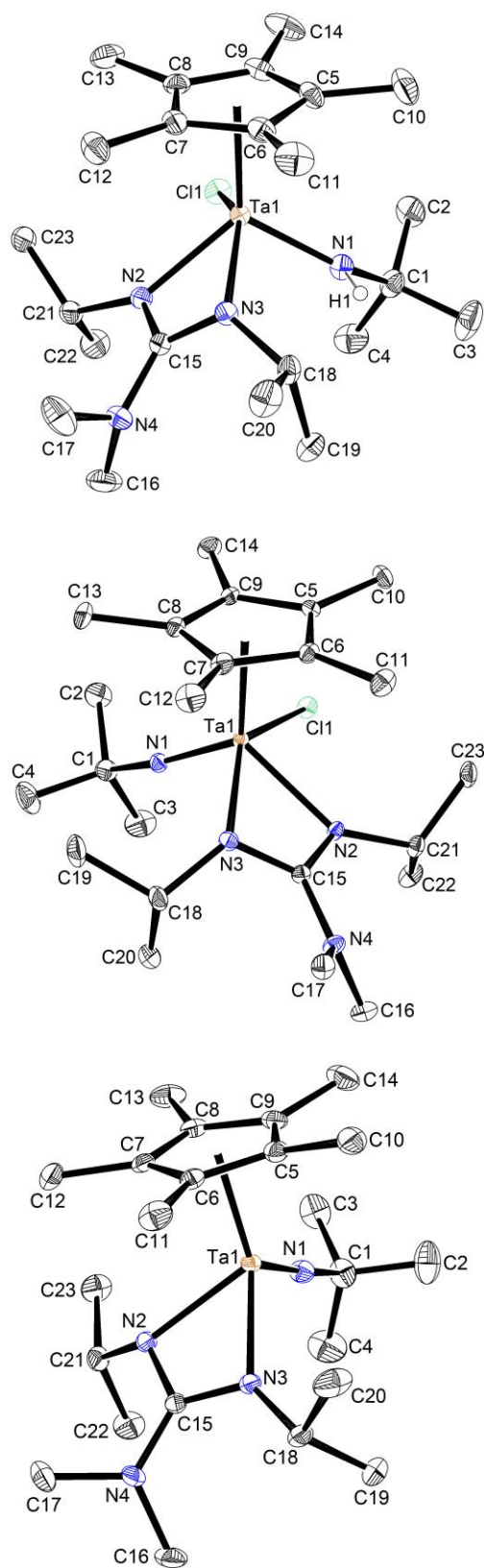


Figure 2.1. Molecular structures (30% thermal ellipsoids) of (top) **2.14**, (middle) **2.15** and (bottom) **2.16**. Hydrogen atoms except for H1 in **2.14** have been removed for the sake of clarity.

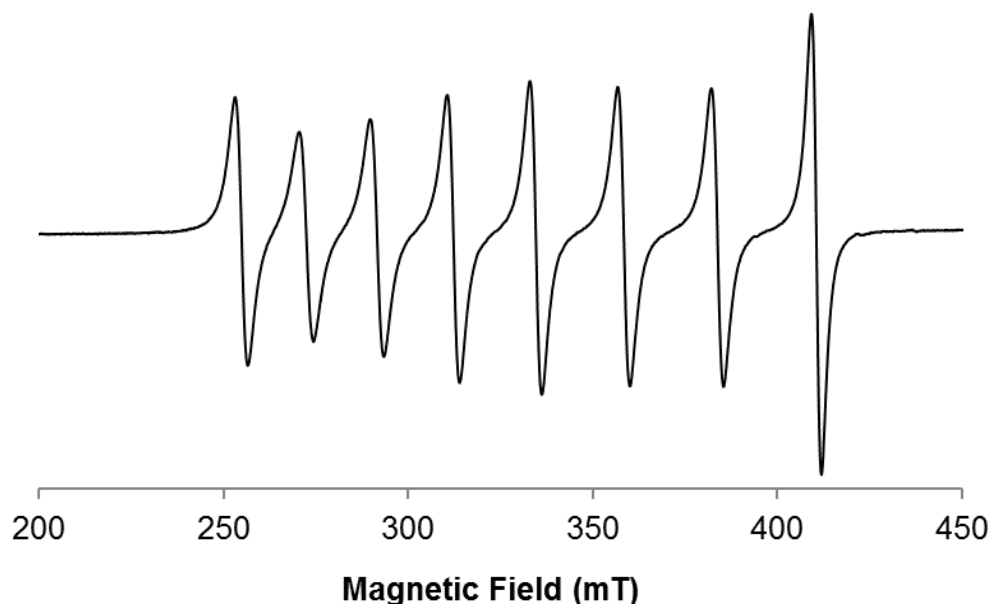


Figure 2.2. X-band EPR spectrum (toluene, 25 °C) of compound **2.16**; $g_{\text{iso}} = 1.975$, $A_{\text{iso}}(^{181}\text{Ta}) = 600$ MHz.

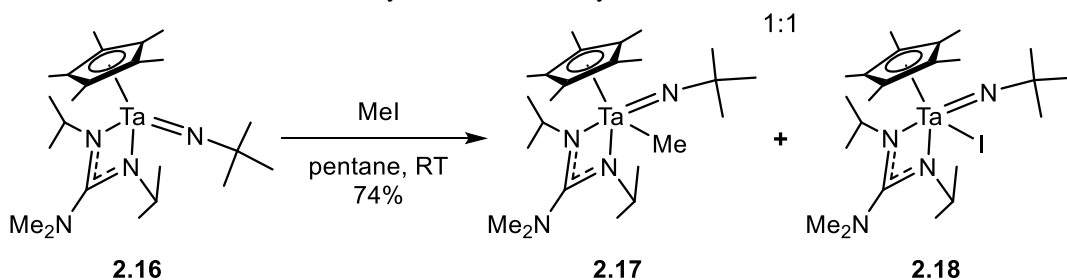
solution was worked-up and crystallized in a concentrated pentane solution at -30 °C to provide a dark red, crystalline material tentatively assigned to **2.16** where elemental analysis and single crystal XRD unequivocally establish the identity of this material as the target CPGU Ta(IV) imido **2.16**. Electron paramagnetic resonance (EPR) was used to further characterize the Ta(IV, d^1) nature of this compound, which resulted in an eight line spectrum indicative of an electron strongly coupled to a spin $7/2$ ^{181}Ta nucleus as shown in Figure 2.2.

2.2.2. Reactivity of a CPGU Ta(IV, d^1) mononuclear imido complex

Having successfully synthesized the target Ta(IV) imido compound **2.16** on a preparative scale, studies were conducted to elucidate the d^1 , Ta(IV) metal-nitrogen bond reactivity. Despite Mountford and co-workers establishing an extensive library of small molecules that undergo cyclo-addition with the related CPAM Ti imido,⁸ a general lack of reactivity of both CPAM and CPGU mononuclear Ta=N bonds was

found considering the inertness of **2.16** towards hydrogenation, hydrosilylation, carbonylation as well as cyclo-addition chemistry with phenylacetylene. Given the radical character of the metal center, it was of interest to see if **2.16** would participate in any one-electron chemistry.⁹ Gratifyingly, after addition of methyl iodide (MeI) to a pentane solution of **2.16**, the color changed within seconds from deep red to pale yellow signifying an oxidation of the metal had occurred. ¹H NMR studies of this

Scheme 2.6. One-electron chemistry of **2.16** with methyl iodide.



transformation concluded that two C_1 symmetric products had been produced in a 1:1 ratio. The identity of these products was established by single crystal XRD to be the iodo product, CPGU Ta(N^tBu)(I) (**2.17**), and the methyl product, CPGU Ta(N^tBu)(Me) (**2.18**), and fractional crystallization of this mixture from pentane resulted in enriched, isolated material as determined by elemental analysis [**2.17** (84%) and **2.18** (88%)]. This reactivity is indicative of a one-electron halogen atom abstraction mechanism with other reported open-shell species displaying similar reactivity.⁹

With CPAM Ta(IV) imido **2.16** serving as a mononuclear analogue to the Ta(IV)(μ -N₂)Ta(IV) dinitrogen complex **2.1**, efforts were focused on evaluating whether the discovered one-electron chemistry of **2.16** would be transferable to **2.1**. As with the reactivity of the model imido **2.16**, an NMR scale reaction of compound **2.1** with MeI resulted in a rapid change in color from dark purple to orange and the

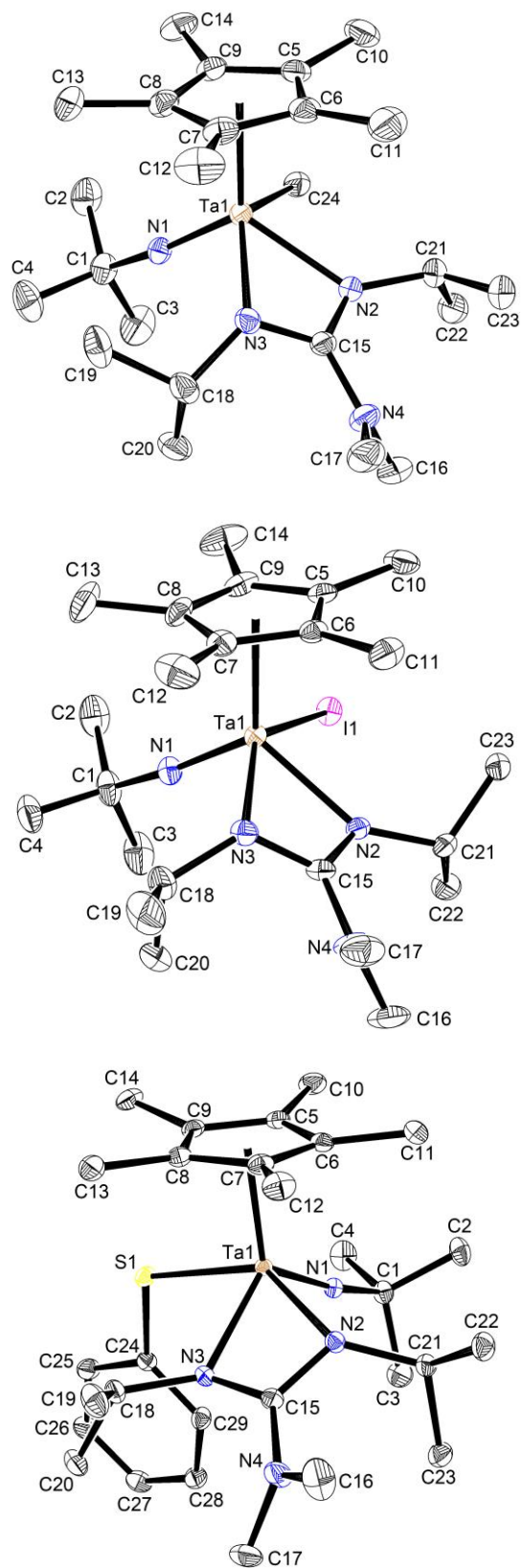
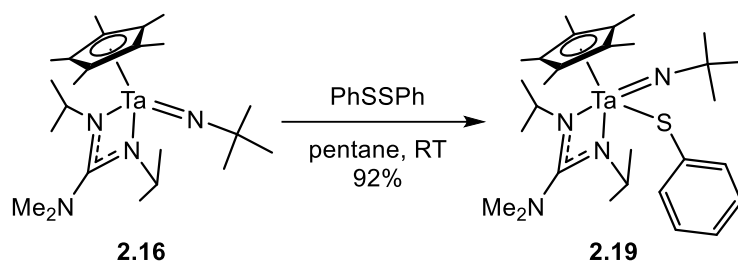


Figure 2.3. Molecular structures (30% thermal ellipsoids) of (top) **2.17**, (middle) **2.18** and (bottom) **2.19**. Hydrogen atoms have been removed for the sake of clarity.

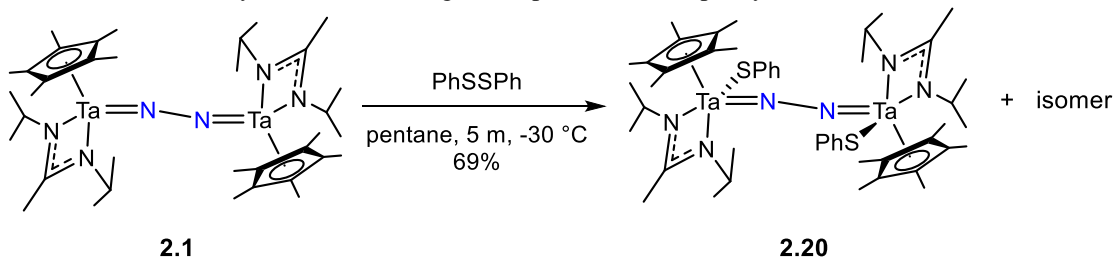
production of a number of diamagnetic compounds as determined by ^1H NMR most likely resulting from the formation of $(\text{I})[\text{Ta}](\mu\text{-N}_2)[\text{Ta}](\text{I})$, $(\text{Me})[\text{Ta}](\mu\text{-N}_2)[\text{Ta}](\text{I})$, $(\text{Me})[\text{Ta}](\mu\text{-N}_2)[\text{Ta}](\text{Me})$ and their isomers.¹⁰ It was thus desirable to develop one-electron chemistry that would result in the formation of only one or two maximum theoretical products to simplify characterization of this one-electron process.

Scheme 2.7. Reactivity of **2.16** with diphenyl disulfide.



Chemistry of the model Ta(IV) imido **2.16** was again explored and it was discovered that diphenyl disulfide (PhSSPh) produced a single product by NMR that was identified as the sulfide product, CPGU Ta(N^tBu)(SPh) (**2.19**) by single crystal XRD and elemental analysis. Adapting this disulfide chemistry to the dinitrogen analogue, rapid reaction of compound **2.1** with PhSSPh occurred to form two products: one that was structurally characterized to be that of the ditantalum dinitrogen disulfide product **2.20** shown in Figure 2.4, and the other, **2.21**, having an elemental composition consistent with being an isomer of **9**, where both products involve the formal 1,4-

Scheme 2.8. Reactivity of CPAM dinitrogen complex **2.1** with diphenyl disulfide.



addition of PhSSPh across the [Ta(IV)]=N-N=[Ta(IV)] core. With this result, chemistry of the model Ta(IV) imido analogue (**2.16**) was successfully applied to the dinitrogen compound **2.1**. The chemistry of both of these species contributes to a dinitrogen and imido CPAM isostructural series spanning groups 4 through 6 and helps establish metal-dependent trends within their respective series.

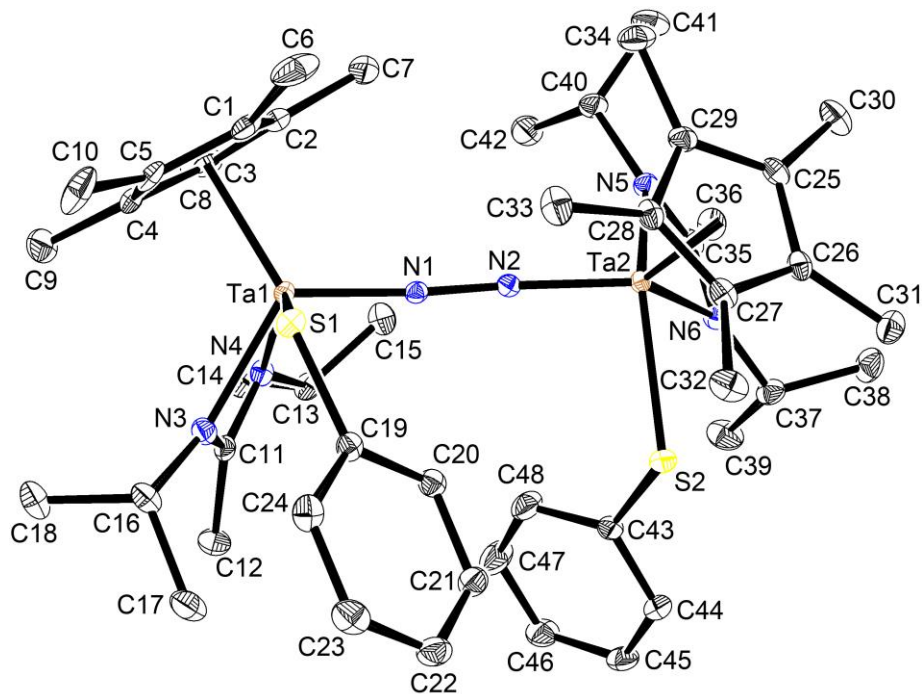


Figure 2.4. Molecular structures (30% thermal ellipsoids) of **2.20**. Hydrogen atoms have been removed for the sake of clarity.

2.3. Conclusion

These results serve to further develop imido chemistry within an isostructural CPAM family spanning groups 4 through 6. While the metal nitrogen bonds of related CPGU Ta(IV) (**2.16**) proved to be non-reactive towards hydrogenation, hydrosilation or carbonylation, the Ta(IV) metal center proved to be reactive towards one-electron chemistry with MeI and PhSSPh. The chemistry of **2.16** was important

to filling a gap in understanding of metal-dependent trends within the CPAM isostructural imido series of groups 4 through 6 and also served as a mononuclear analogue to the dinuclear Ta dinitrogen compound **2.1**. The discovered one-electron chemistry was successfully applied to **2.1** and ultimately contributed to the overall understanding of metal-dependent trends in reactivity of a CPAM dinitrogen complex isostructural series spanning groups 4 through 6.

2.4. Experimental Section

2.4.1. General considerations

All manipulations with air and moisture sensitive compounds were carried out under an inert atmosphere of N₂ or Ar using standard Schlenk-line or glovebox techniques. All solvents were dried (Na for toluene and Na/benzophenone for pentane, Et₂O, and THF) and distilled under N₂ prior to use. Benzene-*d*₆ was dried over Na/K alloy and isolated by vacuum transfer. Celite was oven-dried (150 °C for several days) and all amines were dried over CaH₂ and distilled by short-path distillation prior to use. Cooling for reactions was achieved using the internal freezer of a glovebox maintained at -30 °C. TEMPO, N,N-diisopropylcarbodiimide and lithium dimethylamide (LiNMe₂) were purchased from Sigma-Aldrich and Cp*TaCl₄ was purchased from Strem Chemicals. All chemicals were used as received unless otherwise noted. Compound {Cp*Ta[N(*i*Pr)C(Me)N(*i*Pr)]}₂(μ-η¹:η¹-N₂)¹ was synthesized using reported procedures and isolated in similar yield and purity. All ¹H NMR spectra were recorded at 400.13 MHz. Solution EPR spectra were recorded at Georgetown University on a JEOL continuous wave spectrometer JES-FA200

equipped with an X-band Gunn oscillator bridge and a cylindrical mode cavity employing a modulation frequency of 100 kHz. All spectra were obtained from freshly prepared toluene solutions (5 mM) in a nitrogen-filled glovebox. $A_{\text{iso}}(^{181}\text{Ta})$ values in MHz were determined by the separation of the middle two lines of the eight line pattern. Elemental analyses (C, H, and N) were performed by Midwest Microlab, LLC.

2.4.2. Synthesis of new compounds

Cp*Ta[N(ⁱPr)C(NMe₂)N(ⁱPr)]Cl₃ (2.12). A solution of N,N'-diisopropylcarbodiimide (746 mg, 4.60 mmol) in 10 mL of THF, pre-cooled to -30 °C, was added dropwise to a solution of LiNMe₂ (235 mg, 4.60 mmol) in 10 mL of THF, pre-cooled to -30 °C. The reaction mixture was allowed to warm to room temperature and stirred for 1 h. The resulting pale yellow solution was then cooled to -30 °C and added dropwise to a solution of Cp*TaCl₄ (2.01 g, 4.38 mmol) in 80 mL of THF, pre-cooled to -30 °C, over a period of 5 min. The reaction mixture was allowed to warm to room temperature and stirred for 16 h to produce a red solution, which was followed by removing volatiles *in vacuo* to give a red solid. The red solid was dissolved in toluene and filtered through a short pad of Celite on a glass frit. The filtrate was concentrated, pentane layered on top, and then the mixture was cooled to -30 °C to provide red crystals of **2.12** (2.18 g, 84% yield). Anal. Calc'd for C₁₉H₃₅Cl₃N₃Ta₁: C, 38.50; H, 5.95; N, 7.09; Found: C, 38.81; H, 5.68; N, 7.22. ¹H NMR (400 MHz, benzene-*d*₆): 1.17 (6H, d, CH(CH₃), *J* = 6.7 Hz), 1.88 (6H, d, CH(CH₃)₂, *J* = 6.9 Hz), 2.22 (15H, s, C₅(CH₃)₅), 2.32 (6H, s, N(CH₃)₂), 4.26 (1H, sept, CH(CH₃)₂, *J* = 6.7 Hz), 4.57 (1H, sept, CH(CH₃)₂, *J* = 6.9 Hz).

Cp*Ta[N(ⁱPr)C(NMe₂)N(ⁱPr)]Cl₂ (2.13). Sodium amalgam, 0.5% (w/w) Na/Hg, (16.7 g, 3.64 mmol) was added dropwise to a solution of **2.12** (1.99 g, 3.36 mmol) in 100 mL of Et₂O, pre-cooled to -30 °C. The solution was allowed to warm to room temperature and stirred for 16 h to yield a dark-orange-colored solution, which was followed by removing volatiles *in vacuo* to yield a brown-orange solid. The solid was dissolved in toluene and filtered through a short pad of Celite on a glass frit. The dark red filtrate was concentrated and cooled to -30 °C to yield dark orange crystals of **2.13** (1.59 g, 85% yield). Anal. Calc'd for C₁₉H₃₅N₃Cl₂Ta₁: C, 40.94; H, 6.33; N, 7.54; Found C, 41.11; H, 6.20; N, 7.43.

Cp*Ta[N(ⁱPr)C(NMe₂)N(ⁱPr)][NH(^tBu)]Cl (2.14). A solution of LiNH(^tBu) (123 mg, 1.55 mmol) in 20 mL of Et₂O, pre-cooled to -30 °C, was added dropwise to a solution of **2.13** (823 mg, 1.48 mmol) in 35 mL of Et₂O, pre-cooled to -30 °C, over a period of 5 min. The reaction mixture was allowed to warm to room temperature and stirred for 4 h to produce a purple solution, which was followed by removing *in vacuo* volatiles to yield a purple solid. The solid was dissolved in pentane and filtered through a short pad of Celite on a glass frit. The dark purple filtrate was concentrated and cooled to -30 °C to yield dark purple crystals of **2.14** (805 mg, 92% yield). Anal. Calc'd for C₂₃H₄₅N₄Cl₁Ta₁: C, 46.48; H, 7.64; N, 9.43; Found: C, 46.41; H, 7.39; N, 9.32.

Cp*Ta[N(ⁱPr)C(NMe₂)N(ⁱPr)][N(^tBu)]Cl (2.15). TEMPO (192 mg, 1.23 mmol) was added to a solution of **2.14** (688 mg, 1.16 mmol) in 30 mL of pentane at room temperature and stirred. The solution turned a transparent orange color and the volatiles were removed *in vacuo* to produce an orange-white solid that was then dissolved in a minimal amount of toluene. A small amount of pentane was added and the mixture cooled to -30 °C to provide white crystals of **2.15** (632 mg, 92% yield). Anal. Calc'd for C₂₃H₄₄N₄Cl₁Ta₁: C, 46.58; H, 7.48; N, 9.45; Found: C, 46.77; H, 7.28; N, 9.67. ¹H NMR (400 MHz, benzene-d₆): 1.21 (3H, d, CH(CH₃)₂, *J* = 6.6 Hz), 1.28 (3H, d, CH(CH₃)₂, *J* = 6.6 Hz), 1.33 (3H, d, CH(CH₃)₂, *J* = 6.6 Hz), 1.41 (3H, d, CH(CH₃)₂, *J* = 6.7 Hz), 1.44 (9H, s, C(CH₃)₃), 2.08 (15H, s, C₅(CH₃)₅), 2.35 (6H, s, N(CH₃)₂), 3.68 (1H, sept, CH(CH₃)₂, *J* = 6.6 Hz), 3.80 (1H, sept, CH(CH₃)₂, *J* = 6.6 Hz).

Cp*Ta[N(ⁱPr)C(NMe₂)N(ⁱPr)][N(^tBu)] (2.16). Potassium graphite (KC₈) (90 mg, 0.666 mmol) was transferred over a period of 5 min to a solution of **2.15** (247 mg, 0.416 mmol) in 15 mL of THF, pre-cooled to -30 °C, by slurring with 15 mL of THF that had been pre-cooled to -30 °C. The stirred suspension was allowed to warm to room temperature and stirred for an additional 3 h to provide a red-colored solution containing a black suspension. The volatiles were removed *in vacuo* and the crude material was dissolved in pentane and filtered through a short pad of Celite on a glass frit. The red filtrate was concentrated and cooled to -30 °C overnight and any unreacted **2.15** that crystallized out was removed by decanting. The red mother liquor was then concentrated and cooled to -30 °C for three days to provide red

crystals of **2.16** (197 mg, 85% yield). Anal. Calc'd for $C_{23}H_{44}N_4Ta_1$: C, 49.55; H, 7.95; N, 10.05; Found: C, 49.62; H, 7.71; N, 10.02.

Cp*Ta[N(*i*Pr)C(NMe₂)N(*i*Pr)][N(*t*Bu)](Me) (2.17**) and**

Cp*Ta[N(*i*Pr)C(NMe₂)N(*i*Pr)][N(*t*Bu)](I) (2.18**).** Methyl iodide (6.0 μ L, 0.096 mmol) was added to a solution of **2.16** (54 mg, 0.096 mmol) in 3 mL of pentane at room temperature to provide a clear-colored solution. The volatiles were removed in vacuo to produce a colorless solid, which was fractionally crystallized in pentane at -30 °C to provide opaque light-yellow co-crystals that were enriched with **7** in a 10:90 **2.17**:**2.18** ratio (26 mg, 44% yield). The mother liquor was then allowed to slowly evaporate at -30 °C whereupon white co-crystals enriched with **2.17** in a 90:10 **2.17**:**2.18** ratio were obtained (15 mg, 30% yield). For enriched-**2.17** containing 12 mol% of **2.18**: Anal. Calc'd for $C_{23.9}H_{46.6}N_{4.1}Ta_1$: C, 49.01; H, 8.03; N, 9.57; Found: C, 49.14; H, 7.96; N, 9.50; ¹H NMR (400 MHz, benzene-*d*₆): 0.54 (3H, s, TaCH₃), 1.12 (6H, d, CH(CH₃)₂, *J* = 6.8 Hz), 1.25 (3H, d, CH(CH₃)₂, *J* = 6.6 Hz), 1.41 (3H, d, CH(CH₃)₂, *J* = 6.6 Hz), 1.42 (9H, s, C(CH₃)₃), 2.00 (15H, s, C₅(CH₃)₅), 2.35 (6H, s, N(CH₃)₂), 3.59 (1H, sept, CH(CH₃)₂, *J* = 6.8 Hz), 3.78 (1H, sept, CH(CH₃)₂, *J* = 6.6 Hz). For enriched-**2.18** containing 12 mol% of **2.17**: Anal. Calc'd for $C_{23.1}H_{44.4}N_{4.1}Ta_1$: C, 41.56; H, 6.69; N, 8.38; Found: C, 41.61; H, 6.50; N, 8.40; ¹H NMR (400 MHz, benzene-*d*₆): 1.22 (3H, d, CH(CH₃)₂, *J* = 6.7 Hz), 1.24 (3H, d, CH(CH₃)₂, *J* = 6.8 Hz), 1.27 (3H, d, CH(CH₃)₂, *J* = 6.7 Hz), 1.34 (3H, d, CH(CH₃)₂, *J* = 6.8 Hz), 1.52 (9H, s, C(CH₃)₃), 2.12 (15H, s, C₅(CH₃)₅), 2.29 (6H, s, N(CH₃)₂), 3.70 (1H, sept, CH(CH₃)₂, *J* = 6.8 Hz), 3.86 (1H, sept, CH(CH₃)₂, *J* = 6.7 Hz).

Cp*Ta[N(ⁱPr)C(NMe₂)N(ⁱPr)][N(^tBu)](SPh) (2.19). Diphenyl disulfide (19.9 mg, 0.091 mmol) was added to a stirred solution of **2.16** (102 mg, 0.182 mmol) in 5 mL of pentane at room temperature. After stirring for 2 min, the colorless solution was concentrated *in vacuo* and then cooled to -30 °C to provide colorless crystals of **2.19** (115 mg, 94% yield). Anal. Calc'd for C₂₉H₄₉N₄S₁Ta₁: C, 52.24; H, 7.41; N, 8.40; Found: C, 52.32; H, 7.68; N, 8.54. ¹H NMR (400 MHz, benzene-*d*₆): 0.91 (3H, d, CH(CH₃)₂, *J* = 7.0 Hz), 0.95 (3H, d, CH(CH₃)₂, *J* = 6.7 Hz), 1.27 (9H, s, C(CH₃)₃), 1.30 (3H, d, CH(CH₃)₂, *J* = 6.7 Hz), 1.33 (3H, d, CH(CH₃)₂, *J* = 7.0 Hz), 2.07 (15H, s, C₅(CH₃)₅), 2.33 (6H, s, N(CH₃)₂), 4.04 (1H, sept, CH(CH₃)₂, *J* = 7.0 Hz), 4.12 (1H, sept, CH(CH₃)₂, *J* = 6.7 Hz), 6.96 (1H, m, S(C₆H₅)), 7.20 (2H, m, S(C₆H₅)), 8.03 (2H, m, S(C₆H₅)).

{Cp*Ta[N(ⁱPr)C(Me)N(ⁱPr)](SPh)}₂(μ-η¹:η¹-N₂) (2.20). Diphenyl disulfide (24 mg, 0.111 mmol) was added to a solution of {Cp*Ta[N(ⁱPr)C(Me)N(ⁱPr)]}₂(μ-η¹:η¹-N₂) (**2.1**) (104 mg, 0.111 mmol) in 5 mL of pentane that was pre-cooled to -30 °C. After warming to room temperature and stirring for 5 min, the volatiles were removed *in vacuo* to provide a mixture of a dark-orange oil and a light-orange powder (isomer). The mixture was taken up in 5 mL of Et₂O and cooled to -30 °C, followed by collecting orange solids on a glass-frit that were composed of compound **2.21**. The dark orange filtrate was concentrated *in vacuo* and then cooled to -30 °C to provide dark orange crystals of *meso*-**2.20** (33 mg, 25% yield). The light orange solids collected on the glass-frit were washed with first pentane and then Et₂O. The solids

were then dissolved in a minimal amount of toluene and allowed to precipitate from solution at -30 °C to provide analytically pure orange powder of **2.21** that is an isomer of **2.20** (44 mg, 44% yield). For meso-**2.20**: Anal. Calc'd for C₄₈H₇₄N₆S₂Ta₂: C, 49.65; H, 6.42; N, 7.24; Found: C, 49.15; H, 6.47; N, 7.08. ¹H NMR (400 MHz, benzene-*d*₆): 0.67 (6H, d, CH(CH₃)₂, *J* = 7.2 Hz), 1.00 (6H, d, CH(CH₃)₂, *J* = 7.2 Hz), 1.34 (6H, d, CH(CH₃)₂, *J* = 7.0 Hz), 1.43 (6H, d, CH(CH₃)₂, *J* = 7.0 Hz), 1.69 (6H, s, N(^{*i*}Pr)C(CH₃)N(^{*i*}Pr)), 2.13 (30H, s, C₅(CH₃)₅), 3.86 (2H, sept, CH(CH₃)₂, *J* = 7.0 Hz), 4.48 (2H, sept, CH(CH₃)₂, *J* = 7.2 Hz), 6.95 (2H, m, S(C₆H₅)), 7.21 (4H, m, S(C₆H₅)), 8.07 (4H, m, S(C₆H₅)). For **2.21**: Anal. Calc'd for C₄₈H₇₄N₆S₂Ta₂: C, 49.65; H, 6.42; N, 7.24; Found: C, 50.14; H, 6.65; N, 7.45. ¹H NMR (400 MHz, benzene-*d*₆): 0.67 (6H, d, CH(CH₃)₂, *J* = 6.6 Hz), 0.94 (6H, d, CH(CH₃)₂, *J* = 6.8 Hz), 1.37 (6H, d, CH(CH₃)₂, *J* = 6.6 Hz), 1.64 (6H, broad s, CH(CH₃)₂), 1.69 (6H, s, N(^{*i*}Pr)C(CH₃)N(^{*i*}Pr)), 2.05 (30H, s, C₅(CH₃)₅), 4.03 (2H, broad, CH(CH₃)₂), 4.41 (2H, broad, CH(CH₃)₂), 7.00 (2H, m, S(C₆H₅)), 7.14 (4H, m, S(C₆H₅)), 8.00 (4H, d, S(C₆H₅), *J* = 7.6 Hz).

2.5. References

- (1) (a) Fryzuk, M. D.; Johnson, S. A. *Coord. Chem. Rev.* **2000**, *200-202*, 379-409. (b) Shaver, M. P.; Fryzuk, M. D. *Adv. Synth. Catal.* **2003**, *245*, 1061-1076. (c) Gambarotta, S.; Scott, J. *Angew. Chem. Int. Ed.* **2004**, *43*, 5298-5308. (d) MacKay, B. A.; Fryzuk, M. D. *Chem. Rev.* **2004**, *104*, 385-401. (e) MacLachlan, E. A.; Fryzuk, M. D. *Organometallics* **2006**, *25*, 1530-1543. (f) Chirk, P. J. *Dalton Trans.* **2007**, 16-25. (g) Ohki, Y.; Fryzuk, M. D. *Angew. Chem. Int. Ed.*

- 2007**, *46*, 3180-3183. (h) Fryzuk, M. D. *Acc. Chem. Res.* **2009**, *42*, 127-133. (i) Chirik, P. J. *Organometallics* **2010**, *29*, 1500-1517.
- (2) Pool, J. A.; Lobkovsky, E.; Chirik, P. J. *Nature* **2004**, *42*, 527-530.
- (3) Cummins, C. C.; Baxter, S. M.; Woczenski, P. T. *J. Am. Chem. Soc.* **1988**, *110*, 8731-8733.
- (4) Hirotsu, M.; Fontaine, P. P.; Epshteyn, A.; Zavalij, P. Y.; Sita, L. R. *J. Am. Chem. Soc.* **2007**, *129*, 9284-9285.
- (5) (a) Rocklage, S. M.; Schrock, R. R. *J. Am. Chem. Soc.* **1980**, *102*, 7809-7811. (b) Chao, Y.; Wexler, P. A.; Wigley D. E. *Inorg. Chem.* **1989**, *28*, 3860-3868. (c) Bonanno, J. B.; Wolczanski, P. T.; Lobkovsky, E. B. *J. Am. Chem. Soc.* **1994**, *116*, 11159-11160. (d) Freundlich, J. S.; Schrock, R. R.; Davis, W. M. *J. Am. Chem. Soc.* **1996**, *118*, 3643-3655. (e) Proulx, G.; Bergman, R. G. *Organometallics* **1996**, *15*, 684-692. (f) Bailey, N. J.; Cooper, J. A.; Gailus, H.; Green, M. L. H.; James, J. T.; Leech M. A. *J. Chem. Soc., Dalton Trans.* **1997**, *19*, 3579-3584. (g) Royo, P.; Sánchez-Nieves, J. *J. Organomet. Chem.* **2000**, *597*, 61-68. (h) Anderson, L. L.; Schmidt, J. A. R.; Arnold, J.; Bergman, R. G. *Organometallics* **2006**, *25*, 3394-3406. (i) Tomson, N. C.; Arnold, J. Bergman, R. G. *Dalton Trans.* **2011**, *40*, 7718-7729.
- (6) (a) Kissounko, D. A.; Epshteyn, A.; Fettingner, J. C.; Sita, L. R. *Organometallics* **2006**, *25*, 1076-1078. (b) Yonke, B. L.; Reeds, J. P.; Fontaine, P. P.; Zavalij, P. Y.; Sita, L. R. *Organometallics* **2014**, *33*, 3239-3242.
- (7) (a) Takemoto, S.; Ogura, S.; Yo, H.; Hosokoshi, Y.; Kamikawa, K.; Matsuzaka, H. *Inorg. Chem.* **2006**, *45*, 4871-4873. (b) Cowley, R. E.; Bontchev, R. P.;

- Sorrell, J.; Sarracino, O.; Feng, Y.; Wang, H.; Smith, J. M. *J. Am. Chem. Soc.* **2007**, *129*, 2424-2425. (c) Huynh, H. V.; Meyer, T. J. *Chem. Rev.* **2007**, *107*, 5004-5064. (d) Illuc, V. M.; Hillhouse, G. L. *J. Am. Chem. Soc.* **2010**, *132*, 15148-15150.
- (8) (a) Guiducci, A. E.; Cowley, A. R.; Skinner, M. E. G.; Mountford, P. *J. Chem. Soc., Dalton Trans.* **2001**, 1392-1394. (b) Boyd, C. L.; Clot, E.; Guiducci, A. E.; Mountford, P. *Organometallics* **2005**, *24*, 2347-2367. (c) Guiducci, A. E.; Boyd, C. L.; Clot, E.; Mountford, P. *Dalton Trans.* **2009**, 5960-5979. (d) Tiong, P. J.; Nova, A.; Groom, L. R.; Schwarz, A. D.; Selby, J. D.; Schofield, A. D.; Clot, E.; Mountford, P. *Organometallics* **2011**, *30*, 1182-1201.
- (9) (a) Baird, M. C. *Chem. Rev.* **1988**, *88*, 1217-1227. (b) Huber, T. A.; Macartney, D. H.; Baird, M. C. *Organometallics* **1995**, *14*, 592-602. (c) Koeslag, M. A.; Baird, M. C.; Lovelace, S.; Geiger, W. E. *Organometallics* **1996**, *15*, 3289-3302. (d) Smith, K. M. *Organometallics* **2005**, *24*, 778-784. (e) Smith, K. M. *Coord. Chem. Rev.* **2006**, *250*, 1023-1031. (f) MacLeod, K. C.; Conway, J. L.; Tang, L.; Smith, J. J.; Corcoran, L. D.; Ballem, K. H.; Patrick, B. O.; Smith, K. M. *Organometallics* **2009**, *28*, 6798-6806. (g) MacLeod, K. C.; Patrick, B. O.; Smith, K. M. *Organometallics* **2010**, *29*, 6639-6641. (h) Zhou, W.; Tang, L.; Patrick, B. O.; Smith, K. M. *Organometallics* **2011**, *30*, 603-610.
- (10) Benito-Garagorri, D.; Bernskoetter, W. H.; Lobkovsky, E.; Chirik, P. J. *Organometallics* **2009**, *28*, 4807-4813.

Chapter 3: Chemistry and N-N Cleavage of Tantalum Hydrazido and Hydrazidium Complexes²

² Reproduced in part with permission from Keane, A. J.; Zavalij, P. Y.; Sita, L. R. *J. Am. Chem. Soc.* **2013**, *135*, 9580-9583. Copyright 2013 American Chemical Society.

3.1. Introduction

Over the last ten years, increasing interest in early transition metal hydrazido(2-) complexes has led to the development of rich chemistry that includes catalytic and stoichiometric transformations involving N-N cleavage and N-atom transfer. Early reports of hydrazido complexes have played an integral role in probing intermediates within the catalytic cycle of dinitrogen reduction to ammonia where molybdenum is considered to play an active role. As a result, group 6 hydrazido chemistry has become relatively well established¹ to explain some of the fundamental transformations found within the Chatt cycle.² These studies have not only led to success, but they continue to give insight towards reactivity within this area.³ Recently, building off an early example from Bergman,⁴ studies of group 4 hydrazides by Mountford,⁵ Odom⁶ and Gade⁷ and co-workers have unlocked a variety of catalytic and stoichiometric transformations for the terminal hydrazido(2-), where in some cases N_α-N_β cleavage occurs.⁸

Having characterized the reactivity of the Ta(IV) *tert*-butyl imido (**2.7** and **2.16**),⁹ we set out to isolate and characterize the closely related Ta(IV) terminal hydrazido (**3.5**). Surprisingly, in contrast with groups 4 and 6, group 5 terminal hydrazido(2-) chemistry is rather undeveloped and reactivity has not been fully explored.¹⁰ This is especially true for Ta(IV), where no examples currently exist. Furthermore, Ta(IV) hydrazidium reactivity, where the β nitrogen is alkylated and possesses a formal positive charge, could reveal new information involving N-atom functionalization and N-N cleavage processes. Herein, the successful isolation, characterization and reactivity of Ta(V) and Ta(IV) terminal hydrazido complexes including the characterization and reactivity of their N_β methylation products are

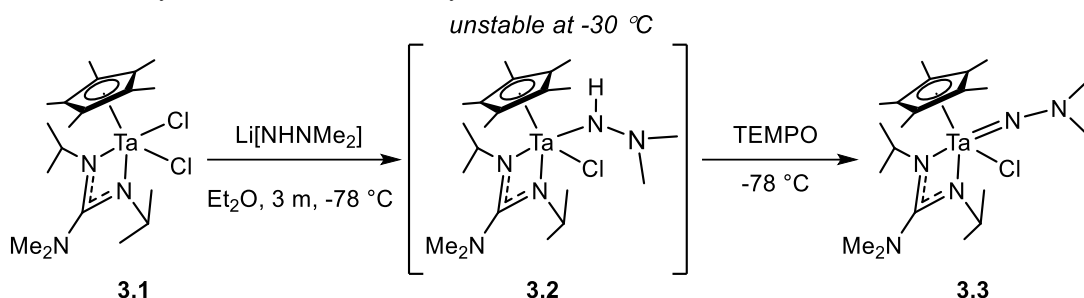
reported. The discovery of N-N cleavage processes with these CPGU ‘hydrazidium’ complexes provides insights into different mechanisms associated with important intermediates found within the Chatt cycle.

3.2. Mononuclear Ta(IV, d¹) Hydrazido Studies

3.2.1. Synthesis and characterization of a mononuclear Ta(IV) hydrazido complex

Having demonstrated a preparative route to the CPGU tantalum *tert*-butyl imido **2.16** as described in Chapter 2, the analogous hydrazido compound, **3.5**, was initially attempted to be prepared *via* imido-hydrazido metathesis. Although used as a successful strategy by Mountford and co-workers to obtain a similar CPAM Ti(IV)[NNMe₂] compound,^{5j} **2.16** proved to be unreactive towards N,N-dimethylhydrazine, H₂NNMe₂, at room temperature and upon heating to 80 °C, produced a complex mixture of unknown diamagnetic products. Efforts towards synthesizing **3.3** using the established synthetic route to **2.16** were complicated by a thermally unstable Ta(IV)[NHNMe₂]Cl intermediate (**3.2**). Synthesis of CPGU Ta(V)[N(^tBu)]Cl (**2.15**) involved the initial preparation of CPGU Ta(IV)[NH(^tBu)]Cl (**2.14**), followed by reacting with TEMPO to produce compound **2.14**. While the compound CPGU Ta(IV)[NH(^tBu)]Cl (**2.14**) fully decomposes after 18 h at room temperature, it was found that the analogous CPGU Ta(IV)[NHNMe₂]Cl compound (**3.2**) fully decomposed within seconds at -30 °C. Despite the complications of the thermally instable **3.2**, it was found that the compound was stable for several minutes at -78 °C. This allowed for the generation of **3.2** *in situ* by reacting CPGU Ta(IV)Cl₂ (**3.1**) with one equivalent of Li[NHNMe₂] at -78 °C, followed by quickly adding

Scheme 3.1. Synthesis of CPAM Ta(V) hydrazido chloride **3.3**.



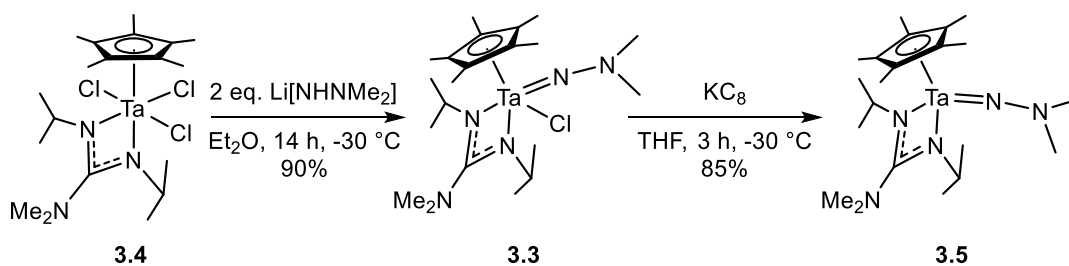
TEMPO to abstract a hydrogen atom ($\text{H}\cdot$) to generate the target CPGU

Ta(V)[NNMe₂]Cl (**3.3**) as shown in Scheme 3.1. Although a synthetic pathway to **3.3**

was established, a more straightforward route was desired. Gratifyingly, as

highlighted in Scheme 3.2, reacting the CPGU Ta(V) trichloride (**3.4**) with two equivalents of Li[NHNMe₂] at -30 °C provided **3.3** in excellent yields at a preparative scale. Compound **3.3**, as well as all compounds reported herein, was subjected to single crystal X-ray Diffraction (XRD) and structurally characterized. Compared to the imido compound CPGU Ta(IV)[N^tBu]Cl (**2.15**), compound **3.3** exhibits a similar pseudo square pyramidal geometry (Figure 3.), featuring a linear Ta1-N1-N2 bond angle of 176.54(13)° that is slightly more obtuse than the 165.0(2)° Ta1-N1-C1 bond angle of **2.15**. Compound **3.3** has a slightly elongated Ta1-N1 bond length of 1.7853(14) Å compared to **2.15** (1.775(2) Å) and a slightly shortened N1-N2 bond length of 1.375(2) Å relative to the N-N bond length of 1.45 Å for the parent

Scheme 3.2. Synthesis of CPAM Ta(IV) Hydrazido **3.5**.



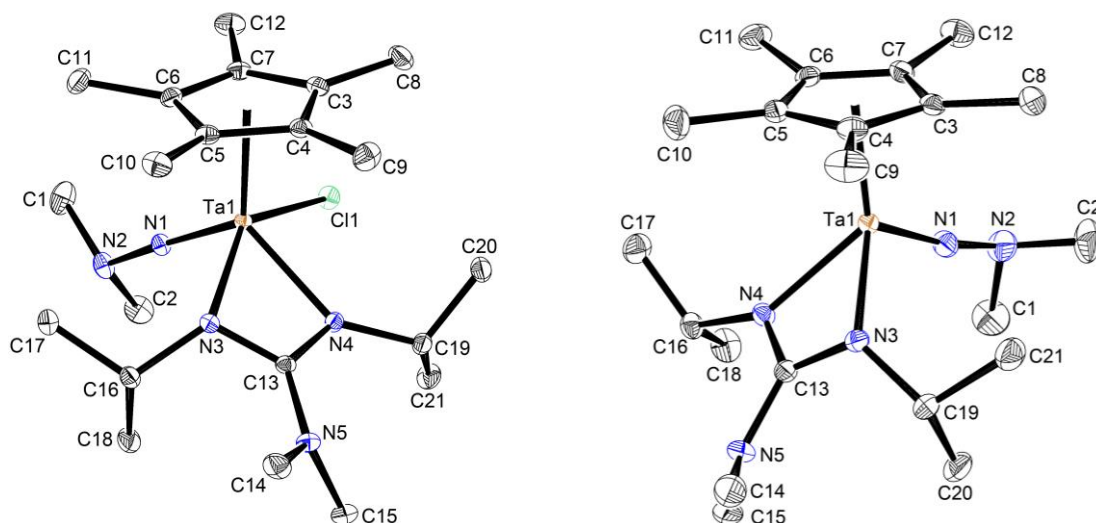


Figure 3.1. Molecular structures (30% thermal ellipsoids) of (left) **3.3** and (right) **3.5**. Hydrogen atoms have been removed for the sake of clarity.

hydrazine, indicating partial double bond character for the N1-N2 bond. The latter structural features have been attributed to the destabilizing effect of the N_{β} lone pair with the $M=N_{\alpha}$ π orbital.^{10,11} Notably, the β nitrogen is pyramidalized ($\sum \angle N2 = 333.24(88)$) which indicates only partial overlap of the lone pair and the $M=N$ π bond. Having successfully developed a route to precursor **3.3**, the synthesis of CPGU Ta(IV)(N^tBu) (**2.16**) was followed. Accordingly, **3.3** was reacted with a slurry of potassium graphite (KC_8) in THF at $-30^{\circ}C$ to provide the cherry red CPGU Ta(IV)(NNMe₂) compound **3.5**. ¹H NMR of **3.5** yielded only broadened resonances due to paramagnetism; therefore, crystallographic and elemental analysis confirmed the mononuclear structure and elemental composition of this compound. Compound **3.5** has a pseudo tetrahedral geometry in the solid state, with a slightly shorter Ta1-N1 bond length of 1.781(3) Å coupled to a longer N1-N2 bond length of 1.398(5) Å, and a slightly more acute Ta1-N1-N2 bond angle of 171.2(3)^o compared to the structural parameters of **3.3**. EPR analysis presented in Figure 3.2 confirmed the

radical nature of the Ta(IV) metal center, showing a signal consistent with a single unpaired electron strongly coupled to the spin 7/2 ^{181}Ta metal center [$g_{\text{iso}} = 1.962$, $A_{\text{iso}}(^{181}\text{Ta}) = 439$ MHz].

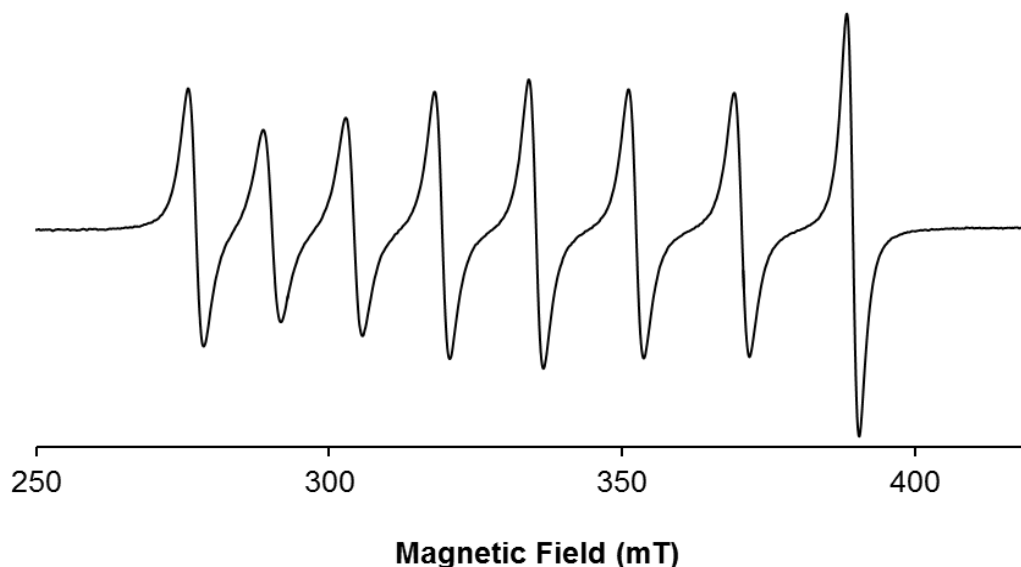


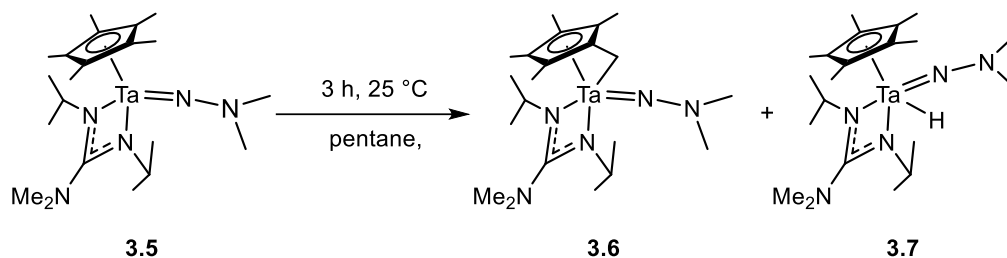
Figure 3.2. X-band EPR spectrum (toluene, 25 °C) of compound **3.5**; $g_{\text{iso}} = 1.962$, $A_{\text{iso}}(^{181}\text{Ta}) = 439$ MHz.

3.2.2. Metal-centered reactivity of a mononuclear Ta(IV) hydrazido complex

Previously reported, the CPGU Ta(IV)[N^tBu] (**2.14**) was found to have a general lack of M=N bond reactivity towards hydrogenation, hydrosilylation and CO; therefore, it was promising that the reduction of sterics in going from the *tert*-butyl imido (**2.14**) to the hydrazido (**3.5**), as well as the N_β destabilization effect would facilitate this type of reactivity. After isolating **3.5**, an immediate, stark contrast to CpGu Ta(IV)][N^tBu] (**3.3**) was observed regarding thermal instability. While **2.14** is indefinitely stable in solution at 25 °C, compound **3.5** quickly decomposes in a concentrated pentane solution over 3 h at this temperature to produce two main diamagnetic products by ^1H NMR. Crystallization of this mixture in pentane at –

30 °C led to the selective isolation of a C_1 symmetric compound containing a ^1H NMR peak at 11.0 ppm that integrated for one, which suggested the formation of a Ta-H bond. Single crystal XRD confirmed the structure to be that of the CPGU Ta(V) hydrazide, hydride compound **3.6**, which rests in a pseudo square pyramidal geometry. Although the second major product proved to be less crystalline, slow evaporation of the mother liquor at -30 °C provided a trace amount of single crystals that were subjected to crystallographic analysis to provide a Cp* activated “tuck-in”

Scheme 3.3. Thermal disproportionation of CPAM Ta(IV) Hydrazido **3.5**.



structure (**3.7**). Efforts at isolating **3.7** at larger scales were unsuccessful; however, ^1H NMR was consistent with this compound being the second disproportionation due to the presence of two diagnostic doublets at 2.8 and 3.0 ppm that are assigned to the diastereotopic methylene protons and consistent with other reported Ta(V) “tuck-in” compounds.¹² This contrast in reactivity between **2.16** and **3.5** is attributed to the less sterically demanding hydrazido moiety, which provides a more readily accessible metal center.

Having characterized the disproportionation of **3.5**, it was of interest to determine whether the hydrazido moiety would show any enhanced reactivity towards hydrogenation, silylation or carbonylation or other one-electron processes as compared to **2.16**.¹³ With competing decomposition pathways, it was necessary to

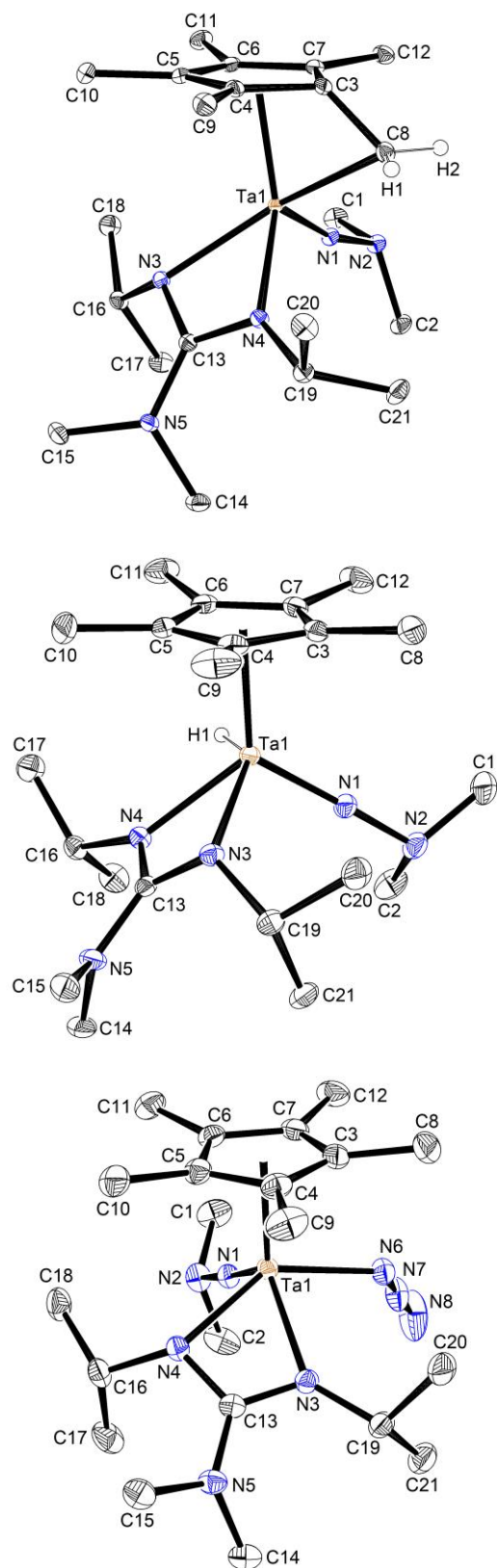
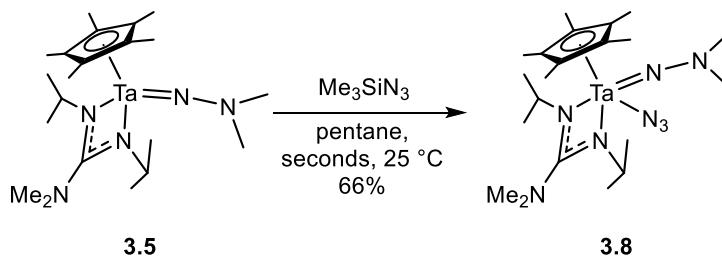


Figure 3.3. Molecular structures (30% thermal ellipsoids) of (top) **3.6**, (middle) **3.7** and (bottom) **3.8**. Hydrogen atoms except for H1 and H2 in **3.6** and H1 in **3.7** have been removed for the sake of clarity.

survey reactivity of **3.5** at -30 °C. It is unknown whether the low temperature may have precluded any reactivity; however, **3.5** was inert towards addition of H₂, PhSiH₃ and CO. Attempts to quantitatively synthesize the hydrazido, hydride compound **3.6** by reacting **3.5** with various hydrogen atom donors including (Bu)₃Sn-H, cyclohexadiene, Ph₃C-H and 9,10-dihydroanthracene also failed. In all cases, allowing reactions to warm to ambient temperature led to disproportionation products. Finally, alkyl or silyl azides have been known to form cycloaddition products with metal-nitrogen multiple bonds.¹⁴ This class of reactivity was thus attempted with **3.5**, where 1 eq. of trimethylsilylazide, Me₃SiN₃, was added to a pentane solution of **3.5** at -30 °C. The solution quickly turned from cherry red to yellow, signifying the oxidation of the Ta(IV) metal center to Ta(V). ¹H

Scheme 3.4. Reactivity of **3.5** with trimethylsilylazide.



NMR was consistent with the formation of a single *C*₁ symmetric product and XRD of single crystals determined the structure to be the azide compound, CPGU Ta(V)[NNMe₂][N₃] (**3.8**). The formation of this azide compound is consistent with one-electron reduction of the Si-N bond, in which a similar process has been reported for an iron hydride compound.¹⁵ In general, **3.5** was more active towards one electron processes than **2.16**, which is attributed to lesser sterics of the hydrazido moiety. Compound **3.5** was also found to readily act as a radical initiator for the

polymerization of styrene in pentane solution, whereas compound **2.16** was completely inert towards the addition of styrene.

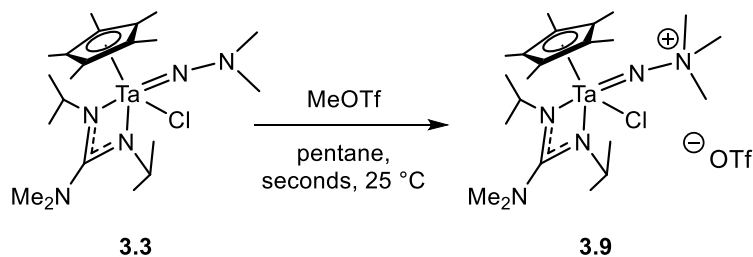
3.3. Tantalum Hydrazidium Complexes and N-N Cleavage

3.3.1. Synthesis of Ta(V) and Ta(IV) hydrazidium complexes

Hydrazide complexes of Group 4 and in particular, group 6, have been used to probe the reactivity of intermediates within the Chatt Cycle. Although examples of group 4 and group 6 hydrazido compounds bearing a positively charged N_{β} have been documented, there are currently no examples of group 5 hydrazidium complexes.

Previous research has shown that group 4 and 6 hydrazides react with alkyl electrophiles to generate a quaternary N_{β} atom.¹⁶ In pentane solution, compound **3.3**

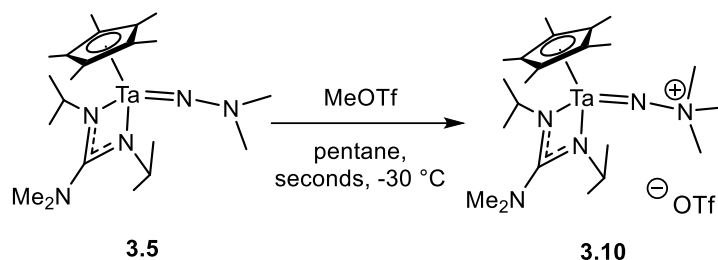
Scheme 3.5. Synthesis of CPAM Ta(V) hydrazidium **3.9**.



reacted with methyl trifluoromethanesulfonate (MeOTf) to produce a white precipitate that was isolated in near quantitative yield for both cases. ¹H NMR was consistent with the methylation of N_{β} to give **3.9**. Interestingly, while **3.3** is yellow, compound **3.9** is colorless which signifies the absence of N_{β} lone pair effects.

Having isolated the mid-valent Ta(IV) hydrazido (**3.5**), it was of interest to see if it would be possible to isolate the Ta(IV) hydrazidium complex (**3.10**). MeOTf was added to a solution of **3.5** in pentane cooled to -30 °C, which led to the precipitation of a light pink powder. This product displayed significantly less kinetic stability to

Scheme 3.6. Synthesis of CPAM Ta(IV) hydrazidium **3.10**.



that of **3.5**, with the light pink powder fully decomposing within several hours and solutions fully decomposing within an hour at room temperature. The paramagnetic properties of **3.10** were further probed by EPR spectroscopy, which again displayed a strongly coupled electron localized on the ^{181}Ta metal center (Figure 3.4).

Unequivocal evidence for the molecular structure of **3.10** was given by crystallographic analysis of single purple crystals that were grown from a toluene solution layered with pentane stored at $-30\text{ }^\circ\text{C}$. The structure, presented in Figure 3.5, shows a tetrahedral geometry analogous to that of **3.5**, with a quaternary N_β and a non-coordinating triflate counter-anion. Compound **3.10** contains an elongated $\text{N}_\alpha\text{-N}_\beta$ bond ($1.417(3)\text{ \AA}$), consistent with the absence of N_β substituent effects. Intriguingly,

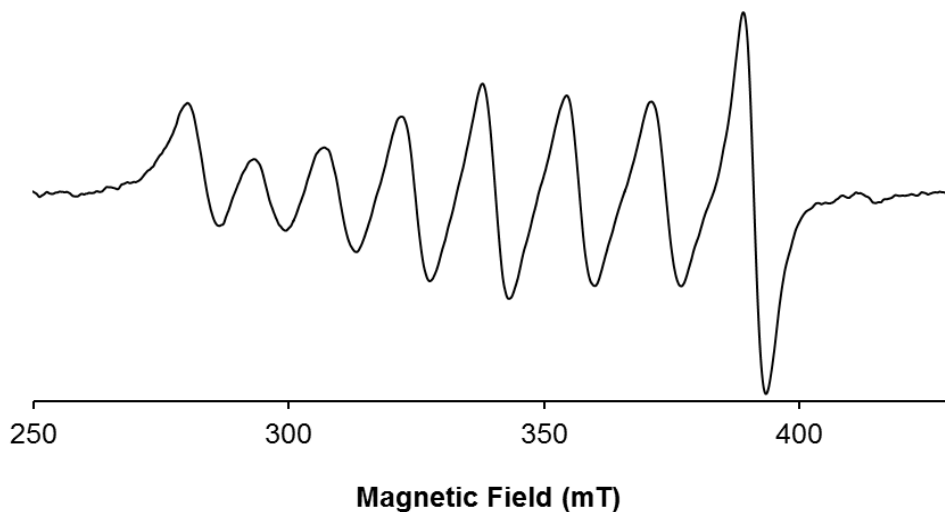


Figure 3.4. X-band EPR spectrum (toluene, $25\text{ }^\circ\text{C}$) of compound **3.10**; $g_{\text{iso}} = 1.921$, $A_{\text{iso}}(^{181}\text{Ta}) = 422\text{ MHz}$.

3.10 has the longest Ta=N_α bond length, 1.806(2) Å, out of all compounds reported despite lacking any N_β lone pair destabilization, which may be due to steric rather than electronic effects.

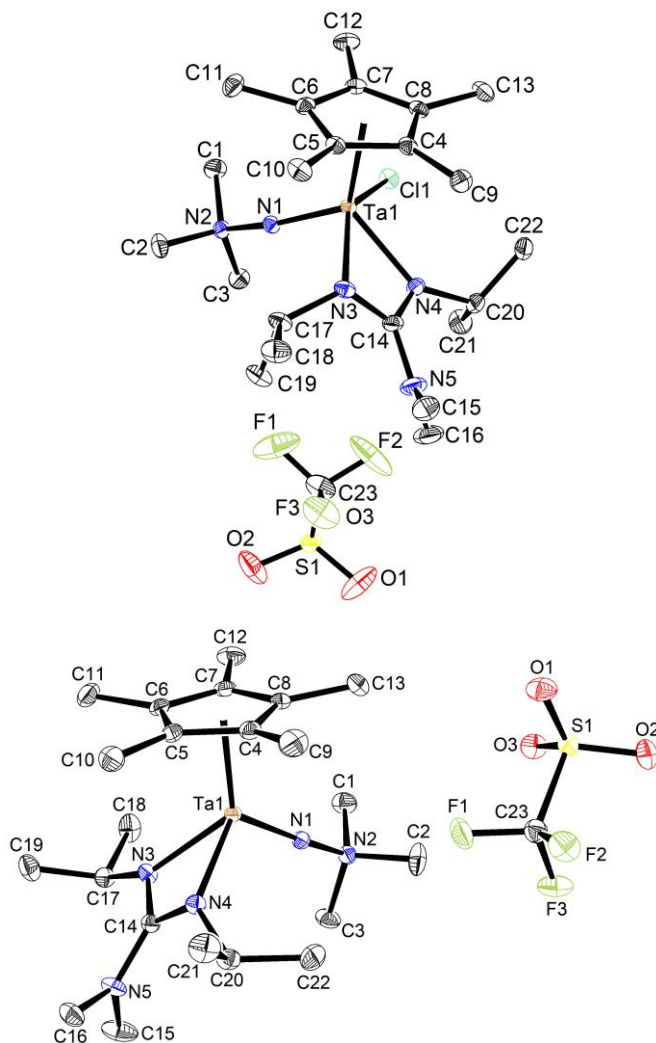
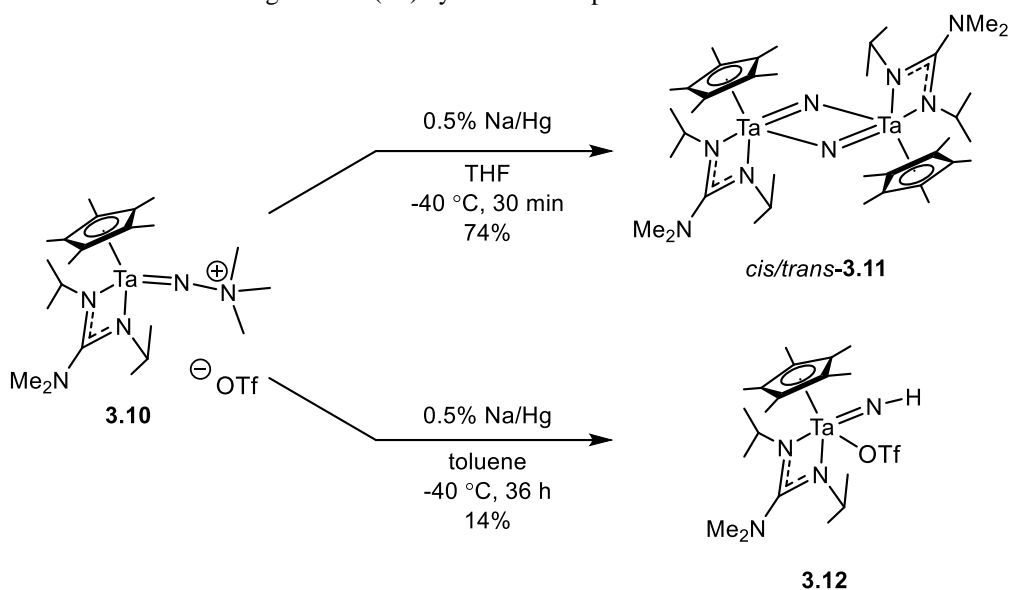


Figure 3.5. Molecular structures (30% thermal ellipsoids) of (top) **3.9** and (bottom) **3.10**. Hydrogen atoms have been removed for the sake of clarity.

3.3.2. Ta(IV) hydrazidium N-N cleavage studies

Once again, reactivity studies of **3.10** were conducted at -30 °C to avoid competing decomposition pathways. Compound **3.10** was not reactive towards hydrogenation. The reductive N_α-N_β cleavage of hydrazidium complexes has been

Scheme 3.7. N-N cleavage of a Ta(IV) hydrazidui complex.



well studied within group 4 and 6 metals as an intermediate process within the Chatt cycle;^{7i,j,17} however, no group 5 hydrazidui N_{α} - N_{β} bond cleavage nor evaluation of whether group 5 can participate in a Chatt type cycle described in Chapter 1. In pink, THF solutions maintained at -30 °C, **3.10** reacted with 1 eq. of sodium amalgam (Na/Hg) over 30 min to produce a yellow solution. Following workup, two products were identified by ¹H NMR as the isomeric N-N cleaved *cis/trans*-**3.11** in 74% yield, which were further established by single crystal XRD studies. As depicted in the top row of Scheme 3.8, the mechanism of this reaction most likely involves reductive N-N cleavage to produce the terminal nitride species **3.13**, which then aggregates to form the dimer product *cis/trans*-**3.11**. In contrast to this reactivity, when the same reaction was performed in toluene solvent, much longer reaction times (36 h) were required to observe the disappearance of pink color. Upon workup and crystallization in a saturated pentane solution at -30 °C, colorless crystals formed. As determined by ¹H NMR, no *cis/trans*-**3.11** had formed; resonances were attributed to a clean C_1

symmetric species where single crystal XRD studies established the identity of the product as the N_{α} - N_{β} cleaved product CPGU Ta(V)(NH)(OTf) (**3.12**) in 14% yield. Compound **3.12** resides in a pseudo square pyramidal geometry with a Ta1-N1 bond length of 1.775(4) Å, which is consistent with Ta(V)=N bonds of other complexes

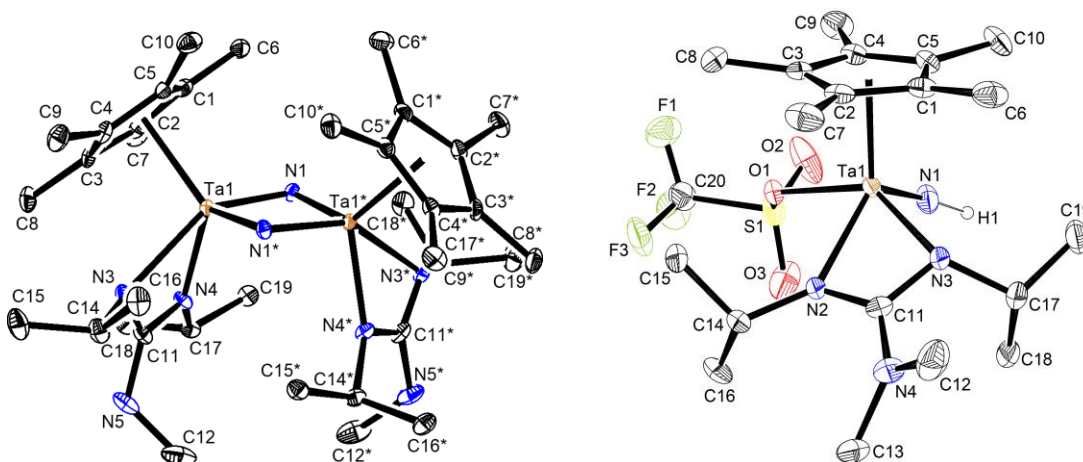
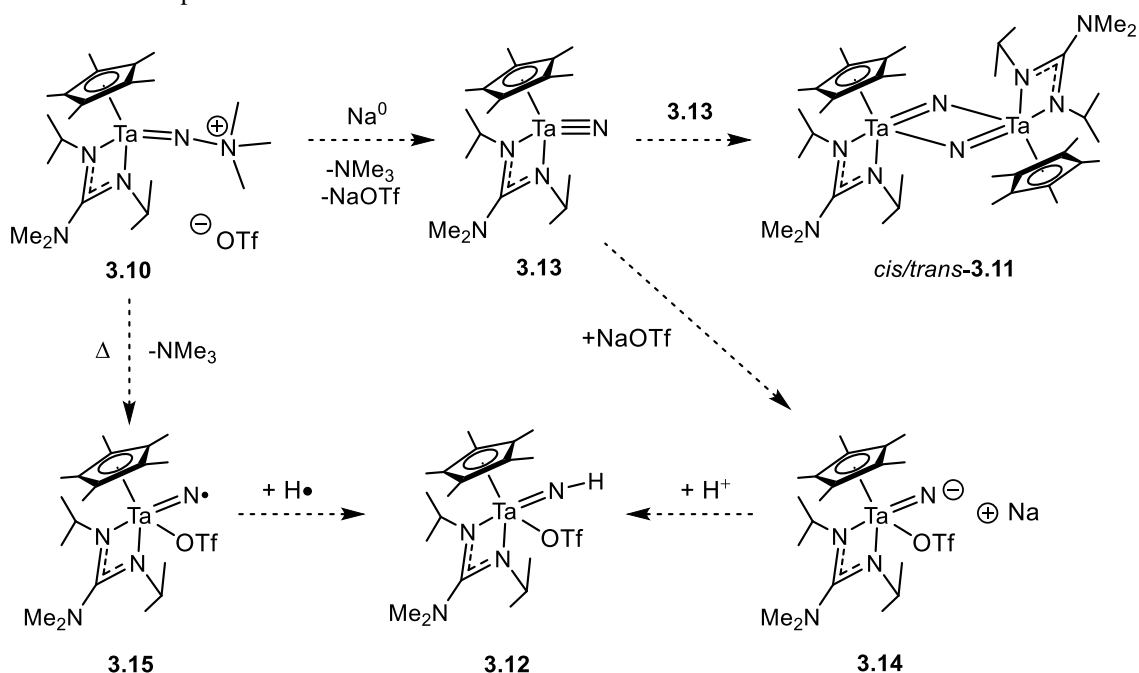


Figure 3.6. Molecular structures (30% thermal ellipsoids) of (left) *cis*-**3.11** and (right) **3.12**. Hydrogen atoms except for H1 in **3.12** have been removed for the sake of clarity.

such as the Ta1-N1 bond length of Ta(V) imido chloride **2.15**, 1.775(2) Å. As a control experiment, a solution of **3.10** in THF was left at room temperature and after 1 h, the solution had lost its pink hue and become colorless. ^1H NMR of the crude product revealed a mixture of diamagnetic species; however, comparison of the spectrum with a pure spectrum parent imide product **3.12** indicated the presence of this compound. Formally, the reaction of **3.10** with Na/Hg in toluene could proceed *via* an intermediate such as **3.14** in Scheme 3.8 which could subsequently pick up an adventitious proton. An alternative mechanism, and one that is more supported by the control experiment is that first trimethylamine, NMe_3 , dissociates to give a nitridyl radical intermediate (**3.15**). This intermediate can then engage in hydrogen atom abstraction with suitable $\text{H}\cdot$ donors that most likely involves H atoms from a Cp^* ligand considering the disproportionation chemistry described in Scheme 3.3.

Scheme 3.8. Proposed mechanisms for the formation of **3.11** and **3.12**.



Precedent for this nitridyl pathway rests on a discovery made by Mindiola's group where a Ti(III) azide complex was shown to extrude N_2 to yield a Ti(IV)[=NH] product, which was hypothesized to proceed through a Ti(IV) nitridyl intermediate that abstracted a hydrogen atom from a tolyl ligand.¹⁸

3.4. Structural and Electronic Comparisons of Ta Imido and Hydrazido Compounds

3.4.1. N_β -substituent effects

It has been well documented that N_β -substituent effects play a large role in the structure and electronic properties of the hydrazido moiety.^{10,19,20} Particularly, N_β has a lone pair that can interact with the M-N π bond and cause a destabilizing interaction. This destabilizing interaction lengthens the M- N_α bond and shortens the N_α - N_β bond. It also has the effect of raising the hydrazido centered HOMO, which generally gives color to high oxidation state early transition metals due to lowering

the energy gap between the HOMO and an unfilled metal *d* orbital.^{10a} These properties are prevalent throughout the results mentioned above. For instance, CPGU Ta(V) imido chloride **2.15** is a colorless compound with a Ta-N bond of 1.775(2) Å, whereas the Ta(V) hydrazido chloride analogue **3.3** is yellow and has an elongated Ta-N bond of 1.7853(14) Å, coupled to a shorter N-N bond length of 1.375(2) Å, signifying N-N partial double bond character (parent hydrazine N-N bond length = 1.45 Å). The extent of pyramidalization in **3.3** is significant with the sum of all angles around N_β ($\sum\angle N_{\beta}$) equal to 333.44(28)°. Comparing Ta(V) and Ta(IV) hydrazides, the N_β substituent effect is significantly less in the midvalent compound. For Ta(IV) imido **2.16**, the Ta-N bond length is 1.785(2) Å, which is slightly longer than that of the Ta(IV) hydrazido (**3.5**) Ta-N bond length of 1.781(3) Å. The lesser degree of

Table 3.1. Structural parameters for imido and hydrazido compounds.

	Ta-N _α (Å)	N _α -N _β (Å)	$\sum\angle N_{\beta}$ (°) ^a
[Ta(V)](N ^t Bu)Cl (2.15)	1.775(2)	-	-
[Ta(V)](NNMe ₂)Cl (3.3)	1.7853(14)	1.375(2)	333.44(28)
[Ta(IV)](N ^t Bu) (2.16)	1.785(2)	-	-
[Ta(IV)](NNMe ₂) (3.5)	1.781(3)	1.398(5)	330.4(8)

^a $\sum\angle N_{\beta}$ = sum of all angles between N_β substituents.

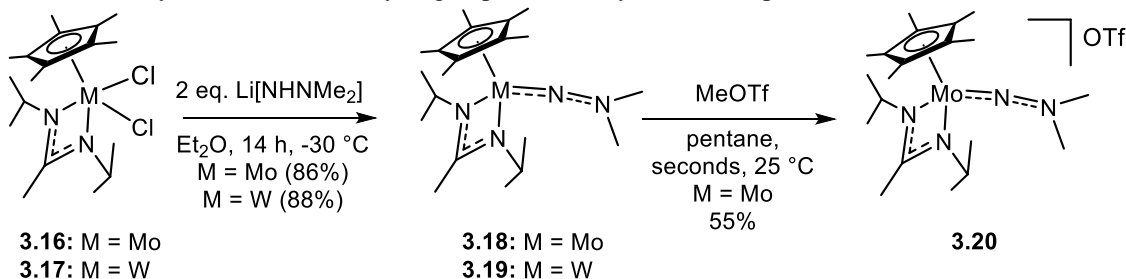
Ta(IV) hydrazido (**3.5**) N_β destabilization is manifested through the longer N-N bond length (1.398(5) Å) and greater extent of pyramidalization ($\sum\angle N_{\beta}$ = 330.4(8)°) as compared to the Ta(V) hydrazido chloride. These observations can be rationalized by the more electron rich Ta(IV) metal center making it less favorable for N_β lone pair donation.

3.5. Hydrazido Studies Extended to Group 6

3.5.1. Synthesis and reactivity of group 6 hydrazido complexes

With the discovery of N-N cleavage pathways for group 5 hydrazido complexes and recent reports from within our group concerning group 6 imido reactivity and catalytic N- and O-atom transfer reactions, we were interested in developing similar chemistry for Mo(IV) and W(IV) d^2 hydrazido complexes. Entry into group 6 hydrazido analogues **3.18** and **3.19** was obtained using two equivalents of Li[NHNMe₂] with the corresponding CPAM MCl₂ precursors [M = Mo (**3.16**), M = W (**3.17**)]. Although **3.18** and **3.19** exhibited low crystallinity, crude product after work-up was of excellent purity as a powder as determined by ¹H NMR and used in all subsequent reactions.

Scheme 3.9. Synthesis and reactivity of group 6 CPAM hydrazido compounds **3.18** and **3.19**.



Silyl (Mo = **3.21**, W = **3.22**) and *tert*-butyl (Mo = **3.23**, W = **3.24**) analogues of **3.18** and **3.19** have previously been found to react with CO and undergo subsequent reductive elimination of an isocyanate.²¹ Results suggest that **3.19** is much less reactive with CO as compared to **3.18**, with **3.19** being unreactive towards carbonylation. This is in keeping with the general trend that Mo is more reactive than W with CO insertion, as well as imido substituent effects laid out thus far with more

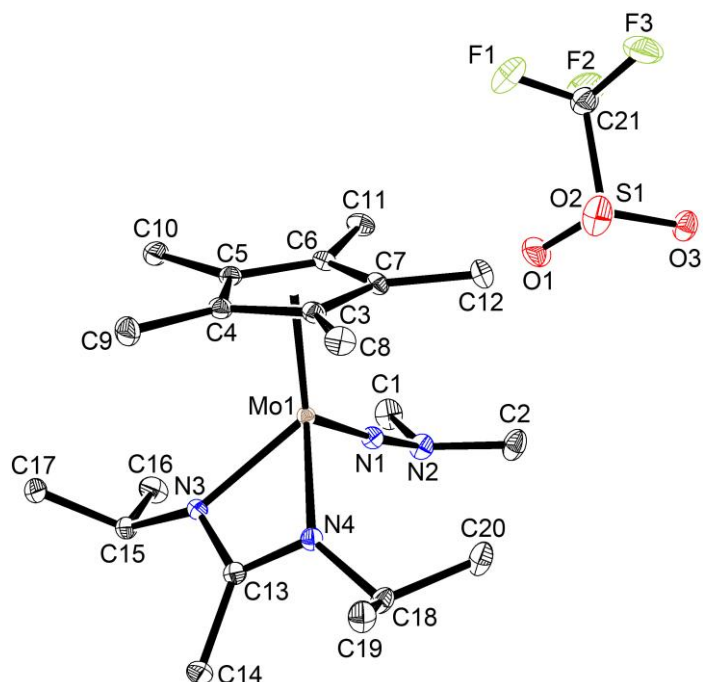


Figure 3.7. Molecular structures (30% thermal ellipsoids) of **3.20**. Hydrogen atoms have been removed for the sake of clarity.

electropositive substituents leading to greater reactivity. Compounds **3.18** and **3.19** were not reactive towards hydrogenation or silylation.

Having studied the reactivity of **3.18** and **3.19** with CO, we wanted to probe the nucleophilicity of N_{β} with electrophilic alkyls to study hydrazidium reactivity and N-N cleavage pathways. Addition of MeOTf to **3.18** and **3.19** led to a brown precipitate. However, single crystal XRD analysis of the Mo product led to a structure consistent with a cationic Mo(V) hydrazido triflate compound (**3.20**) containing a planar N_{β} ($\sum \angle N_{\beta} = 352.13^{\circ}$) and a contracted N1-N2 bond length of 1.325(4) Å. In this case, N_{β} was not alkylated; instead, the metal was oxidized with the formal production of ethane.

An explanation of why carbonyl insertion is less reactive and that alkylation of N_β cannot compete with redox at the metal center stems from the fact that there are two resonance limits for the hydrazide ligand: one is the hydrazido(2-) limit, where

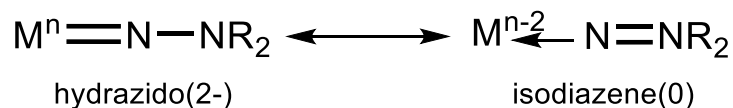


Figure 3.8. Hydrazido(2-) versus isodiazene(0) resonance structures for hydrazido complexes.

there is no lone pair donation from N_β into N_α , and the other is the isodiazene(0) limit, where the N_β lone pair fully donating into N_α and the bonding resembles a dative donor/acceptor relationship. For the Ta hydrazido, N_β is clearly pyramidalized ($\sum \angle N_\beta = 330(8)^\circ$ for **3.5**) signifying the hydrazido limit, but for group 6, the isodiazene limit is dominant. In the isodiazene limit, the N-N bond is stronger and the metal center is electron rich, which is why metal redox is favored and M-N and N-N bonds are unreactive. These results are consistent with the findings of Bercaw's group,^{10a} where they have isolated and structurally characterized Ta(V) hydrazido complexes representative of the hydrazido limit, and W(VI) hydrazide complexes representative of the isodiazene limit.

3.6. Conclusion

In conclusion, the Ta imido studies have been extended to the hydrazido moiety, which includes the first isolation of Ta(IV) hydrazido and Ta(IV) hydrazidium complexes. The hydrazido derivative is unreactive towards cycloaddition reactions, but displayed interesting one-electron reactivity. The Ta(IV) hydrazido derivative (**3.5**) is much more reactive towards disproportionation and other one-electron processes compared to the Ta(IV) imido (**2.14**) due to lesser

sterics, decomposing within hours at room temperature and initiating the polymerization of styrene whereas (**2.16**) was inert to both these processes at room temperature. Having isolated the Ta(IV) hydrazido, the Ta(IV) hydrazidium complex **3.10** was isolated and structurally characterized and was found to be much more susceptible towards thermal disproportionation. Compound **3.10** underwent reductive N_{α} - N_{β} cleavage that gave the hydrogen substituted imido (**3.12**). Future studies will include electrochemical analysis to further probe the reactivity and N-N cleavage of **3.10**, as well as continued research towards the activation and functionalization of dinitrogen.

3.7. Experimental Section

3.7.1. General considerations

All manipulations with air and moisture sensitive compounds were carried out under an inert atmosphere of N_2 or Ar using standard Schlenk-line or glovebox techniques. All solvents were dried (Na for toluene and Na/benzophenone for pentane, Et_2O , and THF) and distilled under N_2 prior to use. Benzene- d_6 and solvents used for sodium amalgam reduction of **3.10** (THF and toluene) were dried over Na/K alloy and isolated by vacuum transfer. Celite was oven-dried ($150\text{ }^{\circ}\text{C}$ for several days) and all amines were dried over CaH_2 and isolated by vacuum transfer before use. Cooling for reactions was achieved using the internal freezer of a glovebox maintained at $-30\text{ }^{\circ}\text{C}$. Chemicals N,N-dimethylhydrazine and methyl trifluoromethanesulfonate (MeOTf) were purchased from Sigma-Aldrich and Cp^*TaCl_4 was purchased from Strem Chemicals. All chemicals were used as

received unless otherwise noted. $\text{Cp}^*\text{Ta}[\text{N}(\text{iPr})\text{C}(\text{NMe}_2)\text{N}(\text{iPr})]\text{Cl}_3$ was prepared according to previously reported procedures and isolated in similar yield and purity.⁹ ^1H NMR spectra were recorded at 400.13 MHz and referenced to SiMe_4 using residual ^1H chemical shifts of C_6D_6 (7.16 ppm) as a standard. ^{19}F NMR spectra were recorded at 376.08 MHz and externally referenced to CFCl_3 using α,α,α -trifluorotoluene (-63.72 ppm) as a standard. Solution EPR spectra were recorded at Georgetown University on a JEOL JES-FA200 continuous wave spectrometer equipped with an X-band Gunn oscillator bridge and a cylindrical mode cavity employing a modulation frequency of 100 kHz. All EPR spectra were obtained from freshly prepared toluene solutions (5 mM) in a nitrogen-filled glovebox and recorded at room temperature. $A_{\text{iso}}(^{181}\text{Ta})$ values in MHz were determined by the separation of the middle two lines of the eight-line pattern. Elemental analyses (C, H, and N) were performed by Midwest Microlab, LLC.

3.7.2. Synthesis of new compounds

$\text{Cp}^*\text{Ta}[\text{N}(\text{iPr})\text{C}(\text{NMe}_2)\text{N}(\text{iPr})][\text{NNMe}_2][\text{Cl}]$ (3.3). A solution of $\text{Li}[\text{NH-NMe}_2]$ (242 mg, 3.67 mmol) in 15 mL of Et_2O was cooled to $-30\text{ }^\circ\text{C}$ and added drop-wise to a solution of $\text{Cp}^*\text{Ta}[\text{N}(\text{iPr})\text{C}(\text{NMe}_2)\text{N}(\text{iPr})]\text{Cl}_3$ (1.06 g, 1.79 mmol) in 30 mL of Et_2O that was pre-cooled to $-30\text{ }^\circ\text{C}$, over a period of 3 min. The reaction mixture was allowed to warm to room temperature and stirred for 14 h to produce a yellow solution. Volatiles were removed *in vacuo* to yield an amber solid. The crude product was extracted with toluene and filtered through a short pad of Celite on a glass frit. The collected filtrate was concentrated and cooled to $-30\text{ }^\circ\text{C}$ to provide yellow crystals of **3.3** (935 mg, 90% yield). Anal. Calc'd for $\text{C}_{21}\text{H}_{41}\text{N}_5\text{ClTa}$: C, 43.49;

H, 7.13; N, 12.08; Found: C, 43.54; H, 6.99; N, 12.09. ^1H NMR (benzene- d_6): δ 1.13 (3H, d, $\text{CH}(\text{CH}_3)$, $J = 6.4$ Hz), 1.34 (3H, d, $\text{CH}(\text{CH}_3)$, $J = 6.4$ Hz), 1.36 (3H, d, $\text{CH}(\text{CH}_3)$, $J = 6.8$ Hz), 1.41 (3H, d, $\text{CH}(\text{CH}_3)$, $J = 6.8$ Hz), 2.10 (15H, s, $\text{C}_5(\text{CH}_3)_5$), 2.37 (6H, s, $\text{N}(\text{CH}_3)_2$), 2.88 (6H, s, $\text{NN}(\text{CH}_3)_2$), 3.78 (1H, sept, $\text{CH}(\text{CH}_3)_2$, $J = 6.4$ Hz), 3.87 (1H, sept, $\text{CH}(\text{CH}_3)_2$, $J = 6.8$ Hz).

$\text{Cp}^*\text{Ta}[\text{N}(\text{iPr})\text{C}(\text{NMe}_2)\text{N}(\text{iPr})][\text{NNMe}_2]$ (3.5). Freshly prepared KC_8 (234 mg, 1.73 mmol) was slurried with 15 mL of THF that had been pre-cooled to -30 °C and transferred over a period of 3 min to a solution of **3.3** (555 mg, 0.96 mmol) in 15 mL of THF that was pre-cooled to -30 °C. Volatiles were immediately removed *in vacuo* to give a black-red solid, which was promptly dissolved in pentane that was pre-cooled to -30 °C and filtered through a short pad of Celite on a glass frit. The dark red filtrate was concentrated and stored at -30 °C overnight to provide dark red crystals of **3.5** (444 mg, 85% yield). Anal. Calc'd for $\text{C}_{21}\text{H}_{41}\text{N}_5\text{Ta}$: C, 46.32; H, 7.59; N, 12.86; Found: C, 46.00; H, 7.32; N, 12.67.

$\text{Cp}^*\text{Ta}[\text{N}(\text{iPr})\text{C}(\text{Me})\text{N}(\text{iPr})][\text{NNMe}_2][\text{H}]$ (3.6) and $(\text{C}_5\text{Me}_4\text{-CH}_2)\text{Ta}[\text{N}(\text{iPr})\text{C}(\text{Me})\text{N}(\text{iPr})][\text{NNMe}_2]$ (3.7). A solution of **3.5** (164 mg, 0.30 mmol) in 1 mL of pentane was left at room temperature for 14 h to provide an amber solution. The solution was then cooled to -30 °C overnight to provide light yellow crystals of **3.6** (36 mg, 22% yield). Slow evaporation of the mother liquor at -30 °C led to an oily mixture of **3.6** and **3.7**, including trace formation of single crystals composed of **3.7**, which were subjected to X-Ray analysis and ^1H NMR (see figure

S2). Anal. Calc'd for $C_{21}H_{42}N_5Ta$ (**3.6**): C, 46.24; H, 7.76; N, 12.84; Found: C, 46.51; H, 7.51; N, 12.61. 1H NMR (benzene- d_6): δ 1.13 (3H, d, $CH(CH_3)$, $J = 6.4$ Hz), 1.19 (3H, d, $CH(CH_3)$, $J = 6.2$ Hz), 1.34 (3H, d, $CH(CH_3)$, $J = 6.4$ Hz), 1.44 (3H, d, $CH(CH_3)$, $J = 6.6$ Hz), 2.20 (15H, s, $C_5(CH_3)_5$), 2.39 (6H, s, $N(CH_3)_2$), 2.73 (6H, s, $NN(CH_3)_2$), 3.69 (1H, sept, $CH(CH_3)_2$, $J = 6.3$ Hz), 3.71 (1H, sept, $CH(CH_3)_2$, $J = 6.4$ Hz), 10.99 (1H, s, TaH). For **3.7**, 1H NMR (benzene- d_6): δ 1.09 (3H, d, $CH(CH_3)$, $J = 6.9$ Hz), 1.14 (3H, d, $CH(CH_3)$, $J = 6.5$ Hz), 1.29 (3H, d, $CH(CH_3)$, $J = 6.5$ Hz), 1.48 (3H, d, $CH(CH_3)$, $J = 6.9$ Hz), 1.49 (3H, s, $C_5(CH_3)_4-CH_2$), 1.92 (3H, s, $C_5(CH_3)_4-CH_2$), 2.14 (3H, s, $C_5(CH_3)_4-CH_2$), 2.19 (3H, s, $C_5(CH_3)_4-CH_2$), 2.39 (6H, s, $N(CH_3)_2$), 2.57 (6H, s, $NN(CH_3)_2$), 2.81 (1H, d, $C_5(CH_3)_4-CH_2$, $J = 5.3$ Hz), 2.99 (1H, d, $C_5(CH_3)_4-CH_2$, $J = 5.3$ Hz), 3.69 (1H, sept, $CH(CH_3)_2$, $J = 6.5$ Hz), 3.86 (1H, sept, $CH(CH_3)_2$, $J = 6.9$ Hz).

Cp*Ta[N(ⁱPr)C(Me)N(ⁱPr)][NNMe₂](N₃) (3.8**). Trimethylsilylazide (TMS-N₃) (64.2 μ L, 0.49 mmol) was added to a solution of **3.5** (53.1 mg, 0.10 mmol) in 3 mL of pentane that was pre-cooled to -30 °C. The mixture was stored at -30 °C for 14 h to provide a yellow solution that contained yellow crystals of **3.8** (38 mg, 66%). Anal. Calc'd for $C_{21}H_{41}N_8Ta_1$: C, 43.00; H, 7.05; N, 19.10; Found: C, 43.12; H, 7.11; N, 19.09. 1H NMR (400 MHz, benzene- d_6): 1.02 (3H, d, $CH(CH_3)$, $J = 6.3$ Hz), 1.19 (3H, d, $CH(CH_3)$, $J = 6.6$ Hz), 1.29 (3H, d, $CH(CH_3)$, $J = 6.6$ Hz), 1.33 (3H, d, $CH(CH_3)$, $J = 6.6$ Hz), 2.01 (15H, s, $C_5(CH_3)_5$), 2.31 (6H, s, $N(CH_3)_2$), 2.98 (6H, s, $NN(CH_3)_2$), 3.72 (1H, sept, $CH(CH_3)_2$, $J = 6.6$ Hz), 3.73 (1H, sept, $CH(CH_3)_2$, $J = 6.6$ Hz).**

Cp*Ta[N(ⁱPr)C(NMe₂)N(ⁱPr)][NNMe₃][Cl]OTf (3.9). MeOTf (39.3 μL, 0.36 mmol) was added to a stirred solution of **3.3** (208 mg, 0.36 mmol) in 2.5 mL of pentane, which led to the formation of a white precipitate. The solid was collected on a frit, washed with pentane and further purified by slow diffusion of pentane into a concentrated benzene solution at room temperature to provide colorless crystals of **3.9** (248 mg, 93% yield). Anal. Calc'd for C₂₃H₄₄N₅O₃S₁F₃ClTa•C₆H₆: C, 42.36; H, 6.13; N, 8.52; Found: C, 42.36; H, 6.15; N, 8.57. ¹H NMR (benzene-*d*₆): δ 1.05 (3H, d, CH(CH₃), *J* = 6.7 Hz), 1.08 (3H, d, CH(CH₃)₂, *J* = 6.6 Hz), 1.09 (3H, d, CH(CH₃)₂, *J* = 6.8 Hz), 1.17 (3H, d, CH(CH₃)₂, *J* = 6.7 Hz), 1.88 (15H, s, C₅(CH₃)₅), 2.20 (6H, s, N(CH₃)₂), 3.35 (9H, s, NN(CH₃)₃), 3.66 (1H, sept, CH(CH₃)₂, *J* = 6.7 Hz), 3.66 (1H, sept, CH(CH₃)₂, *J* = 6.6 Hz). ¹⁹F NMR (benzene-*d*₆): δ -78.87.

Cp*Ta[N(ⁱPr)C(NMe₂)N(ⁱPr)][NNMe₃]OTf (3.10). MeOTf (31.4 μL, 0.29 mmol) was added to a stirred solution of **3.5** (156 mg, 0.29 mmol) in 10 mL of pentane that was pre-cooled to -30 °C, which led to the formation of a light pink precipitate. The solid was collected on a frit, washed with cold pentane and further purified by slow diffusion of pentane into a concentrated toluene solution at -30 °C to provide purple crystals of **3.10** (174 mg, 85% yield). Anal. Calc'd for C₂₃H₄₄N₅O₃S₁F₃Ta: C, 38.98; H, 6.26; N, 9.88; Found: C, 39.20; H, 6.06; N, 9.61.

{Cp*Ta[N(ⁱPr)C(NMe₂)N(ⁱPr)][N]}₂ (*cis/trans*-**3.11**). Compound **3.10** (65.2 mg, 0.09 mmol) was dissolved in 10 mL of THF^{S2} that was pre-cooled to -30 °C and

added to a schlenk flask containing 0.5% w/w sodium amalgam (423 mg, 0.09 mmol of Na). The mixture was quickly transferred to a -40 °C temperature controlled bath and vigorously stirred for 30 min to provide a yellow solution. After removing solvent *in vacuo*, solids were first extracted with pentane and filtered through Celite on a glass frit. Solvent was removed *in vacuo* to provide a yellow oil, which was dissolved in minimal diethylether and stored at -30 °C to provide yellow crystals of *cis*-**3.11** (22.7 mg, 49% yield). Remaining solids from the initial crude mixture were dissolved in hot benzene and filtered through Celite on a glass frit. The filtrate was concentrated and then heated to re-dissolve any solids. The solution was stored at room temperature overnight to provide yellow crystals of *trans*-**3.11** (11.5 mg, 25% yield). Anal. Calc'd for C₃₈H₇₀N₈Ta₂: C, 45.58; H, 7.05; N, 11.20; Found: C, 45.36; H, 7.00; N, 11.22. For *cis*-**3.11**, ¹H NMR (benzene-*d*₆): δ 1.29 (6H, d, CH(CH₃)₂, *J* = 6.6 Hz), 1.32 (6H, d, CH(CH₃)₂, *J* = 6.6 Hz), 2.22 (15H, s, C₅(CH₃)₅), 2.52 (6H, s, N(CH₃)₂), 3.71 (2H, sept, CH(CH₃)₂, *J* = 6.6 Hz). For *trans*-**3.11**, ¹H NMR (benzene-*d*₆): δ 1.39 (6H, d, CH(CH₃)₂, *J* = 6.3 Hz), 1.40 (6H, d, CH(CH₃)₂, *J* = 6.3 Hz), 2.24 (15H, s, C₅(CH₃)₅), 2.42 (6H, s, N(CH₃)₂), 3.70 (2H, sept, CH(CH₃)₂, *J* = 6.3 Hz).

Cp*Ta[N(ⁱPr)C(NMe₂)N(ⁱPr)][NH][OTf] (3.12). Compound **3.10** (133 mg, 0.19 mmol) was dissolved in 10 mL of toluene that was pre-cooled to -30 °C and added to a schlenk flask containing 0.5% w/w sodium amalgam (862 mg, 0.19 mmol of Na). The mixture was quickly transferred to a -40 °C temperature controlled bath and vigorously stirred for 36 h to provide a yellow solution. After removing solvent *in vacuo*, solids were dissolved in benzene and filtered through Celite on a glass frit.

Volatiles were removed *in vacuo* to give a yellow oil. The product was extracted with pentane, concentrated, and cooled to -30 °C to provide colorless crystals of **3.12** (17.5 mg, 14% yield). Anal. Calc'd for C₂₀H₃₆N₄S₁O₃F₃Ta: C, 36.93; H, 5.58; N, 8.61; Found: C, 37.24; H, 5.69; N, 8.31. ¹H NMR (400 MHz, benzene-*d*₆): δ 0.97 (3H, d, CH(CH₃), *J* = 6.2 Hz), 0.98 (3H, d, CH(CH₃)₂, *J* = 6.6 Hz), 1.16 (3H, d, CH(CH₃)₂, *J* = 6.6 Hz), 1.26 (3H, d, CH(CH₃)₂, *J* = 6.6 Hz), 1.94 (15H, s, C₅(CH₃)₅), 2.26 (6H, s, N(CH₃)₂), 3.56 (1H, sept, CH(CH₃)₂, *J* = 6.6 Hz), 3.66 (1H, sept, CH(CH₃)₂, *J* = 6.6 Hz). ¹⁹F NMR (376 MHz, benzene-*d*₆): δ -77.54.

Cp*Mo[N(ⁱPr)C(Me)N(ⁱPr)][NNMe₂] (3.18). A solution of Li[NH-NMe₂] (54.0 mg, 0.82 mmol) in 15 mL of Et₂O was cooled to -30 °C and added drop-wise to a solution of **3.16** (172 mg, 0.39 mmol) in 10 mL of Et₂O that was pre-cooled to -30 °C, over a period of 3 min. The reaction mixture was allowed to warm to room temperature and stirred for 14 h to produce a brown solution. The solution was filtered through a short pad of Celite on a glass frit. Volatiles were removed *in vacuo* to yield a brown powder of **3.18** (144 mg, 86% yield). ¹H NMR (400 MHz, benzene-*d*₆): 0.95 (3H, d, CH(CH₃), *J* = 6.7 Hz), 1.12 (3H, d, CH(CH₃)₂, *J* = 6.6 Hz), 1.63 (3H, s, [N(ⁱPr)C(CH₃)N(ⁱPr)]), 1.90 (15H, s, C₅(CH₃)₅), 2.86 (6H, s, NN(CH₃)₂), 3.30 (1H, sept, CH(CH₃)₂, *J* = 6.6 Hz).

Cp*W[N(ⁱPr)C(Me)N(ⁱPr)][NNMe₂] (3.19). A solution of Li[NH-NMe₂] (69.9 mg, 1.06 mmol) in 15 mL of Et₂O was cooled to -30 °C and added drop-wise to a solution of **3.17** (274 mg, 0.52 mmol) in 10 mL of Et₂O that was pre-cooled to -30 °C, over a

period of 3 min. The reaction mixture was allowed to warm to room temperature and stirred for 14 h to produce a maroon solution. The solution was filtered through a short pad of Celite on a glass frit. Volatiles were removed *in vacuo* to yield a maroon powder of **3.19** (144 mg, 86% yield). ¹H NMR (400 MHz, benzene-*d*₆): 1.00 (3H, d, CH(CH₃), *J* = 6.7 Hz), 1.24 (3H, d, CH(CH₃)₂, *J* = 6.6 Hz), 1.52 (3H, s, [N(ⁱPr)C(CH₃)N(ⁱPr)]), 2.12 (15H, s, C₅(CH₃)₅), 2.86 (6H, s, NN(CH₃)₂), 3.17 (1H, sept, CH(CH₃)₂, *J* = 6.7 Hz).

Cp*Mo[N(ⁱPr)C(Me)N(ⁱPr)][NNMe₂]OTf (3.24). MeOTf (12.3 μL, 0.11 mmol) was added to a stirred solution of **3.18** (48.3 mg, 0.10 mmol) in 5 mL of pentane that was pre-cooled to -30 °C, which led to the formation of a dark yellow precipitate. The solid was collected on a frit to yield a dark brown powder of **3.24** (60.6 mg, 55%).

3.7.3. Supporting NMR spectra

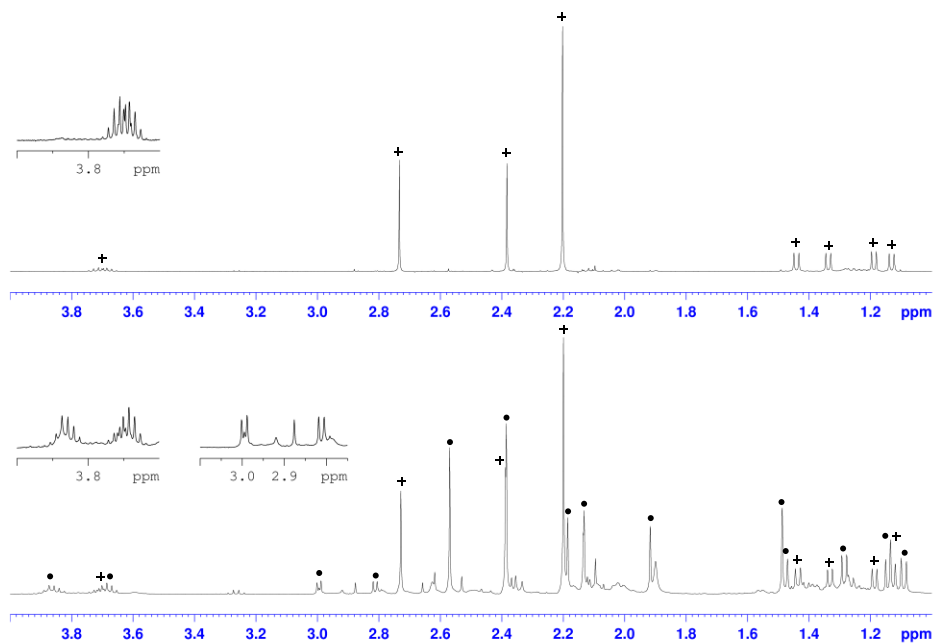


Figure 3.9. ¹H NMR (400.13 MHz, C₆D₆, 25 °C) experiment showing (top) pure **3.7** and (bottom) a mixture of **3.7** (+) and **3.6** (•) that was produced from the thermal disproportionation of **3.5**.

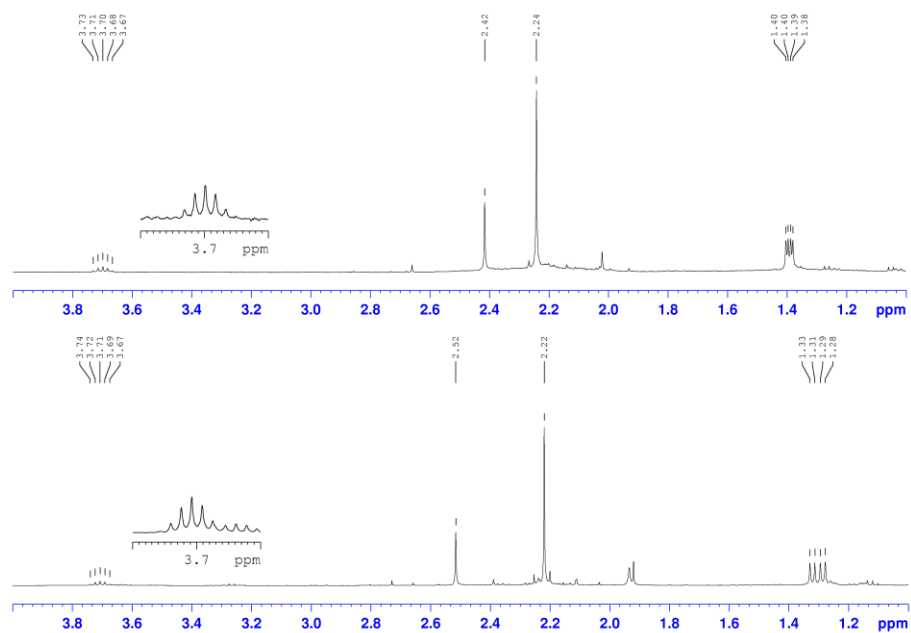


Figure 3.10. ¹H NMR (400.13 MHz, C₆D₆, 25 °C) experiment showing (top) *trans*-**3.11** and (bottom) *trans*-**3.11**, both isolated from reductive N-N cleavage of compound **3.10**.

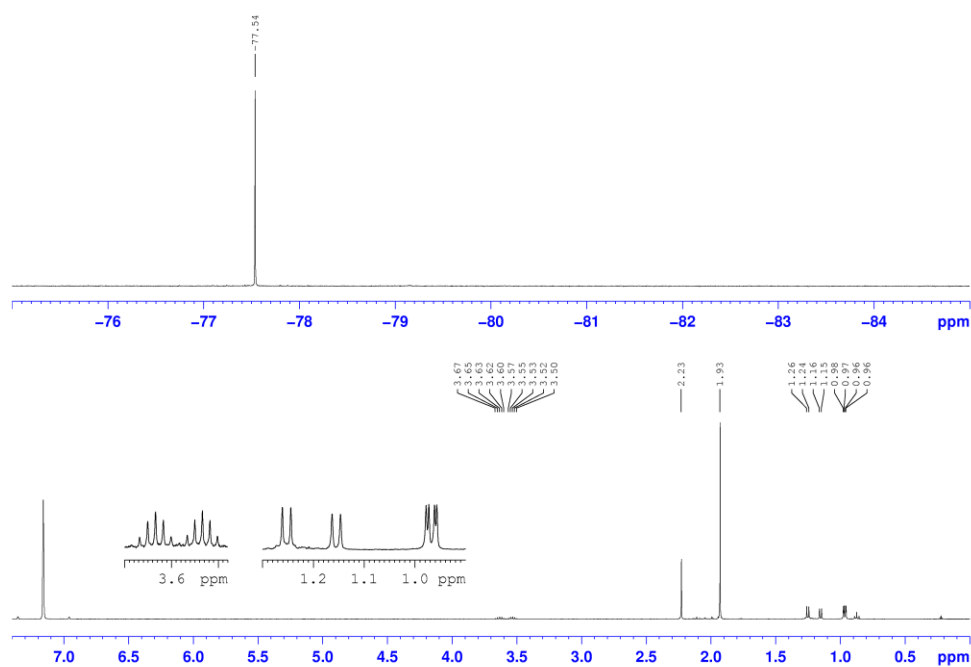


Figure 3.11. (top) ^{19}F NMR (376 MHz, C_6D_6 , 25 °C) and (bottom) ^1H NMR (400.13 MHz, C_6D_6 , 25 °C) of compound **3.12** isolated from N-N cleavage of **3.10** in toluene.

3.8. References

- 1) (a) Zárate, X.; Schott, E.; Carey, D. M.-L.; Bustos, C.; Arratia-Pérez, R. *J. Mol. Struct. Theochem.* **2010**, 957, 126-132. (b) Redshaw, C.; Elsegood, M. R. *J. Inorg. Chem.* **2000**, 39, 5164-5168. (c) Kahlal, S.; Saillard, J.-Y.; Hamon, J.-R.; Manzur, C.; Carrillo, D. *J. Chem. Soc., Dalton Trans.* **1998**, 1229-1240. (d) George, T. A.; Kaul, B. B.; Chen, Q.; Zubieta, J. *Inorg. Chem.* **1993**, 32, 1706-1711. (e) Harada, Y.; Mizobe, Y.; Hidai, M. *J. Organomet. Chem.* **1999**, 24-31. (f) Harada, Y.; Mizobe, Y.; Ishii, Y.; Hidai, M. *Bull. Chem. Soc. Jpn.* **1998**, 71, 2701-2708. (g) Niemoth-Anderson, J. D.; Debord, J. R. D.; George, T. A.; Ross II, C. R.; Stezowski, J. J. *Polyhedron* **1996**, 15, 4031-4040. (h) Vale, M. G.; Schrock R. R. *Inorg. Chem.* **1993**, 32, 2767-2772. (i) Schrock, R. R.; Glassman, T. E.; Vale, M.

- G.; Kol, M. *J. Am. Chem. Soc.* **1993**, *115*, 1760-1772. (i) Glassman, T. E.; Vale, M. G.; Schrock, R. R. *J. Am. Chem. Soc.* **1992**, *114*, 8098-8109. (j) Galindo, A.; Hills, A.; Hughes, D. L.; Richards, R. L.; Hughes, M.; Mason, J. *J. Chem. Soc., Dalton Trans.* **1990**, 283-288. (k) Henderson, R. A.; Leigh, G. J.; Pickett, C. J. *J. Chem. Soc., Dalton Trans.* **1989**, 425-430. (l) Dilworth, J. R.; Morton, S. *Transition Met. Chem.* **1987**, *12*, 41-42. (m) Murray, R. C.; Schrock, R. R. *J. Am. Chem. Soc.* **1985**, *107*, 4557-4558.
- (11) Chatt, J.; Dilworth, J. R.; Richards, R. L. *Chem. Rev.* **1978**, *78*, 589-625.
- (12) (a) Yandulov, D. V.; Schrock, R. R. *Inorg. Chem.* **2005**, *44*, 1103-1117. (b) Weare, W. W.; Dai, X.; Byrnes, M. J.; Chin, J. M.; Schrock, R. R.; Müller, P. *Proc. Natl. Acad. Sci. USA* **2006**, *103*, 17099-17106. Yandulov, D. V.; Schrock, R. R. *Science* **2003**, *301*, 76-78. (c) Yandulov, D. V.; Schrock, R. R. *J. Am. Chem. Soc.* **2002**, *124*, 6252-6253.
- (13) Walsh, P. J.; Carne, M. J.; Bergman, R. G. *J. Am. Chem. Soc.* **1991**, *113*, 6343-6345.
- (14) (a) Tiong, P. J.; Nova, A.; Schwarz, A. D.; Selby, J. D.; Clot, E.; Mountford, P. *Dalton Trans.* **2012**, 2277-2288. (b) Tiong, P. J.; Nova, A.; Clot, E.; Mountford, P. *Chem. Commun.* **2011**, *47*, 3147-3149. (c) Schofield, A. D.; Nova, A.; Selby, J. D.; Schwarz, A. D.; Clot, E.; Mountford, P. *Chem. Eur. J.* **2011**, *17*, 265-285. (d) Selby, J. D.; Feliz, M.; Schwarz, A. D.; Clot, E.; Mountford, P. *Organometallics* **2011**, *30*, 2295-2307. (e) Tiong, P. J.; Nova, A.; Groom, L. R.; Schwarz, A. D.; Selby, J. D.; Schofield, A. D.; Clot, E.; Mountford, P. *Organometallics*, **2011**, *30*, 1182-1201. (f) Tiong, P.-J.; Schofield, A. D.; Selby, J. D.; Nova, A.; Clot, E.;

- Mountford, P. *Chem. Commun.* **2010**, *46*, 85-87. (g) Schofield, A. D.; Nova, A.; Selby, J. D.; Manley, C. D.; Schwarz, A. D.; Clot, E.; Mountford, P. *J. Am. Chem. Soc.* **2010**, *132*, 10484-10497. (h) Clulow, A. J.; Selby, J. D.; Cushion, M. G.; Schwarz, A. D.; Mountford, P. *Inorg. Chem.* **2008**, *47*, 12049-12062. (i) Selby, J. D.; Manley, C. D.; Schwarz, A. D.; Clot, E.; Mountford, P. *Organometallics*, **2008**, *27*, 6479-6494. (j) Selby, J. D.; Schulten, C.; Schwarz, A. D.; Stasch, A.; Clot, E.; Jones, C.; Mountford, P. *Chem. Commun.* **2008**, 5101-5103. (k) Selby, J. D.; Manley, C. D.; Feliz, M.; Schwarz, A. D.; Clot, E.; Mountford, P. *Chem. Commun.* **2007**, 4937-4939.
- (15) (a) Patel, S.; Li, Y.; Odom, A. L. *Inorg. Chem.* **2007**, *46*, 6373-6381. (b) Banerjee, S.; Odom, A. L. *Organometallics* **2006**, *25*, 3099-3101. (c) Li, Y.; Shi, Y.; Odom, A. L. *J. Am. Chem. Soc.* **2004**, *126*, 1794-1803. (d) Cao, C.; Shi, Y.; Odom, A. L. *Org. Lett.* **2002**, *4*, 2853-2856.
- (16) (a) Gehrman, T.; Scholl, S. A.; Fillol, J. L.; Wadepohl, H.; Gade, L. H. *Chem. Eur. J.* **2012**, *18*, 3925-3941. (b) Gehrman, T.; Fillol, J. L.; Scholl, S. A.; Wadepohl, H.; Gade, L. H. *Angew. Chem. Int. Ed.* **2011**, *50*, 5757-5761. (c) Gehrman, T.; Fillol, J. L.; Wadepohl, H.; Gade, L. H. *Organometallics* **2010**, *29*, 28-31. (d) Weitershaus, K.; Wadepohl, H.; Gade, L. H. *Organometallics* **2009**, *28*, 3381-3389. (e) Weitershaus, K.; Fillol, J. L.; Wadepohl, H.; Gade, L. H. *Organometallics*, **2009**, *28*, 4747-4757. (f) Gehrman, T.; Fillol, J. L.; Wadepohl, H.; Gade, L. H. *Angew. Chem. Int. Ed.* **2009**, *48*, 2152-2156. (g) Herrman, H.; Fillol, J. L.; Gehrman, T.; Enders, M.; Wadepohl, H.; Gade, L. H. *Chem. Eur. J.* **2008**, *14*, 8131-8146. (h) Herrmann, H.; Wadepohl, H.; Gade, L. H. *Dalton Trans.*

- 2008**, 2111-2119. (i) Herrman, H.; Gehrman, T.; Wadepohl, H.; Gade, L. H. *Dalton Trans.* **2008**, 6231-6241. (j) Herrman, H.; Fillol, J. L.; Wadepohl, H.; Gade, L. H. *Organometallics* **2008**, *27*, 172-174. (k) Herrmann, H.; Fillol, J. L.; Wadepohl, H.; Gade, L. H. *Angew. Chem. Int. Ed.* **2007**, *46*, 8426-8430.
- (17) Mindiola, D. J. *Angew. Chem. Int. Ed.* **2008**, *47*, 1557-1559.
- (18) Yonke, B. L.; Keane, A. J.; Zavalij, P. Y.; Sita, L. R. *Organometallics* **2012**, *31*, 345-355.
- (19) (a) Tonks, I. A., Durrell, A. C.; Gray, H. B.; Bercaw, J. E. *J. Am. Chem. Soc.* **2012**, *134*, 7301-7304. (b) Tonks, I. A.; Bercaw, J. E. *Inorg. Chem.* **2010**, *49*, 4648-4656. (c) Banerjee, S.; Odom, A. L. *Dalton Trans.* **2008**, 2005-2008. Sebe, E.; Heeg, M. J.; Winter, C. H. *Polyhedron* **2006**, *25*, 2109-2118. Green, M. L. H.; James, J. T.; Saunders, J. F.; Souter, J. *J. Chem. Soc., Dalton Trans.* **1997**, 1281-1288.
- (20) For DFT and experimental studies on effect of N β , see: 1a, 1c, 5e, 5i, 6a, 7g, 14a, b.
- (21) Riley, P. N.; Parker, J. R.; Fanwick, P. E.; Rothwell, I. P. *Organometallics* **1999**, *18*, 3579-3583.
- (22) For reactivity of silanes with a hydrazido, see: 5a, b.
- (23) For silyl azide reagents reacting with a hydrazido, see: 7e, 7f.
- (24) Yu, Y.; Sadique, A. R.; Smith, J. M.; Dugan, T. R.; Cowley, R. E.; Brennessel, W. W.; Flaschenriem, C. J.; Bill, E.; Cundari, T. R.; Holland, P. L. *J. Am. Chem. Soc.* **2009**, *130*, 6624-6638.
- (25) For N β alkylation, see: 1g, 5a, 6a, 1g.

- (26) Ishino, H.; Tokunaga, S.; Seino, H.; Ishii, Y.; Hidai, M. *Inorg. Chem.* **1999**, *38*, 2489-2496.
- (27) Tran, B. L.; Washington, M. P.; Henckel, D. A.; Gao, X.; Park, H.; Pink, M.; Mindiola, D. J. *Chem. Commun.* **2012**, *48*, 1529-1531.
- (28) For studies relating to the structure and electronic properties of the hydrazido ligand, see: 5e, 5i, 6a, 7g.
- (29) (a) Zárata, X.; Schott, E.; Carey, D. M.-L.; Bustos, C.; Arratia-Pérez, R. *J. Mol. Struct. Theochem.* **2010**, *957*, 126-132. (b) George, T. A.; Kaul, B. B.; Chen, Q.; Zubieta, J. *Inorg. Chem.* **1993**, *32*, 1706-1711.
- (30) Yonke, B. L.; Reeds, J. P.; Fontaine, P. P.; Zavalij, P. Y.; Sita, L. R. *Organometallics* **2014**, *33*, 3239-3242.

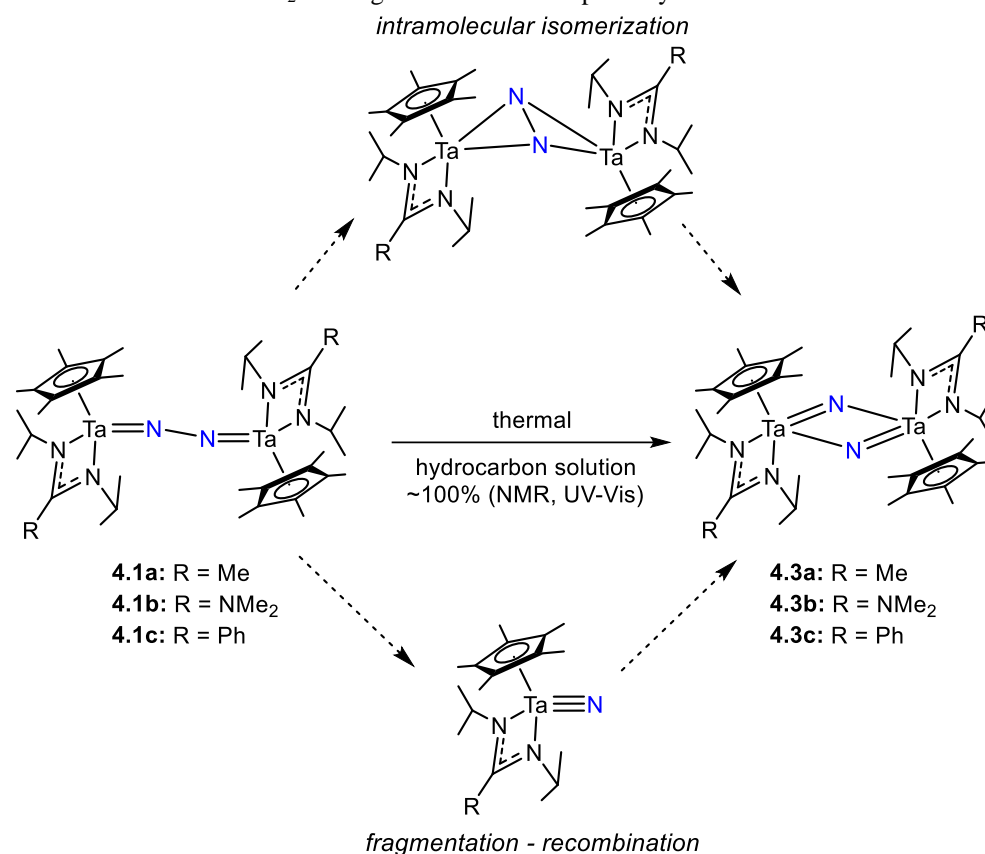
Chapter 4: Group 5 Thermal N₂ Cleavage Studies³

³ Reproduced in part with permission from Keane, A. J.; Yonke, B. L.; Hirotsu, M.; Zavalij, P. Y.; Sita, L. R. *J. Am. Chem. Soc.* **2014**, *136*, 9906-9909. Copyright 2014 American Chemical Society.

4.1. Introduction

Dinitrogen fixation has been an important academic focus in part due to the significant challenge that cleaving dinitrogen presents, but more practically, for taking advantage of the massive resource of N-atoms from nitrogen gas readily available in Earth's atmosphere, which either go unused, or are used at a high energy cost for the production of ammonia.^{1,2} A key challenge for developing N₂ fixation catalysts is to develop systems capable of cleaving the strong N≡N triple bond (bond dissociation energy = 226 kcal/mol). Many important examples of energy efficient dinitrogen cleavage have been documented that include photolytic,³ thermal,⁴ reductive,⁵ ligand-induced,⁶ and hydrosilylation⁷ induced N₂ cleavage.⁹ To date, however, only one report has obtained quantitative data on the activation barrier of N₂ cleavage,^{4b} and is limited to a specific case, lacking robustness towards derivatization of substituents and metals to provide similar chemistry. Recently, our group reported a paramagnetic linear dinitrogen complex, {Cp*Ta[N(ⁱPr)C(Me)N(ⁱPr)]}₂(μ-η¹:η¹-N₂) (**4.1a**), that undergoes thermal N-N cleavage to provide {Cp*Ta[N(ⁱPr)C(Me)N(ⁱPr)](N)}₂ (**4.3a**) and extended this work to the dimethyl amino (**4.1b** and **4.3b**) and phenyl (**4.1c** and **4.3c**) derivatives that also participated in this thermal N-N cleavage chemistry as shown in Scheme 4.1.¹⁰ Interestingly, substitution of the R group located at the distal position of the amidinate led to the qualitative observation that dinitrogen compounds **4.1a-c** have considerably different kinetic stabilities in solution (in order of increasing stability, R = Me, R = NMe₂, and finally R = Ph).¹¹ Mechanistically, these transformations could hypothetically proceed via two routes as depicted in Scheme 4.1: *intramolecular* N-N cleavage, and

Scheme 4.1. Tantalum mediated N₂ cleavage and mechanistic pathways.



fragmentation and recombination involving the production of 2 eq. of Ta nitrides that subsequently recombine to form the final cleaved N₂ compound. It was thus of interest to gain a fundamental understanding of the discrepancies in kinetic stability of compounds **4.1a-c** and obtain a clear picture of the reaction profile for these N₂ cleavage transformations. Further questions also centered around whether other metals in group 5 (Nb and V) would also participate in this N₂ cleavage transformation. This chapter extends the established CPAM Ta N₂ chemistry to the lighter congeners Nb and V and presents the detailed kinetic and mechanistic studies of N₂ cleavage of these compounds that detail the reaction coordinate and free energy barriers for the given transformations.

4.2. Tantalum mediated N-N cleavage

4.2.1. Discussion of structural perturbations of pre-cleaved and cleaved dinitrogen complexes as a function of the amidinate derivative

While **4.1a** (R = Me) crystallizes in the C_{2h} point group, both **4.1b** (R = NMe₂) and **4.1c** (R = Ph) are C_1 symmetric, and have a slightly lesser extent of N₂ activation [N1-N2 = 1.306(5) Å, 1.308(2) Å respectively *vis-à-vis* 1.313(4) Å] with longer Ta1-N1 bond lengths [1.812(5) Å, 1.8111(18) Å respectively *vis-à-vis* 1.807(2) Å]. One clear trend in going from **4.1a** to **4.1b** and **4.1c** is that the Ct-Ta1-Ta2-Ct angle, which is *trans* (180°) for **4.1a**, approaches a staggered orientation in going to **4.1b** and **4.1c** (133.09° and 66.97° respectively). This is largely attributed to the non-bonding sterics between the Cp* and the distal substituent of the amidinate

Table 4.1. Structural parameters for group 5 pre-cleaved and cleaved dinitrogen compounds.¹⁰

	$d(\text{M1-N1})$ (Å)	$d(\text{M2-N1})$ (Å)	$d(\text{N1-N2})$ (Å)	$\angle(\text{M1-N1-N2})$ (°)
4.1a	1.807(2)	-	1.313(4)	172.7(3)
4.1b	1.812(5)	-	1.306(5)	167.2(4)
4.1c	1.8111(18)	-	1.308(5)	175.93(15)
4.2b	1.8230(14)	-	1.300(3)	167.17(17)
4.5	1.7795(11)	-	1.225(2)	166.96(14)
4.3a^a	1.883(3)	1.923(3)	2.563	-
4.3b^a	1.8805(14)	1.9550(14)	2.592	-
4.3c^a	1.9096(17)	1.9188(16)	2.619	-
4.4a^b	1.8959(18)	1.9133(18)	2.561	-
4.4b^b	1.8895(12)	1.9192(12)	2.583	-

^a*trans* isomer, ^b*cis* isomer.

on the proximal metal center, which is highlighted by the spacefill models of **4.1a-c** in . Similar to thermal N₂ cleavage of **4.1a** that produces **4.3a**, both **4.1b** and **4.2c** were found to readily cleave dinitrogen to produce **4.3b** and **4.3c**. The dimethylamino (**4.3b**) and phenyl (**4.3c**) derivatives of the cleaved dinitrogen compound only had small effects on the core Ta₂N₂ geometry, with **4.3b** having a slightly more asymmetrical core [Ta1-N1 = 1.9550(14) Å, Ta1-N1A = 1.8805(14) Å] compared to **4.3a** [Ta1-N1 = 1.923(3) Å, Ta1-N1A = 1.883(3) Å], while **4.3c** has a

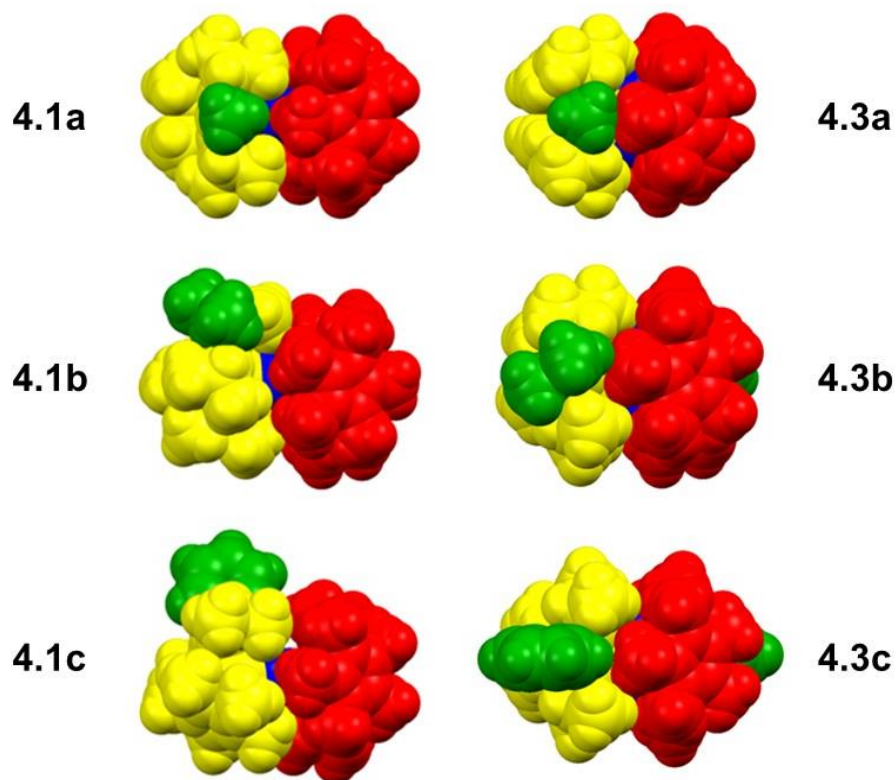


Figure 4.1. Spacefill models for (left column) pre-cleaved **4.1a-c** and (right column) cleaved *trans* **4.3a-c** with view of red Cp* remaining constant.

more symmetrical core [Ta1-N1 = 1.9188(16) Å, Ta1-N1A = 1.9096(17) Å]. The largest effects of the dimethylamino and phenyl derivatives are again found with non-bonding steric interactions between the R group and the Cp* on the proximal Ta center. While **4.1b** and **4.1c** are able to rotate to relieve this strain, **4.3b** and **4.3c** are

both locked in the *trans* orientation, which maximizes the steric interaction. This effect is observed by the deflection of the R group away from the nearby Cp* ligand for **4.3b** and **4.3c** [Ta1-C10-N13 = 177.61° (**4.3b**), Ta1-C20-C21 = 173.39° (**4.3c**) *vis-à-vis* Ta1-C1-C2 = 163.35° (**4.3a**)] as shown by the spacefill models in Figure 4.1.

4.2.2. Kinetic and mechanistic studies regarding N₂ cleavage

Surprisingly, while **4.1a-c** only differ slightly in distal amidinate substituents, they were previously found to widely vary in thermal stability.¹² To investigate this feature and further explore the reaction profiles, temperature and concentration dependent kinetics were obtained. For each N₂ cleavage reaction (**4.1a-c** to **4.3a-c**), conversion of dark purple solutions of the pre-cleaved N₂ compounds to their corresponding yellow cleaved compounds were followed at 625 nm using UV-vis spectroscopy. Concentration dependent kinetics and initial rate studies confirmed the 1st order nature of these transformations and the rate constants were invariant over the concentrations studied for all three derivatives.¹³ For temperature dependent studies, five data points were measured in triplicate for each derivative with varying temperature ranges (40 – 60 °C for **1**, 55 – 80 °C for **2**, and 70 – 95 °C for **3**). The average rate constants were plotted versus temperature and fit to the Eyring equation, $k = (k_B T/h) \exp(\Delta S^\ddagger/R) \exp(-\Delta H^\ddagger/RT)$, as shown in Figure 4.4. Activation parameters were extracted from the Eyring fit and are presented in Table 4.2. While the novelty of obtaining several derivatives that maintain similar N₂ cleavage chemistry and can be kinetically followed is substantial, more importantly, the ability to tune the free energy barrier for N₂ cleavage and obtain quantitative kinetic data on the reaction coordinate is currently unprecedented for any known N₂ cleavage system. To begin,

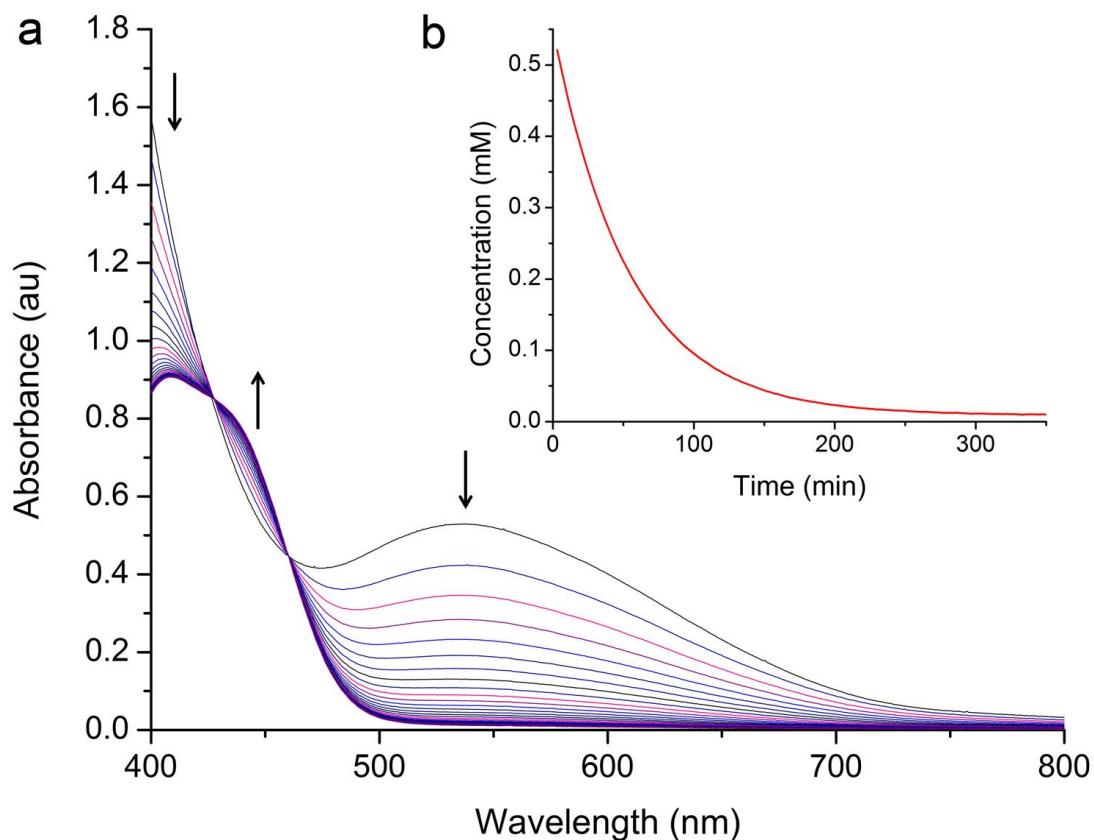


Figure 4.2. (a) Scanning UV-vis spectroscopy for $(^{15}\text{N}_2, 98\%)\text{-4.1a} \rightarrow (^{15}\text{N}_2, 98\%)\text{-4.3a}$ at $T = 318.15$ K. (b) Kinetic analysis of $[\text{4.1a}]_t$ vs. time as monitored at $\lambda = 625$ nm.

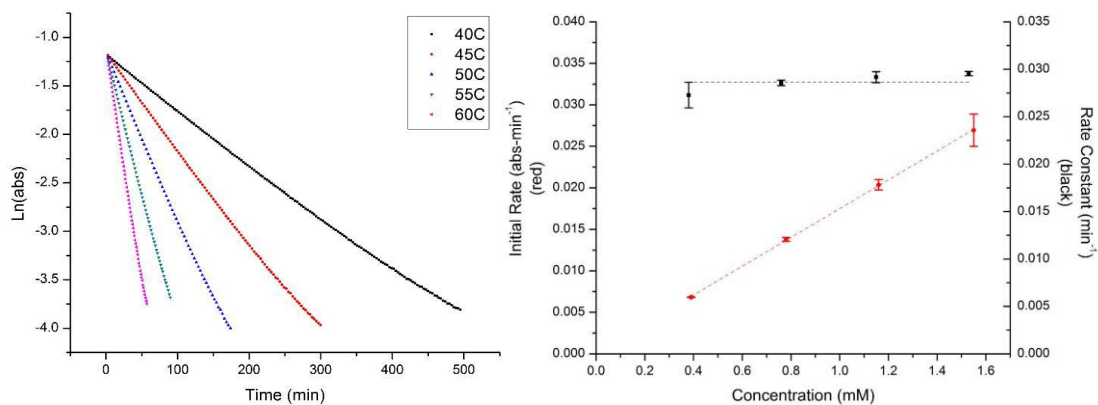


Figure 4.3. (left) temperature dependent first order $\ln(A) = -kt + A_0$ plots for the conversion of $(^{15}\text{N}_2, 98\%)\text{-4.1a}$ to $(^{15}\text{N}_2, 98\%)\text{-4.3a}$ and (right) concentration dependence of rate constants and initial rates for the conversion of $(^{15}\text{N}_2, 98\%)\text{-4.1a}$ to $(^{15}\text{N}_2, 98\%)\text{-4.3a}$.

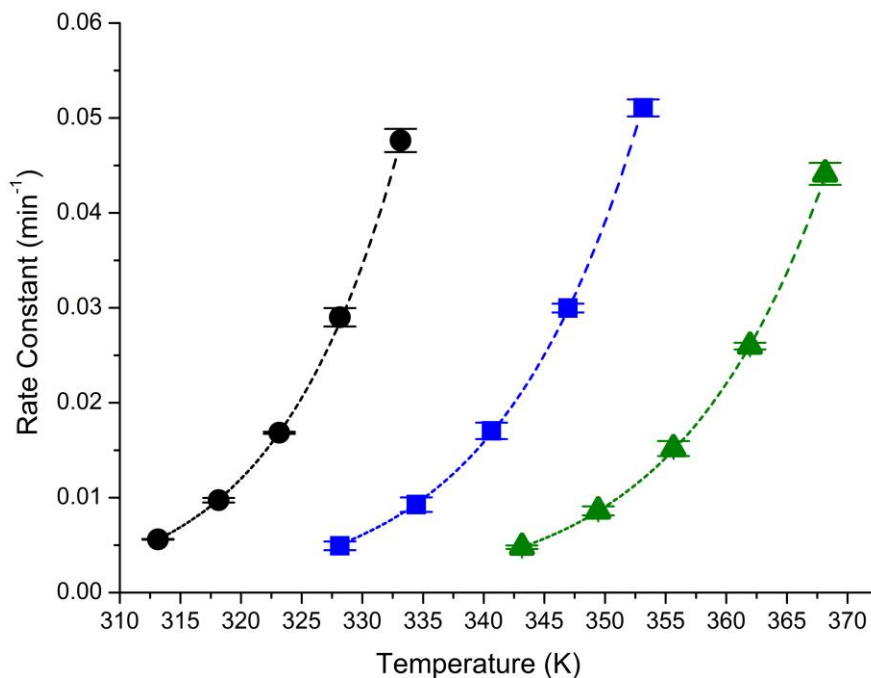


Figure 4.4. Temperature-dependent first-order rate constants with least-squares fit to the Eyring equation, $k = (k_B T/h) \exp(\Delta S^\ddagger/R) \exp(-\Delta H^\ddagger/RT)$, for the conversion of **4.1a** to **4.3a** (circle), **4.1c** to **4.3c** (square) and **4.1b** to **4.3b** (triangle).

the experimental values for ΔG^\ddagger are consistent with the qualitative trends in kinetic stability of **4.1a-c** [$\Delta G^\ddagger(338.15 \text{ K}) = 24.3(3)$, $25.5(3)$, and $26.6(3)$ kcal/mol for **4.1a**, **4.1b**, and **4.1c** respectively]. Interestingly, all ΔS^\ddagger values are negative, which indicates a contraction of the dinuclear core in the rate determining step. As shown in Table 4.2, the greatest contributing factor for the increase in ΔG^\ddagger of **4.1b** and **4.1c** versus **4.1a** is from the large *ca.* 6 cal/mol-K decrease in ΔS^\ddagger for NMe₂ and Ph derivatives [$\Delta S^\ddagger = -8.4(9)$, $-14.6(8)$, and $-14.4(8)$ cal/mol-K for **4.1a**, **4.1b**, and **4.1c** respectively]. This decrease in ΔS^\ddagger is attributed to the higher order required to reach a contracted transition state for the NMe₂ and Ph derivatives, which originates from increased non-bonding sterics of the R group and the Cp* on the proximal Ta metal center (*vide supra*). While **4.1b** and **4.1c** have similar ΔS^\ddagger values (and comparatively similar sterics), **4.1b** has the lowest ΔH^\ddagger compared to both **4.1a** and **4.1c**

Table 4.2. Experimentally-derived activation parameters for thermal conversion of **4.1a-c** to **4.3a-c**.

	ΔG^\ddagger (kcal/mol) ^{a,b}	ΔH^\ddagger (kcal/mol) ^b	ΔS^\ddagger (cal/mol-K) ^b
4.1a	24.3(3)	21.5(3)	-8.4(9)
4.1a (¹⁵ N ₂)	24.4(2)	21.8(2)	-7.4(6)
4.1b	25.5(3)	20.6(3)	-14.6(8)
4.1c	26.6(3)	21.7(3)	-14.4(8)
4.2b	24.4(1)	20.2(1)	-12.4(5)

^acalculated at 338.15K, ^berror reported at the 95% confidence interval.

[$\Delta H^\ddagger = 20.6(3)$ kcal/mol for **4.1b** *vis-à-vis* 21.5(3) and 21.7(3) kcal/mol for **4.1a** and **4.1c**]. Indeed, electronic factors may come into play as **4.1b** has the most electron rich derivative, NMe₂, which can further stabilize a transition state with increased positive charge [*i.e.* Ta(V), Ta(V)] relative to the alkyl and phenyl substituents of **4.1a** and **4.1c**.

4.2.3. Kinetic isotope effects and crossover experiments

With access to the ¹⁵N₂ version of **4.1a**, kinetic isotope effects (KIEs) were pursued. Experimental Eyring values for **4.1a**-¹⁵N₂ were measured in the same fashion as **4.1a**, which yielded activation parameters $\Delta G^\ddagger(338.15\text{ K}) = 24.4(2)$ kcal/mol, $\Delta H^\ddagger = 21.8(2)$ kcal/mol, and $\Delta S^\ddagger = -7.4(6)$ cal/mol-K. Theoretically, the KIE value, $k(^{14}\text{N}_2/^{15}\text{N}_2)$, for thermal dissociation of N₂ and alkyl nitrenes is 1.21 and 1.14 respectively at 298 K.¹² Experimental data obtained for Cummins' system yielded a KIE of 1.15, which was rationalized as a primary KIE for complete N-N scission.¹² A small isotopic effect [$k(^{14}\text{N}_2/^{15}\text{N}_2) = 1.03(3)$] was measured at 318.15 K for our CPAM mediated system. This small KIE indicates that N-N scission is not part of the rate determining step - rather, a shift in coordination and/or slight

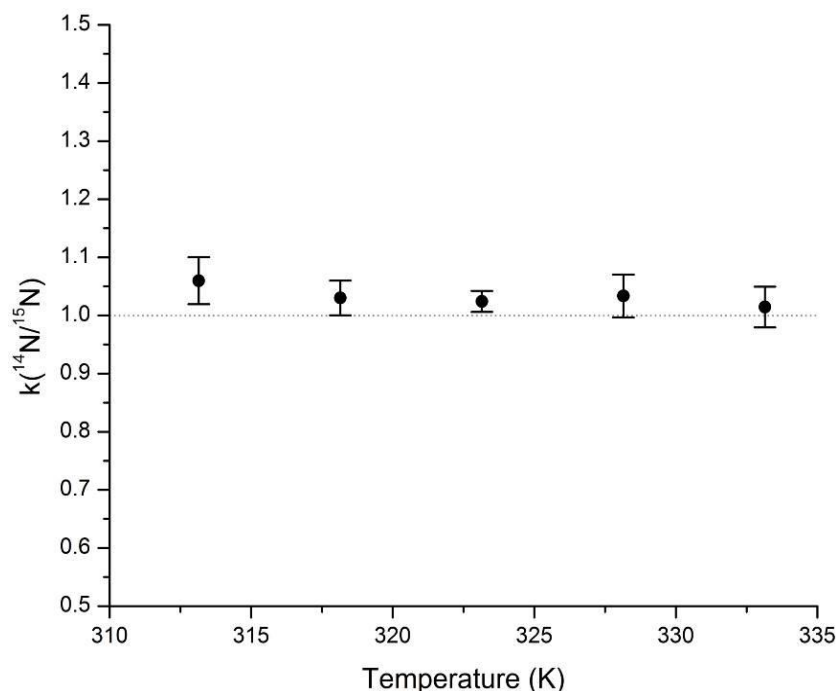


Figure 4.5. Kinetic isotope effect $k(^{14}\text{N})/k(^{15}\text{N})$ for the conversion of **4.1a** to **4.3a**.

activation of the N_2 ligand is taking place. At this point, valuable insights into the N_2 cleavage reaction profile have been obtained. The negative ΔS^\ddagger values and small KIEs support the *intramolecular* mechanism particularly well; however, *fragmentation and recombination* could still theoretically fit the reaction profile (*e.g.* the negative ΔS^\ddagger values and small $^{14}\text{N}_2/^{15}\text{N}_2$ KIE would indicate that the rate determining step is contracted and occurs prior to any significant N-N cleavage and fragmentation). To make a distinction between these two mechanisms, crossover experiments were employed. Specifically, a concentrated mixture of **4.1a** and **4.1b** was heated to 80 °C in THF and the products were analyzed by ESI-MS. Compounds **4.3a** and **4.3b** have $[\text{M} + \text{H}]^+$ values of 943.21 and 1001.26 m/z respectively and the theoretical crossover product, $\{\text{Cp}^*\text{Ta}[\text{N}(\text{iPr})\text{C}(\text{Me})\text{N}(\text{iPr})]\}\{\text{Cp}^*\text{Ta}[\text{N}(\text{iPr})\text{C}(\text{NMe}_2)\text{N}(\text{iPr})]\}(\mu\text{-}\eta^1\text{:}\eta^1\text{-N}_2)$, has a theoretical value of 972.25 m/z. ESI-MS of the crude product mixture revealed the

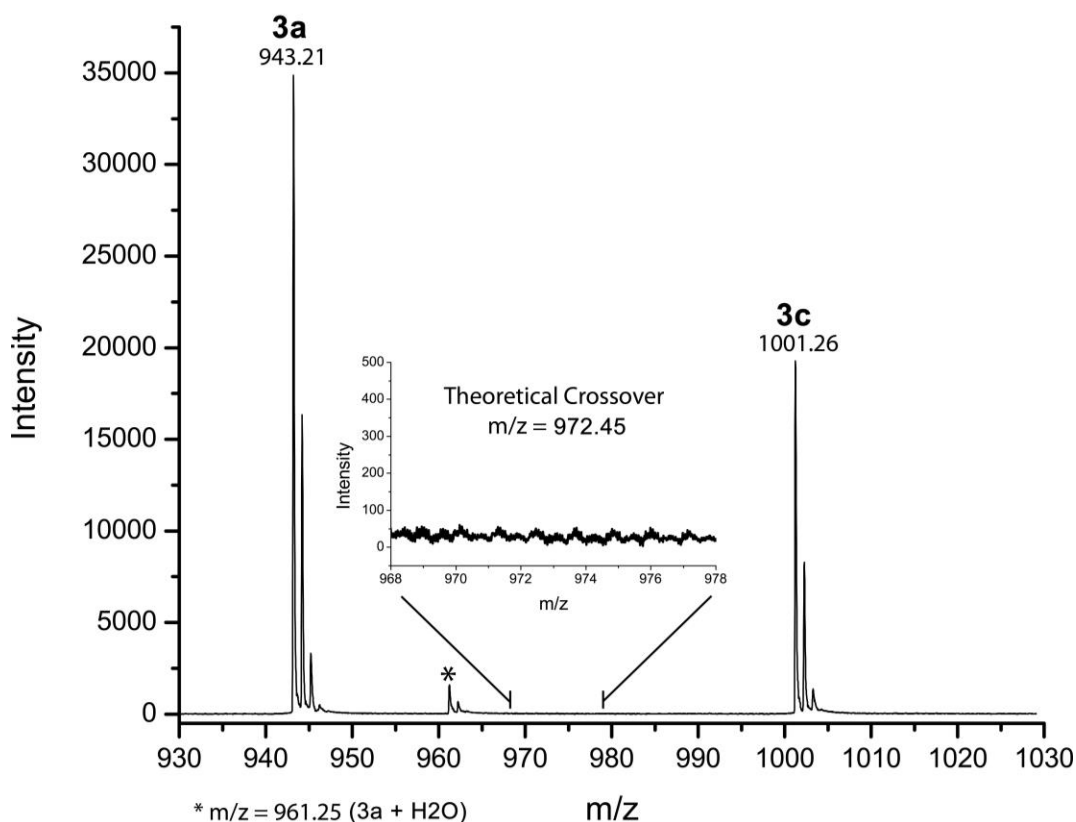
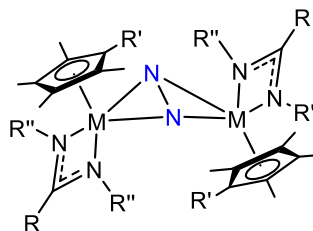


Figure 4.6. Crossover study: ESI-MS (positive ion mode) of products from heating a mixture of **4.1a** and **4.1b** in THF for 3.5 h. No theoretical crossover product was observed.

presence of non-crossover products **4.3a** and **4.3b** with the absence of a crossover product as shown in Figure 4.6. This indicates that the system does not undergo fragmentation to produce mononuclear nitrides under the conditions studied; rather, it proceeds through an *intramolecular isomerization* mechanism.

Cummins' and co-workers have established that their Mo trisanilide dinitrogen complex proceeds through a 'zig-zag' transition state.^{4b} For the present system, we have proposed a contracted, $\eta^2:\eta^2\text{-N}_2$ bridging state transition state, which is mainly based on group 4 CPAM side-bound dinitrogen compounds (Figure 4.7).¹³ The metals in these dinuclear complexes only have four electrons to donate into the N_2 ligand $[\text{M}(\text{IV}, d^0), [\text{N}_2]^{4-}]$, which falls short of the six electron requirement to



- a:** M = Zr; R = NMe₂; R' = Me; R'' = ⁱPr; *d*(NN) = 1.518(2) Å
b: M = Hf; R = NMe₂; R' = Me; R'' = ⁱPr; *d*(NN) = 1.581(4) Å
c: M = Hf; R = NMe₂; R' = H; R'' = ⁱPr; *d*(NN) = 1.600(6) Å
d: M = Hf; R = Me; R' = Me; R'' = ⁱPr; *d*(NN) = 1.611(4) Å
e: M = Hf; R = Me; R' = H; R'' = ⁱPr; *d*(NN) = 1.630(4) Å
f: M = Hf; R = Me; R' = Me; R'' = Et; *d*(NN) = 1.635(5) Å

Figure 4.7. Structural parameters for group 4 side-bound dinitrogen complexes.

formally cleave N₂ by populating its σ^* and 2 π^* orbitals. Therefore, these complexes can be viewed as arrested transition states that fall along the pathway to hypothetical N₂ cleavage if sufficient electrons were to be present. As displayed in Figure 4.7, N₂ activation increases with decreasing sterics of the amidinate and Cp* ligand as demonstrated by *d*(NN) bond lengths. The increased N₂ activation with smaller substituents in these complexes compares favorably to the kinetic studies of Ta mediated N₂ cleavage, where less bulky substituents decrease the free energy barrier to N₂ cleavage.

Indeed, Musaev has computationally studied our system using the stripped $\{(C_5H_5)Ta[N(Me)C(H)N(Me)]\}_2(\mu-\eta^1:\eta^1-N_2)$ framework and predicted that the reaction profile follows a dimeric pathway with the calculated rate determining step involving side-on, end-on N₂ bonding ($\mu-\eta^1:\eta^2-N_2$) shifting to side-on, side-on N₂ bonding ($\mu-\eta^2:\eta^2-N_2$) with concomitant activation of N₂.¹⁴ This predicted rate determining transition state is consistent with the small, experimentally observed secondary kinetic

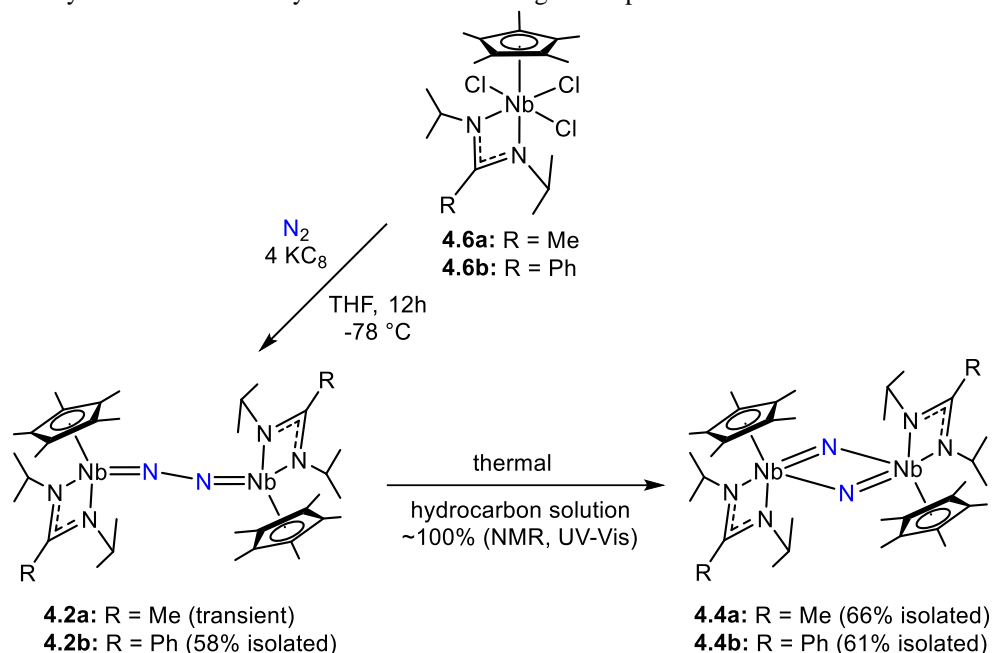
isotope effects and the predicted reaction coordinate compares favorably with other experimental mechanistic studies presented in this chapter.

4.3. CPAM Niobium Mediated N₂ cleavage

4.3.1. Development of a well-defined Nb N₂ cleavage system

Having analyzed the reaction profiles for Ta mediated N₂ cleavage, we were curious as to whether other metals in group 5 (Nb and V) would engage in similar N₂ cleavage chemistry. CPAM Niobium trichloride precursor, using the same Cp* amidinate ligand framework with a methyl group as the distal substituent (R = Me), was reduced with 4 eq. of KC₈ in THF solution employing a similar procedure to its previously described Ta analogue. While carefully maintaining ~ -20 °C during work-up, only diamagnetic products were observed by ¹H-NMR. Crystallization of the product in minimal pentane at -30 °C yielded orange single crystals, which were subsequently analyzed by XRD. The analysis revealed that indeed niobium can participate in the same N₂ cleavage process to produce the bis(μ-N) product **4.4a**. Furthermore, the inability to observe or isolate any paramagnetic pre-cleaved N₂ complex **4.2a** indicated that the activation barrier to N₂ cleavage is substantially lower for Nb. It was therefore of interest to pursue a kinetically stabilized version of **4.2a** to establish a well-defined process for Nb mediated N₂ cleavage that would be amenable to kinetic studies. Using lessons learned from substituent effects for Ta regarding kinetic stability (*vide supra*), the phenyl derivative was targeted to achieve this desired result. Gratifyingly, reducing the Nb trichloride precursor employing a phenyl group as the distal substituent (R = Ph) yielded dark green crystals that were

Scheme 4.2. Synthesis and reactivity of CPAM Nb dinitrogen complexes.



identified by XRD to be the end-on bridging N_2 compound **4.2b**. Compound **4.2b** bears some similarities to **4.1a** as they both crystallize in the C_{2h} point group. This is, however, a departure from the solid state structure of the pre-cleaved Ta N_2 complex (R = Ph) **4.3a**, which adopts a staggered C_1 symmetric conformation as opposed to the C_{2h} anti conformation of **4.1a** and **4.2b**. Compared to **4.1c**, **4.2b** has a further activated N_2 moiety with an N1-N2 bond length of 1.300(3) Å (*vis-à-vis* 1.308(2) Å for **4.1c**) and a slightly longer metal nitrogen bond length, Nb1-N1 = 1.8230(14) Å (*vis-à-vis* Ta1-N1 = 1.8111(18) for **4.1c**). Monitoring by ^1H NMR, paramagnetic resonances of **4.2b** were observed to convert into a single diamagnetic, C_{2h} symmetric product after heating to 60 °C for 2.5 h.¹⁵ Elemental analysis and single crystal XRD confirmed the identity of the product to be the cleaved N_2 complex **4.4b**, which has comparable M-N bond lengths to the Ta cleaved N_2 compounds [Nb1-N1 = 1.9192(12) Å and Nb1-N1A = 1.8895(12) Å].

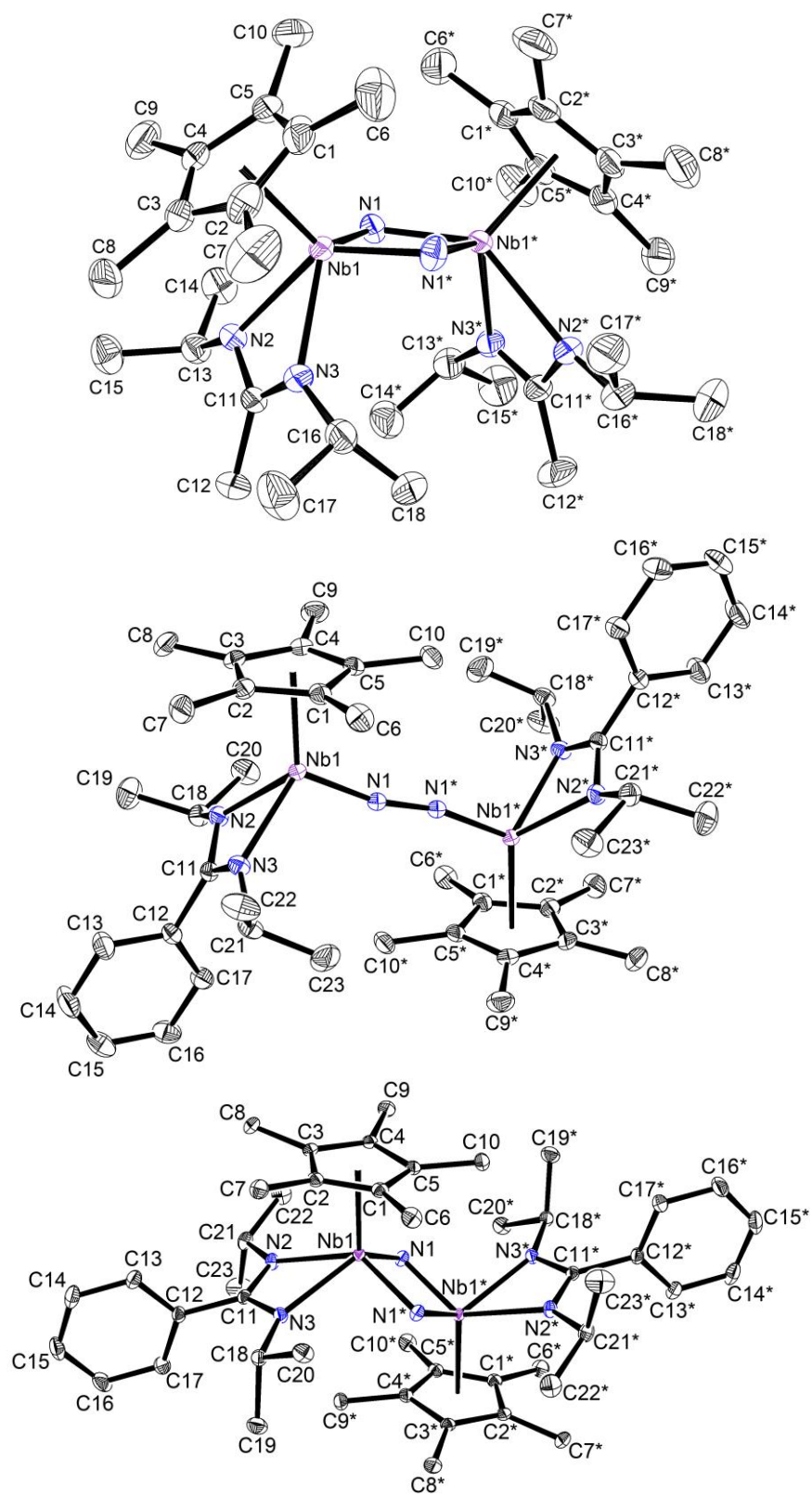


Figure 4.8. Molecular structures (30% thermal ellipsoids) of (top) **4.4a**, (middle) **4.2b** and (bottom) **4.4b**. Hydrogen atoms have been removed for the sake of clarity.

4.3.2. Niobium mediated N₂ cleavage kinetics

Having now established a well-defined Nb-mediated N₂ cleavage system, quantitative kinetic data was obtained in order to directly compare the Ta/Nb mediated N₂ cleavage systems. Temperature dependent rate constants for the conversion of olive green **4.2b** to orange **4.4b** were obtained within the range of 40 °C and 60 °C using UV/Vis spectroscopy by monitoring absorbance data at 625 nm. These rate constants were fit to the Eyring equation, $k = (k_B T/h) \exp(\Delta S^\ddagger/R) \exp(-\Delta H^\ddagger/RT)$, and the resulting activation parameters are presented in Table 4.2. Interestingly, the conversion of **4.2b** to **4.4b** nearly mimics the kinetics for the conversion of **4.1a** to **4.1c** (M = Ta, R = Me) in the temperature range studied, which is also indicated by their similar $\Delta G^\ddagger(338.15K)$ values of 24.4(1) and 24.3(3) kcal/mol respectively. Comparing to the more closely related conversion of **4.1c** to **4.3c** (M = Ta, R = Ph), Nb-mediated **4.2b** to **4.4b** has a lower free energy of activation [$\Delta G^\ddagger(338.15K) = 26.6(3)$ kcal/mol for **3** to **6**]. The ΔS^\ddagger value for the conversion of **4.2b** to **4.4b** (-12.4 cal/mol-K) is relatively large and negative, albeit slightly less negative than the ΔS^\ddagger value for the conversion of **4.1c** to **4.3c** (-14.4(8) cal/mol-K). However, the most significant contribution to the 2.2 kcal/mol decrease of $\Delta G^\ddagger(338.15K)$ for Nb is the 1.5 kcal/mol decrease in the enthalpic barrier for **4.1c** to **4.3c** vs. **4.2b** to **4.4c** (21.7(3) and 20.2(1) kcal/mol respectively). These results confirm that niobium does indeed have an intrinsically lower barrier to N₂ cleavage relative to tantalum, and that the phenyl group is critical to obtaining a kinetically stabilized, pre-cleaved Nb N₂ complex (**4.2b**).

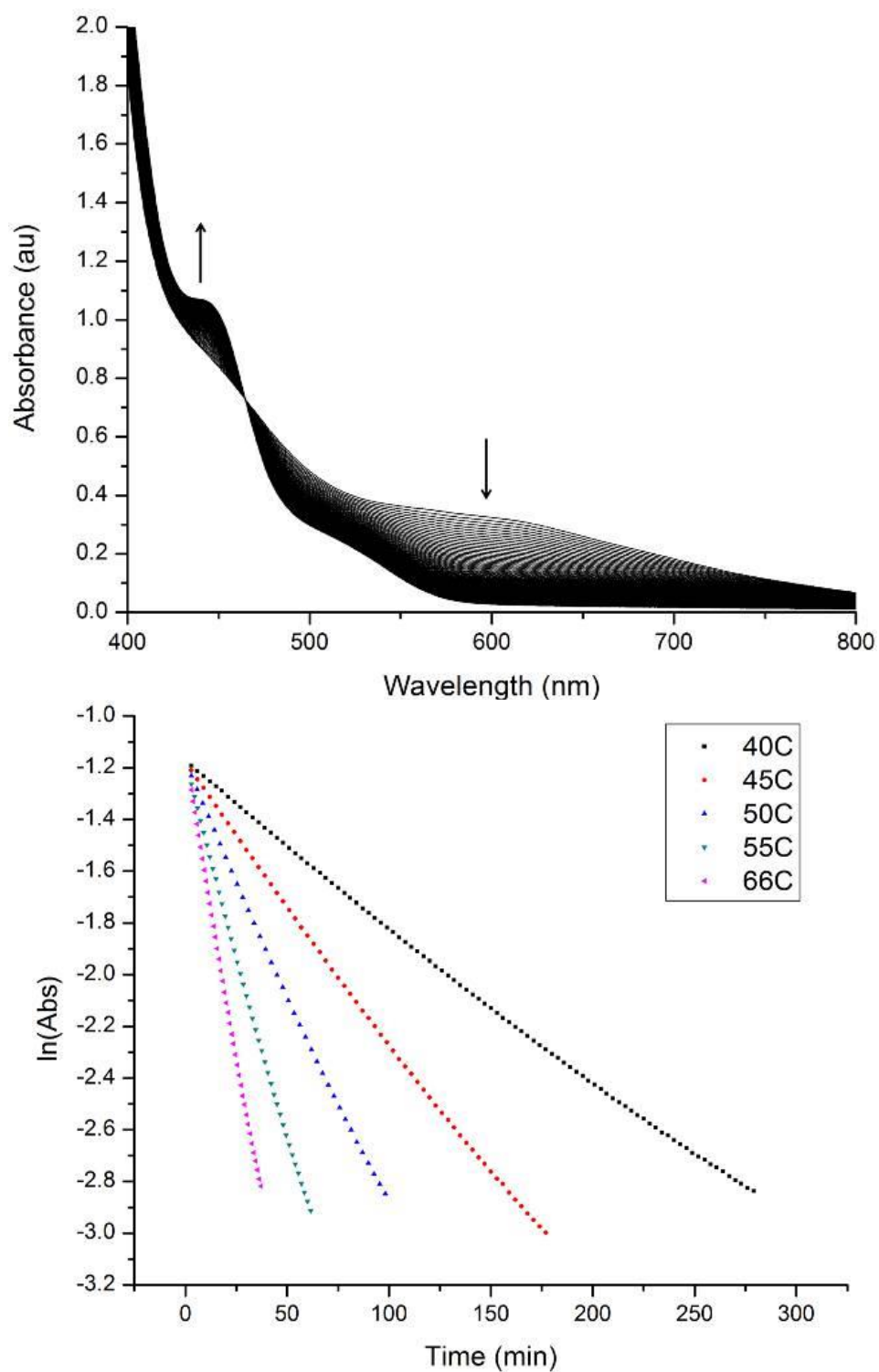


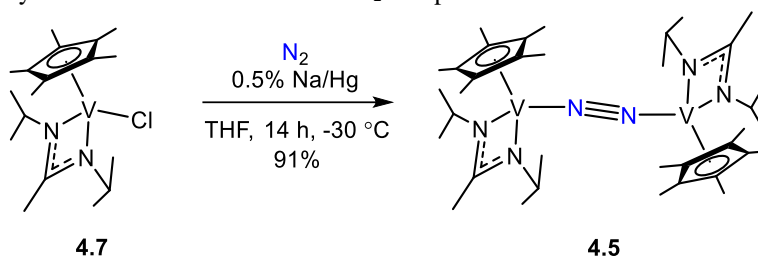
Figure 4.9. (top) Scanning UV-vis spectroscopy for **4.2b** \rightarrow **4.4b** ($T = 338.15$ K, $\Delta t = 3$ min) and (bottom) temperature dependent first order $\ln(A) = -kt + A_0$ plots for the conversion of **4.2b** to **4.4a**.

4.4. CPAM Vanadium N₂ chemistry

4.4.1. Synthesis and reactivity of a CPAM vanadium N₂ complex

To complete the survey of group 5 mediated N₂ cleavage, the vanadium derivative **4.5** was synthesized in a straight-forward manner by reducing the CPAM V(III) monochloride precursor (**4.7**) with sodium amalgam in the presence of N₂. The isolation of **4.5** was unequivocally

Scheme 4.3. Synthesis of a CPAM vanadium N₂ complex.



established by single crystal XRD and elemental analysis, with structural parameters involving shorter metal nitrogen bond lengths (V1-N1 = 1.7795(11) Å) compared to both Ta and Nb, along with a shorter N1-N1a bond length of 1.225(2) Å relative to both Ta and Nb. While reactivity under elevated temperatures or photolytic conditions would either imply N-N cleavage (*vide supra*) or N₂ extrusion,¹⁶ no

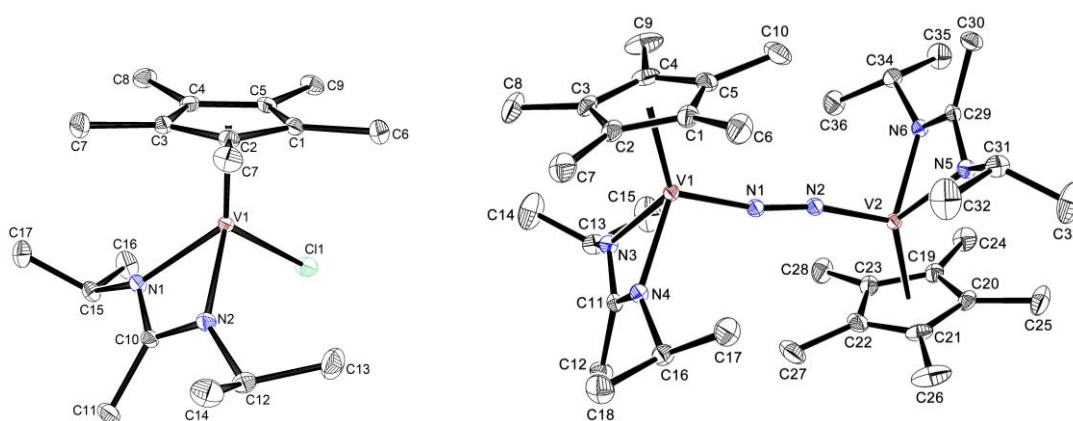


Figure 4.10. Molecular structures (30% thermal ellipsoids) of (left) **4.7** and (right) **4.5**. Hydrogen atoms have been removed for the sake of clarity.

change was observed by ^1H NMR after heating a solution of **4.5** in C_6D_6 at 95°C for 14 h or exposing to UV light for 4 h. A mismatch in V d and N_2 π^* orbitals (as indicated by the shorter N-N bond) as well as differing electronic states compared to **4.1a-c**, **4.2a** and **4.2b** could be prohibitive to N_2 cleavage taking place.¹⁶

Reactivity studies were pursued to further probe the nature of N_2 bonding of **4.5** as well gain a general understanding of its chemical reactivity. Considering the poorly activated N_2 ligand of **4.5** as manifested by the N1-N1a bond of $1.225(2)$ Å, it was suspected that this compound might participate in N_2 displacement chemistry

Scheme 4.4. CPAM vanadium N_2 displacement chemistry.

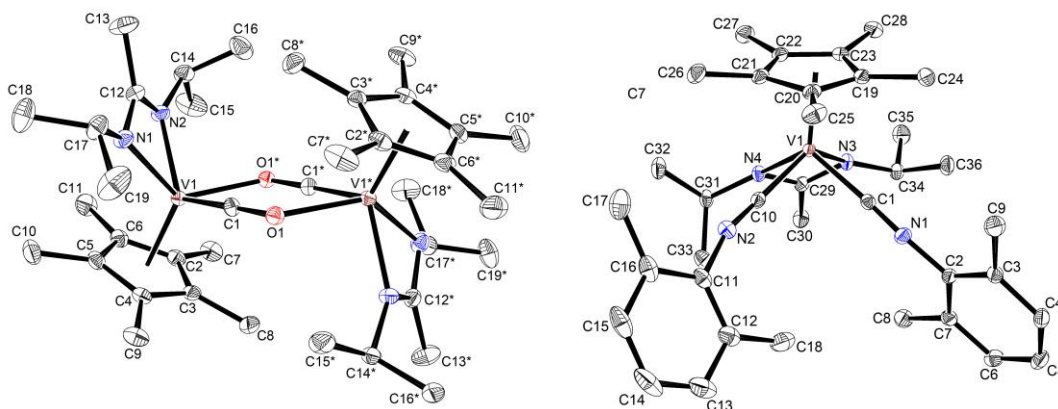
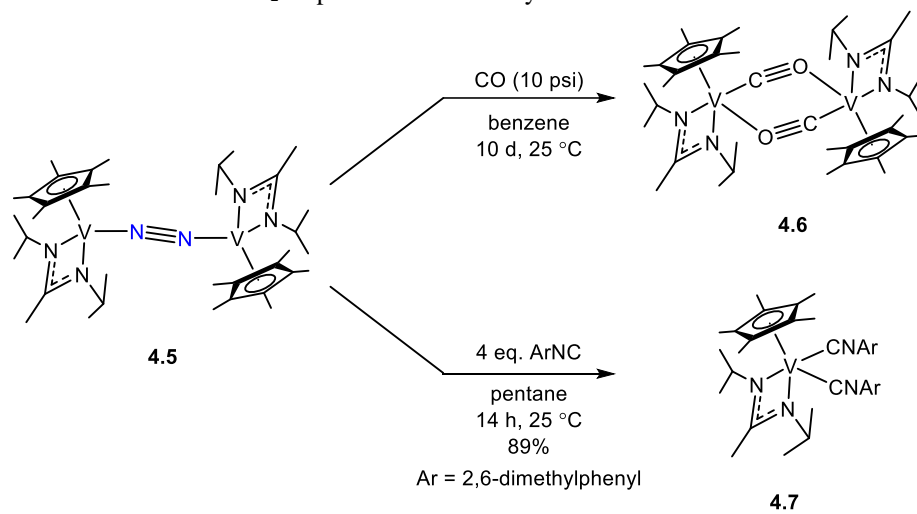


Figure 4.11. Molecular structures (30% thermal ellipsoids) of (left) **4.6** and (right) **4.7**. Hydrogen atoms have been removed for the sake of clarity.

similar to group 6 (Mo and W) CPAM dinitrogen complexes that readily react with CO and isocyanide reagents to provide bis-carbonyl and bis-isocyanide complexes respectively. Indeed, as depicted in Scheme 4.4, **4.5** reacted with both CO and 2,6-dimethylphenyl isocyanide to provide the dinuclear carbonyl compound **4.6** and the mononuclear bis-isocyanide compound **4.7**.

4.5. Conclusion

In summary, kinetic and mechanistic studies regarding thermal Ta-mediated dinitrogen cleavage involving previously established pre-cleaved dinitrogen compounds **4.1a-c** and cleaved dinitrogen compounds **4.3a-c** were undertaken. Crossover experiments established the *intramolecular isomerization* pathway while temperature and concentration dependent kinetics provided quantitative data on the reaction profiles. It was discovered that small perturbations in the amidinate framework had large effects on the kinetic stability of **4.1a-c**. These studies were extended to Nb, which displayed much lower kinetic stability of pre-cleaved dinitrogen complexes relative to Ta and required using a bulky amidinate (R = Ph) to successfully isolate a pre-cleaved Nb dinitrogen compound (**4.2b**). Temperature dependent kinetics were also acquired for this Nb analogue and compared with values obtained for Ta. These comparisons led to the conclusion that Nb has an intrinsically lower barrier for N₂ cleavage. The vanadium analogue did not display thermal nor photochemical N₂ cleavage; however it was demonstrated that **4.5** was a valuable V(II) synthon where N₂ was displaced to provide isocyanide and carbonyl compounds (**4.6** and **4.7**). Collectively, these results demonstrate the

robustness of the CPAM ligand framework towards developing group 5 N₂ cleavage chemistry while also establishing the ability to fine-tune the energy barrier for thermal N₂ cleavage based on the identity of the amidinate and metal employed.

4.6. Experimental Section

4.6.1. General considerations

All manipulations with air and moisture sensitive compounds were carried out under N₂ or Ar atmospheres with standard Schlenk or glovebox techniques. All solvents were dried (Na for toluene and Na/benzophenone for pentane, Et₂O, and THF) and distilled under N₂ prior to use. Benzene-*d*₆, toluene-*d*₈ and methylcyclohexane were dried over Na/K alloy and isolated by vacuum transfer prior to use. Celite was oven dried (150 °C for several days) prior to use. Cooling was performed in the internal freezer of a glovebox maintained at -30 °C. N,N'-diisopropylcarbodiimide, PhLi (1.8M in *n*-butylether), LiNMe₂, MeLi, and methylcyclohexane (spectrophotometric grade) were purchased from Sigma-Aldrich, Cp*TaCl₄ and NbCl₅ were purchased from Strem Chemicals, and ¹⁵N₂ (98% ¹⁵N enriched) was purchased from Cambridge Isotope Laboratories. All purchased chemicals were used as received unless otherwise noted. Compounds **4.1a-c**, **4.3a-c**, **4.1a-¹⁵N₂**,¹⁰ Cp*NbCl₄¹⁷ and [Cp*V(μ-Cl)₂]₃¹⁸ were prepared according to previously reported procedures in similar yield and purity. ¹H NMR spectra were recorded at 400.13 MHz and referenced to SiMe₄ using residual ¹H chemical shifts of *d*₆-benzene. Mass spectrometry measurements were performed on a JEOL AccuTOF-CS mass

spectrometer using electrospray ionization. Elemental analyses were carried out by Midwest Microlab, LLC.

4.6.2. Synthesis of new compounds

{Cp*Nb[N(ⁱPr)C(Ph)N(ⁱPr)]}₂(μ-η¹:η¹-N₂) (4.2b). Compound **7b** (148 mg, 0.28 mmol) and KC₈ (151 mg, 1.11 mmol) were placed in a storage tube with a Teflon valved stopper under an argon atmosphere. The storage tube was evacuated and cooled to -196 °C with 10 mL of THF added to the storage tube by vacuum transfer. The tube was charged with dinitrogen (~1 atm) at -196 °C, sealed, and warmed to -78 °C. After stirring at -78 °C for 12 h, the reaction was allowed to warm to 0 °C and stirred for 1 h. Volatiles were removed *in vacuo* at 0 °C to give a black solid. The solid residue was extracted with -30 °C pentane and immediately filtered through a dry pad of Celite on a glass frit. The filtrate was concentrated and cooled to -30 °C to give black crystals of **2b** (71 mg, 58% yield). Anal. calc'd for C₄₆H₆₈N₆Nb₂: C, 62.02; H, 7.69; N, 9.43; Found: C, 62.25; H, 7.62; N, 9.31.

{Cp*Nb[N(ⁱPr)C(Me)N(ⁱPr)](μ-N)}₂ (4.4a). Compound **7a** (100 mg, 0.21 mmol) and KC₈ (114 mg, 0.84 mmol) were placed in a storage tube with a Teflon valved stopper under an argon atmosphere. The storage tube was evacuated and cooled to -196 °C with 10 mL of THF added to the storage tube by vacuum transfer. The tube was charged with dinitrogen (~1 atm) at -196 °C, sealed, and warmed to -78 °C. After stirring at -78 °C for 10 h, the reaction was allowed to warm to 0 °C and stirred for 1 h. Volatiles were removed *in vacuo* to give a black solid. The solid residue was extracted with -30 °C pentane and immediately filtered through a dry pad of Celite

on a glass frit. Volatiles were removed *in vacuo*, and crude NMR revealed a mixture of *cis/trans*-**4.4a** had formed. Crystallization of the mixture with minimal pentane at -30 °C led to the isolation of orange crystals of *cis*-**4.4a**, along with *trans*-**4.4a** (52.4 mg, 66% yield). ¹H NMR (benzene-*d*₆): (*cis*-**4a**) δ 1.17 (6H, d, *J* = 7.0 Hz, CH(CH₃)₂), 1.34 (6H, d, *J* = 6.8 Hz, CH(CH₃)₂), 1.66 (3H, s, N(^{*i*}Pr)C(CH₃)N(^{*i*}Pr)), 2.09 (15H, s, C₅(CH₃)₅), 3.45 (1H, sept, *J* = 6.8 Hz, CH(CH₃)₂). (*trans*-**4a**) δ 1.18 (6H, d, *J* = 6.4 Hz, CH(CH₃)₂), 1.44 (6H, d, *J* = 6.4 Hz, CH(CH₃)₂), 1.65 (3H, s, N(^{*i*}Pr)C(CH₃)N(^{*i*}Pr)), 2.10 (15H, s, C₅(CH₃)₅), 3.50 (1H, sept, *J* = 6.4 Hz, CH(CH₃)₂).

{Cp***Nb**[N(^{*i*}Pr)C(Ph)N(^{*i*}Pr)](μ-N)}₂ (**4b**). A solution of **2b** (49 mg, 0.05 mmol) in 1 mL of benzene was transferred into a J Young tube with a teflon stopper. The contents of the J. Young tube were heated at 60 °C for 14 h to give an orange solution. Solvents were removed *in vacuo* to give an orange solid. The solid was dissolved in minimal pentane and cooled to -30 °C to give orange crystals of **4b** (30 mg, 61% yield). Anal. calc'd for C₄₆H₆₈N₆Nb₂: C, 62.02; H, 7.69; N, 9.43; Found: C, 62.07; H, 7.57; N, 9.39. ¹H NMR (benzene-*d*₆): δ 1.12 (12H, d, CH(CH₃)₂), 1.30 (12H, d, CH(CH₃)₂), 2.31 (30H, s, C₅(CH₃)₅), 3.64 (4H, sept, CH(CH₃)₂), 7.07-7.22 (6H, m, C(C₆H₅)), 7.24-7.30 (2H, m, C(C₆H₅)), 7.33-7.39 (2H, m, C(C₆H₅)).

{Cp***V**[N(^{*i*}Pr)C(Me)N(^{*i*}Pr)](μ-η¹:η¹-N₂)} (**5**). In an N₂ glovebox, compound **8** (504 mg, 1.39 mmol) was dissolved in 20 mL of THF and cooled to -30 °C. To the stirred solution, 0.5% w/w sodium amalgam (7.03 g, 1.53 mmol of Na) was added and the solution was allowed to warm to room temperature and stirred for 14 h. Solvents

were removed *in vacuo* to give a green solid, which was subsequently dissolved in pentane and filtered through Celite on a glass frit. The filtrate was concentrated to saturation and stored at -30 °C to give green crystals of **8** (432 mg, 91% yield). Anal. calc'd for C₃₆H₆₄N₆V₂: C, 63.32; H, 9.45; N, 12.31; Found: C, 63.09; H, 9.19; N, 12.25.

Cp*Nb[N(ⁱPr)C(Me)N(ⁱPr)]Cl₃ (7a). A -30 °C solution of Li[N(ⁱPr)C(Me)N(ⁱPr)] (418 mg, 2.84 mmol) in 20 mL of Et₂O was added dropwise to a -30 °C suspension of Cp*NbCl₄ (1.00 g, 2.71 mmol) in 40 mL of Et₂O. The suspension was allowed to warm to room temperature and stirred for 14 h to give a purple solution. Volatiles were removed *in vacuo*, and the crude product was dissolved in toluene and filtered through a pad of Celite on a glass frit. The resulting purple filtrate was concentrated and cooled to -30 °C to give dark purple crystals of **7a** (562 mg, 44% yield). Anal. calc'd for C₁₈H₃₂N₂Cl₃Nb₁: C, 45.45; H, 6.78; N, 5.89; Found: C, 45.23; H 6.87; N, 5.64. ¹H NMR (benzene-*d*₆): δ 1.00 (6H, d, *J* = 7.0 Hz, CH(CH₃)₂), 1.52 (3H, s, N(ⁱPr)C(CH₃)N(ⁱPr)), 1.75 (6H, d, *J* = 7.0 Hz, CH(CH₃)₂), 2.00 (15H, s, C₅(CH₃)₅), 4.41 (1H, sept, *J* = 7.0 Hz, CH(CH₃)₂), 4.95 (1H, br, CH(CH₃)₂).

Cp*Nb[N(ⁱPr)C(Ph)N(ⁱPr)]Cl₃ (7b). A -30 °C solution of Li[N(ⁱPr)C(Ph)N(ⁱPr)]•*n*-Bu₂O (451 mg, 1.34 mmol) in 20 mL of Et₂O was added dropwise to a -30 °C suspension of Cp*NbCl₄ (473 mg, 1.28 mmol) in 40 mL of Et₂O. The suspension was allowed to warm to room temperature and stirred for 14 h to give a purple solution. Volatiles were removed *in vacuo*, and the crude product was dissolved in toluene and

filtered through a pad of Celite on a glass frit. The resulting purple filtrate was concentrated and cooled to -30 °C to give dark purple crystals of **7b** (411 mg, 61% yield). Anal. calc'd for C₂₃H₃₄N₂Cl₃Nb₁: C, 51.37; H, 6.37; N, 5.21; Found: C, 51.76; H 6.36; N, 5.06. ¹H NMR (benzene-*d*₆): δ 1.00 (6H, d, *J* = 7.0 Hz, CH(CH₃)₂), 1.52 (3H, s, N(^{*i*}Pr)C(CH₃)N(^{*i*}Pr)), 1.75 (6H, d, *J* = 7.0 Hz, CH(CH₃)₂), 2.01 (15H, s, C₅(CH₃)₅), 4.41 (1H, sept, *J* = 7.0 Hz, CH(CH₃)₂), 4.95 (1H, br, *J* = 7.04 Hz, CH(CH₃)₂).

Cp*V[N(^{*i*}Pr)C(Me)N(^{*i*}Pr)]Cl (8**). A -30 °C solution of Li[N(^{*i*}Pr)C(Me)N(^{*i*}Pr)] (178 mg, 1.21 mmol) in 10 mL of Et₂O was added dropwise to a -30 °C suspension of [Cp*V(μ-Cl)₂]₃ (306 mg, 0.40 mmol) in 20 mL of Et₂O. The reaction was allowed to warm to room temperature and stir for 14 h to give a maroon solution. Solvents were removed *in vacuo* to give a maroon solid, which was subsequently dissolved in pentane and filtered through Celite on a glass frit. The filtrate was concentrated to saturation and stored at -30 °C to give maroon crystals of **8** (354 mg, 82% yield). Anal. calc'd for C₁₈H₃₂N₂Cl₁V₁: C, 59.58; H, 8.89; N, 7.72; Found: C, 59.69; H, 8.72; N, 7.86.**

Cp*V[N(^{*i*}Pr)C(Me)N(^{*i*}Pr)][CN(2,6-Me₂C₆H₃)₂] (10**). Compound **5** (102 mg, 0.15 mmol) in 5 mL of pentane was added to a suspension of 2,6-xylisocyanide (79 mg, 0.60 mmol) in 5 mL of pentane and stirred at room temperature. After reacting for 14 h to give a red solution, the solution was filtered through Celite supported by Kimwipe in a glass pipette. The filtrate was concentrated and stored at -30 °C to give**

dark red crystals of **10** (157 mg, 89% yield). Anal. calc'd for C₃₆H₅₀N₄V₁: C, 73.32; H, 8.55; N, 9.50; Found: C, 73.86; H, 8.54; N, 9.67. IR (KBr) $\nu_{\text{CN}} = 1902 \text{ cm}^{-1}$ (s), 1992 cm^{-1} (s).

4.6.3. Mechanistic experiments

Kinetic Studies. Solutions of pre-cleaved N₂ complexes for Eyring analysis were prepared in an argon filled glovebox by dissolving 0.03 mmol – 0.08 mmol of **4.1a-c** or **4.2b** in 40.4 g of methylcyclohexane that was pre-cooled to -30 °C to give solutions with concentrations between 0.55 mM and 1.53 mM. These solutions were subsequently analyzed at 5 different temperatures in triplicate within the range of 40 °C to 95 °C. Stock solutions for concentration dependence analysis were prepared by dissolving **4.1a-c** (0.04 mmol – 0.05 mmol) in 23 g of methylcyclohexane that was pre-cooled to -30 °C. Dilutions of the stock solution were performed by mass to give solutions that were 0.75, 0.50, and 0.25 times the concentration of the stock solution. Solutions were stored and maintained at -30 °C and used immediately after preparation, with aliquots analyzed consecutively until the data set was complete.

For sample analysis, a teflon sealed, 1 cm path length quartz cuvette was charged with a magnetic stir bar and 3 mL of a sample solution. The cuvette was pumped out of the glovebox and then inserted into an Agilent Cary 60 Spectrophotometer equipped with a Quantum Northwest temperature controlled cuvette holder that was pre-equilibrated at the desired temperature, with data collection starting simultaneously. The cuvette solution was stirred while scans from 800 – 350 nm were collected at a rate to give 30 to 164 data points per run.

First-order rate constants for all kinetic runs were determined by a least-squares fit of absorbance data, monitored at 625 nm, to the equation $\ln(A) = -kt + A_0$ using the LINEST function in Excel. The first 3 min of data acquisition were excluded to account for temperature equilibration of the cuvette solution, and the number of data points included was determined by a standard of linearity ($R^2 > 0.9985$) for each kinetic run. Using this standard, up to 4.2 half-lives of first-order linear data were observed for the compounds examined. Initial rates from absorbance vs. time plots were determined by a least-squares linear fit of the first 5 data points after the temperature equilibration period using the LINEST function in Excel. All rate constants and initial rates were analyzed in triplicate.

Temperature dependent rate constants collected for each compound were least-squares fitted to the Eyring equation, $k = (k_B T/h) \exp(\Delta S^\ddagger/R) \exp(-\Delta H^\ddagger/RT)$, using OriginPro 8 software. All rate constant, initial rate, and activation parameter errors are reported at the 95% confidence interval.¹⁹

Crossover Experiment. Compounds **4.1a** (9.5 mg, 0.01 mmol) and **4.1c** (14.9 mg, 0.01 mmol) were dissolved in 0.25 mL of THF in a Teflon sealed NMR tube and heated to 70 °C for 3.5 hours to produce a yellow solution. The solution was diluted with THF to give a total volume of 2 mL, which was then analyzed by ESI-MS (positive ion mode). Only peaks corresponding to **4.3a** ($[M + H]^+ = 943.21$ m/z) and **4.3c** ($[M + H]^+ = 1001.26$ m/z) were present and no crossover product, $\{\text{Cp}^*\text{Ta}[\text{N}(\text{iPr})\text{C}(\text{Me})\text{N}(\text{iPr})]\}(\mu\text{-}\eta^1\text{:}\eta^1\text{:N}_2)\{\text{Cp}^*\text{Ta}[\text{N}(\text{iPr})\text{C}(\text{Me})\text{N}(\text{iPr})]\}$ ($[M + H]^+ = 972.45$), was observed.

4.6.4. Supporting NMR and UV-vis spectra

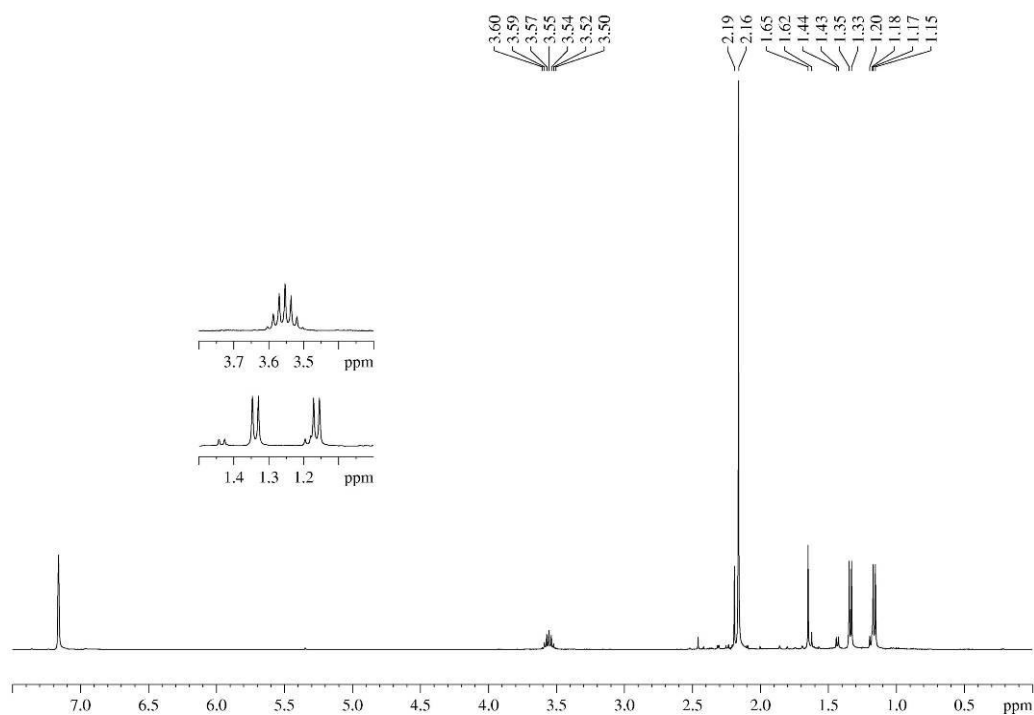


Figure 4.12. ¹H NMR (400.13 MHz, C₆D₆, 25 °C) experiment showing crude products (*cis/trans*-4.3a) obtained from thermolysis of 4.1a at 70 °C for 2 h.

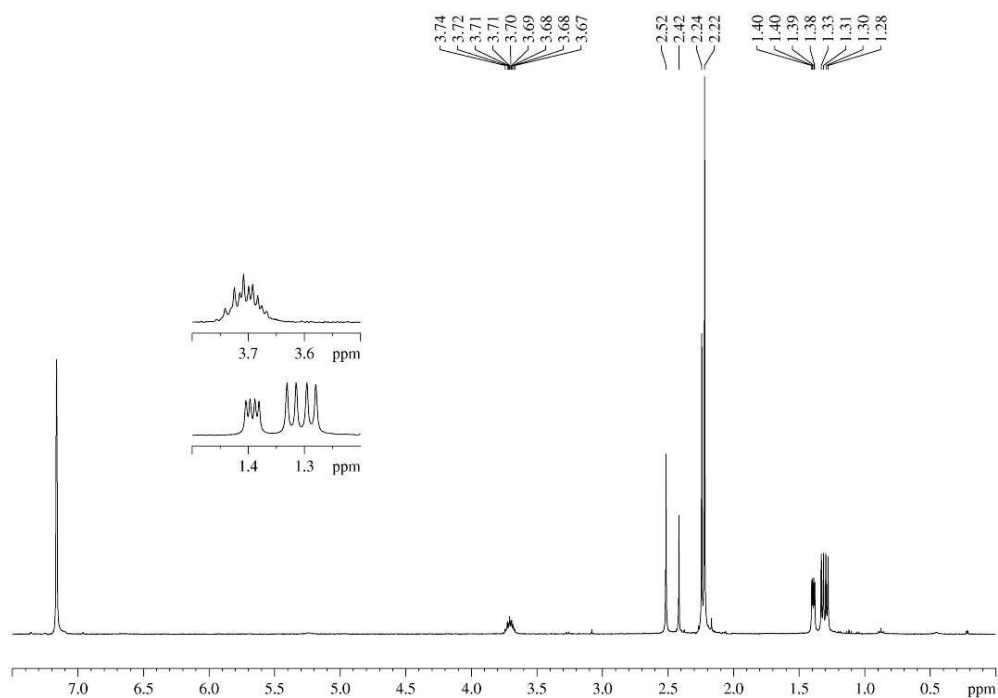


Figure 4.13. ¹H NMR (400.13 MHz, C₆D₆, 25 °C) experiment showing crude products (*cis/trans*-4.3b) obtained from thermolysis of 4.1b at 70 °C for 2 h.

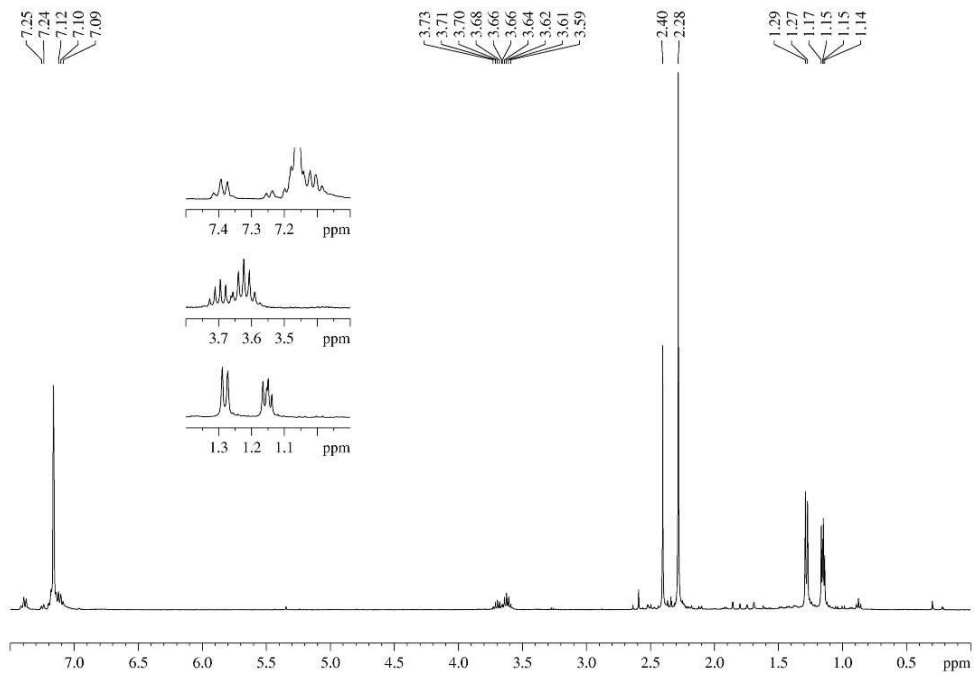


Figure 4.14. ¹H NMR (400.13 MHz, C₆D₆, 25 °C) experiment showing crude products (*cis/trans*-**4.3c**) obtained from thermolysis of **4.1c** at 85 °C for 2.5 h.

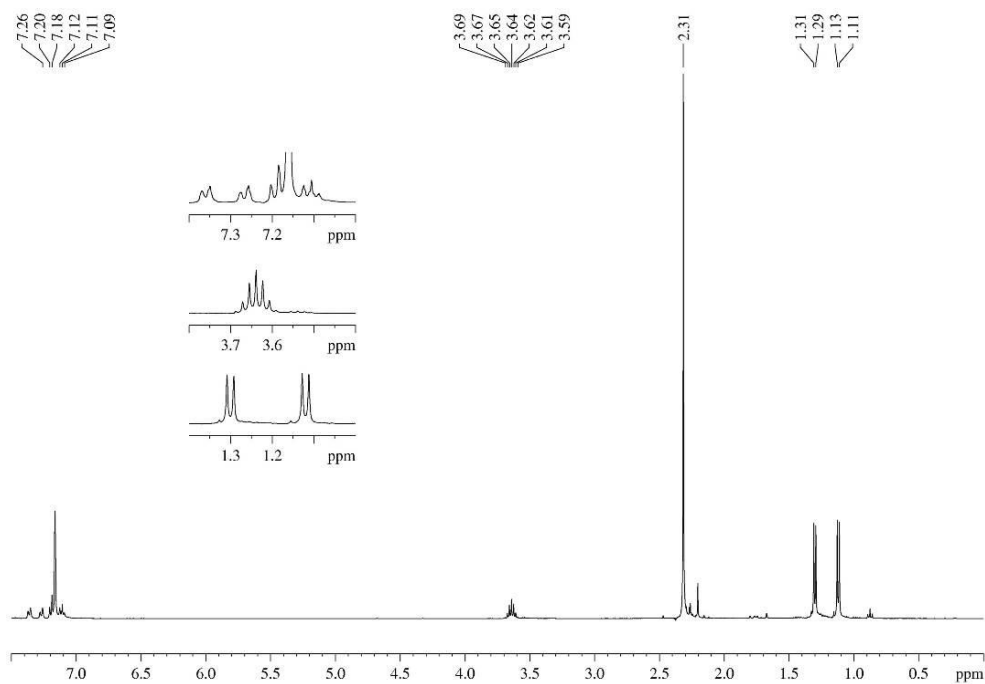


Figure 4.15. ¹H NMR (400.13 MHz, C₆D₆, 25 °C) experiment showing crude products (*trans*-**4.4b**) obtained from thermolysis of **4.2b** at 70 °C for 2 h.

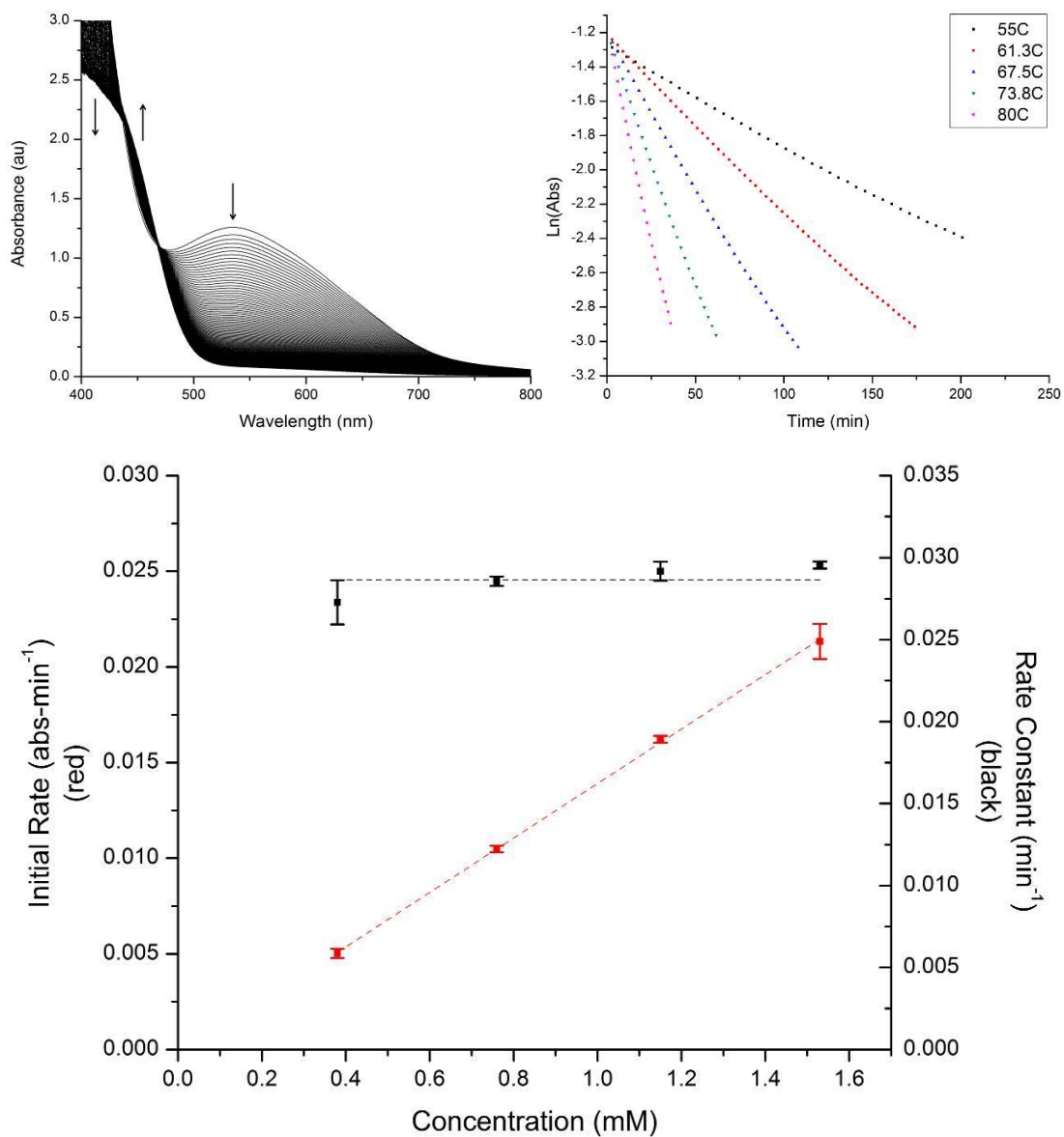


Figure 4.16. (top left) UV-vis scanning kinetics at 334.45 K, $\Delta t = 3$ min, (top right) temperature dependent first order $\ln(A) = -kt + A_0$ plots, and (bottom) rate constant and initial rate concentration dependence for the conversion of **4.1b** to **4.3b**. Error bars are at the 95% confidence interval.

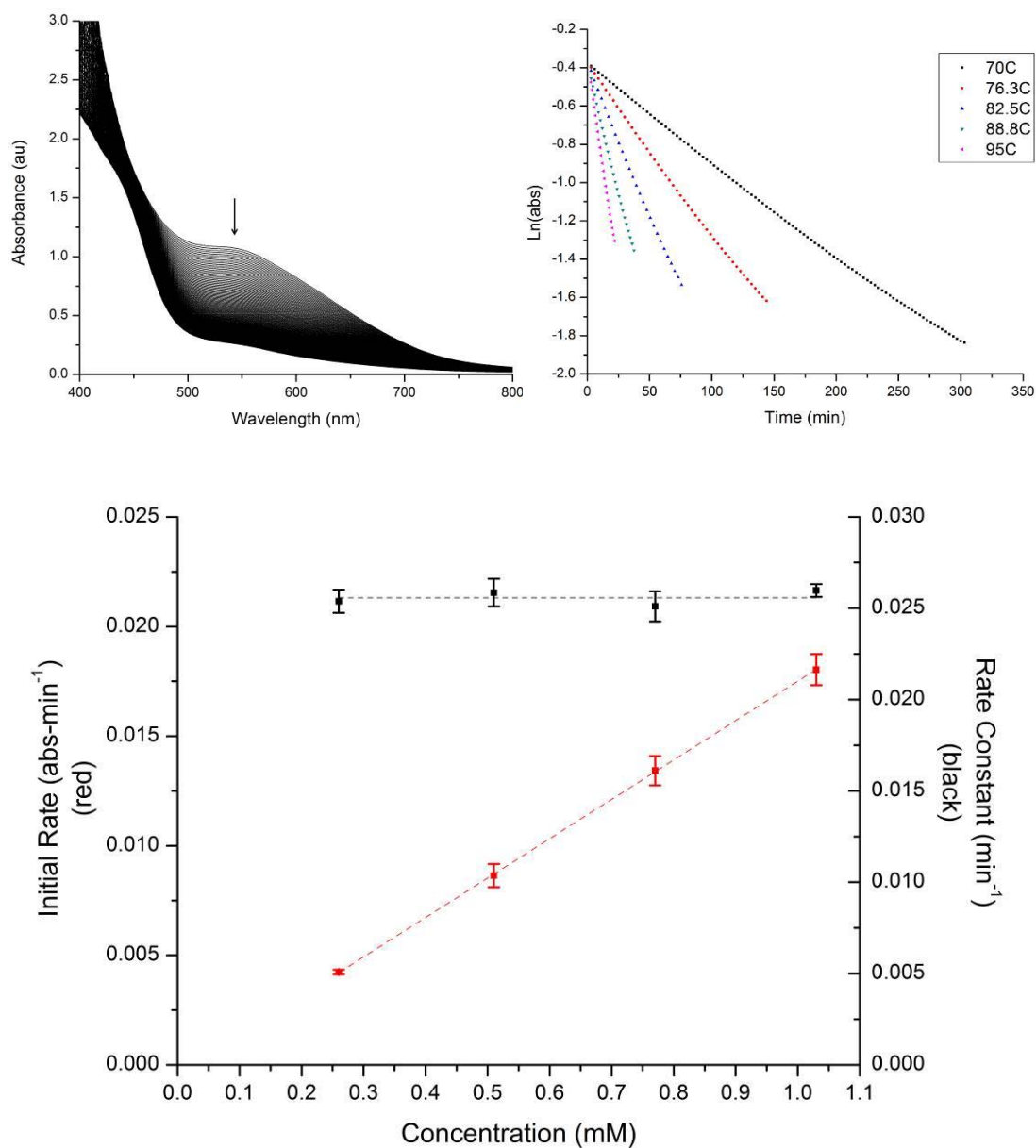


Figure 4.17. (top left) UV-vis scanning kinetics at 343.15 K, $\Delta t = 3$ min, (top right) temperature dependent first order $\ln(A) = -kt + A_0$ plots, and (bottom) rate constant and initial rate concentration dependence for the conversion of **4.1c** to **4.3c**. Error bars are at the 95% confidence interval.

4.7. References

- 1) Smil, V. *Enriching the Earth: Fritz Haber, Carl Bosch, and the Transformation of World Food Production*, MIT Press, Cambridge, MA, 2001.

- 2) For a recent reviews, see: (a) Fryzuk, M. D.; Johnson, S. A. *Coord. Chem. Rev.* **2000**, 379-409. (b) Shaver, M. P.; Fryzuk, M. D.; *Adv. Synth. Catal.* **2003**, 345, 1061-1076. (c) Gambarotta, S.; Scott, J. *Angew. Chem., Int. Ed.* **2004**, 43, 5298-5308. (d) MacKay, B. A.; Fryzuk, M. D. *Chem. Rev.* **2004**, 104, 385-402. (e) MacLachlan, E. A.; Fryzuk, M. D. *Organometallics* **2006**, 25, 1530-1543. (f) Chirik, P. J. *Dalton Trans.* **2007**, 16-25. (g) Ohki, Y.; Fryzuk, M. D. *Angew. Chem., Int. Ed.* **2007**, 46, 3180-3183. (h) Chirik, P. J. *Organometallics* **2010**, 29, 1500-1517. (i) Hinrichsen, S.; Broda, H.; Gradert, C.; Söncksen, L.; Tucek, F. *Annu. Rep. Prog. Chem., Sect. A: Inorg. Chem.* **2012**, 108, 17-47.
- 3) (a) Solari, E.; Da Silva, C.; Iacono, B.; Hesschenbrouck, J.; Rizzoli, C.; Scopelliti, R.; Floriani, C. *Angew. Chem., Int. Ed.* **2001**, 40, 3907-3909. (b) Curley, J. J.; Cook, T. R.; Reece, S. Y.; Müller, P.; Cummins, C. C. *J. Am. Chem. Soc.* **2008**, 130, 9394-9405. (c) Huss, A. S.; Curley, J. J.; Cummins, C. C. *J. Phys. Chem. B* **2013**, 117, 1429-1436. (d) Rebreyend, C.; de Bruin, B. *Angew. Chem. Int. Ed.* **2014**, doi: 10.1002/anie.201409727. (e) Miyazaki, T.; Tanaka, H.; Tanabe, Y.; Yuki, M.; Nakajima, K.; Yoshizawa, K.; Nishibayashi, Y. *Angew. Chem. Int. Ed.* **2014**, 53, 11488-11492.
- 4) (a) Laplaza, C. E.; Cummins, C. C. *Science* **1995**, 268, 861-863. (b) Laplaza, C. E.; Johnson, M. J. A.; Peters, J. C.; Odom, A. L.; Kim, E.; Cummins, C. C.; George, G. N.; Pickering, I. J. *J. Am. Chem. Soc.* **1996**, 118, 8623-8638. (c) Curley, J. J.; Cook, T. R.; Reece, S. Y.; Müller, P.; Cummins, C. C. *J. Am. Chem. Soc.* **2008**, 130, 9394-9405.

- 5) (a) Mindiola, D. J.; Meyer, K.; Cherry, J.-P. F.; Baker, T. A.; Cummins, C. C. *Organometallics* **2000**, *19*, 1622-1624. (b) Yandulov, D. V.; Schrock, R. R. *Science* **2003**, *301*, 76-78. (c) Yandulov, D. V.; Schrock, R. R. *Inorg. Chem.* **2005**, *44*, 1103. (d) Schrock, R. R. *Acc. Chem. Res.* **2005**, *38*, 955. (e) Weare, W. W.; Dai, X.; Byrnes, M. J.; Chin, J. M.; Schrock, R. R.; Müller, P. *Proc. Nat. Acad. Sci. USA* **2006**, *103*, 17099. (f) Vidyaratne, I.; Crewdson, P.; Lefebvre, E.; Gambarotta, S. *Inorg. Chem.* **2007**, *46*, 8836-8842.
- 6) (a) Knobloch, D. J.; Lobkovsky, E.; Chirik, P. J. *Nat. Chem.* **2010**, *2*, 30-35. (b) Knobloch, D. J.; Semproni, S. P.; Lobkovsky, E.; Chirik, P. J. *J. Am. Chem. Soc.* **2012**, *134*, 3377-3386. (c) Semproni, S. P.; Milsmann, C.; Chirik, P. J. *Angew. Chem. Int. Ed.* **2012**, *51*, 5213-5216.
- 7) (a) Fryzuk, M. D. *Acc. Chem. Res.* **2009**, *42*, 127-133. (b) Ballmann, J.; Yeo, A.; Patrick, B. O.; Fryzuk, M. D. *Angew. Chem. Int. Ed.* **2011**, *50*, 507-510. (c) Semproni, S. P.; Lobkovsky, E.; Chirik, P. J. *J. Am. Chem. Soc.* **2011**, *133*, 10406-10409.
- 8) (a) Nikiforov, G. B.; Vidyaratne, I.; Gambarotta, S.; Korobkov, I. *Angew. Chem. Int. Ed.* **2009**, *48*, 7551-7555. (b) Shima, T.; Hu, S.; Luo, G.; Kang, X.; Luo, Y.; Hou, Z. *Science* **2013**, *340*, 1549-1552.
- 9) For a recent review on iron and molybdenum mediated N₂ cleavage, see: MacLeod, K. C.; Holland, P. L. *Nat. Chem.* **2013**, *5*, 559-565.
- 10) Hirotsu, M.; Fontaine, P. P.; Epshteyn, A.; Zavalij, P. Y.; Sita, L. R. *J. Am. Chem. Soc.* **2007**, *129*, 9284-9285.

- 11) For amidinate distal substituent effects regarding living polymerization, see:
Zhang, Y.; Reeder, E. K.; Keaton, R. J.; Sita, L. R. *Organometallics* **2004**, *23*, 3512-3520.
- 12) Cummins' reported value and calculated theoretical KIE values can be found in ref. 4b.
- 13) Hirotsu, M.; Fontaine, P. P.; Zavalij, P. Y.; Sita, L. R. *J. Am. Chem. Soc.* **2007**, *129*, 12690-12692.
- 14) Zhang, W.; Tang, Y.; Lei, M.; Morokuma, K.; Musaev, D. G. *Inorg. Chem.* **2011**, *50*, 9481-9490.
- 15) Fryzuk, M. D.; Kozak, C. M.; Bowdridge, M. R.; Patrick, B. O.; Rettig, S. J. *J. Am. Chem. Soc.* **2002**, *124*, 8389-8397.
- 16) Tran, B. L.; Pinter, B.; Nichols, A. J.; Konopka, F. T.; Thompson, R.; Chen, C.-H.; Krzystek, J.; Ozarowski, A.; Telser, J.; Baik, M.-H.; Meyer, K.; Mindiola, D. J. *J. Am. Chem. Soc.* **2012**, *134*, 13035-13045.
- 17) Mata, J. D. L.; Fandos, R.; Gómez, M.; Gómez-Sal, P.; Martinez-Carrera, S.; Royo, P. *Organometallics* **1990**, *8*, 2846-2850.
- 18) Abernethy, C. D.; Bottomley, F.; Decken, A. *Organometallics* **1997**, *16*, 1865-1869.
- 19) Error at the 95% confidence interval was calculated using the student's *t* distribution, see: Wilson, E. B., Jr. *An Introduction to Scientific Research*; Dover: New York, 1990.

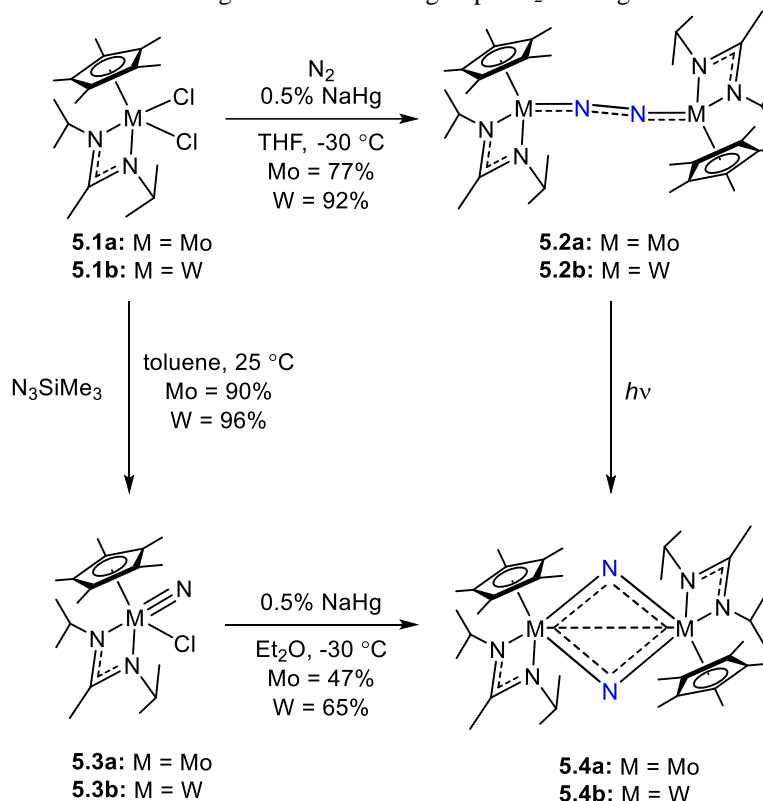
Chapter 5: Group 6 CPAM N₂ Fixation

5.1. Introduction

Homogenous metal systems that involve catalytic formation of ammonia or silyl amines have greatly progressed over the last several years;¹ however, a catalytically competent system capable of producing more complex molecules involving N-C bond forming nitrogen fixation remains to be discovered. Current examples of non-catalytic N-C bond forming nitrogen fixation reside almost exclusively within the early transition metal series. Aside from an early example of N-C bond forming N₂ fixation to provide N,N-dimethyl acetamide,² Cummins and co-workers have established a foundation of closed-cycle N₂ fixation systems that involve individual chemical steps and include either thermal N₂ cleavage with Mo dinuclear compounds,³ or reductive N₂ cleavage with mixed Nb/Mo dinuclear compounds.⁴ The resulting Mo or Nb nitride has been shown to react with acyl chlorides to provide nitrile compounds with N-atoms derived from N₂. Within group 4, Chirik and co-workers have developed hafnium metallocene dinitrogen complexes that undergo ligand-induced N₂ cleavage to provide a μ -nitrido intermediate that can be functionalized to obtain coordinated oxamides,^{5,6} formamides⁷ and carbodiimides⁸ that require liberation by quenching with HCl. Production of cyanate salts have also been targeted as viable products for achieving a catalytic N-C bonding N₂ fixation cycle.⁹ Most recently, a closed synthetic cycle employing a vanadium system capable of fixating N₂ to provide potassium cyanate, KNCO.¹⁰

Considering potential intermediates that are along the pathway of dinitrogen fixation, metal nitrido compounds represent important intermediates to investigate. Previously, a group member of the Sita lab, Brendan Yonke, developed and synthetic

Scheme 5.1. Previous research involving CPAM mediated group 6 N₂ cleavage.



route to Group 6 CPAM nitride complexes. As depicted in Scheme 5.1, bis- μ -nitrido complexes **5.4a** and **5.4b** were prepared by first obtaining the nitrido chloride complexes **5.3a** and **5.3b** by addition of trimethylsilylazide (Me_3SiN_3) to the dichloride precursors **5.1a** and **5.1b** and reducing them with sodium amalgam (NaHg) to provide the nitrido complexes **5.4a** and **5.4b** in good yields. Following the complete characterization of these nitrido complexes, Brendan Yonke discovered that Group 6 dinitrogen complexes (**5.2a** and **5.2b**), while thermally robust (temperatures up to 100 °C), undergo photochemical N_2 cleavage to provide the same bis- μ -nitrido complexes **5.4a** and **5.4b**.

In this chapter, further investigations into the nature of group 6 N_2 photocleavage are described. The chemistry of metal nitrides obtained from N_2 cleavage is successfully developed and applied to dinitrogen cleavage chemistry.

Ultimately, this chemistry provides access to organic products derived from N₂ and establishes a unique foundation for future studies in developing a true catalytic system capable of fixating N₂ to N-C based organic products.

5.2. Group 6 Photolytic N₂ Cleavage Studies

5.2.1. UV-vis and NMR studies of photolytic Mo and W mediated N₂ cleavage

It was of interest to further explore group 6 photolytic N₂ cleavage considering that tungsten cleavage had not previously been monitored to completion nor by UV/Vis spectroscopy within our group. For the molybdenum dinitrogen analogue, UV-vis kinetics regarding photocleavage of N₂ using a 1000W Xe/Hg lamp with selective irradiation at 330 nm (20 nm band pass) had been previously been obtained; however, considering photolytic N₂ fixation studies within this chapter were performed with a Rayonet carousel of 16 medium-pressure Hg lamps (*vide infra*), it was important to study UV-vis kinetic profiles under these new photolytic conditions. To begin, an NMR scale solution of the CPAM tungsten dinitrogen complex **5.2b** was observed to quantitatively convert to the diamagnetic cleaved N₂ complex **5.4b** through *ca.* 50% conversion (60 h of irradiation) *via* ¹H NMR, whereafter it became clear that **5.4b** was itself photoreactive as well, converting to a new unidentified product by the time the starting N₂ complex had been fully consumed. These results were also supported by UV-vis kinetics, where solutions of the tungsten dinitrogen compound **5.2b** were irradiated and UV-vis spectra collected at timed intervals to provide a series of spectra that produced well-resolved isosbestic over 9 h of irradiation as shown in Figure 5.2, but became less resolved upon further irradiation.

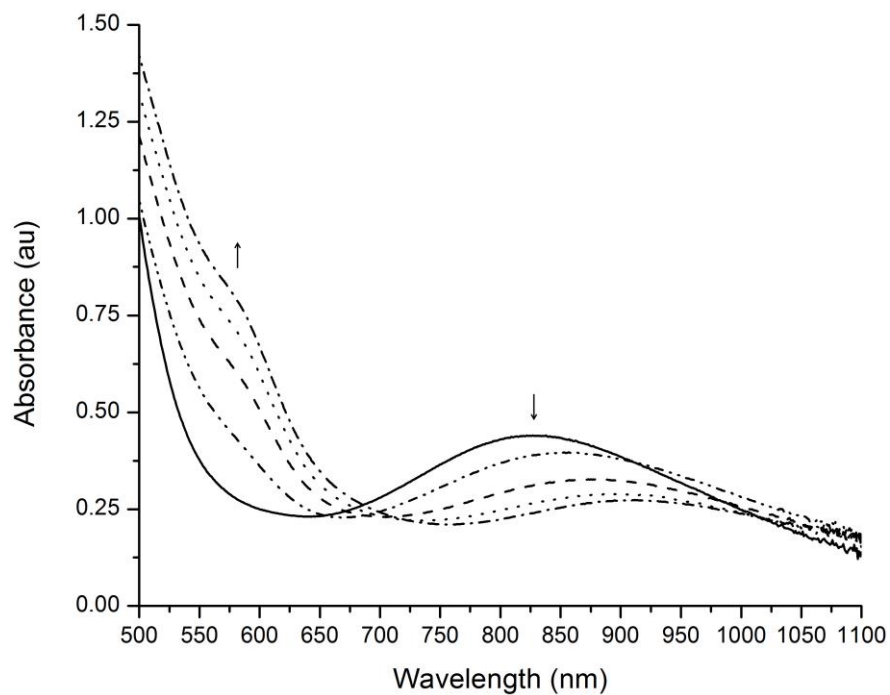


Figure 5.1. UV-vis spectra of **5.2a** ($c = 0.87$ mM in methylcyclohexane) taken during photolysis (Quartz, med. Pressure Hg lamps) after timed intervals ($\Delta t \approx 1$ h for total 4 h).

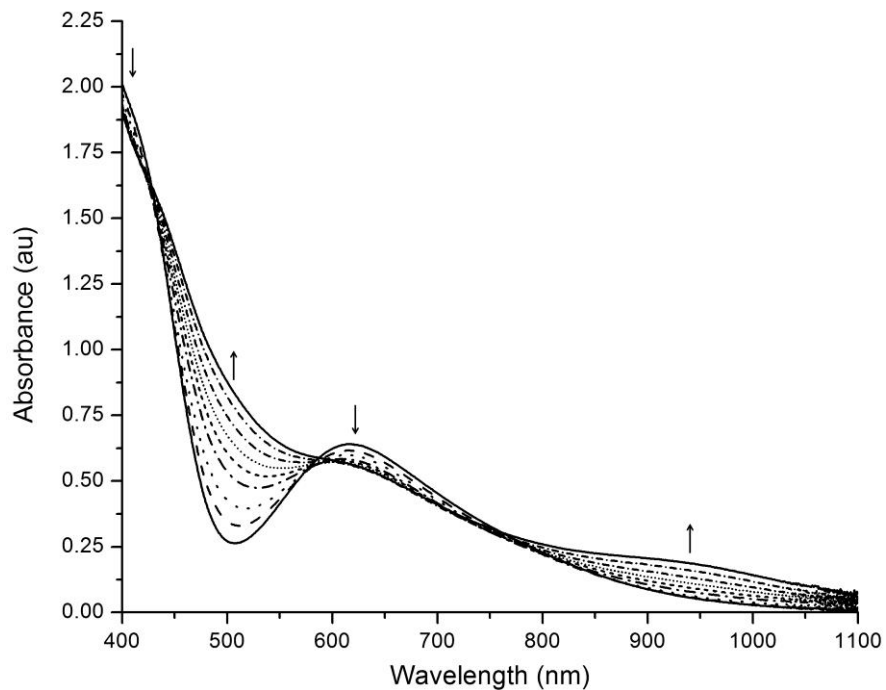
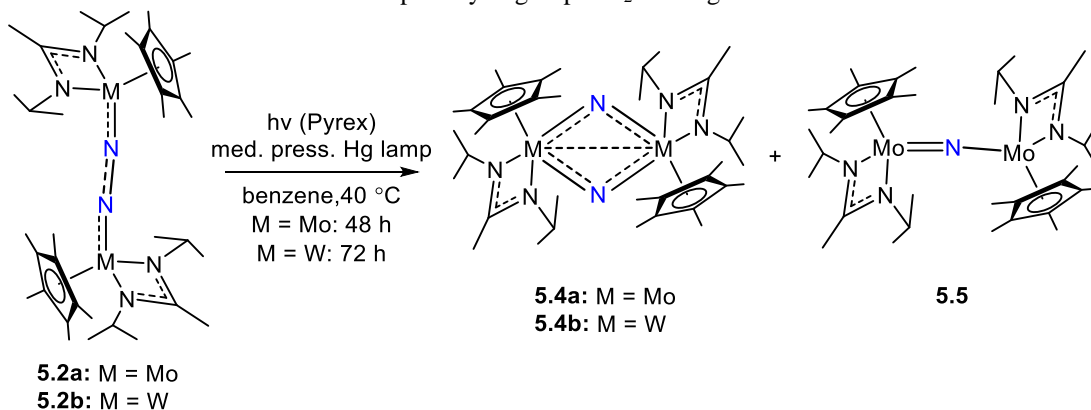


Figure 5.2. UV-vis spectra of **5.2b** ($c = 0.86$ mM in methylcyclohexane) taken during photolysis (Quartz, med. pressure Hg lamps) after timed intervals ($\Delta t \approx 1$ h for total of 9 h).

Scheme 5.2. Products obtained from photolytic group 6 N₂ cleavage.



For the molybdenum analogue, ¹H NMR studies proved less useful as only the consumption of the initial dinitrogen compound **5.2a** was able to be observed due to the paramagnetic nature of the products. Irradiation of a cuvette solution containing the molybdenum analogue **5.2a** was followed by timed intervals of UV-vis spectra and clearly produced a series of spectra that lacked the presence of isosbestic points, indicating the production of two (or more) photoproducts. This result for molybdenum prompted further studies with large scale photochemical Mo N₂ cleavage reactions to identify any additional products formed other than **5.4a**.

Therefore, 110 mg of **5.2a** was irradiated and monitored by ¹H NMR until all of **5.2a**

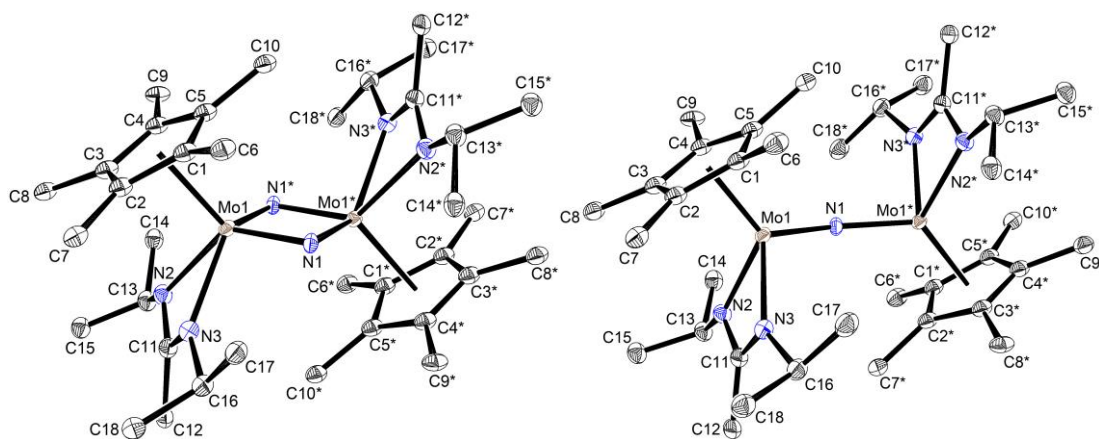


Figure 5.3. Molecular structures (30% thermal ellipsoids) within a co-crystal containing **5.4a** and **5.5** (ratio of **5.4a** to **5.5** is 1 to 3). (left) **5.4a** and (right) **5.5**. Hydrogen atoms have been removed for the sake of clarity.

was consumed. Crystallization of the crude product in a concentrated pentane solution at -30 °C led to the formation of black single crystals that were subjected to single crystal XRD analysis. Gratifyingly, these crystals were identified as a 3:1 co-crystal of a new mono- μ -nitrido compound (**5.5**) and the previously characterized bis- μ -nitrido **5.4a** as shown in Figure 5.3. Formation of **5.5** has precedent with other established dinuclear Mo photolytic N₂ cleavage systems by Floriani¹¹ and Cummins¹² where both have isolated mono- μ -nitrido compounds that are products of N₂ cleavage and N₂ extrusion pathways from the initial dinuclear [Mo]-N-N-[Mo] compound under photolytic conditions. It is proposed that a similar mechanism is in effect for the current system under study. The collective results presented in this section give further understanding to the photochemical transformations of the group 6 dinitrogen complexes **5.2a** and **5.2b**.

5.3. Reactivity of Group 6 CPAM Nitride Complexes

5.3.1. Structural and electronic properties of group 6 CPAM bis- μ -nitrido complexes

Having established further insight into the CPAM Group 6 photolytic N₂ cleavage system, focus was directed towards understanding the reactivity of the Mo (**5.4a**) and W (**5.4b**) bis- μ -nitrido species. Both of these species represent rare

Table 5.1. Structural parameters for bis- μ -nitrido complexes **5.4a** and **5.4b**.

	$d(\text{M1-N1})$ (Å)	$d(\text{M1-N1a})$ (Å)	$d(\text{N1-N1a})$ (Å)	$d(\text{M1-M1a})$ (Å)
5.4a	1.9636(13)	1.9636(13)	2.70	2.6764(3)
5.4b	1.912(2)	1.908(2)	2.75	2.6560(3)

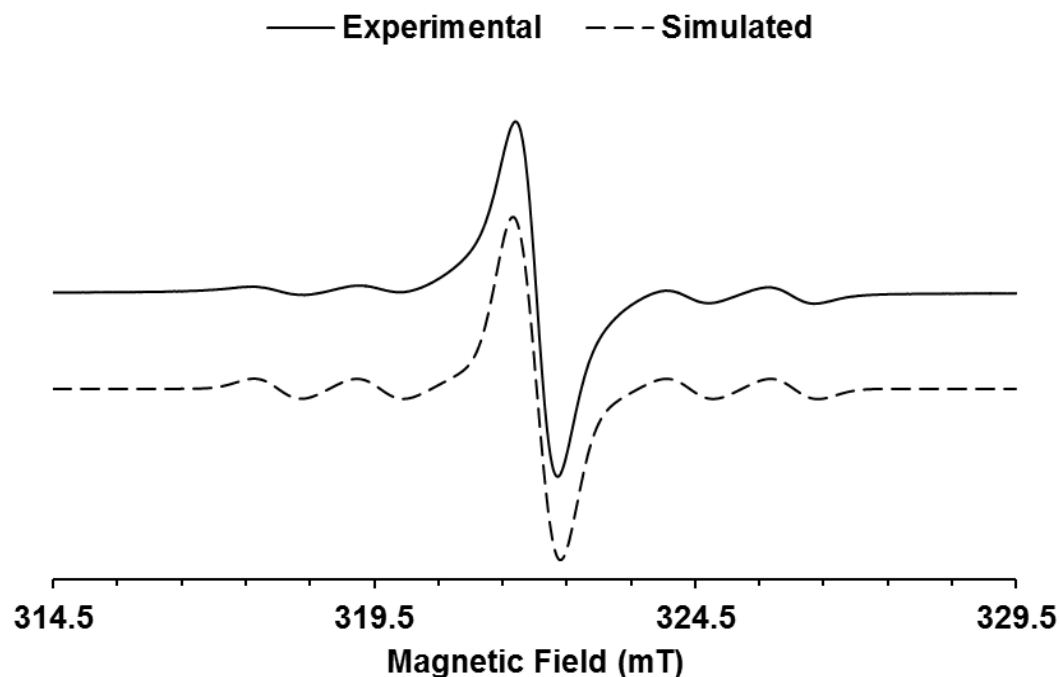


Figure 5.4. X-band EPR spectrum (toluene, 25 °C) of compound **5.4a**; $g_{\text{iso}} = 1.975$, $A_{\text{iso}}(^{95/97}\text{Mo}) = 40$ MHz. Simulation was produced by EasySpin.

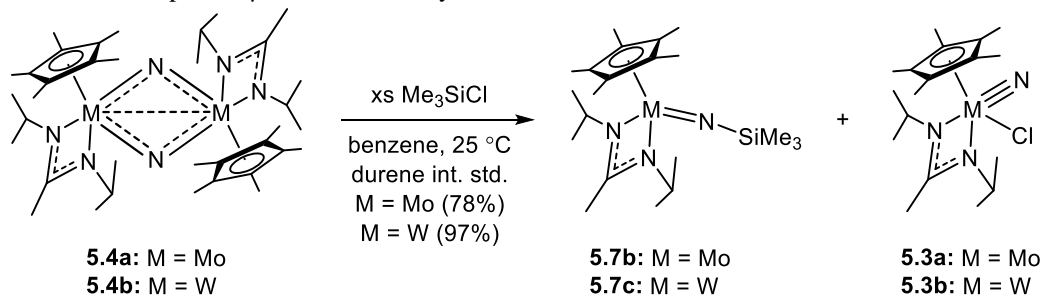
examples of Mo(V) and W(V) nitride species, where the only other example in group 6 is a Cr(V) bridging nitride complex.¹³ While the tungsten analogue is diamagnetic, the molybdenum analogue is paramagnetic. Previously, Brendan Yonke established the fluxional properties of the tungsten analogue with VT-NMR. Due to the paramagnetic nature of **5.4a**, EPR was used to further probe the electronic properties. As depicted in Figure 5.4, the room temperature isotropic EPR spectrum of **5.4a** is consistent with an electron coupled to a Mo nucleus ($^{95}\text{Mo} = 16\%$ abundance, spin 5/2; $^{97}\text{Mo} = 10\%$ abundance, spin 5/2). Notably, the absence of any additional coupling that might arise from a triplet state of **5.4a** was absent, which raised the question of whether a monomer-dimer equilibrium was present in solution. Variable temperature EPR was pursued to probe whether lower temperatures would reveal a

triplet state; however, no additional coupling was observed at 103 K or in toluene glass at 89 K.

5.3.2. Reaction of nitride complexes with silylating agents

We have established that CPAM Mo and W imido complexes undergo imido group transfer to CO and aryl isocyanides to provide isocyanates and carbodiimides respectively (see Appendix A). Coupled with the photolytic N₂ cleavage chemistry discussed (*vide supra*), it was clear that if Mo or W imido species could be obtained

Scheme 5.3. Group 6 bis- μ -nitrido reactivity with Me₃SiCl.

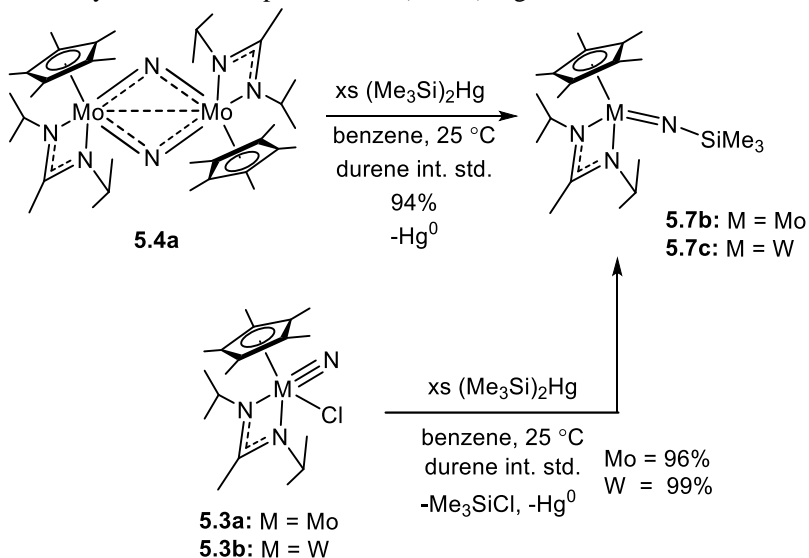


from the dinuclear nitride compounds **5.4a** and **5.4b**, N₂ fixation to isocyanates and carbodiimides could be feasible. Therefore, efforts were focused on evaluating the reactivity of the bridging nitride complexes to achieve this desired result. To begin, while dihydrogen and phenylsilane are known to add across metal-nitrogen bonds, both **5.4a** and **5.4b** were inert towards these reagents. Surprisingly, addition of a slight excess trimethylsilyl chloride (Me₃SiCl) to benzene-*d*₆ solutions of **5.4a** and **5.4b** within minutes led to the production of a C₁ symmetric species and a C_s symmetric species for both Mo and W analogues by ¹H NMR. These products were confirmed to be the previously characterized trimethylsilyl imido species **5.7a** and **5.7b**, and nitrido chloride species **5.3a** and **5.3b**, which was a very exciting result.¹⁴

Integration versus a durene internal standard revealed excellent yields for tungsten and high yields for molybdenum, as depicted in Scheme 5.3. It is proposed that the mechanism of this reaction involves the addition one eq. of Me_3SiCl across a metal nitrogen bond followed by cleavage of the second metal nitrogen bond via disproportionation to provide the M(IV) imido and M(VI) nitrido chloride. This was an important result, because it indicated that it might be possible to obtain group 6 imido complexes containing N-atoms derived from N_2 (Section 5.3). While this was a significant discovery, it was of interest to explore the silylation chemistry further to determine whether imido complexes **5.7b** and **5.7c** could be obtained in quantitative yield from **5.4a** and **5.4b** respectively. It was reasoned that bis(trimethylsilyl)mercury, $(\text{Me}_3\text{Si})_2\text{Hg}$, would be an excellent reagent for this purpose.¹⁵ Gratifyingly, it was found that the Mo analogue **5.4a** readily reacted with $(\text{Me}_3\text{Si})_2\text{Hg}$ to provide the target imido (**5.7b**) in near quantitative yield with respect to a durene internal standard (94%), with concomitant production of elemental mercury; however, the W analogue **5.4b** was inert to this reagent. The reason for this discrepancy could potentially be due to a higher barrier for splitting the W_2N_2 dimer versus the Mo_2N_2 dimer. Chemistry of the nitrido chloride compounds **5.3a** and **5.3b** were also investigated with $(\text{Me}_3\text{Si})_2\text{Hg}$. Interestingly, both **5.3a** and **5.3b** readily react with $(\text{Me}_3\text{Si})_2\text{Hg}$ to provide the imido complexes of interest (**5.7b** and **5.7c**), with concomitant formation of Me_3SiCl and elemental mercury. It is noted that in these reactivity studies, excess equivalents of $(\text{Me}_3\text{Si})_2\text{Hg}$ did not further react with the generated M(IV) imido species to provide the hypothetical M(III) bis-silyl amido or silyl amine products. This is important, because imido and N-atom transfer

chemistry has been well developed across the transition metal series and provides access to a variety of organic molecules of scientific and commercial interest.¹⁶

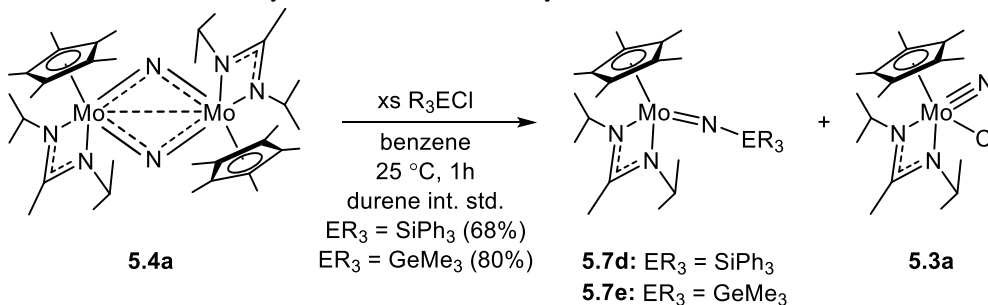
Scheme 5.4. Reactivity of nitride compounds with $(\text{Me}_3\text{Si})_2\text{Hg}$.



5.3.3. Extension of silyl chemistry to group 14 monochloride reagents, R_3ECl

After the discovery of group 6 CPAM nitride functionalization chemistry with trimethylsilyl reagents, it was realized that other group 14 analogues as well as a greater variety of substituents on the group 14 atom might participate in similar chemistry. To begin, Ph_3SiCl was investigated to determine whether sterics (or electronics, considering the greater stability of the Ph_3Si radical) could impose a

Scheme 5.5. CPAM Molybdenum nitride chemistry with R_3ECl .⁴

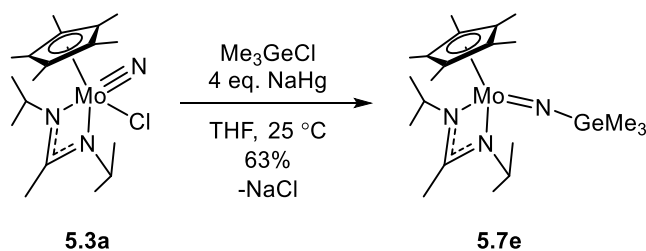


⁴ Reagents $^i\text{Pr}_3\text{SiCl}$, PhMe_2SiCl and Ph_2MeSiCl also participate in this chemistry.

limiting factor on this chemistry. It was found that Ph_3SiCl quickly reacts with **5.4a** in benzene- d_6 solution to provide the nitride chloride **5.3a** as well as new C_s symmetric peaks corresponding to the new silyl substituted imido complex **5.7d** (Scheme 5.5). To explore heavier group 14 imido group substituents, a slight excess of the trimethyl germanium analogue, Me_3GeCl , was added to a benzene- d_6 solution of **5.4a**. After reacting for 1 h, ^1H NMR revealed the production of a new C_s symmetric species that was attributed to the germanium substituted imido (**5.7e**) and a C_1 symmetric species with resonances corresponding to the nitrido chloride, **5.3a**.

It was desired to obtain these new imido complexes in larger quantities; therefore, a preparative synthesis was developed. Performing a large scale addition of Me_3GeCl to **5.4a** would provide theoretical maximum yield of *ca.* 50%. It was envisioned, however, that the nitride chloride co-product (**5.3a**) could simply be recycled back to the nitrido compound **5.4a** by employing 0.5% NaHg in excess as a reducing agent. Based on this initial thought, a preparative route was developed by reacting **5.3a** with a 4 eq. excess of 0.5% NaHg, followed by adding successive aliquots of Me_3GeCl (0.5 eq, 0.25 eq., 0.125 eq.). In between each aliquot, time was allotted for generated **5.3a** to be recycled back to **5.4a**. This procedure was successfully implemented, which allowed for the isolation of analytically pure

Scheme 5.6. Preparative synthesis of **5.7e**.⁵



⁵ This preparative route has been established for **5.7b-e**.

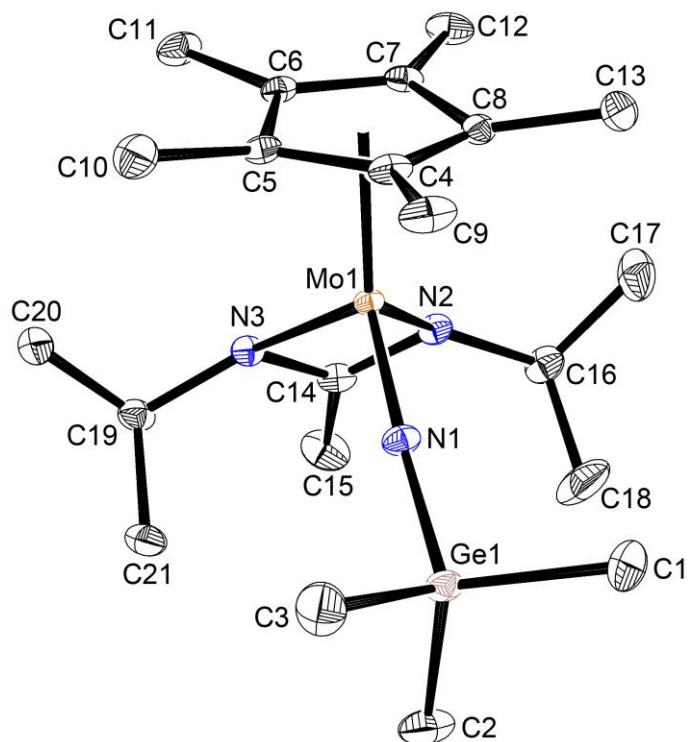


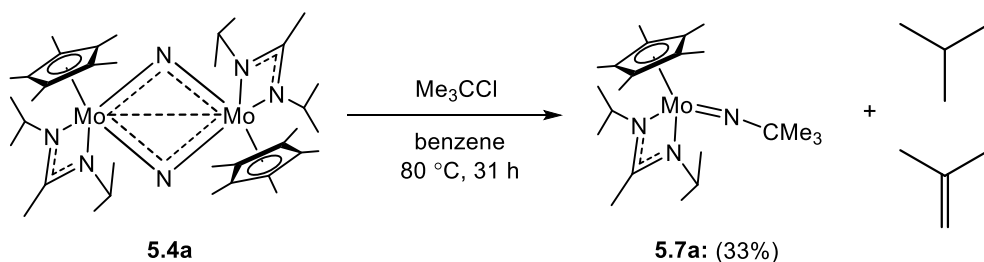
Figure 5.5. Molecular structure (30% thermal ellipsoids) of **5.7e**. Hydrogen atoms have been removed for the sake of clarity.

material. Single crystals were grown and analyzed by XRD to verify the product as the desired germanium imido **5.7e**. Interestingly, the synthesis of **5.7e** constitutes a particularly rare example of a transition metal germanium imido,¹⁷ of which only one other example of its type has been reported. Characterization of this imido complex also contributes to a CPAM Group 14 series of imido substituents (*i.e.* C, Si, Ge), which establishes the ability to study trends in imido group transfer chemistry with carbon monoxide and aryl isocyanides. It is curious whether this analogue has the potential to accelerate nitrogen group transfer, or more importantly, open new classes of reactivity for the Mo and W CPAM imido group.

To complete the survey of Group 14 ER_3Cl reagents reactivity of **5.4a**, *tert*-butyl chloride ($E = C$, $R = Me$) was pursued. No reaction was observed by 1H NMR

after leaving the reaction in a J. Young NMR tube overnight to react at 25 °C. The sample was thus subsequently heated to 80 °C for 31 h, at which time, ^1H NMR revealed the production of the previously characterized *tert*-butyl imido **5.7a** in 33% yield (durene internal standard), along with the formation of isobutene and isobutane (Scheme 5.7). The formation of isobutene and isobutane clearly indicates that *tert*-butyl radicals had formed, and the lower yield of **5.6** can be attributed to the formation of these products in place of coupling with a Mo(V) nitride.

Scheme 5.7. Molybdenum bis- μ -nitrido reactivity with *tert*-butyl chloride.



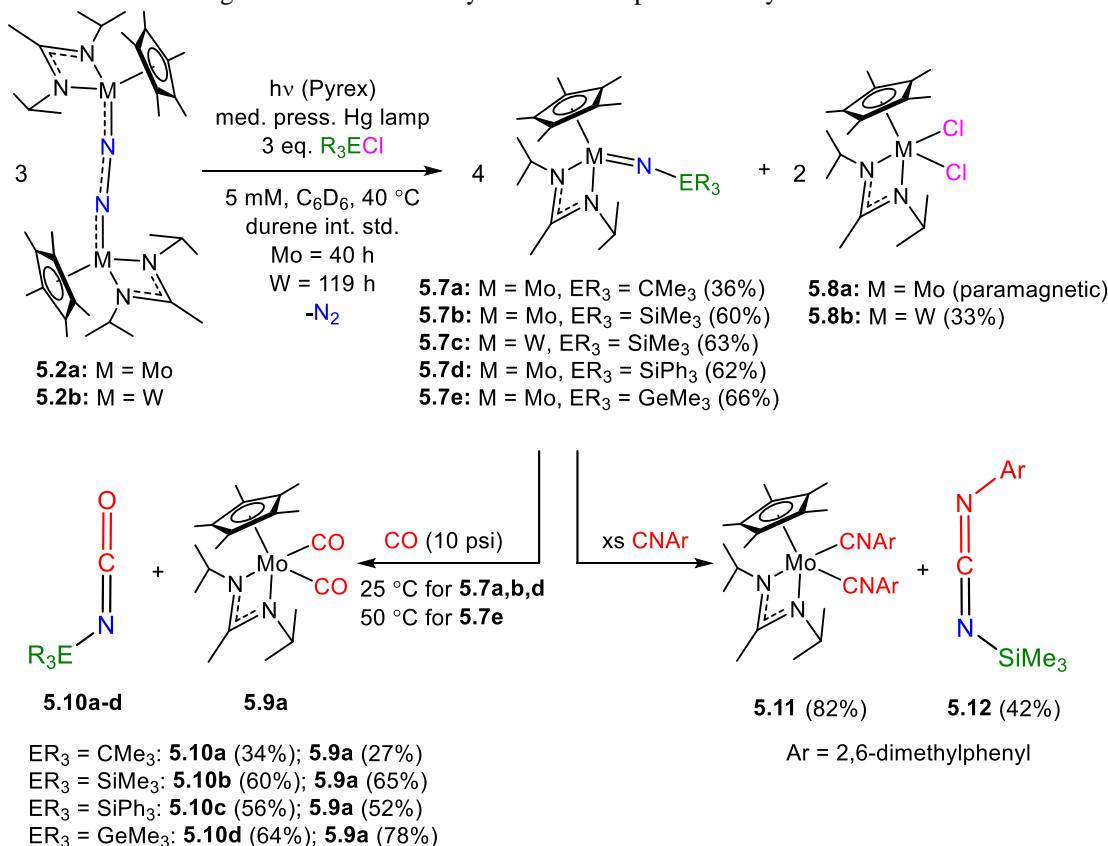
5.4. Dinitrogen Functionalization

5.4.1. Imido complexes derived from dinitrogen

Having successfully established that imido complexes could be obtained from Group 6 metal nitride complexes, it was important to determine whether the nitride functionalization chemistry could be applied to the products obtained from photolytic N_2 cleavage presented in Section 5.2. To begin, a 5 mM benzene- d_6 solution of tungsten dinitrogen complex **5.2b** was prepared in a Teflon sealed Pyrex J. Young NMR tube and exposed to UV light (medium pressure Hg lamps) in the presence of 3 eq. of trimethylsilyl chloride (Me_3SiCl). Monitoring by ^1H NMR, the complete

disappearance of **5.2b** and clean production of two diamagnetic species was noted after 119 h of UV irradiation. The new diamagnetic peaks were identified as the previously characterized tungsten silyl imido **5.7** and tungsten dichloride **5.8b** in 63% and 34% yield respectively (97% total) versus a durene internal standard. A similar result was achieved with the Mo dinitrogen complex **5.2a**, where the imido complex was obtained in 60% yield with the formation of characteristic paramagnetic resonances corresponding to the dichloride **5.8a**. Considering the yields of the tungsten reaction, the stoichiometry is according to what is shown on the top row of Scheme 5.8 and occurs with formal loss of 1 eq. of N₂. The formation of the dichloride compounds also is consistent with the loss of N₂, and this could occur either *via* photo N₂ extrusion or oxidative halogen atom abstraction of Me₃SiCl with concomitant loss of N₂, where any formation of Me₃Si• radicals can reductively couple with any nitride complexes that are formed to provide the imido products. It is noted that if a radical mechanism is in play, there would be less control over yields in slightly different conditions; however, it was found that the yields found in Scheme 5.8 were reproducible over several experiments even with slightly different conditions that implies a more controlled mechanism with respect to N₂ functionalization. Gratifyingly, using all R₃ECl reagents employed in nitride chemistry (*vide supra*) reacted readily with the photoproduct generated from **5.2a** in similar yields except for Me₃CCl, which again required heating to form the imido complex **5.7a** as well as isobutane and isobutene co-products that signify a radical mechanism.

Scheme 5.8. Dinitrogen functionalization by Mo and W to provide isocyanates and carbodiimides.⁶



This result of obtaining imido complexes derived N₂ is exciting because nitrene group transfer (NTG) to CO to provide isocyanates has already been established by our group. These studies have also been expanded to aryl isocyanide substrates that react with imido complexes to provide carbodiimides as described in Appendix A. Thus, as described in Scheme 5.8, the imido complexes **5.7a-e** readily reacted with CO to provide their corresponding isocyanates and bis-carbonyl co-product (**5.9a**). Compound **5.7b** reacted with 2,6-dimethylphenyl isocyanide to provide the carbodiimide **5.11** and the corresponding bis-isocyanate **5.12**. While imido complexes have previously been obtained from N₂, this is the first example of obtaining organic products that uses traditional NGT chemistry. This is important

⁶ In the first step, Me₃SiOTf is also suitable for obtaining the silyl-substituted imido **5.7b**.

considering that imido complexes are known to react with a variety of substrates to provide a variety organic molecules (isocyanates, carbodiimides, aziridines, diazenes, C-H amination, etc.). For obtaining N-C based organic molecules derived from N₂, imido complexes are an ideal intermediate considering the chemistry that has been developed over the last 40 years and establishes precedent in reconciling N₂ fixation with nitrene transfer chemistry.

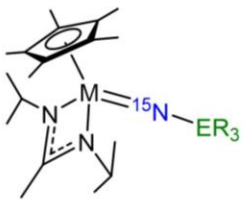
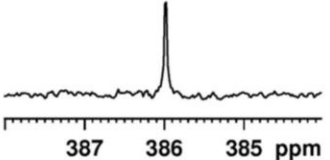
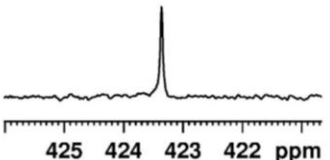
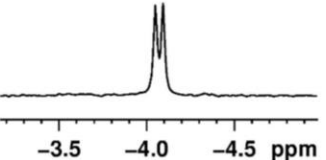
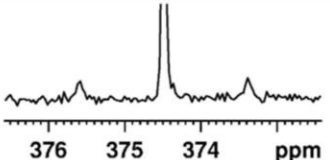
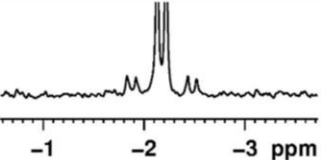
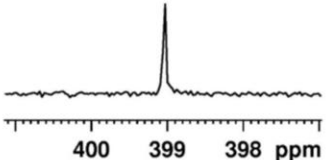
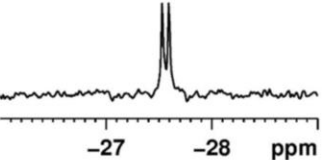
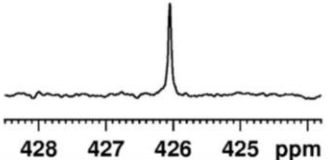
5.4.2. Labeling studies and multinuclear NMR

To further prove the formation of these N₂-derived products, isotope labeling experiments were employed. Specifically, ¹⁵N-**5.2a** and ¹⁵N-**5.2b** (15N, 98% enriched) that were synthesized using ¹⁵N labeled N₂ gas were subjected to the same N₂ functionalization experiments as outlined in Scheme 5.8. Imido products **5.7a-e** that were generated from irradiating ¹⁵N-**5.2a** and ¹⁵N-**5.2b** in the presence of the desired R₃ECl reagent were subjected to ¹⁵N NMR and for silicon containing compounds, ²⁹Si NMR. All chemical shifts and coupling constants can be found in Section 5.7.6. To begin, all ¹⁵N NMR and ²⁹Si NMR collected were consistent with the assigned CPAM imido structure. For example, analyzing a sample of ¹⁵N-**5.7b** with ¹⁵N NMR (50.68 MHz, benzene-*d*₆, 25 °C) yielded a singlet at δ 423.36 ppm and for ²⁹Si NMR (DEPT-35, 99.36 MHz, benzene-*d*₆, 25 °C), a doublet at δ -4.07 (*J*_{29Si-¹⁵N} = 4.4 Hz) showing coupling to the ¹⁵N atom. Similarly for the tungsten analogue ¹⁵N-**5.7c**, ¹⁵N NMR (50.68 MHz, benzene-*d*₆, 25 °C) yielded a singlet at δ 374.48 ppm with tungsten satellites (¹⁸³W = 14.31% abundance, ¹*J*_{15N-183W} = 111.7 Hz and for ²⁹Si NMR (DEPT-35, 99.36 MHz, benzene-*d*₆, 25 °C), a doublet with tungsten

satellites at δ -2.18 ppm ($^1J_{29\text{Si}-15\text{N}} = 8.7$ Hz, $^2J_{29\text{Si}-183\text{W}} = 59.1$ Hz). Table 5.2 presents the spectral data for all imido complexes ^{15}N -**5.7a-e**.

After all ^{15}N imido complexes were analyzed, they were exposed to either ^{13}CO (^{13}C , 99% enriched) or 2,6-dimethylphenyl isocyanide according to Scheme 5.8 to provide doubly labeled [$^{13}\text{C},^{15}\text{N}$]-isocyanates **5.10a-d** and [^{15}N]-carbodiimide **5.12** organic products. Once again, all of these products subjected to ^{13}C , ^{15}N and ^{29}Si

Table 5.2. Multinuclear NMR of ^{15}N -labeled imido complexes **5.7a-e**.

	^{15}N NMR (50.68 MHz)	^{29}Si NMR (99.36 MHz)
Mo, CMe₃ 5.7a		
Mo, SiMe₃ 5.7b		
W, SiMe₃ 5.7c		
Mo, SiPh₃ 5.7d		
Mo, GeMe₃ 5.7e		

NMR to fully characterize and establish the incorporation of isotopic labels. All NMR resonances were located and are consistent with the assigned structures (see Section 5.6.6 for a complete list of chemical shifts and coupling constants). The NMR spectra that is most descriptive of double label incorporation (^{13}C , ^{15}N) for the isocyanate compounds are the DEPT-35 ^{29}Si NMR spectra for the silyl substituted derivatives (**5.10b** and **5.10c**), where coupling is shown to both ^{15}N and ^{13}C nuclei (for **5.10b**: δ 3.91 [$^1J_{29\text{Si}-15\text{N}} = 14.7$ Hz, $^2J_{29\text{Si}-13\text{C}} = 8.5$ Hz]; for **5.10c**: δ -21.08 [$^1J_{29\text{Si}-15\text{N}} = 18.6$ Hz, $^2J_{29\text{Si}-13\text{C}} = 8.8$ Hz]). For the carbodiimide product **5.12**, it was necessary to obtain heteronuclear NMR considering that silyl substituted carbodiimides are known to isomerize to the corresponding cyanimide. As evidenced

Table 5.3. Multinuclear NMR (benzene- d_6 , 25 °C) of doubly labeled [^{13}C , ^{15}N]-isocyanates **5.10a-d** and labeled [^{15}N]-carbodiimide **5.12**.

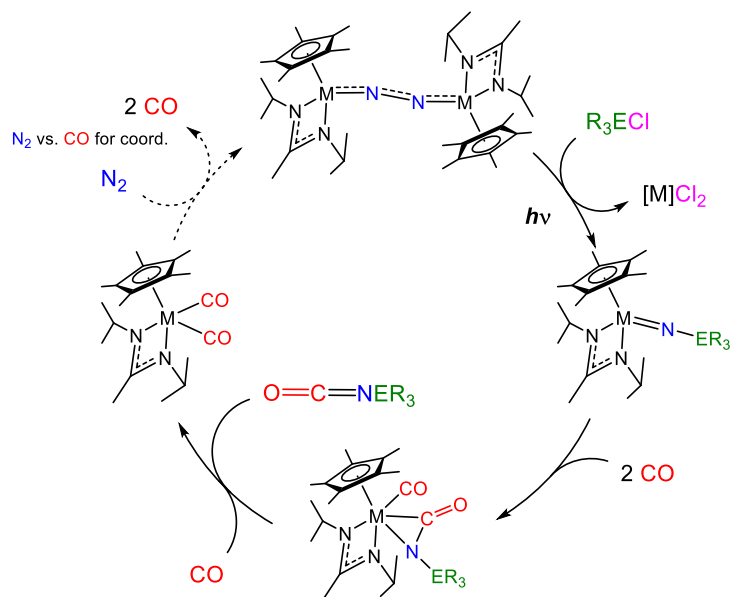
	^{13}C NMR (125.76 MHz)	^{15}N NMR (50.68 MHz)	^{29}Si NMR (99.36 MHz)
$\text{O}=\text{C}=\text{NMe}_3$ ^{13}C and ^{15}N labeled 5.10a			-----
$\text{O}=\text{C}=\text{NSiMe}_3$ ^{13}C and ^{15}N labeled 5.10b			
$\text{O}=\text{C}=\text{NSiPh}_3$ ^{13}C and ^{15}N labeled 5.10c			
$\text{O}=\text{C}=\text{NGeMe}_3$ ^{13}C and ^{15}N labeled 5.10d			-----
$\text{Ar}'\text{N}=\text{C}=\text{NSiMe}_3$ ^{15}N labeled 5.12	-----		

by ^{29}Si NMR, a doublet was located at δ 1.78 $^1J_{29\text{Si}-15\text{N}} = 14.0$ Hz indicating coupling of the ^{29}Si and ^{15}N nuclei was found with a coupling constant of $^1J_{29\text{Si}-15\text{N}} = 14.0$ Hz. This coupling constant is similar to the coupling constants of silyl substituted isocyanates, affirming the Si- ^{15}N connectivity and establishing the identity of this product as the carbodiimide **5.12**.

5.5. On Pursuing Catalysis

5.5.1. Catalytic implications of discovered dinitrogen functionalization

Considering the chemistry described in this chapter, a natural pathway for recycling the metal species to obtain multiple equivalents of organic product can be hypothesized (Scheme 5.9). As shown, the dinitrogen complex can be photocleaved in the presence of R_3ECl reagents to provide the imido and metal dichloride. The metal dichloride can be recycled back to the dinitrogen complex by reduction under **Scheme 5.9**. Hypothetical cycle for production of isocyanates derived from N_2 .



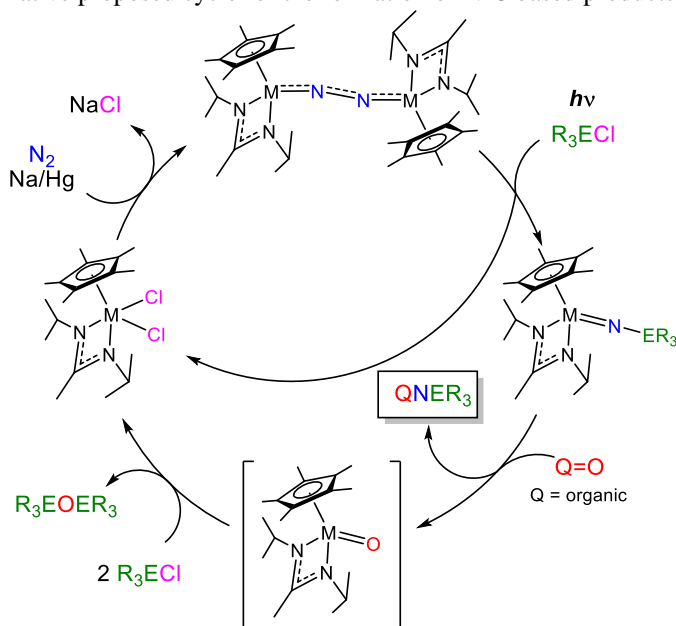
an atmosphere of N₂. Following reaction of the imido complex with CO, the isocyanate is formed along with a metal dicarbonyl co-product. The greatest challenge in this cycle is the re-coordination of N₂. Carbon monoxide coordinates very strongly to reduced metal centers, whereas dinitrogen is a very poor ligand. Experiments attempting to re-coordinate N₂ directly from the bis-carbonyl species using 30 psi of N₂, UV transparent media and UV irradiation provided evidence that no N₂ re-coordination was taking place. This is the main challenge when using a strongly coordinating substrate for nitrene group transfer – it is difficult to later displace when N₂ is attempting to coordinate to the metal center. Although chemistry involving a series of transformations has been developed by Wesley Farrell to overcome this issue involving isolated steps using chemistry developed by Jonathan Reeds (the light mediated conversion of bis-carbonyl species to metal oxo compound in the presence of CO₂) and chemistry developed by Gerard Parkins (conversion of group 6 metallocene oxo complexes to the metal dichloride using 2 eq. of Me₃SiCl that can be reduced under the presence of N₂ to provide the starting N₂ material for a second cycle). There is still a significant challenge in re-coordinating dinitrogen in a mixed N₂/CO atmosphere.

5.5.2. Future direction for pursuing catalytic formation of N-C based products

Ideally, a catalytic system that can be that can take place in a single reaction vessel under N₂ atmosphere and in the presence of desired reagents/substrates would be most feasible. As mentioned in the previous section, the main challenge inhibiting catalysis is the imido group transfer substrate carbon monoxide. While this reagent gives the desired isocyanate product, it inhibits any re-coordination of N₂. Thus, to

produced in this cycle can be converted back into the dinitrogen complex to undergo a subsequent photocleavage step. Ideally, the photophysics of dinitrogen cleavage can be further elucidated to provide the bis(μ -nitrido) in quantitative yield (without photo N_2 extrusion) and the reagent $Hg(SiMe_3)_2$ can be employed to quantitatively obtain the imido species without any metal chloride by-products.

Scheme 5.11. Alternative proposed cycle for the formation of N-C based products derived from N_2 .



A second hypothetical cycle (Scheme 5.11) that uses chemistry developed by Wesley Farrell involving the conversion of metal oxo species to the metal dichloride can be hypothesized. This includes the use of oxygen based substrates for imido group transfer. For example, aldehyde, ketone, isocyanate and CO_2 substrates ($Q=O$ as described in Scheme 5.11) are known to react with imido species to obtain organic products with a metal oxo co-product.¹⁶ This oxo species can be converted to the metal dichloride using R_3ECl reagents with production of R_3EOER_3 . The dichloride can subsequently be converted into the dinitrogen complex *via* reduction for further turnover. Again, for this cycle to operate in true catalytic form, the substrate ($Q=O$)

needs to be non-competitive with N₂ for recoordination. A comprehensive analysis of substrate scope of the imido compounds needs to be undertaken.

5.6. Conclusion

Chemistry of group 6 metal nitride complexes has been developed to obtain imido complexes. This chemistry has been successfully extended to dinitrogen functionalization studies. Labeling experiments have unequivocally established the source of nitrogen atoms found in these organic product as ¹⁵N labeled N₂ gas. The implications of these have been discussed, which includes using imido compounds to provide organic N-C based products for the first time in the context of N₂ fixation. These discoveries establish a foundation for pursuing a system capable of catalytically obtaining N-C based organic products directly from N₂.

5.7. Experimental Section

5.7.1. General considerations

All manipulations with air and moisture sensitive compounds were carried out under N₂ or Ar atmospheres with standard Schlenk or glovebox techniques. Et₂O and THF were distilled from Na/benzophenone under N₂ prior to use. Toluene and pentane were dried and deoxygenated by passage over activated alumina and a copper catalyst within a PureSolv solvent purification system manufactured by Innovative Technologies and collected under N₂ prior to use. Benzene-*d*₆ and toluene-*d*₈ were dried over Na/K alloy and isolated by vacuum transfer prior to use. Celite was oven dried (150 °C for several days) prior to use. Cooling was performed in the internal freezer of a glovebox maintained at -30 °C. Trimethylsilyl azide, trimethylsilyl

chloride, triphenylsilyl chloride, trimethylgermanium chloride and *tert*-butyl chloride were purchased from Sigma Aldrich and used as received. Complexes **5.2**,¹⁹ [¹⁵N₂]-**5.2**,¹⁸ **5.4**,¹⁹ and Hg(SiMe₃)₂²⁰ were prepared according to the previously reported procedures in similar yield and purity. All room temperature ¹H NMR were recorded at 400.13 MHz and referenced to SiMe₄ using residual ¹H chemical shifts of benzene-*d*₆. ¹³C NMR spectra were recorded at 125.76 MHz and calibrated to residual ¹³C chemical shifts of benzene-*d*₆. ¹⁵N NMR spectra were recorded at 50.68 MHz and externally referenced to NH_{3(l)} using neat MeNO₂ (380.2 ppm) as a standard. ²⁹Si DEPT-35 NMR were recorded at 99.36 MHz and externally referenced to a solution of SiMe₄ in benzene-*d*₆. Photochemical reactions were performed using a Rayonet[®] Photochemical Reactor containing a carousel of 16 ultraviolet medium-pressure mercury lamps (catalogue number: RPR-3500A). Elemental analyses were carried out by Midwest Microlab, LLC.

5.7.2. Synthesis of new compounds

Cp*Mo[N(^{*i*}Pr)C(Me)N(^{*i*}Pr)](NSiPh₃) (5.7d). Sodium Amalgam (0.5% w/w) (5.88 g, 1.28 mmol Na) was added to a -30 °C solution of **5.4a** (179 mg, 0.42 mmol) in 5 mL of THF. After stirring for 2 h at room temperature, the solution was decanted into a vial containing Ph₃SiCl (62.5 mg, 0.21 mmol) in 3 mL and stirred for 1.5 h. The solution was then transferred back to vial containing sodium amalgam and stirred for 2 h. The solution was decanted into a vial containing Ph₃SiCl (31.2 mg, 0.11 mmol) and stirred for 4 h, which was followed by transferring the solution back to the vial containing sodium amalgam and stirred for 2 h. The solution was finally decanted into a vial containing Ph₃SiCl (15.5 mg, 0.05 mmol), stirred for 3 h, followed by

removing volatiles *in vacuo* to give a dark red oil. The crude product was dissolved in pentane and filtered through Celite supported by a plug of KimWipe in a glass pipet and removal of volatiles yielded a red oil containing **5.7d** and a small amount of Ph₃SiCl impurity that was identified by NMR and not purified further (217 mg, 75%). ¹H NMR (400.13 MHz, benzene-*d*₆, 25 °C): 0.96 (6H, d, *J* = 6.4 Hz, CH(CH₃)₂), 1.12 (6H, d, *J* = 6.4 Hz, CH(CH₃)₂), 1.58 (3H, br, NC(CH₃)N), 1.84 (15H, s, C₅(CH₃)₅), 3.21 (2H, sept, *J* = 6.4 Hz, CH(CH₃)₂), 7.24 (9H, m, Si(C₆H₅)₃), 7.93 (6H, m, Si(C₆H₅)₃).

Cp*Mo[N(ⁱPr)C(Me)N(ⁱPr)][NGeMe₃] (5.7e). Sodium Amalgam (0.5% w/w) (10.90 g, 2.37 mmol Na) was added to a -30 °C solution of **5.4a** (250 mg, 0.59 mmol) in 5 mL of THF. After stirring for 3 h at room temperature, Me₃GeCl (36.6 μL, 0.30 mmol) was added *via* microsyringe. The solution was stirred for 1 h and then a second aliquot of Me₃GeCl (18.3 μL, 0.15 mmol) was added. After stirring for 2 h, a third aliquot of Me₃GeCl (9.2 μL, 0.07 mmol) was added followed by 14 h of stirring at room temperature. Volatiles were removed *in vacuo* to give a black solid, which was dissolved in pentane and filtered through Celite supported by a plug of Kimwipe in a glass pipet. The filtrate was concentrated and crystallized from a concentrated pentane solution at -30 °C to give dark red crystals of **5.7e** (187 mg, 63% yield). Anal. Calc'd for C₂₁H₄₁N₃Ge₁Mo₁: C, 50.03; H, 8.20; N, 8.34; Found: C, 50.22; H, 8.08; N, 8.17. ¹H NMR (400.13 MHz, benzene-*d*₆, 25 °C): 1.06 (6H, d, *J* = 6.4 Hz, CH(CH₃)₂), 1.24 (6H, d, *J* = 6.4 Hz, CH(CH₃)₂), 1.58 (3H, s, NC(CH₃)N), 1.93 (15H, s, C₅(CH₃)₅), 3.22 (2H, sept, *J* = 6.4 Hz, CH(CH₃)₂).

Large scale photolysis of 5.2a. One benzene- d_6 solution to monitor reaction progress and two unlabeled toluene solutions of **5.2a** were prepared in Pyrex J. Young tubes: 36.4 mg of **5.2a** in 2 mL of benzene- d_6 , 36.8 mg of **5.2a** in 2 mL of toluene and 36.7 mg of **5.2a** in 2 mL of toluene. The solutions were photolyzed for 63.5 h where ^1H NMR of the benzene- d_6 NMR tube revealed the complete disappearance of **5.2a**. The solutions were combined in a vial, and volatiles were removed *in vacuo*. After recrystallizing in minimal pentane, black crystals were isolated from the mother liquor (69.4 mg). Single crystals were identified by X-ray Diffraction to be a 3:1 co-crystal of **5.4a** and **5.5**.

5.7.3. ^1H NMR N_2 photocleavage experiments

Photolysis of 5.2b followed by ^1H NMR. A solution of **5.2b** (9.3 mg, 0.01 mmol) in 0.7 mL of benzene- d_6 was prepared in a Teflon sealed Pyrex J. Young NMR tube. Photolysis of this material was monitored by ^1H NMR and after 60 h of exposure, the *ca.* 50% conversion of **5.2b** to **5.4b** was noted. See Figure 5.6 for corresponding spectra.

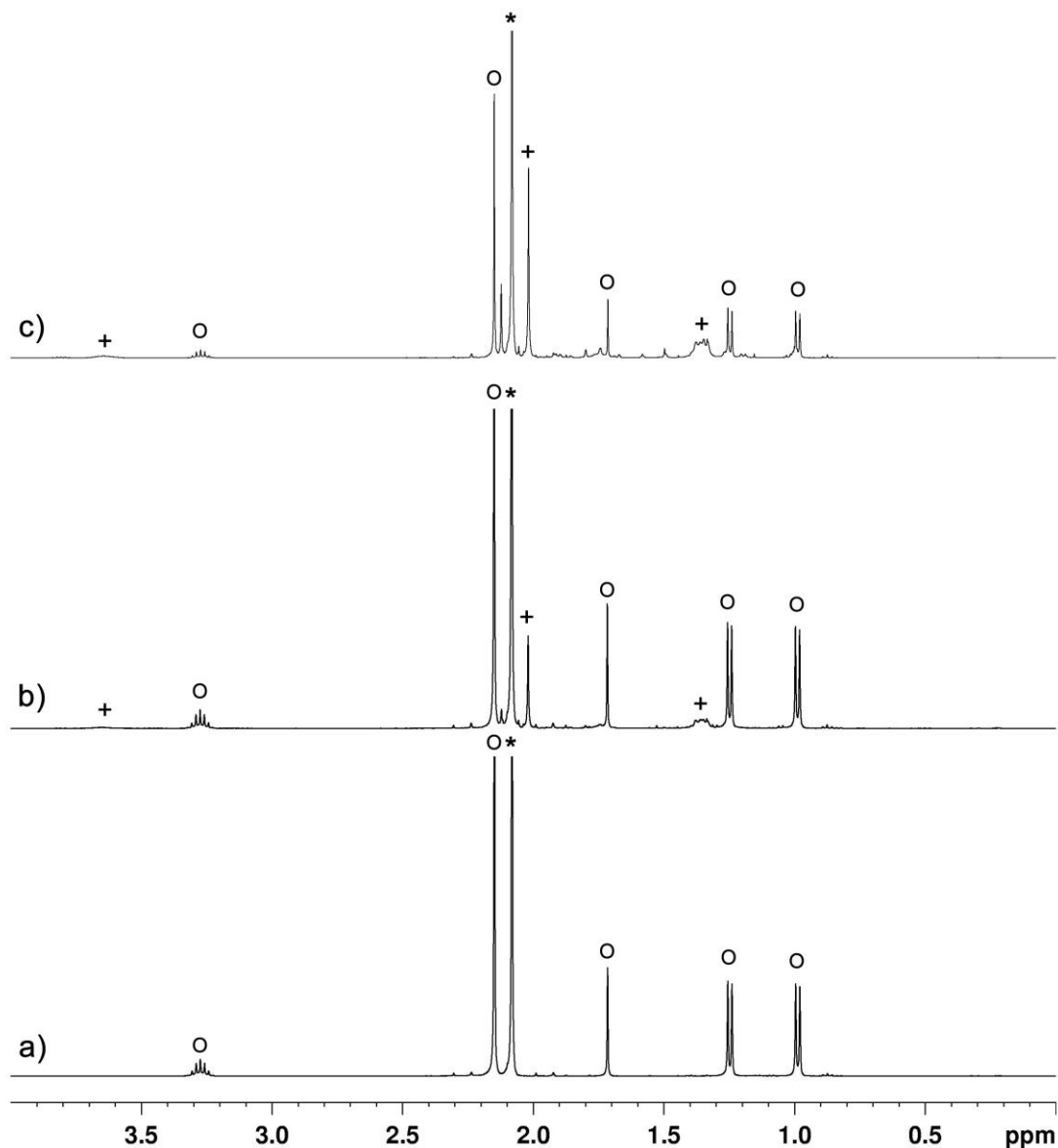


Figure 5.6. ^1H NMR (400.13 MHz, benzene- d_6 , 25 $^\circ\text{C}$) of **5.2b** (o) exposed to UV light after (a) 0 h, (b) 15.5 h, and (c) 60 h, showing production of **5.4b** (+).

5.7.4. ^1H NMR experiments of Mo and W nitride complexes with R_3ECl ($\text{R} = \text{Me}, \text{Ph};$
 $\text{E} = \text{C}, \text{Si}, \text{Ge}$)

Reactivity of 5.4a with *tert*-butyl chloride. In a Teflon sealed NMR tube, a solution of **5.4a** (9.6 mg, 0.012 mmol) and durene (4.7 mg, 0.035 mmol) in 0.5 mL of benzene- d_6 was prepared and an initial ^1H NMR was obtained. *tert*-butyl chloride (6.8

μL , 0.062 mmol) was added and mixed well. After reacting for 31 h at 80 °C, another ^1H NMR was obtained to reveal the production of **5.7a** (33% yield, durene internal standard), isobutene (-) and isobutane (l). See **Figure 5.7** for corresponding NMR spectra.

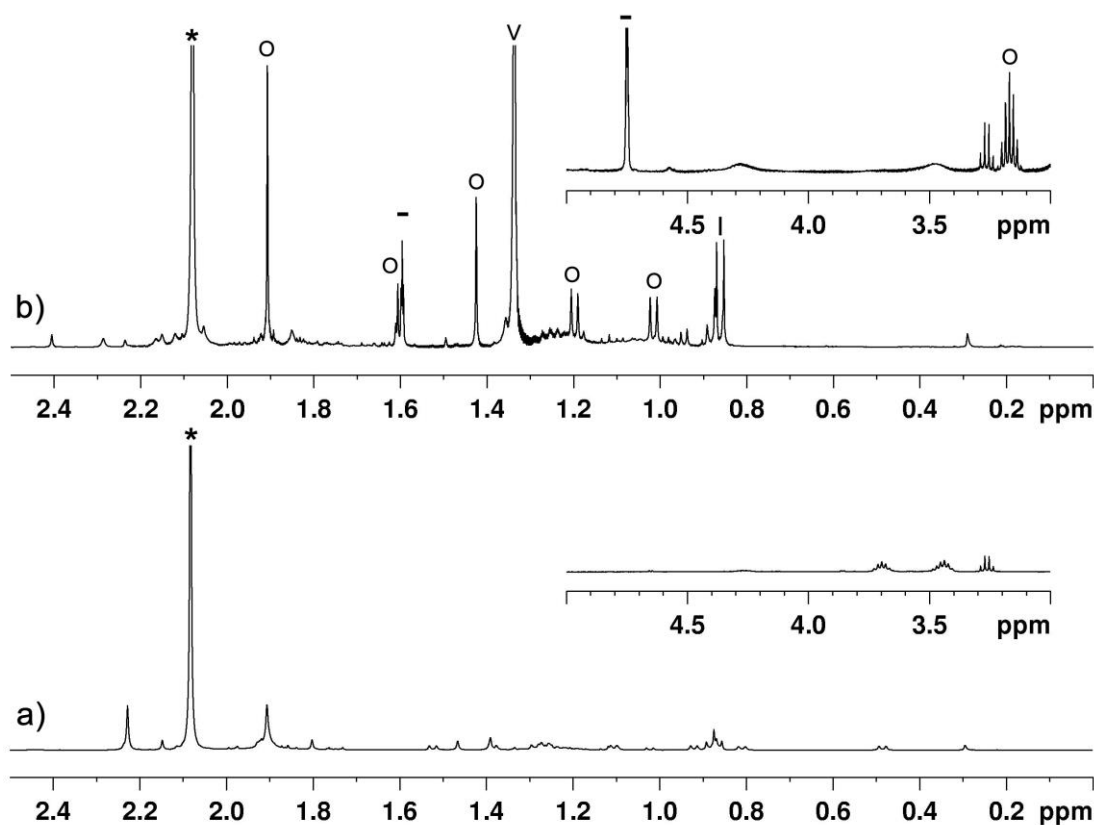


Figure 5.7. ^1H NMR (400.13 MHz, benzene- d_6 , 25 °C) of (a) initial **5.4a** and durene (*). (b) Reactivity of **5.4a** with Me_3CCl (V) after heating at 80 °C for 31h to give **5.7a** (o), isobutene (-) and isobutane (l).

Reactivity of 5.4a with Me_3SiCl . In a Teflon sealed NMR tube, a solution of **5.4a** (12.2 mg, 0.016 mmol) and durene (2.9 mg, 0.022 mmol) in benzene- d_6 was prepared and an initial ^1H NMR was taken. Me_3SiCl (7.8 μL , 0.063 mmol) was added and mixed well, with an immediate color change being observed. After reacting for 18 h, another ^1H NMR was obtained to reveal the production of **5.7b** (51% yield, durene

internal standard) and **5.3a** (27% yield, durene internal standard). See Figure 5.8 for corresponding NMR spectra.

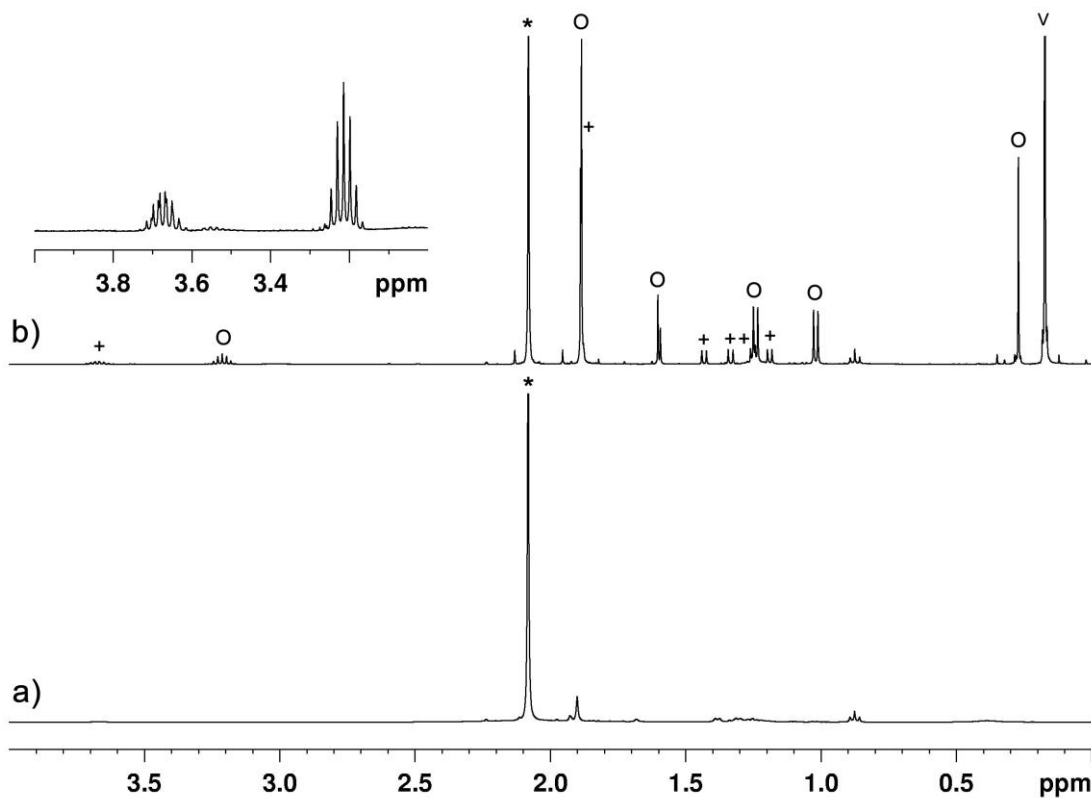


Figure 5.8. ¹H NMR (400.13 MHz, benzene-*d*₆, 25 °C) of (a) initial **5.4a** and durene (*). (b) Reactivity of **5.4a** with Me₃SiCl over 18 h to produce **5.7b** (+) and **5.3a** (O).

Reactivity of 5.4b with Me₃SiCl. In a Teflon sealed NMR tube, a solution of **5.4b** (10.0 mg, 0.011 mmol) and durene (3.3 mg, 0.025 mmol) in 0.5 mL of benzene-*d*₆ was prepared and an initial ¹H NMR was obtained. Me₃SiCl (5.2 μL, 0.042 mmol) was added and mixed well, with an immediate color change being observed. After reacting for 18 h, another ¹H NMR was obtained to reveal the production of **5.7c**

(52% yield, durene internal standard) and **5.3b** (45% yield, durene internal standard).

See Figure 5.9 for corresponding NMR spectra.

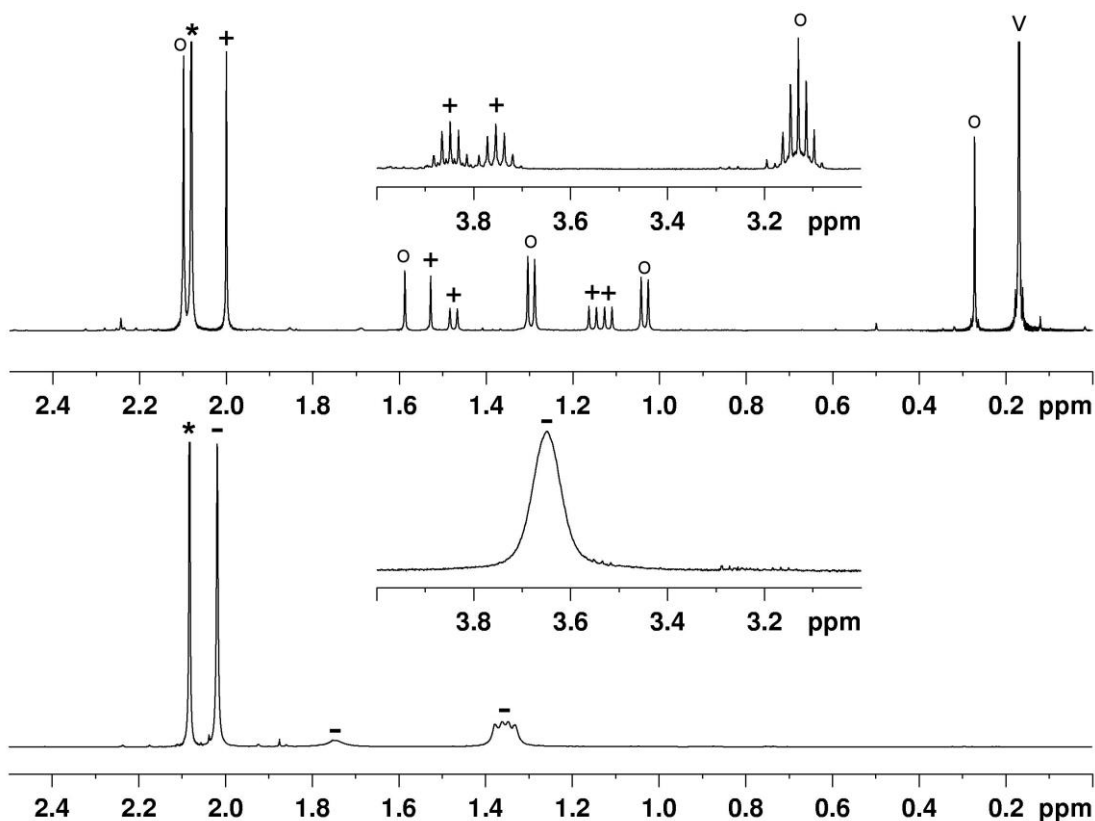


Figure 5.9. ^1H NMR (400.13 MHz, benzene- d_6 , 25 $^\circ\text{C}$) of (bottom) initial **5.4b** (-) and durene (*). (top) reactivity of **5.4b** with Me_3SiCl (V) over 18 h to produce **5.7c** (o) and **5.3b** (+).

Reactivity of 5.4a with $(\text{Me}_3\text{Si})_2\text{Hg}$. In a Teflon sealed NMR tube, a solution of **5.4a** (8.9 mg, 0.012 mmol) and durene (5.1 mg, 0.038 mmol) in 0.5 mL of benzene- d_6 was prepared and an initial ^1H NMR was obtained. $(\text{Me}_3\text{Si})_2\text{Hg}$ (12.0 mg, 0.035 mmol) was added and mixed well. After reacting for 18 h, another ^1H NMR was obtained to reveal the production of **5.7b** (94% yield, durene internal standard). See Figure 5.10 for corresponding NMR spectra.

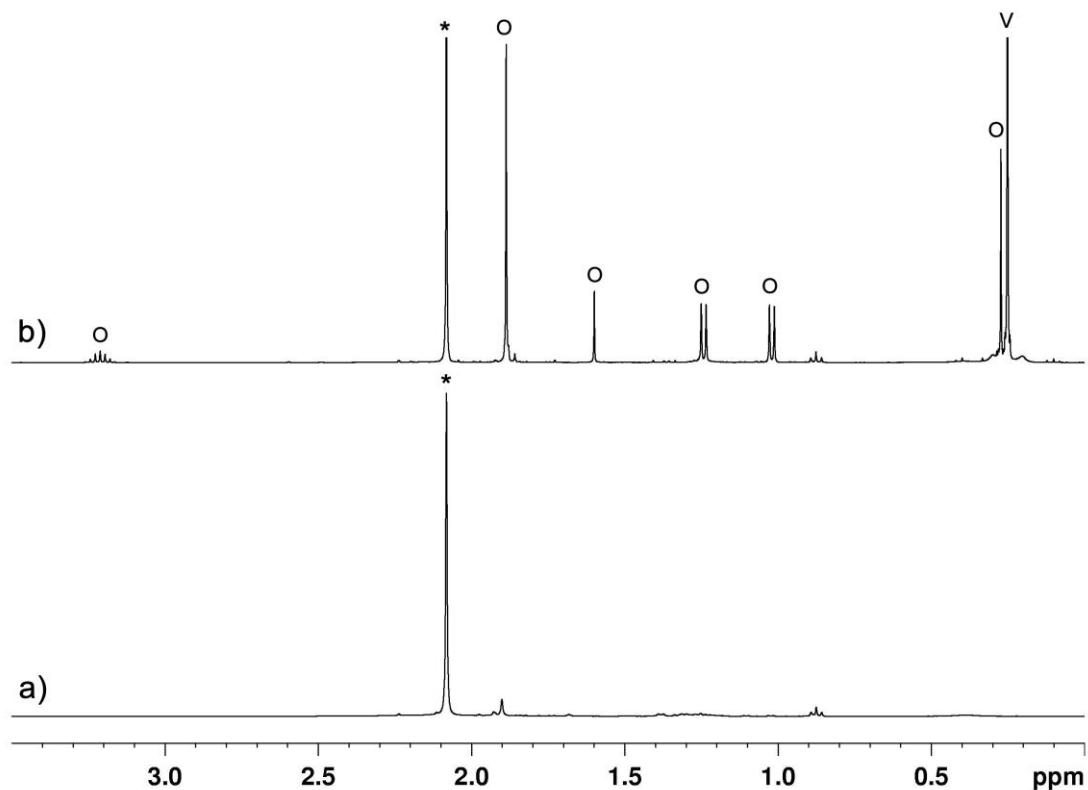


Figure 5.10. ^1H NMR (400.13 MHz, benzene- d_6 , 25 $^\circ\text{C}$) of (a) initial **5.4a** and durene (*). (b) Reactivity of **5.4a** with $(\text{Me}_3\text{Si})_2\text{Hg}$ over 18 h to give **5.7b** (o).

Reactivity of 5.4a with Ph_3SiCl . In a Teflon sealed NMR tube, a solution of **5.4a** (12.2 mg, 0.016 mmol) and durene (8.1 mg, 0.060 mmol) in 0.5 mL of benzene- d_6 was prepared and an initial ^1H NMR was obtained. Ph_3SiCl (14 mg, 0.047 mmol) was added and mixed well. After reacting for 20 min at room temperature, another ^1H NMR was obtained to reveal the production of **5.7d** (46% yield, durene internal standard) and **5.3a** (22% yield, durene internal standard). See Figure 5.11 for corresponding NMR spectra.

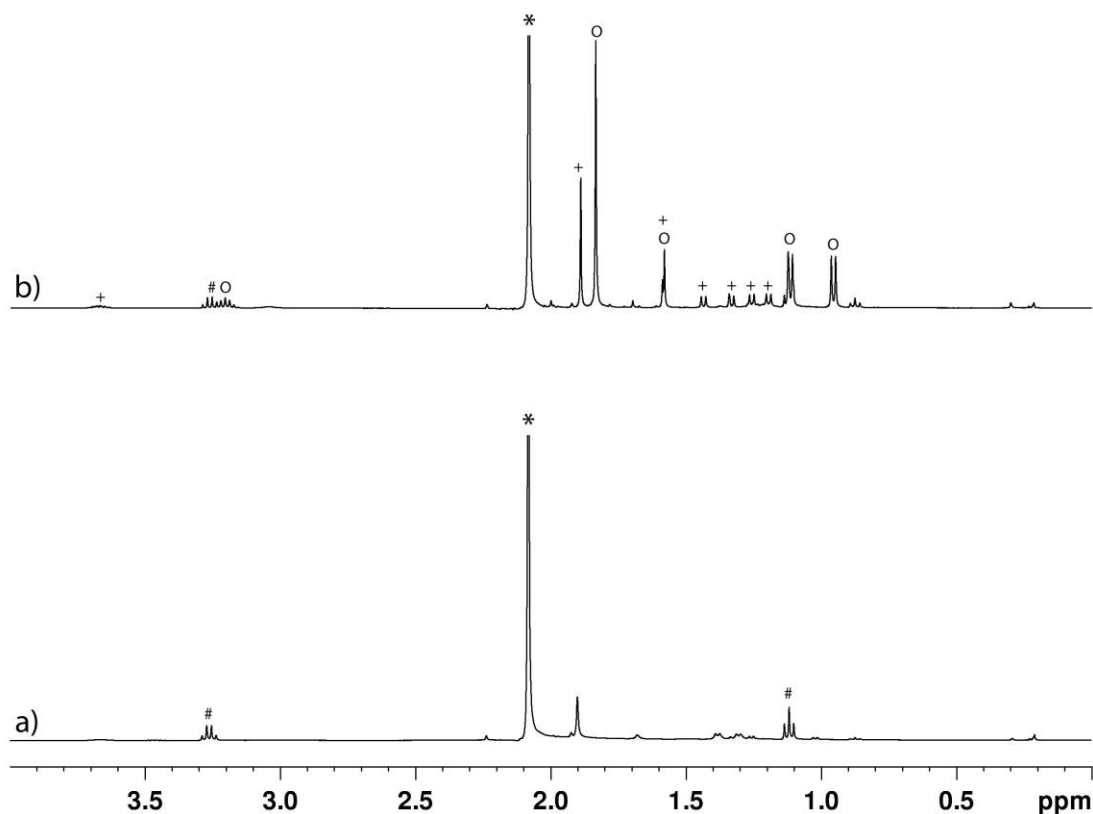


Figure 5.11. ^1H NMR (400.13 MHz, benzene- d_6 , 25 °C) of (a) initial **5.4a** and durene (*). (b) Reactivity of **5.4a** with Ph_3SiCl for 15 min to give **5.7d** (o) and **5.3a** (+). The symbol # denotes diethyl ether impurities.

Reactivity of 5.4a with Me_3GeCl . In a Teflon sealed NMR tube, a solution of **5.4a** (10.1 mg, 0.013 mmol) and durene (4.5 mg, 0.034 mmol) in 0.5 mL of benzene- d_6 was prepared and an initial ^1H NMR was obtained. Me_3GeCl (6.5 μL , 0.053 mmol) was added and mixed well. After reacting for 1 h at room temperature, another ^1H NMR was obtained to reveal the production of **5.7e** (53% yield, durene internal standard) and $[\text{Mo}](\text{N})\text{Cl}$ (27% yield, durene internal standard). See Figure 5.12 for corresponding NMR spectra.

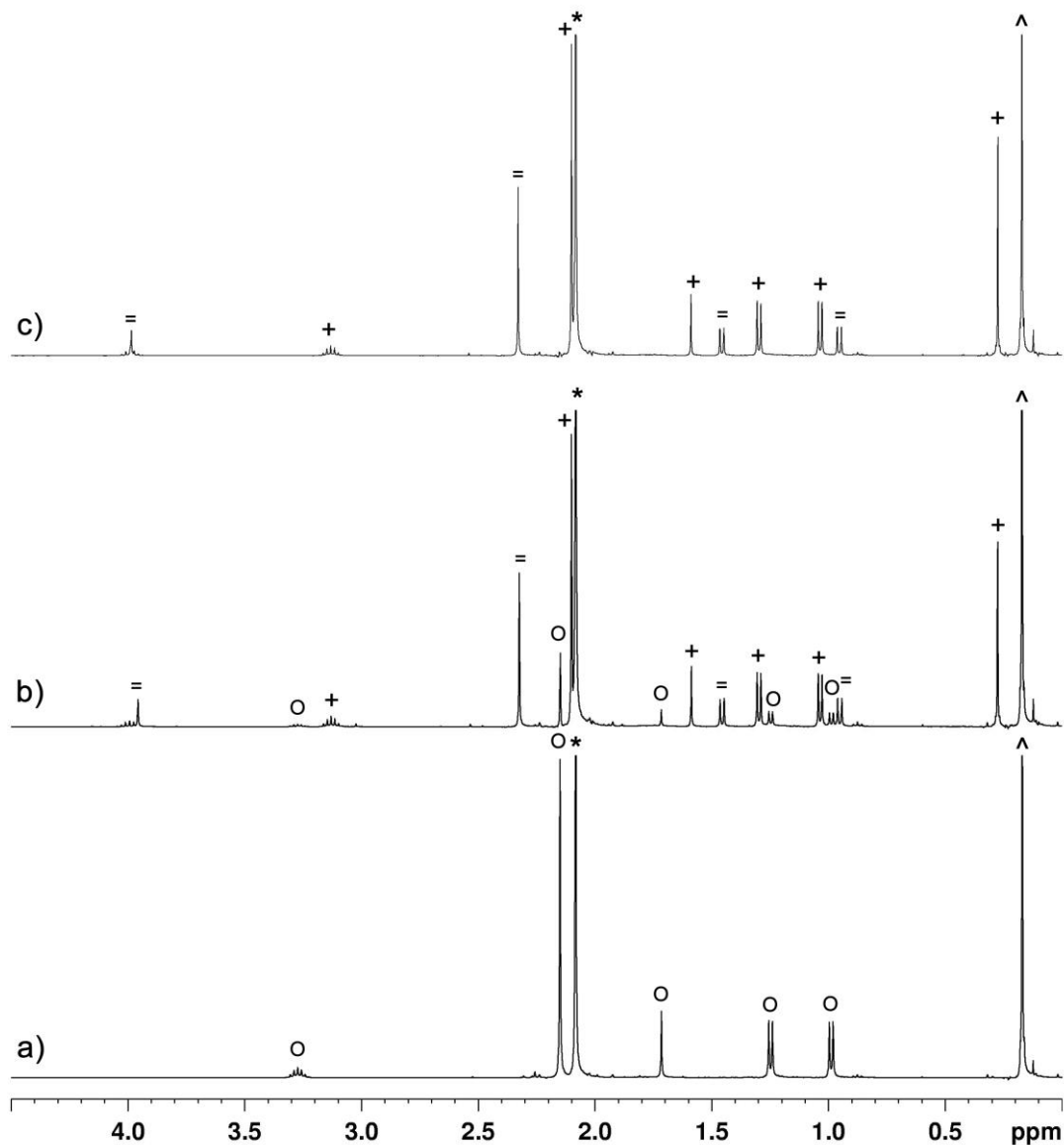


Figure 5.13. ¹H NMR (400.13 MHz, benzene-*d*₆, 25 °C) of (a) initial **5.2b** (O), durene (*), and Me₃SiCl (^), (b) after photolyzing for 49 h showing partial conversion to **5.7c** (+) and **5.8b** (=) and (c) after photolyzing for 119 h to complete the conversion to **5.7c** and **5.8b**.

Production of *tert*-butyl isocyanate (5.10a) from 5.2a. A solution of **5.2a** (11.5 mg, 0.015 mmol) and durene (4.0 mg, 0.030 mmol) in 0.7 mL of benzene-*d*₆ was prepared in a Teflon sealed Pyrex NMR tube. Photolysis of this material was monitored by ¹H NMR and following 70 h of irradiation, the complete consumption of **5.2a** and the production of paramagnetic species were noted. *Tert*-butyl chloride (8.2 μL, 0.074

mmol) was added and mixed well. After reacting for 27 h at 80 °C, another ^1H NMR spectrum was obtained to reveal the production of **5.7a** (36% yield, durene internal standard), isobutene, isobutene, as well as paramagnetic shifts of **5.8a**. The tube was degassed with three freeze-pump-thaw cycles and then charged with 5 psi of carbon monoxide for 23 h to provide **5.9a** (34% yield, durene internal standard) and Me_3CNCO (**5.10a**) (27% yield, durene internal standard). See Figure 5.14 for corresponding NMR spectra.

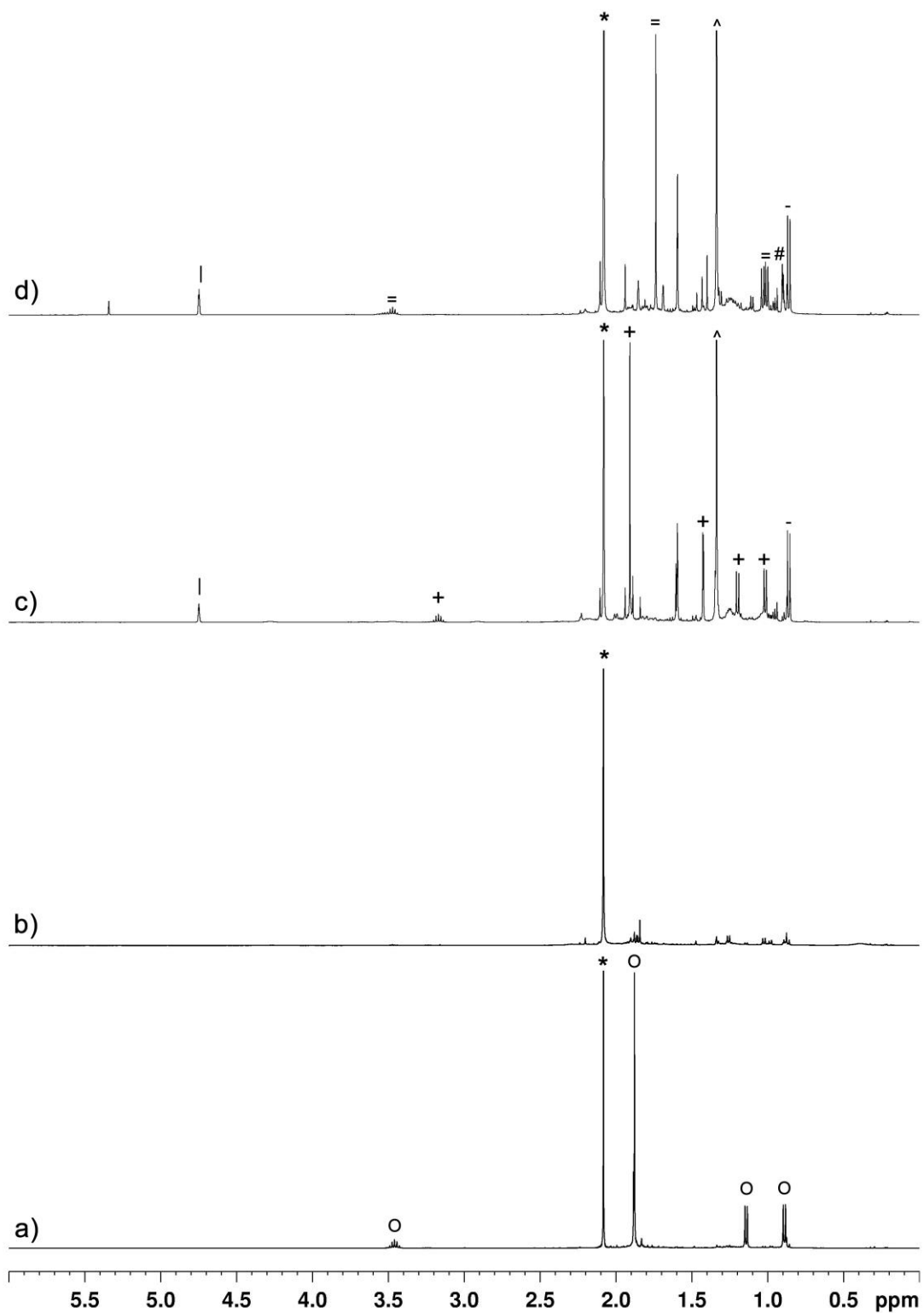


Figure 5.14. ^1H NMR (400.13 MHz, benzene- d_6 , 25 °C) of (a) initial **5.2a** (O) and durene (*), (b) after photolyzing for 65 h, (c) after adding *tert*-butyl chloride (^) and heating to provide **5.7a** (+), isobutene (l) and isobutane (-) followed by (d) reacting with carbon monoxide for 23 h to provide **5.9a** (=) and Me₃CNCO (**5.10a**).

Production of trimethylsilyl isocyanate (5.10b) from 5.2a. A solution of **5.2a** (11.2 mg, 0.014 mmol), durene (3.3 mg, 0.025 mmol) and Me₃SiCl (9.2 μL, 0.072 mmol) in 0.7 mL of benzene-*d*₆ was prepared in a Teflon sealed Pyrex NMR tube. Photolysis of this material was monitored by ¹H NMR and after 40 h of exposure, the complete consumption of **5.2a** and the production of **5.7b** (60% yield, durene internal standard) and paramagnetic shifts of **5.8a** was revealed. Subsequently, the NMR tube was degassed with three freeze-pump-thaw cycles and charged with 10 psi of carbon monoxide. After reacting for 14 h, a ¹H NMR spectrum was obtained to reveal the formation of **5.9a** (65% yield, durene internal standard) and Me₃SiNCO (**5.10b**) (60% yield, durene internal standard). See Figure 5.15 for corresponding NMR spectra.

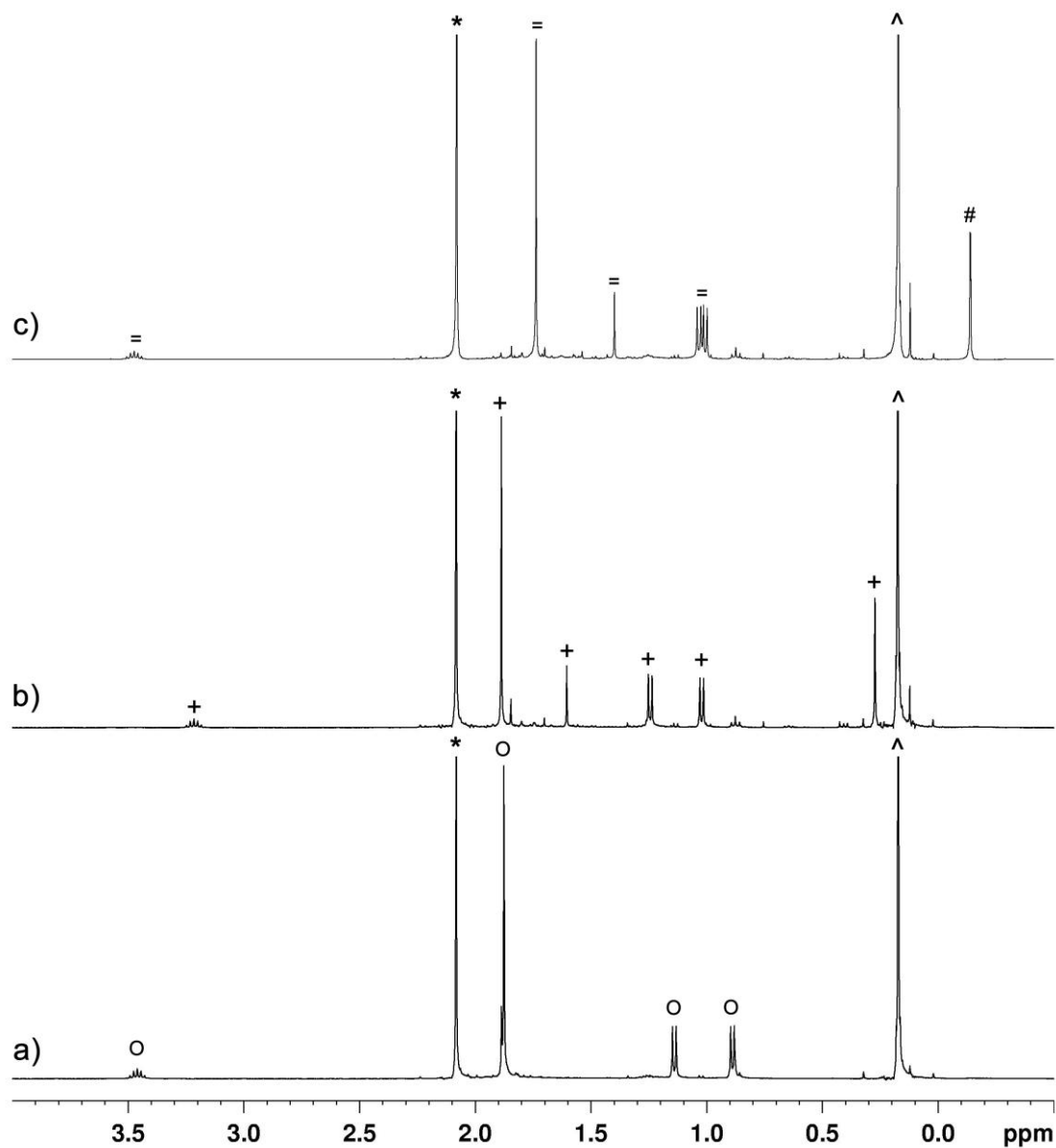


Figure 5.15. ¹H NMR (400.13 MHz, benzene-*d*₆, 25 °C) of (a) initial **5.2a** and durene (*), (b) after photolyzing for 65 h, (c) after adding Ph₃SiCl (^) to provide **5.7b** (+) followed by (d) reacting with CO to provide **5.9a** (=) and Me₃SiNCO (**5.10b**).

Production of triphenylsilyl isocyanate (5.10c) from 5.2a. A solution of **5.2a** (12.1 mg, 0.016 mmol) and durene (5.0 mg, 0.037 mmol) in 0.7 mL of benzene-*d*₆ was prepared in a Teflon sealed Pyrex NMR tube. Photolysis of this material was monitored by ¹H NMR and after 65 h of exposure, the complete consumption of **5.2a**

and the production of paramagnetic shifts of **5.9a** were noted. Triphenylsilyl chloride (13.8 mg, 0.047 mmol) was added and mixed well. After reacting for 4 h, another ^1H NMR spectrum was obtained to reveal the production of **5.7d** (62% yield, durene internal standard) and paramagnetic resonances of **5.8a**. The tube was degassed with three freeze-pump-thaw cycles and then charged with 1 atm of carbon monoxide for 39 h to provide **5.9a** (52% yield, durene internal standard) and Ph_3SiNCO (**5.10c**) (56% yield, durene internal standard). See Figure 5.16 for corresponding NMR spectra.

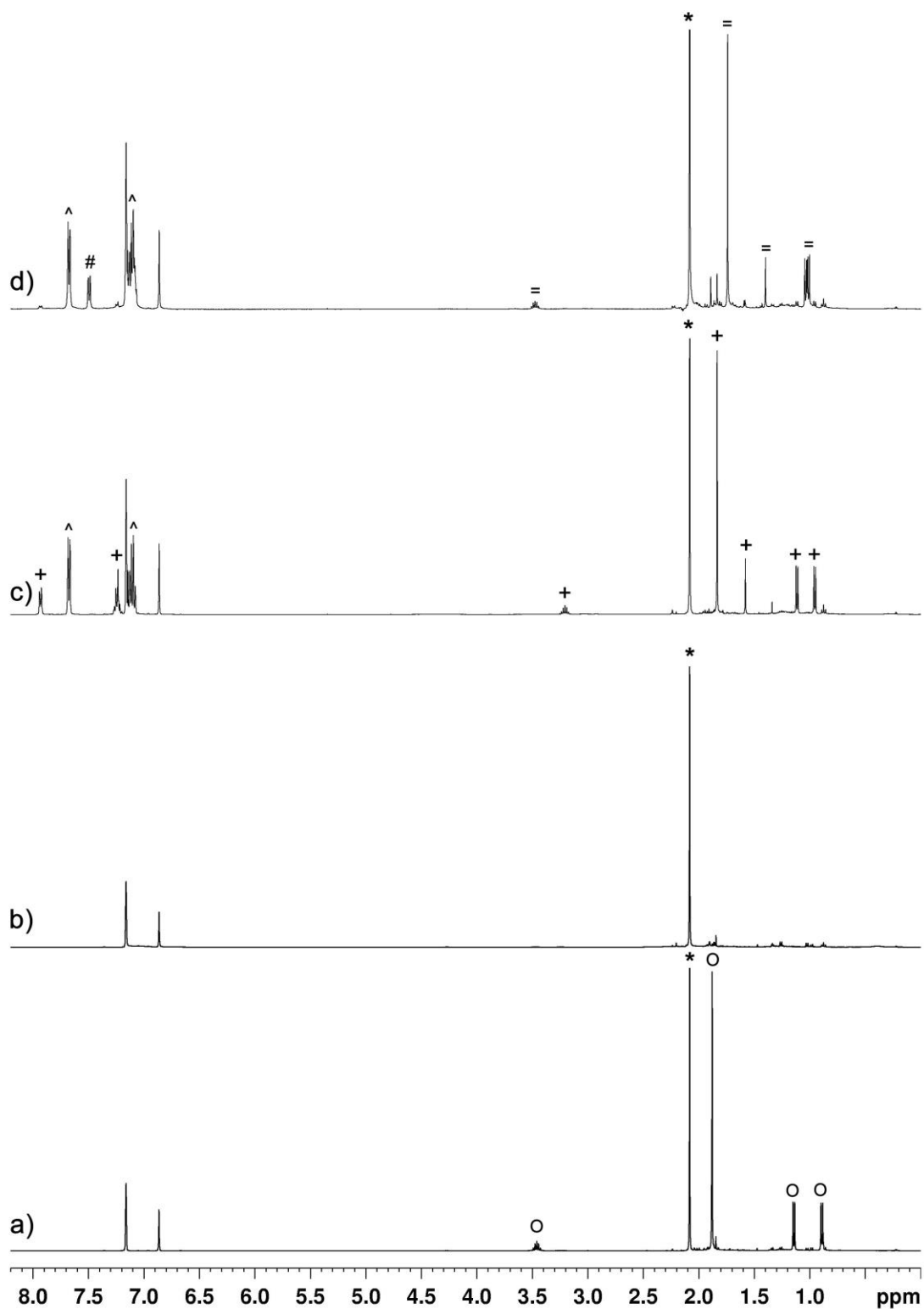


Figure 5.16. ^1H NMR (400.13 MHz, benzene- d_6 , 25 °C) of (a) initial **5.2a** (O) and durene (*), (b) after photolyzing for 65 h, (c) after adding Ph_3SiCl (^) to provide **5.7d** (+) followed by (d) reacting with CO to provide **5.9a** (=) and Ph_3SiNCO (**5.10c**).

Production of trimethylgermyl isocyanate (5.10d) from 5.2a. A solution of **5.2a** (15.3 mg, 0.020 mmol) and durene (7.7 mg, 0.057 mmol) in 0.7 mL of benzene-*d*₆ was prepared in a Teflon sealed Pyrex NMR tube. Photolysis of this material was monitored by ¹H NMR and after 82.5 h of exposure, the complete consumption of **5.2a** and the production of paramagnetic resonances were noted. Trimethylgermyl chloride (12.2 μL, 0.099 mmol) was added and mixed well. After reacting for 2 h, another ¹H NMR spectrum was obtained to reveal the production of **5.7e** (66% yield, durene internal standard) and paramagnetic resonances of **5.8a**. The tube was degassed with three freeze-pump-thaw cycles and then charged with 1 atm of carbon monoxide and heated to 50 °C for 10 h to provide **5.9a** (78% yield, durene internal standard) and Me₃GeNCO (**5.10d**) (64% yield, durene internal standard). See Figure 5.17 for corresponding NMR spectra.

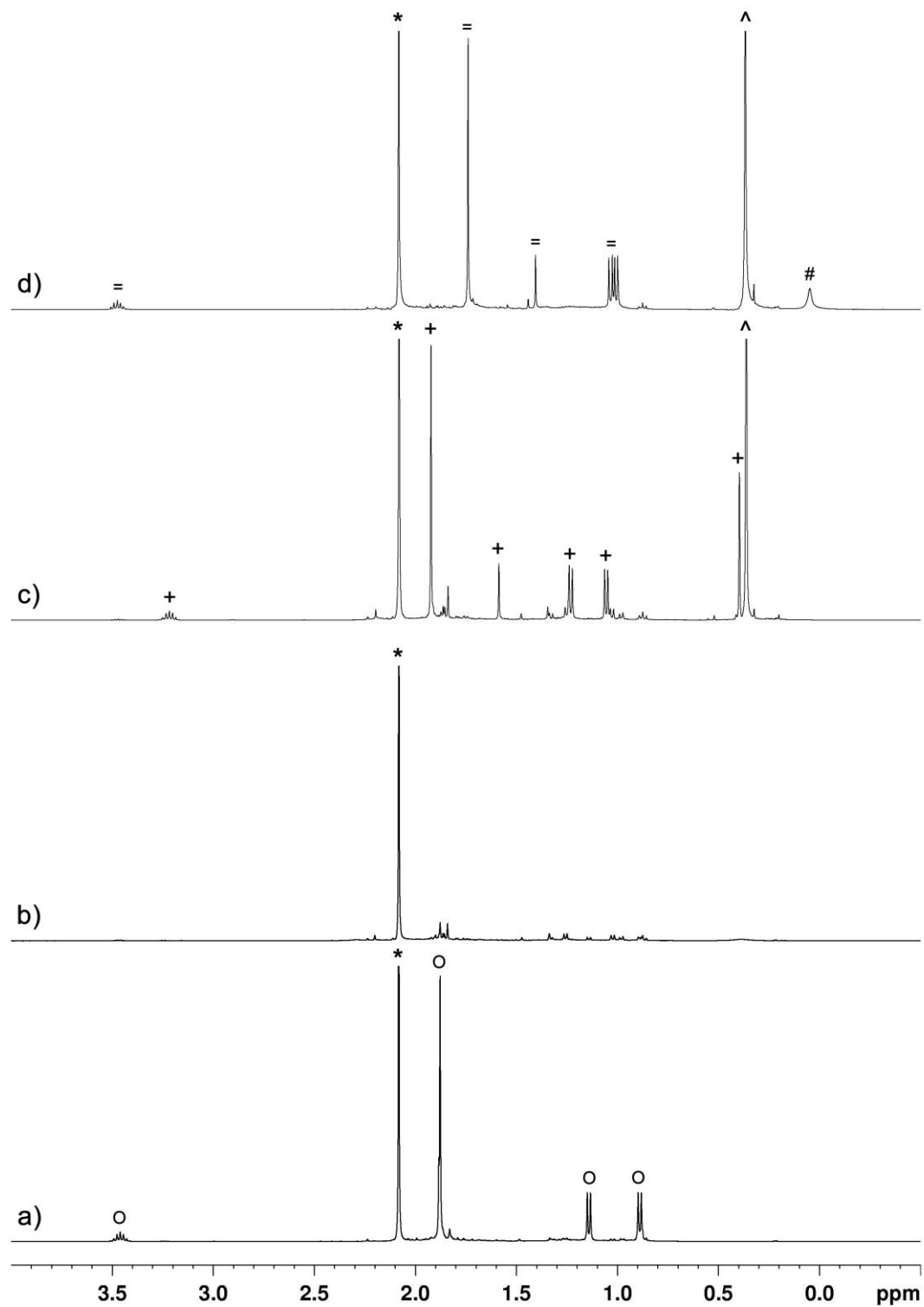


Figure 5.17. ¹H NMR (400.13 MHz, benzene-*d*₆, 25 °C) of (a) initial **5.2a** and durene (*), (b) after photolyzing for 82.5 h, (c) after adding Me₃GeCl (^) to provide **5.7e** (+) followed by (d) reacting with CO to provide **5.9a** (=) and Me₃GeNCO (**5.10d**).

Production of Me₃SiNCNAr' (5.12) (Ar' = 2,6-dimethylphenyl) from 5.2a. A solution of **5.2a** (12.0 mg, 0.016 mmol), durene (3.3 mg, 0.030 mmol) and Me₃SiCl (9.6 μL, 0.077 mmol) in 0.7 mL of benzene-*d*₆ was prepared in a Teflon sealed Pyrex NMR tube. Photolysis of this material was monitored by ¹H NMR and after 94 h of irradiation, the complete consumption of **5.2a** and the production of **5.7b** (65% yield, durene internal standard) and paramagnetic shifts of **5.8a** was revealed. Subsequently, the NMR tube was charged with 2,6-dimethylphenyl isocyanide (CNAr') (12.4 mg, 0.095 mmol). After reacting for 8 h, a ¹H NMR spectrum was obtained and revealed the formation of **5.11** (82% yield, durene internal standard) and Me₃SiNCNAr' (**5.12**) (42% yield, durene internal standard). See Figure 5.18 for corresponding NMR spectra.

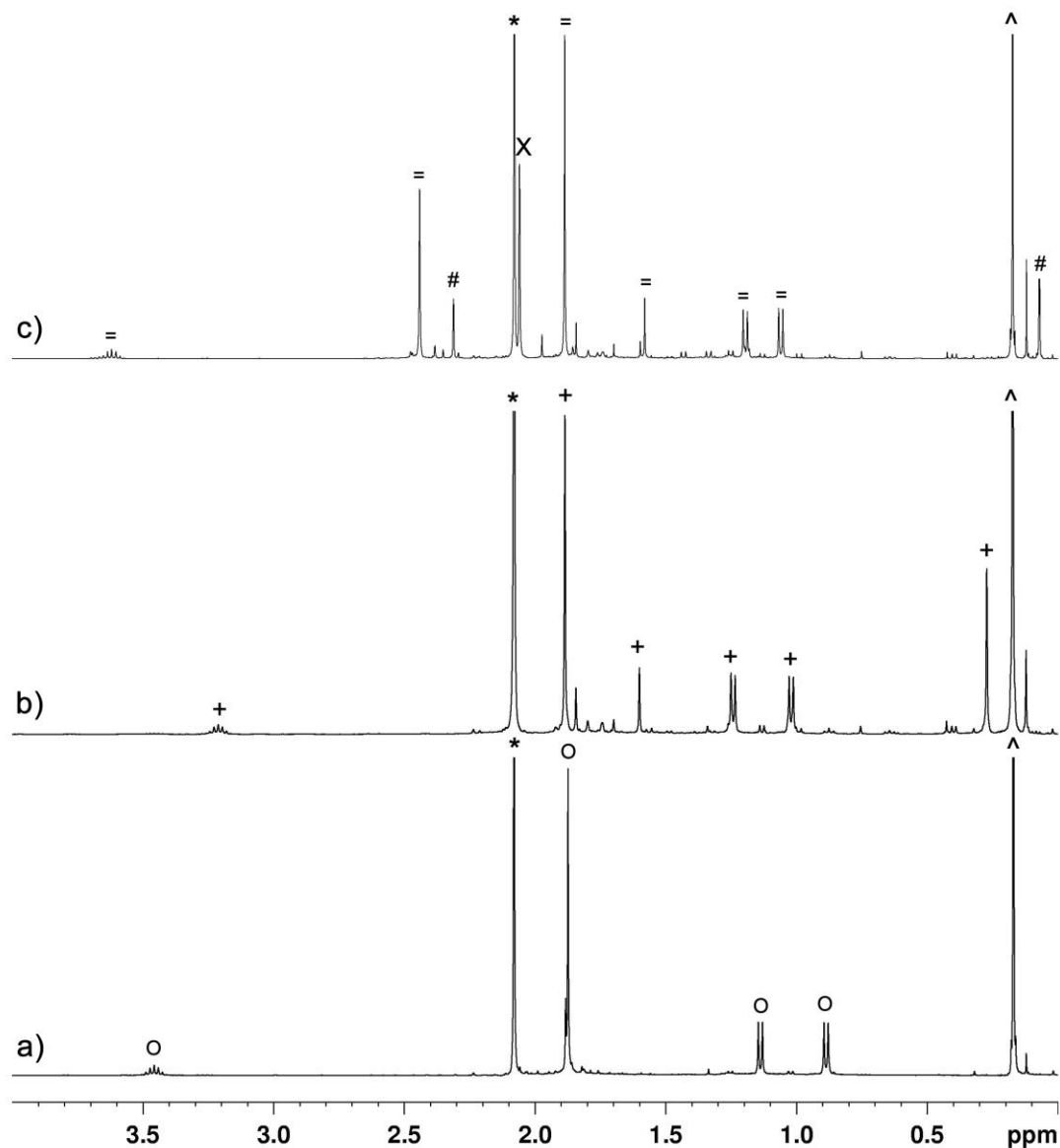


Figure 5.18. ¹H NMR (400.13 MHz, benzene-*d*₆, 25 °C) of (a) initial **5.2a** (O), Me₃SiCl (V) and durene (*), (b) after photolyzing for 94 h to produce **5.7b** (I) and (c) 8 h after addition of 2,6-dimethylphenyl isocyanide (CNAr') (X) to produce **5.11** (-) and Me₃SiNCNAr (**5.12**) (+).

5.7.6. Labeling studies and multinuclear NMR of group 6 ¹⁵N imido species, [¹³C, ¹⁵N]-isocyanates and ¹⁵N-carbodiimides

General preparation of group 6 ¹⁵N labeled metal imido species. ¹⁵N labeled imido species were prepared on an NMR scale from [¹⁵N]-**5.2a** or [¹⁵N]-**5.2b** (¹⁵N,

98% enriched). ^{15}N labeled Me_3Si substituted Mo and W imido compounds were prepared in similar yields with respect to durene according to procedures outlined in Section 5.7.5 by irradiating $^{15}\text{N-5.2a}$ or $^{15}\text{N-5.2b}$ in a Teflon sealed NMR tube in the presence of Me_3SiCl . ^{15}N labeled Me_3C , Ph_3Si and Me_3Ge substituted Mo imido compounds were prepared in similar yields with respect to durene according to procedures outlined in Section 5.7.5 by first irradiating $^{15}\text{N-5.2a}$ in a Teflon sealed NMR tube until full conversion to its photoproducts had occurred, followed by addition of Me_3CCl , Ph_3SiCl or Me_3GeCl .

$\text{Cp}^*\text{Mo}[\text{N}(\text{iPr})\text{C}(\text{Me})\text{N}(\text{iPr})][^{15}\text{N}\text{CMe}_3]$ ($^{15}\text{N-5.7a}$): ^1H NMR (400.13 MHz, benzene- d_6 , 25 °C): δ 1.43 (9H, d, $^3J_{1\text{H}-15\text{N}} = 1.8$ Hz, $\text{MoNC}(\text{CH}_3)_3$). ^{15}N NMR (50.68 MHz, benzene- d_6 , 25 °C): δ 385.98 (1N, s, $\text{MoNC}(\text{CH}_3)_3$).

$\text{Cp}^*\text{Mo}[\text{N}(\text{iPr})\text{C}(\text{Me})\text{N}(\text{iPr})][^{15}\text{NSiMe}_3]$ ($^{15}\text{N-5.7b}$): ^1H NMR (400.13 MHz, benzene- d_6 , 25 °C): δ 0.27 (9H, d, $^3J_{1\text{H}-15\text{N}} = 0.8$ Hz, $\text{MoNSi}(\text{CH}_3)_3$). ^{15}N NMR (50.68 MHz, benzene- d_6 , 25 °C): δ 423.36 (1N, s, $\text{MoNSi}(\text{CH}_3)_3$). ^{29}Si DEPT-35 NMR (99.36 MHz, benzene- d_6 , 25 °C): δ -4.07 (1Si, d, $^1J_{29\text{Si}-15\text{N}} = 4.4$ Hz, $\text{MoNSi}(\text{CH}_3)_3$).

$\text{Cp}^*\text{W}[\text{N}(\text{iPr})\text{C}(\text{Me})\text{N}(\text{iPr})][^{15}\text{NSiMe}_3]$ ($^{15}\text{N-5.7c}$): ^1H NMR (400.13 MHz, benzene- d_6 , 25 °C): δ 0.27 (9H, d, $^3J_{1\text{H}-15\text{N}} = 0.8$ Hz, $\text{WNSi}(\text{CH}_3)_3$). ^{15}N NMR (50.68 MHz, benzene- d_6 , 25 °C): δ 374.48 (1N, $^1J(^{15}\text{N}-^{183}\text{W}) = 111.7$ Hz, $\text{WNSi}(\text{CH}_3)_3$).

^{29}Si DEPT-35 NMR (99.36 MHz, benzene- d_6 , 25 °C): δ -2.18 (1Si, $^1J_{^{29}\text{Si}-^{15}\text{N}} = 8.7$ Hz, $^2J_{^{29}\text{Si}-^{183}\text{W}} = 59.1$ Hz WNSi(CH $_3$) $_3$).

Cp*Mo[N(*i*Pr)C(Me)N(*i*Pr)][$^{15}\text{NSiPh}_3$] (^{15}N -5.7d): ^{15}N NMR (50.68 MHz, benzene- d_6 , 25 °C): δ 399.03 (1N, s, MoNSiPh $_3$). ^{29}Si DEPT-35 NMR (99.36 MHz, benzene- d_6 , 25 °C): δ -27.57 (1Si, d, $^1J_{^{29}\text{Si}-^{15}\text{N}} = 6.5$ Hz, MoNSiPh $_3$).

Cp*Mo[N(*i*Pr)C(Me)N(*i*Pr)][$^{15}\text{NGeMe}_3$] (^{15}N -5.7e): ^{15}N NMR (50.68 MHz, benzene- d_6 , 25 °C): δ 426.04 (1N, s, MoNGe(CH $_3$) $_3$).

General preparation of [^{13}C , ^{15}N]-isocyanates and ^{15}N -Me $_3$ SiNCNAr (Ar = 2,6-dimethylphenyl). [^{13}C , ^{15}N]-isocyanates were prepared in similar yields with respect to durene by degassing a sample of the desired ^{15}N labelled substituted Mo Imido with three freeze-pump-thaw cycles, followed by charging with isotopically labelled ^{13}CO (^{13}C , 99% enriched) according to procedures outlined in Section 5.7.5 and were prepared in similar yields with respect to durene. Me $_3$ Si ^{15}N CNAr was prepared according to procedures outlined in Section 5.7.5 in similar yield by reacting a sample of ^{15}N -5.7b with unlabeled CNAr.

[^{13}C , ^{15}N]-*tert*-butyl isocyanate ([^{13}C , ^{15}N]-5.10a): ^{13}C NMR (125.76 MHz, benzene- d_6 , 25 °C): δ 123.70 (1C, d, $^1J_{^{13}\text{C}-^{15}\text{N}} = 40.6$ Hz, (CH $_3$) $_3$ CNCO). ^{15}N NMR (50.68 MHz, benzene- d_6 , 25 °C): δ 54.99 (1N, d, $^1J_{^{15}\text{N}-^{13}\text{C}} = 40.6$ Hz, (CH $_3$) $_3$ CNCO).

[¹³C,¹⁵N]-trimethylsilyl isocyanate ([¹³C,¹⁵N]-5.10b): ¹H NMR (400.13 MHz, benzene-*d*₆, 25 °C): δ -0.14 (9H, d, ³*J*_{1H-15N} = 1.3 Hz, (CH₃)₃SiNCO). ¹³C NMR (125.76 MHz, benzene-*d*₆, 25 °C): δ 124.41 (1C, d, ¹*J*_{13C-15N} = 42.7 Hz, (CH₃)₃SiNCO). ¹⁵N NMR (50.68 MHz, benzene-*d*₆, 25 °C): δ 33.69 (1N, d, ¹*J*_{15N-13C} = 42.7 Hz, (CH₃)₃SiNCO). ²⁹Si DEPT-35 NMR (99.36 MHz, benzene-*d*₆, 25 °C): δ 3.91 (1Si, dd, ¹*J*_{29Si-15N} = 14.7 Hz, ²*J*_{29Si-13C} = 8.5 Hz, (CH₃)₃SiNCO).

[¹³C,¹⁵N]-triphenylsilyl isocyanate ([¹³C,¹⁵N]-5.10c): ¹³C NMR (125.76 MHz, benzene-*d*₆, 25 °C): δ 125.80 (1C, d, ¹*J*_{13C-15N} = 43.0 Hz, (Ph)₃SiNCO). ¹⁵N NMR (50.68 MHz, benzene-*d*₆, 25 °C): δ 29.86 (1N, d, ¹*J*_{15N-13C} = 43.0 Hz, (Ph)₃SiNCO). ²⁹Si DEPT-35 NMR (99.36 MHz, benzene-*d*₆, 25 °C): δ -21.08 (1Si, dd, ¹*J*_{29Si-15N} = 18.6 Hz, ²*J*_{29Si-13C} = 8.8 Hz, (Ph)₃SiNCO).

[¹³C,¹⁵N]-trimethylgermyl isocyanate ([¹³C,¹⁵N]-5.10d): ¹H NMR (400.13 MHz, benzene-*d*₆, 25 °C): δ 0.05 (9H, br, (CH₃)₃GeNCO). ¹³C NMR (125.76 MHz, benzene-*d*₆, 25 °C): δ 127.19 (1C, d, ¹*J*_{13C-15N} = 33.7 Hz, (CH₃)₃GeNCO). ¹⁵N NMR (50.68 MHz, benzene-*d*₆, 25 °C): δ 31.90 (1N, d, ¹*J*_{15N-13C} = 33.7 Hz, (CH₃)₃GeNCO).

¹⁵N-trimethylsilyl-N'-2,6-dimethylphenyl carbodiimide (¹⁵N-5.12): ¹H NMR (400.13 MHz, benzene-*d*₆, 25 °C): δ 0.07 (9H, d, ³*J*_{1H-15N} = 1.2 Hz, ((CH₃)₃SiNCNAr), 2.31 (6H, s, NCN(2,6-(CH₃)₂(C₆H₃))), 6.82-6.92 (3H, m, NCN(2,6-(CH₃)₂(C₆H₃))). ¹³C NMR (125.76 MHz, benzene-*d*₆, 25 °C): δ 0.64 (3C, ³*J*_{13C-15N} = 2.3 Hz, ((CH₃)₃SiNCNAr). ¹⁵N NMR (50.68 MHz, benzene-*d*₆, 25 °C):

δ 70.23 (1N, (CH₃)₃SiNCNAr). ²⁹Si DEPT-35 NMR (99.36 MHz, benzene-*d*₆, 25 °C): δ 1.78 (1Si, d, ¹J_{29Si-15N} = 14.0 Hz, (CH₃)₃SiNCNAr).

5.8. References

- 1) MacLeod, K. C.; Holland, P. L. *Nature Chem.* **2013**, *5*, 559-565.
- 2) Sobota, P.; Janas, Z. *J. Organomet. Chem.* **1984**, *276*, 171-176.
- 3) Curley, J. J.; Sceats, E. L.; Cummins, C. C. *J. Am. Chem. Soc.* **2006**, *128*, 14036-14037.
- 4) Figueroa, J. S.; Piro, N. A.; Clough, C. R.; Cummins, C. C. *J. Am. Chem. Soc.* **2006**, *128*, 940-950.
- 5) Knobloch, D. J.; Lobkovsky, E.; Chirik, P. J. *J. Am. Chem. Soc.* **2010**, *132*, 10553-10564.
- 6) Knobloch, D. J.; Lobkovsky, E.; Chirik, P. J. *J. Am. Chem. Soc.* **2010**, *132*, 15340-15350.
- 7) Semproni, S. P., Lobkovsky, E. & Chirik, P. J. *J. Am. Chem. Soc.* **2011**, *133*, 10406-10409.
- 8) Semproni, S. P.; Chirik, P. J. *J. Am. Chem. Soc.* **2013**, *135*, 11373-11383.
- 9) Cozzolino, A. F.; Silvia, J. S.; Lopez, N.; Cummins, C. C. *Dalton Trans.* **2014**, *43*, 4639-4652.
- 10) Ishida, Y.; Kawaguchi, H. *J. Am. Chem. Soc.* **2014**, *136*, 16990-16993.
- 11) Solari, E.; Da Silva, C.; Iacono, B.; Hesschenbrouck, J.; Rizolli, C.; Scopelliti, R.; Floriani, C. *Angew. Chem. Int. Ed.* **2001**, *40*, 3907-3909.
- 12) Curely, J. J.; Cook, T. R.; Reece, S. Y.; Muller, P.; Cummins, C. C. *J. Am. Chem. Soc.* **2008**, *130*, 9394-9405.

- 13) Odom, A. L.; Cummins, C. C. *Organometallics* **1996**, *15*, 898-900.
- 14) (a) Tonzetich, Z. J.; Schrock, R. R.; Wampler, K. M.; Bailey, B. C.; Cummins, C. C.; Muller, P. *Inorg. Chem.* **2008**, *47*, 1560-1567. (b) Clough, C. R.; Mueller, P.; Cummins, C. C. *Dalton Trans.* **2008**, 4458-4463. (c) Silvia, J. S.; Cummins, C. C. *J. Am. Chem. Soc.* **2010**, *132*, 2169-2171. (d) Curley, J. J.; Cozzolino, A. F.; Cummins, C. C. *Dalton Trans.* **2011**, *40*, 2429-2432. (e) Scepaniak, J. J.; Bontchev, R. P.; Johnson, D. L.; Smith, J. M. *Angew. Chem. Int. Ed.* **2011**, *50*, 6630-6633. (f) Cleaves, P. A.; King, D. M.; Kefalidis, C. E.; Maron, L.; Tuna, F.; McInnes, E. J. L.; McMaster, J.; Lewis, W.; Blake, A. J.; Liddle, S. T. *Angew. Chem. Int. Ed.* **2014**, *53*, 10412-10415. (g) Klopsch, I.; Finger, M.; Würtele, C.; Milde, B.; Werz, D. B.; Schneider, S. *J. Am. Chem. Soc.* **2014**, *136*, 6881-6883.
- 15) Arnold, J.; Tilley, T. D.; Rheingold, A. L.; Geib, S. J. *Organometallics* **1987**, *6*, 473-479.
- 16) (a) Blake, A. J.; McInnes, J. M.; Mountford, P.; Nikonov, G. I.; Swallow, D.; Watkin, D. J. *J. Chem. Soc., Dalton Trans.* **1999**, 379-391. (b) Royo, P.; Sánchez-Nieves, J. *J. Organomet. Chem.* **2000**, *597*, 61-68. (c) Kilgore, U. J.; Basuli, F.; Huffman, J. C.; Mindiola, D. J. *Inorg. Chem.* **2006**, *45*, 487-489. (e) Ward, B. D.; Clot, E.; Dubberley, S. R.; Gade, L. H.; Mountford, P. *Chem. Commun.* **2002**, 2618-2619.
- 17) Weber, K.; Korn, K.; Schorm, A.; Kipke, J.; Lemke, M.; Khvorost, A.; Harms, K.; Sundermeyer, J. *Zeits. Anorg. Alleg. Chem.* **2003**, *629*, 744-754.
- 18) Fontaine, P. P.; Yonke, B. L.; Zavalij, P. Y.; Sita, L. R. *J. Am. Chem. Soc.* **2010**, *132*, 12273-12285.

- 19) Yonke, B. L., Ph.D. Thesis, University of Maryland – College Park, **2012**.
- 20) Eaborn, C.; Jackson, R. A.; Walsingham, R. W. *J. Chem. Soc. C.* **1967**, 2188-2191.

Chapter 6: Implications of Research and Future

Work

6.1. Implications of Discoveries

A significant advancement made in this thesis work was the development of group 6 CPAM metal nitride chemistry that imparted the ability to obtain imido complexes directly from dinitrogen. The synthesis of a variety of substituted imido complexes was established to provide the ability to tune sterics and electronics for controlling reactivity and unlocking new classes of chemistry for nitrene group transfer. It was demonstrated that N-C based organic products could be obtained directly from N₂ *via* imido complexes. For the first time, this reconciles N₂ fixation chemistry with 40 years of developments in imido chemistry. This discovery has broad implications, considering nitrene group transfer and N₂ cleavage chemistry have been independently and extensively developed across the transition metal series. When considering intermediates along the pathway of N₂ fixation to N-C based organic products, imido complexes represent the ideal intermediate, considering their diverse reactivity that can provide a variety of organic products of commercial interest. These discoveries establish a foundation to pursue a catalytic variant for CPAM supported Mo and W metals.

Other advancements made include the investigation of CPAM group 5 metal mediated N₂ cleavage. Considering that only one other N₂ cleavage system exists that allows the researcher to obtain quantitative data on reaction kinetics of the N₂ cleavage step, the CPAM ligand set provided a rare N₂ cleavage system that also allowed for quantitative data to be obtained on kinetics. Mechanistic work provided more detail on the reaction coordinate that involves and intramolecular isomerization mechanism with a contracted rate determining transition state. These studies also

extended group 5 dinitrogen chemistry to Nb and V, which fills in a missing gap in the CPAM N₂ complex isostructural series. Eight of nine early transition metal CPAM N₂ complexes have now been isolated and structurally characterized, which provides information on metal dependent trends on N₂ coordination and activation.

Finally, group 5 work on CPAM imido and hydrazido complexes completed a reactivity study of an isostructural series of imido complexes spanning groups 4 – 6. Hydrazido and hydrazidium reactivity studies relevant to the Chatt cycle were conducted and provided a picture of N-N cleavage pathways using a unique Ta(IV) metal center.

6.2. Future Work

A comprehensive evaluation of group 6 CPAM imido chemistry is needed to gain a fundamental understanding of reactivity and imido substituent effects. This involves obtaining kinetic and mechanistic data on nitrene group transfer to known substrates that engage in imido group transfer (CO, isocyanides, CO₂) and understanding how substituent effects (sterics and electronics) affect the rate of transfer. This nitrene group transfer needs to be expanded to additional substrates that react under mild conditions. Understanding imido substituent effects may lead to discoveries with either accelerating kinetics or providing access to new classes of nitrene group transfer (*i.e.* transfer to olefins, aldehydes, ketones, etc.). Only a small amount of imido group substituents were studied here but the chemistry provides access to a large collection of substituents for further study (*e.g.* consider Hg(C₆F₅)₂ or MeH₂SiCl and similar reagents for making substantial changes to the electronics and sterics of the imido group). The sterics of the CPAM ligand framework can also

be reduced to enhance reactivity or unlock new chemistry. Less activated substrates that are less competitive with N_2 for coordination to the metal center need to be targeted as discussed in Section 5.5.2. The goal should be to develop a simple, accessible catalytic N_2 fixation system that can operate in a single reaction vessel.

The photophysics of group 6 photolytic N_2 cleavage needs to be further understood. Preliminary results by Brendan Yonke suggest that it might be possible to obtain the dinuclear Mo bis(μ -nitrido) in quantitative yield from the pre-cleaved N_2 complexes using selective irradiation of 336 nm light (1000W Hg/Xe lamp, 20 nm band pass). This would be a significant result considering the Mo bis(μ -nitrido) reacts with $Hg(SiMe_3)_2$ quantitatively to provide the imido complex. This would allow for 100% efficiency in the N-N cleavage and functionalization step and eliminates the need for R_3ECl species that produce the imido (~60% efficiency) and metal chloride co-products that need to be reduced to coordinate N_2 . Using the $Hg(SiMe_3)_2$ route would also eliminate the need for reducing agents all together considering that there would be no metal chloride products formed – reductive elimination of the organic product provides a reduced metal center capable of picking up N_2 .

Finally, obtaining group 6 CPAM dinitrogen complexes that thermally cleave N_2 would be desirable. As previously proposed by Brendan Yonke, obtaining group 6 CPAM complexes that are isoelectronic with group 5 dinitrogen complexes that thermally cleave N_2 might work. Although Brendan attempted to do this by oxidizing both metal centers in the tungsten CPAM dinitrogen complex with ferrocenium BAr^F_4 (obtaining a di-cation that is isoelectronic with the group 5 dinitrogen complexes), it

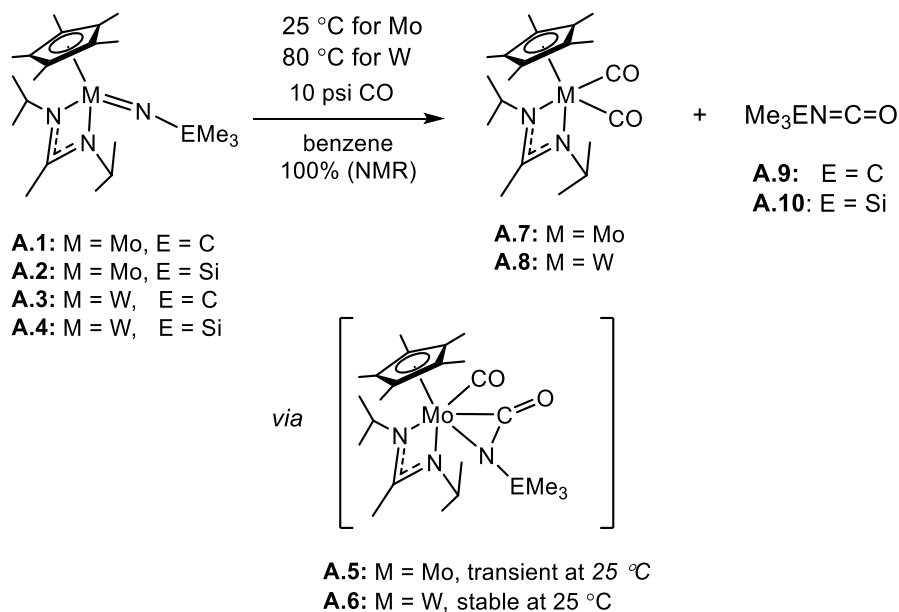
failed to cleave N_2 most likely due to increased sterics from two large BAr^F_4 counter anions. Another proposal would be to try to synthesize the tungsten or molybdenum dinitrogen complex with the deprotonated 'ene-amidinate'. For tungsten, the $Cl[W]-NN-[W](Cl)$ complex is known. Simple deprotonation of the X type amidinates with bulky bases might deprotonate to form the X_2 type, thereby increasing the metal oxidation state by one for both metal centers making an isoelectronic analogue of the group 5 CPAM dinitrogen complexes without the bulky counter-anions.

Appendix A: Group 6 Nitrene Transfer to Isocyanides

A.1. Introduction

Previously, our group has established that molybdenum and tungsten *tert*-butyl and trimethylsilyl imido CPAM compounds $\text{Cp}^*[\text{N}(\textit{i}\text{Pr})\text{C}(\text{Me})\text{N}(\textit{i}\text{Pr})]\text{M}[\text{EMe}_3]$ [$\text{M} = \text{Mo}$: $\text{E} = \text{C}$ (**A.1**), $\text{E} = \text{Si}$ (**A.2**); W : $\text{E} = \text{C}$ (**A.3**), Si (**A.4**)] undergo imido group transfer to carbon monoxide (CO) to provide the corresponding isocyanates in quantitative yield by NMR.¹ Considering the fact that several examples of imido group transfer to the related isocyanide substrates to provide carbodiimides have been

Scheme A.1. Group 6 nitrene transfer to carbon monoxide.



established,²⁻⁸ it was of interest to expand the scope of this chemistry within our system and determine whether similar chemistry was feasible. It had been documented within our lab that *tert*-butyl isocyanide did not react with the CPAM Mo silyl imido (**A.2**) when heated to elevated temperatures (*ca.* 100 °C). In the literature, examples of imido group transfer to CO and isocyanides have appeared in tandem – therefore, it was warranted to pursue other substituted isocyanide substrates

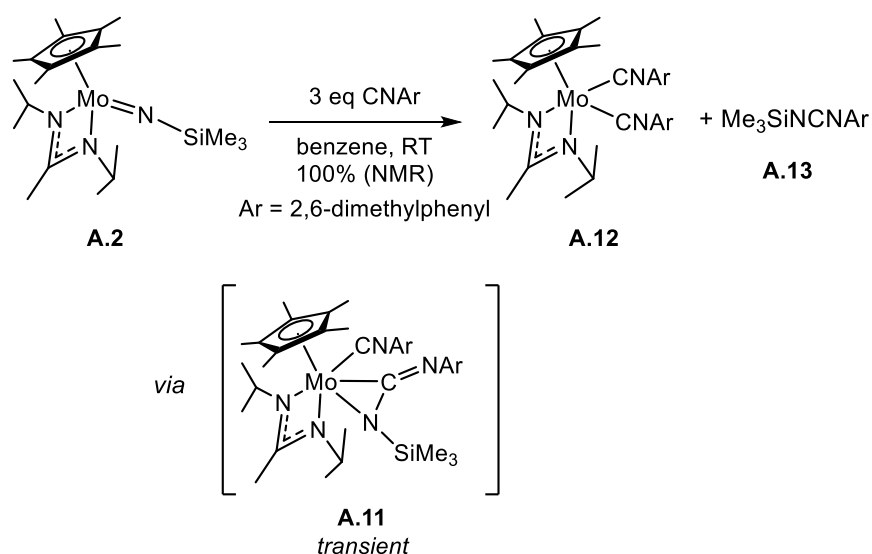
with different steric and electronic properties to fully evaluate whether this chemistry would be achievable with our system.

A.2. Group 6 Imido Group Transfer Chemistry

A.2.1. Extension of imido group transfer chemistry to aryl isocyanide substrates

It is noted that benzyl isocyanide was not reactive with the CPAM Mo silyl imido (**A.2**) at elevated temperatures; however, it was discovered that 3 eq. of 2,6-dimethylphenyl isocyanide (CNAr) reacted over 12 h at room temperature to cleanly produce the previously characterized CPAM Mo(CNAr)₂ **A.12** and a new

Scheme A.2. Group 6 nitrene transfer to aryl isocyanides.



carbodiimide, ArN=C=NSiMe₃ (**A.13**), that was characterized by NMR and ESI-MS (Scheme A.2). Interestingly, while monitoring this reaction by ¹H NMR spectroscopy, an NMR spectrum obtained 15 m after addition of CNAr revealed the presence of a transient C₁ symmetric species (**A.11**) along with unreacted **A.2** and final products **A.12** and **A.13** as shown in Figure A..

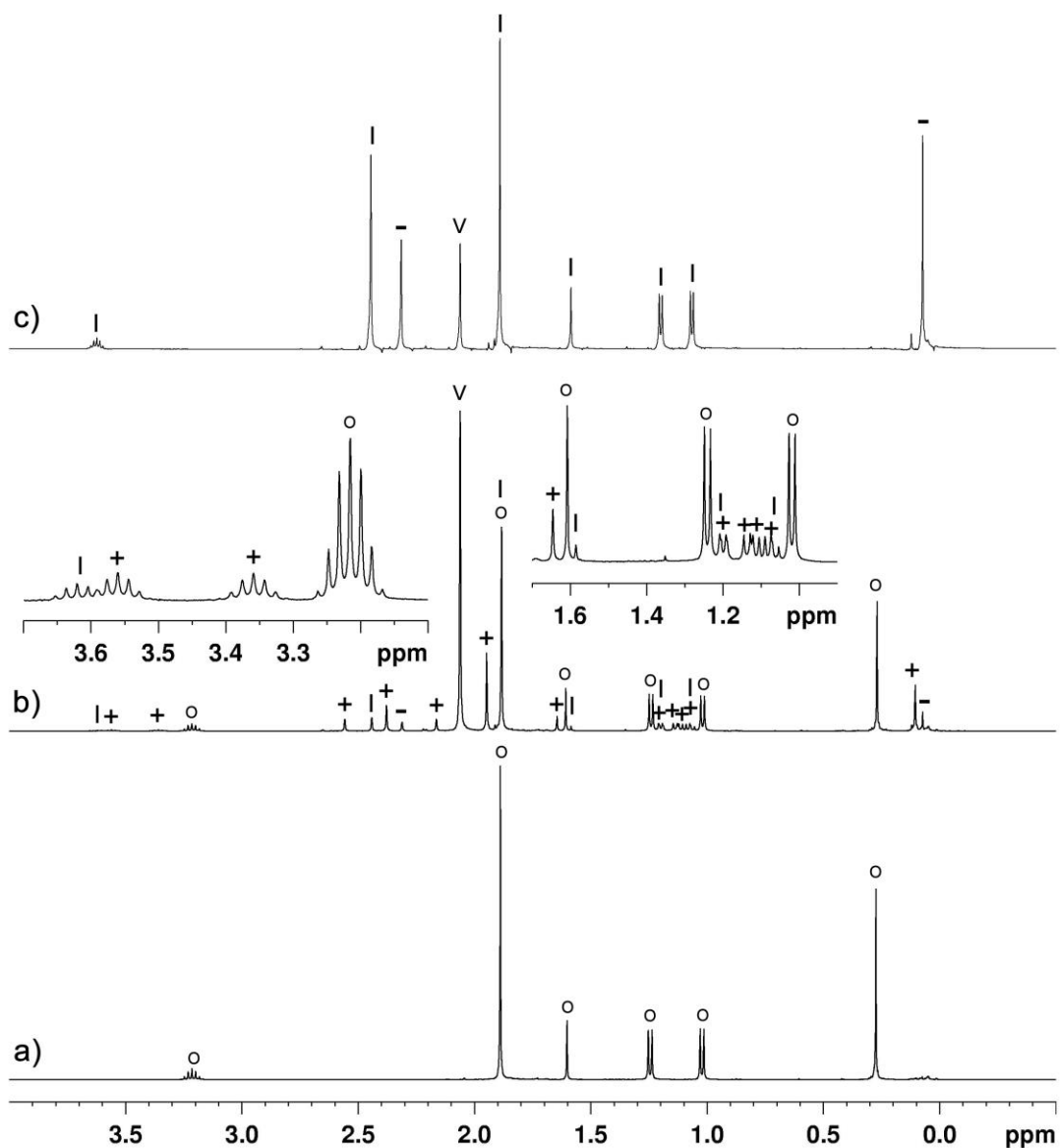


Figure A.1. ^1H NMR spectrum (400 MHz, benzene- d_6 , 25 $^\circ\text{C}$) of (a) pure **A.4** (O), (b) after reacting with 2,6-dimethylphenyl isocyanide (CNAr) (V) at room temperature for 15 m revealing a transient C_1 symmetric species attributed to **A.11** (+), with partial conversion to **A.12** (I), and $\text{Me}_3\text{Si-N}=\text{C}=\text{N-Ar}$ (**A.13**) (-), and (c) complete conversion to **A.12** (I) and $\text{Me}_3\text{Si-N}=\text{C}=\text{N-Ar}$ (**A.13**) (-) after reacting for 12 h.

Previously, our group has published chemistry regarding imido group transfer to CO that involved a similar transient C_1 symmetric species, $[\text{Mo}](\text{CO})(\eta^2\text{-(N,C)-Me}_3\text{SiNCO})$. In this case, the analogous tungsten chemistry allowed for the isolation and structural characterization of this intermediate due to higher thermal barriers for reductive elimination from the metal. It was

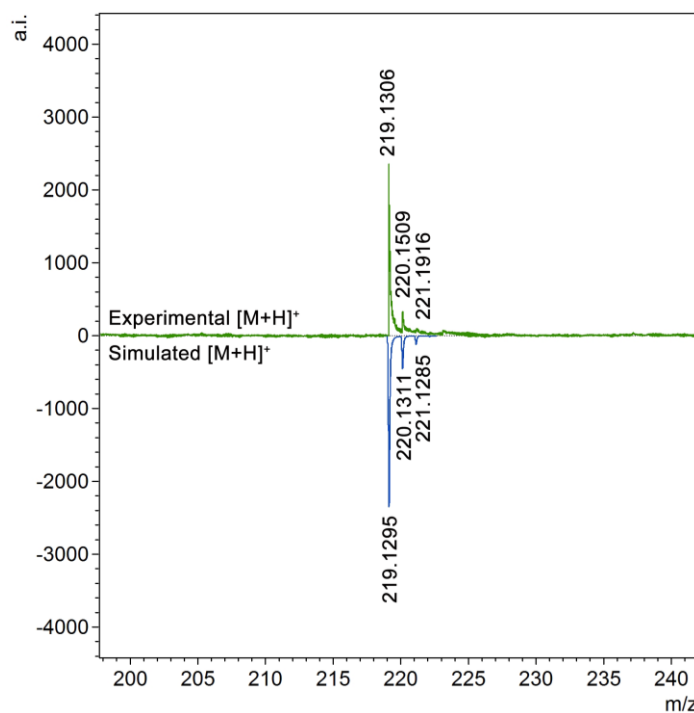
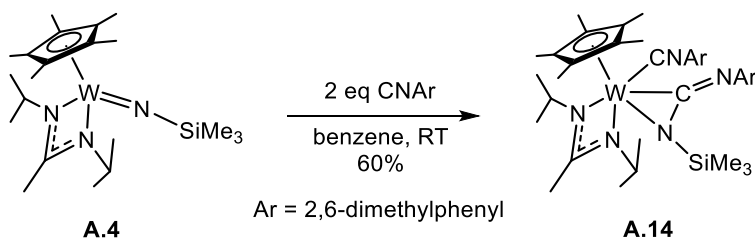


Figure A.2. ESI-MS (positive ion mode) of carbodiimide $\text{ArN}=\text{C}=\text{NSiMe}_3$ (**A.13**) (Ar = 2,6-dimethylphenyl).

therefore hypothesized that the transient C_1 symmetric species observed during imido group transfer to CNAr was the analogous side-bound carbodiimide compound **A.11**. Thus, 2 eq. of CNAr were reacted with the tungsten silyl imido **A.4** to provide the expected C_1 symmetric compound after 15 h of reaction time. Subsequent isolation of this compound by crystallization within concentrated pentane solutions allowed for the isolation of analytically pure crystals that were subjected to single crystal XRD analysis and structurally characterized as the CPAM tungsten $\eta^2\text{-Me}_3\text{SiN}=\text{C}=\text{NAr}$ compound, **A.14**.

Scheme A.3. Synthesis and isolation of a tungsten η^2 -carbodiimide complex.



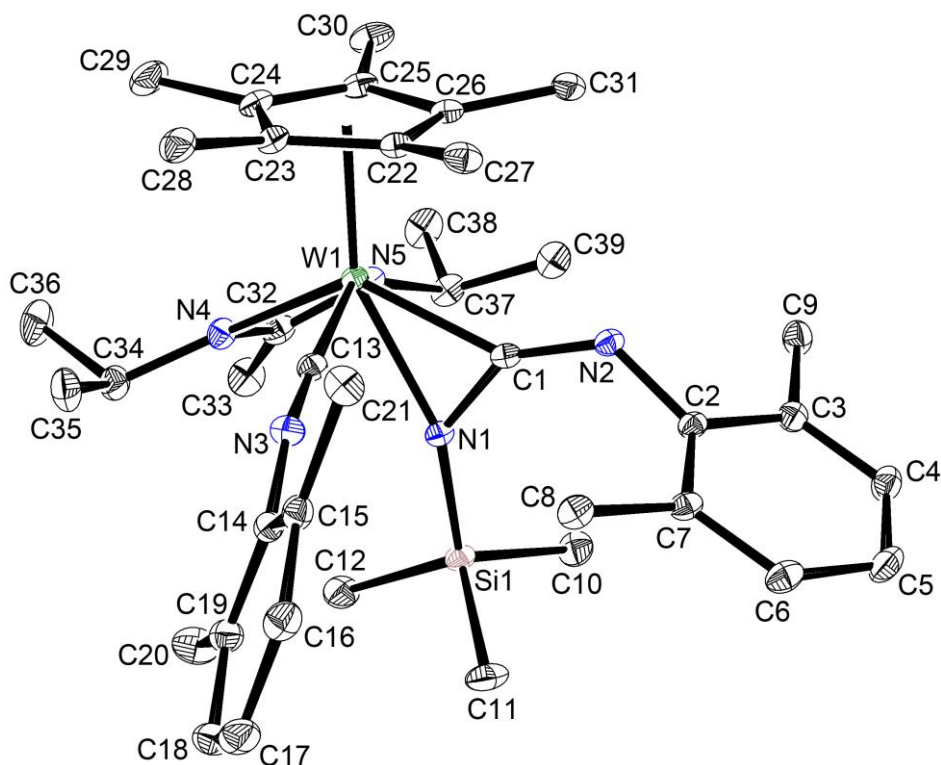


Figure A.3. Molecular structures (30% thermal ellipsoids) of **A.14**. Hydrogen atoms have been removed for the sake of clarity.

A.3. Conclusion

In summary, established chemistry regarding imido group transfer to CO with group 6 imido complexes (Mo and W) was extended to isocyanides that allowed for the production of carbodiimides. The higher barrier of carbodiimide reductive elimination with tungsten was exploited to isolate and structurally characterize the η^2 -carbodiimide, isocyanide compound **A.14**, which serves to establish group 6 CPAM imido group transfer to isocyanide substrates as well-defined process.

A.4. Experimental Section

A.4.1. General considerations

All manipulations with air and moisture sensitive compounds were carried out under an inert atmosphere of N₂ or Ar using standard Schlenk-line or glovebox techniques. All solvents were dried (Na for toluene and Na/benzophenone for pentane, Et₂O, and THF) and distilled under N₂ prior to use. Benzene-*d*₆ was dried over Na/K alloy and isolated by vacuum transfer. Celite was oven-dried (150 °C for several days). Cooling for reactions was achieved using the internal freezer of a glovebox maintained at -30 °C. 2,6-dimethylphenyl isocyanide was purchased from Sigma-Aldrich. All chemicals were used as received unless otherwise noted. Compounds **A.2** and **A.4** were synthesized using reported procedures and isolated in similar yield and purity. All ¹H NMR spectra were recorded at 400.13 MHz. Elemental analyses (C, H, and N) were performed by Midwest Microlab, LLC.

A.4.2. Synthesis of new compounds

Me₃SiN=C=NAr (Ar = 2,6-dimethylphenyl) (A.13). ¹H NMR (400.13 MHz, benzene-*d*₆, 25 °C): δ 0.07 (9H, s, ((CH₃)₃SiNCNAr), 2.31 (6H, s, NCN(2,6-(CH₃)₂(C₆H₃))), 6.82-6.92 (3H, m, NCN(2,6-(CH₃)₂(C₆H₃))). ¹³C NMR (125.76 MHz, benzene-*d*₆, 25 °C): δ 0.64 ((CH₃)₃SiNCNAr), 19.2 (NCN(2,6-(CH₃)₂(C₆H₃))), 123.65 (NCN), 128.51 (Me₃SiNCN-2,6-(CH₃)₂(C₆H₃)), 132.56 (Me₃SiNCN-2,6-(CH₃)₂(C₆H₃)), 137.30 (Me₃SiNCN-2,6-(CH₃)₂(C₆H₃))). ESI-MS (positive ion mode): [M+H]⁺ Calc'd: 219.1295; Found: 219.1306.

Cp*W[N(ⁱPr)C(Me)N(ⁱPr)](CNAr)(η^2 -Me₃SiN-C=NAr) (Ar = 2,6-

dimethylphenyl) (A.14). A teflon sealed NMR tube was charged with A.4 (73.9 mg, 0.135 mmol), 2,6-dimethylphenyl isocyanide (35.4 mg, 0.270 mmol) and 0.5 mL of benzene-*d*₆. The contents were mixed well and allowed to sit for 15 h at 25 °C.

Volatiles were removed *in vacuo* to yield a red oily solid, which was dissolved in pentane and filtered through Celite supported by Kimwipe in a glass pipette. The filtrate was concentrated *in vacuo* and cooled to -30 °C to yield red crystals of **A.14** (66 mg, 60% yield). Anal. Calc'd for C₄₈H₇₄N₆S₂Ta₂: C, 57.84; H, 7.34; N, 8.65; Found: C, 57.85; H, 7.29; N, 8.74. ¹H NMR (400 MHz, benzene-*d*₆): 0.15 (9H, s, Si(CH₃)₃), 1.07 (3H, d, *J* = 6.2 Hz, CH(CH₃)₂), 1.12 (3H, d, *J* = 6.6 Hz, CH(CH₃)₂), 1.17 (3H, d, *J* = 6.6 Hz, CH(CH₃)₂), 1.19 (3H, d, *J* = 6.6 Hz, CH(CH₃)₂), 1.58 (3H, s, NC(CH₃)N), 2.04 (15H, s, C₅(CH₃)₅), 2.25 (3H, s, 2,6-CH₃Ph), 2.42 (6H, s, NCN(2,6-CH₃Ph), 2.57 (3H, s, 2,6-CH₃Ph), 3.46 (1H, sept, *J* = 6.6, CH(CH₃)₂), 3.63 (1H, sept, *J* = 6.3, CH(CH₃)₂).

A.5. References

- 1) Yonke, B. L.; Reeds, J. P.; Fontaine, P. P.; Zavalij, P. Y.; Sita, L. R. *Organometallics* **2014**, *33*, 3239-3242.
- 2) Goure, E.; Avenier, F.; Dubourdeaux, P.; Seneque, O.; Albrieux, F.; Lebrun, C.; Clemancey, M.; Maldivi, P.; Latour, J.-M. *Angew. Chem. Int. Ed.* **2014**, *53*, 1580-1584.
- 3) Nguyen, A. I.; Zarkesh, R. A.; Lacy, D. C.; Thorson, M. K.; Heyduk, A. F. *Chem. Sci.* **2011**, *2*, 166-169.
- 4) Laskowski, C. A.; Hillhouse, G. L. *Organometallics* **2009**, *28*, 6114-6120.

- 5) Mindiola, D. J.; Hillhouse, G. L. *Chem. Commun.* **2002**, 1840-1841.
- 6) Cowley, R. E.; Golder, M. R.; Eckert, N. A.; Al-Afyouni, M. H.; Holland, P. L. *Organometallics* **2013**, 32, 5289-5298.
- 7) Cowley, R. E.; Eckert, N. A.; Elhaik, J.; Holland, P. L. *Chem. Commun.* **2009**, 1760-1762.
- 8) Wiese, S.; Aguila, J. B.; Kogut, E.; Warren, T. H. *Organometallics* **2013**, 32, 2300-2308.